Université de Strasbourg

Ecole Doctorale des Sciences Chimiques

THESE

Présentée en vue de l'obtention du titre de

DOCTEUR DE L'UNIVERSITE DE STRASBOURG

Antibody-functionalized carbon nanotubes towards a targeted anticancer therapy

Par Enrica Venturelli

Soutenue publiquement le 27 Septembre 2011 devant la commission d'examen :

Prof. Cécile Zakri	Rapporteur
Prof. Ester Vazquez Fernandez-Pacheco	Rapporteur
Prof. Marcel Hibert	Examinateur
Prof. Khuloud Al-Jamal	Examinateur
Dr. Cécilia Ménard-Moyon	Membre invité
Dr. Sylviane Muller	Membre invité
Dr. Alberto Bianco	Directeur de Thèse

Université de Strasbourg

Ecole Doctorale des Sciences Chimiques

THESE

Présentée en vue de l'obtention du titre de

DOCTEUR DE L'UNIVERSITE DE STRASBOURG

Antibody-functionalized carbon nanotubes towards a targeted anticancer therapy

Par Enrica Venturelli

Soutenue publiquement le 27 Septembre 2011 devant la commission d'examen:

Prof. Cécile Zakri	Rapporteur
Prof. Ester Vazquez Fernandez-Pacheco	Rapporteur
Prof. Marcel Hibert	Examinateur
Prof. Khuloud Al-Jamal	Examinateur
Dr. Cécilia Ménard-Moyon	Membre invité
Dr. Sylviane Muller	Membre invité
Dr. Alberto Bianco	Directeur de Thèse

Acknowledgments

I wish to acknowledge all the people who collaborated to the development this Thesis.

First, I would like to thank my supervisor Dr. Alberto Bianco for giving me the opportunity to develop this Thesis. I learned a lot with this interesting and multidisciplinary project.

I would like to thank the jury members Prof. Marcel Hibert, Prof. Cécile Zakri, Prof. Ester Vazquez Fernandez-Pacheco and Prof. Khuloud Al-Jamal for accepting to read and judge my work.

I would like also to thank Dr. Sylviane Muller for having accepted me in the laboratory.

I am grateful to Dr. Cécilia Mènard-Moyon for her help and suggestions during these three years.

I would like also to thank the French collaborators Dr. Jean-Paul Briand for peptide synthesis, Dr. Olivier Chaloin for SPR measurements, Dr. Marion Décossas and Dr. Mathieu Erhardt for their help with electron microscopy, Dr. Cristian Smulski, Dr. Julie Russier and Dr. Hélène Dumortier for their help, advices in biology and contributions to the Thesis.
I would like also to acknowledge all the members of the ANTICARB Project. Especially, I am grateful to Prof. Kostas Kostarelos and his group in London for their contributions to this work with the *in vitro* and *in vivo* experiments and to Prof. Maurizio Prato, Dr. Tatiana Da Ros, Dr. Chiara Fabbro and Dr. Francesca Maria Toma for their fruitful discussions and help on the thermogravimetric characterization. I am also grateful to Dr. Martyn Robinson and Laura Newnham (UCB) for providing the different antibodies and to Dr. Julien Amadou (Nanocyl) for the MWCNTs.

Thanks to all the people I met in the lab during these three years especially Alessia, Giuseppe, Pauline, Cristian, Claire, Marie-Charlotte, Joël and Paul.

A special thanks to my parents and my sister for their help and support in everything.

Finally, I would like to thank the European Union FP7 ANTICARB Program (HEALTH-2007-201587) and CNRS for the financial support.

Thanks to all of you.

Abbreviations

Å	Angstrom
Ab	Antibody
AcOEt	Ethyl acetate
AFM	Atomic Force Microscopy
Biot	Biotin
β-Me	β-mercaptoethanol
BMP-2	Bone morphogenetic protein 2
Boc	*tert*-butyloxycarbonyl
Boc_2O	Di-*tert*-butyl dicarbonate
BOP	Benzotriazole-1-yl-oxy-tris-(dimethylamino)-phosphonium hexafluorophosphate
CHI	Chitosan
CLSM	Confocal laser scanning microscopy
CNT	Carbon nanotube
CVD	Chemical vapor deposition
DAPI	4′,6-diamidino-2-phenylindole
DCC	*N-N'*-dicyclohexylcarbodiimide
DCM	Dichloromethane
DDS	Drug delivery system
DFO	Desferrioxamine B
DIC	Differential interference contrast
DIEA	*N,N*-diisopropylethylamine
DMF	*N,N*-dimethylformamide
DMSO	Dymethylsulfoxide
DNA	Deoxyribonucleic acid
DOX	Doxorubicin
DOTA	1,4,7,10-tetraazacyclododecane-1,4,7,10-tetraacetic acid
DTPA	Diethylenetriaminepentaacetic acid
EDC	1-ethyl-3-(3-dimethylaminopropyl) carbodiimide
EDTA	Ethylenediaminetetraacetic acid
EEA	Early endosome antigen
EGF	Epidermal growth factor
EPR	Enhanced permeability and retention

ESI	Electrospray ionization mass spectrometer
Et_2O	Diethyl ether
f-CNTs	Functionalized CNTs
Fab	Fragment antigen binding
FACS	Fluorescence assisted cell sorter
FBS	Fetal bovine serum
FET	Field effect transistor
FITC	Fluorescein isothiocyanate
Fmoc	Fluorenyl-methoxy-carbonyl
FT-IR	Fourier transform infrared
HCl	Hydrochloric acid
HCPT	Hydroxycamptothecin
HEPES	4-(2-hydroxyethyl)-1-piperazineethanesulfonic acid
hMSC	Human mesenchymal stem cells
HOBt	1-hydroxy-benzotriazole
HPLC	High performance liquid chromatography
HRP	Horseradish peroxidase
ID	Injected dose
Ig	Immunoglobulin
IRMS	Isotope ratio mass spectrometry
K_D	Equilibrium dissociation constant
LDH	Lactate dehydrogenase
MeOH	Methanol
MTX	Methotrexate
MWCNT	Multi-walled carbon nanotube
MWCO	Molecular weight cut-off
MUC1	Mucin 1
NHS	*N*-hydroxy succinimide
NIR	Near-infrared
NMR	Nuclear magnetic resonance
ox-CNT	Oxidized carbon nanotubes
PAT	Photoacoustic tomography
PBS	Phosphate buffered saline
pDNA	Plasmid DNA

PEG	Polyethylene glycol
PEM	Polymorphic epithelial mucin
PI	Propidium iodide
PL-PEG	Phospholipid-polyethylene glycol
PLA	Polylactic acid
PSF	Phagolysosomal simulant fluid
PTFE	Polytetrafluoroethylene
qPCR	Quantitative real time polymerase chain reaction
RES	Reticuloendothelial system
RNA	Ribonucleic acid
RNAi	RNA interference
scFv	Single-chain variable fragment
siRNA	Small interfering RNA
SPECT	Single photon emission computed tomography
SPR	Surface plasmon resonance
ssDNA	Single stranded DNA
STM	Scanning tunneling microscopy
SWCNT	Single-walled carbon nanotube
tBu	*tert*-butyl
TEM	Transmission electron microscopy
TGA	Thermogravimetric analysis
THF	Tetrahydrofuran
TMB	3,3',5,5'-tetramethylbenzidine
t_R	Retention time
TUNEL	Terminal deoxynucleotidyl transferase mediated dUTP nick end labeling
UV-Vis	Ultraviolet-visible
VHH	Variable domain of heavy chain of heavy-chain antibodies
VNTR	Variable number tandem repeat

Abstract

Carbon nanotubes (CNTs) are a new allotropic form of carbon including graphite, diamond and fullerenes. Discovered in the 1950/1960s and described as carbon filaments, only in 1991 they were characterized at the atomic level by S. Iijima. Carbon nanotubes are composed only of carbon atoms organized in graphene sheets and rolled up into a seamless tubular shape. Depending on the number of graphene layers from which a single nanotube is composed, CNTs are classified as single-walled carbon nanotubes (SWCNTs) or multi-walled carbon nanotubes (MWCNTs). SWCNTs are formed by a single graphene sheet and have a diameter of 0.4-3 nm and lengths ranging from a few nanometers up to several micrometers. MWCNTs have much larger diameters (10-100 nm) as they are constituted of multiple concentric layers of graphene and can reach tenth of micrometers in length.

CNTs present interesting physical properties that stimulated applications in several research fields like nanotechnologies or materials science. Recent studies on the ability of CNTs to form supramolecular complexes with nucleic acids or proteins triggered their applications in the biomedical domain. For example, they can be used as sensor to detect genetic or molecular abnormalities, as substrates for tissue regeneration or as drug delivery systems.

In this thesis, I focused my interest on the design and synthesis of antibody-CNT (Ab-CNT) conjugates for targeted cancer therapy. The nanotubes are used as delivery system whereas the antibody is the targeting moiety for cancer cells. Nowadays antibodies represent a promising anticancer therapy, however they have not been utilized against intracellular targets because of their low aptitude to traverse the plasma membrane. On the contrary, CNTs have shown the ability to easily cross cell membrane mainly *via* two mechanisms: endocytosis or passive diffusion (“nanoneedle” mechanism).

In this context, the first part of this work was focused on the development of a hybrid platform able to target cancer cells using MWCNTs. Before using CNTs in nanomedicine, it is necessary to chemically functionalize their surface to increase their dispersibility in aqueous milieu and render them more biocompatible than the pristine CNTs. For this purpose, we exploited two strategies to functionalize MWCNTs: the 1,3 dipolar cycloaddition reaction of azomethine ylides to derivatize the sidewall and the amidation to introduce functions at the tips of the tubes.

The functional groups were further coupled with the antibody or a tracking probe (*i.e.* fluorescein or radioisotope) to perform *in vitro* or *in vivo* studies. The obtained constructs were fully characterized by complementary techniques (thermogravimetric analysis, transmission electron microscopy, gel electrophoresis and surface plasmon resonance [SPR]). SPR analysis showed that the affinity of the antibody towards its antigen was not affected by the conjugation to the carbon nanotubes.

However, *in vitro* studies revealed that the internalization of mono-functionalized Ab-CNT conjugates by cells overexpressing the antigen (protein MUC1) was limited. We hypothesized that the low uptake could be due to the size of the conjugate and/or to the low dispersibility degree of the construct.

These results aimed us therefore to develop a second generation of constructs based on doubly functionalized CNTs. These conjugates were prepared starting from carbon nanotubes produced by different suppliers and presenting therefore a different aspect ratio (length to diameter ratio) and dispersibility degree. Changes in these features allowed us to study the effect of the morphology of the CNTs on the internalization process. The findings suggested that the carbon nanotubes presenting a more distorted structure were more easily uptaken by cells. We also investigated the influence of the size of the antibody on the cellular internalization. We prepared conjugates by binding fragments of the antibody (Fab and scFv) to MWCNTs. The SPR results confirmed that the ability to recognize the antigen was not affected by the binding to carbon nanotubes. We observed that the size of the protein and therefore of the final construct is an important parameter that affects the internalization process. Complementary studies to fully understand the role of the protein in the cellular uptake are in progress.

Finally, we expanded the study to the preparation of a therapeutic conjugate. In this case, we coupled a fragment of a heavy-chain antibody (VHH, intrabody) presenting both targeting and therapeutic activity towards cancer cells. SPR confirmed the conservation of the recognition capacity of the bound intrabody towards its antigen but further studies to assess the therapeutic activity are currently ongoing.

An important aspect related to the biomedical applications of these constructs concerns the evaluation of their potential toxicity. We studied the cell viability of different cell lines like breast or lung cancer cells as well as cell lines of the immune system, after incubation with the Ab-CNT conjugates. Results did not show marked signs of short-term toxicity, confirming that the chemical

functionalization is a powerful way to render carbon nanotubes biocompatible. However, further studies are currently perfrmed to assess the possible long-term toxicological effects.

In vivo studies were also done to study the pharmacological parameters, such as tissue distribution and pharmacokinetic profiles.

In conclusion, we reported the functionalization of carbon nanotubes with an antibody (or its fragments) for potential application in targeted cancer therapy. The prepared constructs showed no short-term toxicity and can deliver the antibody (or its fragments) inside cells. Preliminary experiments showed that Ab-CNTs tend to target cells overexpressing the antigen but further studies will be performed in order to understand the role of the antibody in cellular uptake. Antibody-functionalized carbon nanotubes could find in the future interesting applications as therapeutic tools against cancer.

Résumé de Thèse

I: Introduction générale sur les nanotubes de carbone et leurs applications

Les nanotubes de carbone (CNTs) sont une nouvelle forme allotropique du carbone telle que le graphite, le diamant et les fullerènes. Ils ont été découverts dans les années 1950/1960 [Bacon, R., 1960; Oberlin, A., *et al*. 1976; Monthioux, M., *et al.* 2006] et décrits comme étant des filaments de carbone. Toutefois, ce n'est qu'en 1991 que leur structure a été décrite à l'échelle atomique par S. Iijima [Iijima, S. 1991]. Au niveau structurel, les atomes de carbone sont organisés en feuillets de graphène enroulés pour former un cylindre qui peut être fermé ou ouvert aux extrémités. Ils sont classés selon deux types principaux: les nanotubes à simple paroi (SWCNTs pour *Single-Walled Carbon Nanotubes*) et les nanotubes à parois multiples (MWCNTs pour *Multi-Walled Carbon Nanotubes*) (Figure 1). Les SWCNTs sont constitués d'un seul feuillet de graphène tandis que les MWCNTs sont constitués de plusieurs feuillets de graphène enroulés de façon concentrique. Les SWCNTs ont un diamètre qui varie de 0,4 à 3 nm et une longueur comprise entre quelques centaines de nanomètres et plusieurs micromètres. Quant aux MWCNTs, ils ont un diamètre qui peut atteindre 100 nm et une longueur de quelques dizaines de micromètres.

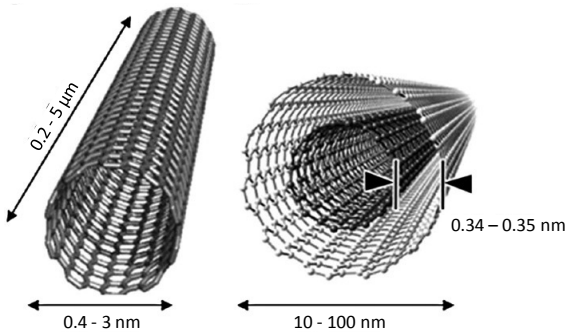

Figure 1: Nanotubes de carbone à simple paroi et à parois multiples.

La combinaison des propriétés mécaniques, thermiques, électriques et chimiques fait des nanotubes de carbone un matériau unique dans les domaines des nanotechnologies et des nanosciences. Les nanotubes ont également trouvé des applications en nanomédecine [Kostarelos, K., *et al*. 2009; Lu, F., *et al*. 2009] puisqu'ils peuvent former des complexes supramoléculaires avec des protéines ou des acides nucléiques, notamment. Ils peuvent être utilisés comme capteurs pour détecter des anomalies moléculaires ou génétiques. Ils trouvent aussi des applications comme substrats pour la régénération de tissus ou comme vecteurs pour la délivrance de médicaments [Prato, M., *et al.* 2008; Ménard-Moyon, C., *et al.* 2010a].

Afin d'élargir le champ d'application des nanotubes au domaine biomédical, il est nécessaire de fonctionnaliser leur surface pour les rendre solubles dans les milieux aqueux et donc pour les rendre plus biocompatibles que les nanotubes natifs non-fonctionnalisés.

Les approches pour fonctionnaliser les nanotubes peuvent être classées selon deux catégories :

- formation de liaisons covalentes *via* des réactions sur la surface des CNTs (*i.e.* fonctionnalisation de la paroi, des extrémités ou des défauts présents sur le tube)
- formation d'interactions non-covalentes avec la surface des nanotubes (par exemple, adsorption de polymères ou de surfactants à la surface des nanotubes).

Dans ce contexte, mon projet de doctorat avait pour objectif le développement de conjugués à base de nanotubes de carbone et d'anticorps (Ab) pour des applications dans le domaine de la nanomédecine, en particulier pour développer une thérapie contre le cancer. En exploitant des stratégies basées sur des réactions de cycloaddition 1,3-dipolaire d'ylures d'azométhine et/ou d'amidation, nous avons pu introduire des groupements réactifs sur la paroi et aux extrémités des nanotubes pour pouvoir accrocher sélectivement et d'une façon stable l'anticorps. En effet, seule la formation d'une liaison covalente entre les nanotubes et l'anticorps permet de fournir des conjugués chimiquement stables.

Dans ce projet, les nanotubes ont été utilisés comme vecteurs pour la délivrance de molécules biologiquement actives à l'intérieur des cellules tumorales ciblées par l'anticorps. Actuellement, les anticorps ne sont pas utilisés contre des cibles intracellulaires à cause de leur faible aptitude à traverser la membrane plasmique. Par contre, il a été montré que les nanotubes ont la capacité de traverser la membrane cellulaire *via* différents mécanismes : soit par endocytose, soit par un mécanisme énergiquement indépendant mimant l'action d'une nanoaiguille.

Néanmoins, l'utilisation des nanotubes à des fins biomédicales a généré dans la communauté scientifique des préoccupations quant à leur possible toxicité et leurs effets à long terme. De nombreuses études *in vitro* et *in vivo* ont établi que la toxicité parfois observée est liée à plusieurs facteurs tels que la morphologie (longueur, diamètre, présence de défauts structurels), le type et le degré de fonctionnalisation ainsi que la méthode et la durée d'exposition.

Récemment, nous avons démontré au laboratoire que les nanotubes de carbone peuvent être dégradés en milieu biologique par des enzymes oxydants [Russier, J., *et al.* 2011], ce qui a permis de renforcer l'optimisme pour le développement des applications des nanotubes en médicine et biologie.

La première étape dans la préparation des nanotubes de carbone fonctionnalisés avec un anticorps a été le choix de l'immunoglobuline G (IgG) hCTM01 anti-MUC1 [Adair, J. R., *et al.* 1993]. Cet anticorps reconnaît les récepteurs MUC1 qui sont surexprimés par les cellules tumorales présentes dans plusieurs types de cancer comme le cancer colorectal ou le cancer du sein [Niv, Y. 2008]. Dans la première partie de cette étude, nous nous sommes intéressés au développement d'un modèle hybride Ab-CNT capable de cibler les cellules tumorales. Dans la deuxième partie, nous avons étendu l'étude à la préparation d'un conjugué Ab-CNT dans lequel la protéine présente à la fois des propriétés de ciblage des cellules tumorales et des propriétés thérapeutiques.

II: Mono-fonctionnalisation de nanotubes de carbone

La première étape de la synthèse des conjugués Ab-CNT a reposé sur l'oxydation des nanotubes en milieu acide. Ce procédé nous a permis de raccourcir les nanotubes (de plusieurs microns jusqu'à quelques centaines de nanomètres) car l'oxydation est conduite sous l'effet d'ultrasons. Ce traitement nous a également permis d'introduire des acides carboxyliques majoritairement sur les pointes des nanotubes, mais aussi au niveau des défauts structurels de la paroi qui sont plus sensibles au traitement oxydant. Ces groupes carboxyliques ont ensuite été dérivatisés avec du diamino-triéthylèneglycol pour obtenir des nanotubes fonctionnalisés avec des amines, localisées principalement aux extrémités des nanotubes [Samorì, C., *et al.* 2010a]. Ces amines ont ensuite été fonctionnalisées avec une sonde fluorescente (FITC: isothiocyanate de fluorescéine) ou avec un agent chélatant (DTPA: acide diéthylènetriamine-*N,N,N',N'',N''*-pentaacétique) qui peut complexer différents radioisotopes. La présence de la fluorescéine nous a permis de localiser les nanotubes à l'intérieur des cellules en utilisant la microscopie de fluorescence. Après chélation du radioisotope ^{111}In par le DTPA, les nanotubes fonctionnalisés ont été utilisés pour de l'imagerie *in vivo* (tomographie d'émission monophotonique), en collaboration avec le groupe du Prof. Kostas Kostarelos à Londres.

La deuxième zone réactive des nanotubes est la paroi. Celle-ci a pu être fonctionnalisée par une réaction de cycloaddition 1,3-dipolaire d'ylures d'azométhine qui permet d'introduire des cycles pyrrolidines à la surface des nanotubes. Ces cycles contiennent une chaîne triéthylèneglycol portant une fonction amine primaire, ce qui a permis de rendre les nanotubes plus solubles dans l'eau et donc d'améliorer leur biocompatibilité [Georgiakilas, V., *et al*. 2002a].

Afin de conjuguer l'anticorps aux nanotubes, nous avons choisi deux stratégies: l'amidation (Schéma 1) et la liaison chimique sélective (Schéma 2). La première stratégie a reposé sur une réaction d'amidation classique entre les groupes carboxyliques présents aux pointes des nanotubes

et les fonctions amines des chaînes latérales de l'acide aminé lysine présent à la surface de l'anticorps. Comme illustré sur le Schéma 1, les groupes COOH des nanotubes oxydés **C1** ont été activés avec du *N*-hydroxysuccinimide et les esters (**C11**) ainsi obtenus ont été couplés directement avec les amines de l'anticorps.

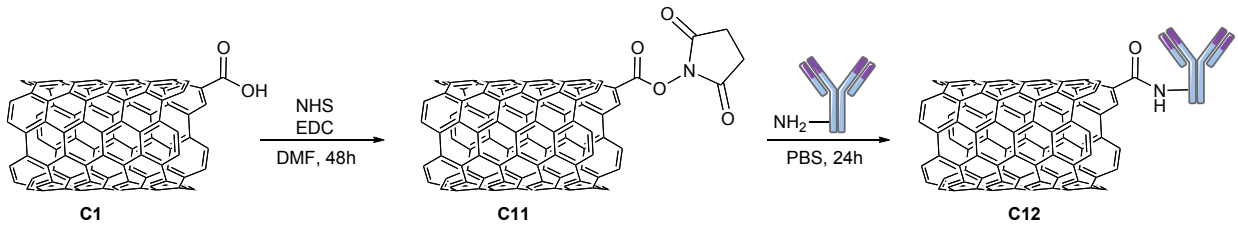

Schéma 1: Synthèse du conjugué Ab-MWCNTs **C12** *via* une réaction d'amidation.

Dans la deuxième approche, les fonctions amines sur les parois des nanotubes **C4** ont été modifiées avec une fonction maléimide (**C13**) qui réagit sélectivement avec un groupement thiol introduit préalablement dans la structure de l'anticorps par réaction avec le réactif de Traut (2-iminothiolane). Ce composé réagit d'une façon spontanée et sélective avec les amines de la chaîne latérale des lysines présentes dans la structure de l'anticorps.

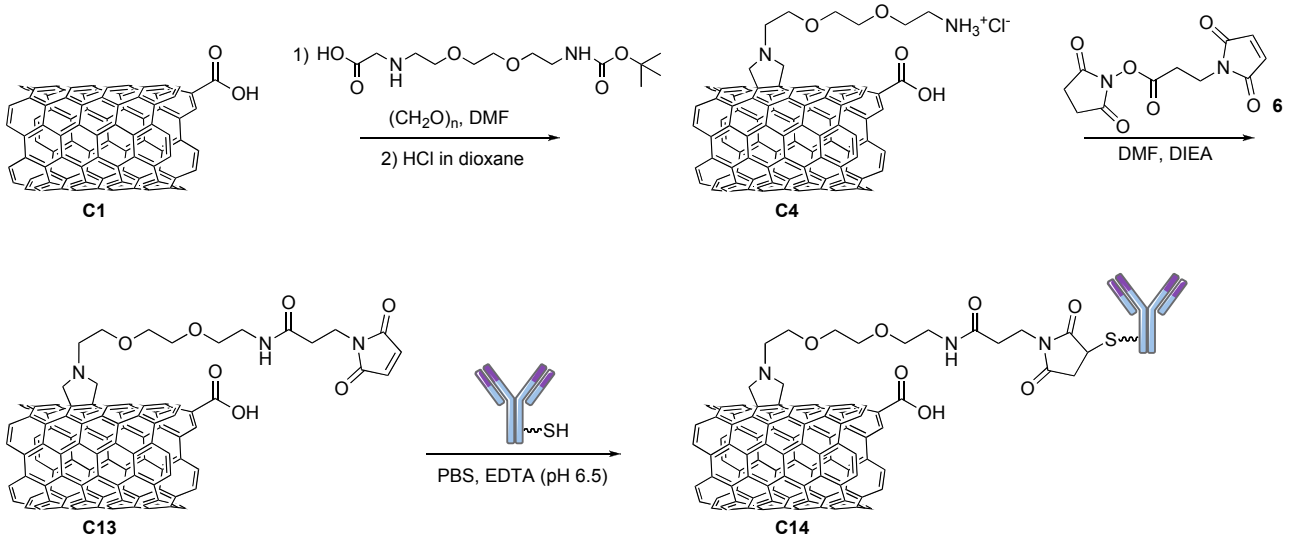

Schéma 2: Synthèse du conjugué Ab-MWCNTs **C14** *via* une réaction de cycloaddition 1,3 dipolaire suivie du couplage maléimide/thiol.

Les deux conjugués **C12** et **C14** ont été caractérisés par différentes techniques complémentaires afin d'étudier les propriétés de surface des nanotubes et d'évaluer l'activité biologique des conjugués synthétisés. En particulier, la surface des nanotubes a été observée par microscopie à transmission électronique après chaque étape de fonctionnalisation. Les images, comparées à celles des nanotubes natifs, montrent que la structure des nanotubes est toujours conservée et n'a pas été altérée par les différents traitements.

La présence de l'anticorps dans les conjugués a été déterminée en utilisant trois techniques :

l'analyse thermogravimétrique, le gel d'électrophorèse et la résonance plasmonique de surface.

L'analyse thermogravimétrique nous a permis de déterminer la quantité d'anticorps conjugué aux tubes car cette technique est basée sur la décomposition thermique sous atmosphère inerte des groupes fonctionnels ancrés à la surface des tubes qui, eux, sont stables dans ces conditions.

Le gel d'électrophorèse nous a offert la possibilité d'évaluer la nature de la liaison entre les tubes et l'anticorps (covalente ou non), mais aussi de déterminer si l'anticorps était toujours intact après greffage sur les nanotubes. Les résultats montrent que l'anticorps n'a pas été dégradé et que la liaison est de type covalent.

L'affinité de l'anticorps a été évaluée par résonance plasmonique de surface. Cette technique permet de quantifier l'efficacité de reconnaissance entre l'anticorps et son antigène. Les résultats sont très encourageants car l'anticorps couplé aux nanotubes a conservé la capacité de reconnaissance de son antigène.

En collaboration avec l'équipe du Prof. K. Kostarelos à Londres, nous avons conduit des études *in vitro* pour évaluer la capacité des conjugués préparés à être internalisés dans les cellules. Ces études ont montré que les conjugués ne se localisent pas à l'intérieur des cellules mais restent à la surface de la membrane cellulaire. Ceci est probablement lié au fait que le conjugué Ab-MWCNTs possède une taille trop grande pour traverser la membrane ou que le conjugué possède une trop faible dispersibilité dans le milieu de culture dans lequel les études ont été conduites.

Nous avons donc envisagé deux stratégies pour résoudre ces problèmes. La première approche a reposé sur l'utilisation d'un autre type de nanotubes produit par l'entreprise NanoAmor et qui présente une meilleure dispersibilité ainsi qu'une quantité de défauts structurels plus importante par rapport au premier type de nanotubes utilisé (produit par la société Nanocyl). La deuxième stratégie était basée sur le changement de la taille de la protéine couplée aux nanotubes. A la place de l'immunoglobuline, nous avons utilisé des fragments de l'anticorps biologiquement actifs, notamment le Fab (*fragment antigen binding*) et le fragment variable simple chaîne scFv (*single chain variable fragment*). Le Fab est le fragment de l'anticorps comprenant le site de liaison à l'antigène. Il a donc la même affinité pour l'antigène que l'anticorps, mais il a une taille de 48 kDa alors que l'anticorps a une taille de 150 kDa. Le scFv est un fragment plus petit (21 kDa) qui conserve les propriétés de l'anticorps puisqu'il est constitué uniquement des régions variables des chaînes constituant l'immunoglobuline.

III: Multi-fonctionnalisation de nanotubes de carbone

Sur la base des résultats obtenus avec les nanotubes mono-fonctionnalisés avec l'anticorps, nous avons développé une deuxième génération de conjugués Ab-CNT dans le but de combiner au sein du même conjugué les propriétés de ciblage de l'anticorps (ou de ces fragments) ainsi que les propriétés de traçabilité de sondes telles que la fluorescéine ou le radioisotope ^{111}In pour de l'imagerie *in vitro* et imagerie *in vivo*, respectivement.

Dans le cadre de ce projet, nous avons aussi eu la possibilité de développer un conjugué thérapeutique capable de cibler les cellules tumorales et en même temps d'exercer une activité thérapeutique.

Pour préparer ces conjugués nous avons utilisé une approche de double fonctionnalisation de CNTs. La paroi des nanotubes a été fonctionnalisée avec les immunoglobulines (ou des fragments) tandis que les pointes ont été derivatisées avec les sondes pour l'imagerie. Pour introduire les groupements réactifs nous avons de nouveau exploité la réaction de cycloaddition 1,3-dipolaire, suivie d'une réaction d'amidation pour fonctionnaliser les pointes des nanotubes oxydés (Schéma 3).

Cette approche nous a permis de double fonctionnaliser les nanotubes de façon covalente, en conférant une bonne stabilité chimique aux conjugués tout en limitant la présence de molécules simplement adsorbées qui pourraient être larguées de la surface des nanotubes une fois administrées *in vivo*. De plus, cette stratégie permet de contrôler tout le processus de fonctionnalisation puisque les deux fonctionnalités se trouvent à deux positions non-compétitives. En outre, grâce à la présence de deux groupements protecteurs orthogonaux tels que le *tert*-butoxycarbonyle (Boc) et le phtalimide (Pht) nous avons pu fonctionnaliser les amines présentes sur la paroi ou aux pointes de façon sélective (Schéma 3).

Les nanotubes fonctionnalisés ont été ensuite observés au microscope à transmission électronique et caractérisés par le test de Kaiser et par analyse thermogravimétrique pour déterminer le degré de fonctionnalisation après chaque étape.

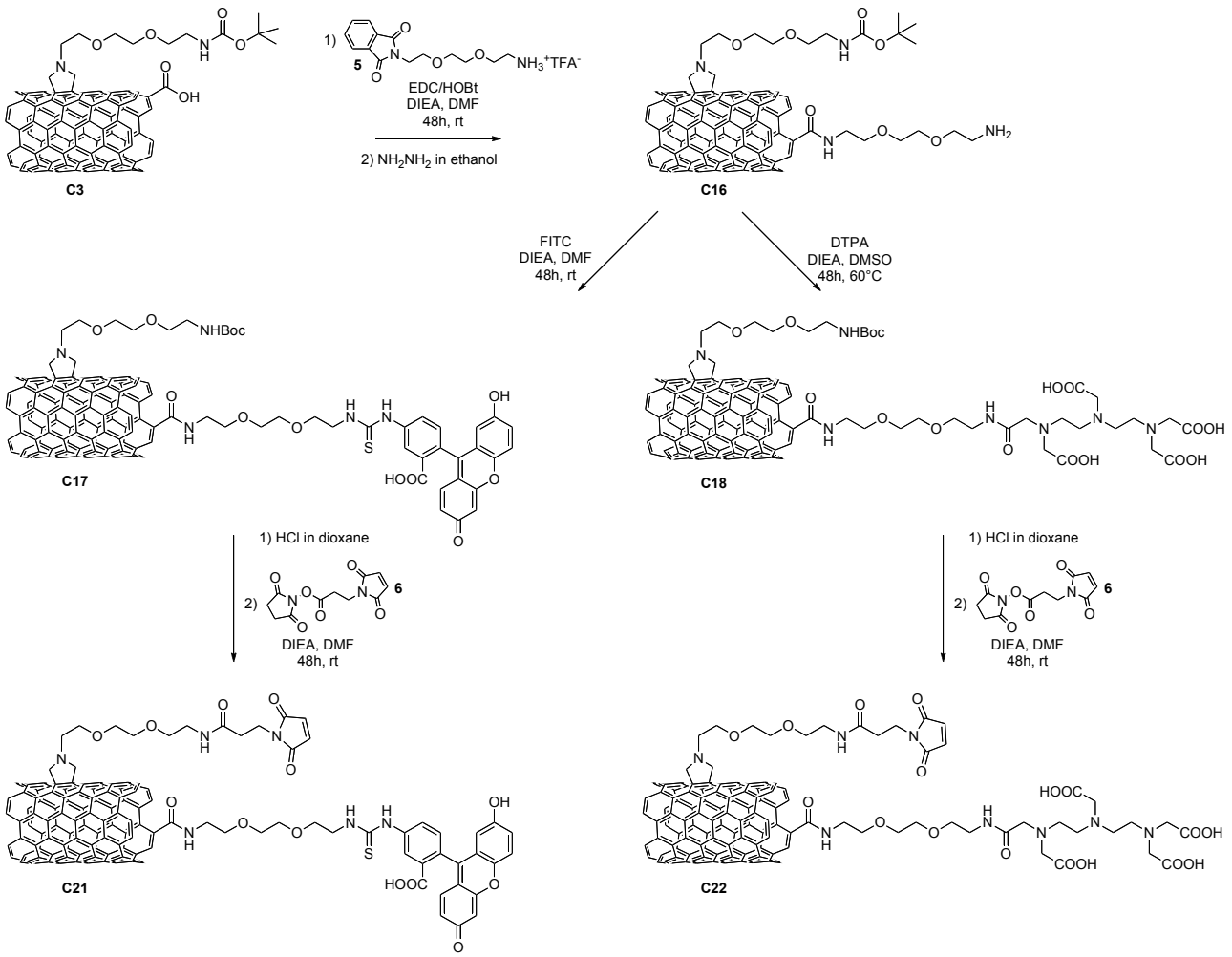

Schéma 3: Préparation des nanotubes doublement fonctionnalisés avec le groupe maléimide et une sonde pour l'imagerie (FITC ou DTPA).

Les nanotubes doublement fonctionnalisés FITC-MWCNTs-maléimide **C21** ou DTPA-MWCNTs-maléimide **C22** ont été couplés à l'anticorps ou à ses fragments. L'anticorps a été préalablement derivatisé avec le réactif de Traut pour introduire des groupements thiols comme décrit auparavant. Les fragments Fab et scFv possèdent par contre des fonctions thiols sur leur surface mais ces groupes SH ont tendance à s'oxyder facilement pour former des ponts disulfures. Toutefois un traitement préalable avec un agent réducteur tel que la 2-mercaptoethylamine, nous a permis d'obtenir des fonctions SH libres qui ont pu être utilisées pour former la liaison covalente entre les nanotubes et les fragments (Schéma 4).

Les conjugués préparés ont été caractérisés par microscopie à transmission électronique, analyse thermogravimétrique, gel d'électrophorèse et résonance plasmonique de surface. Les résultats ont montré que la liaison entre les nanotubes et les protéines (anticorps, Fab et scFv) est de type covalent et qu'une fois liés à la surface des nanotubes, l'anticorps ou ses fragments sont toujours biologiquement actifs.

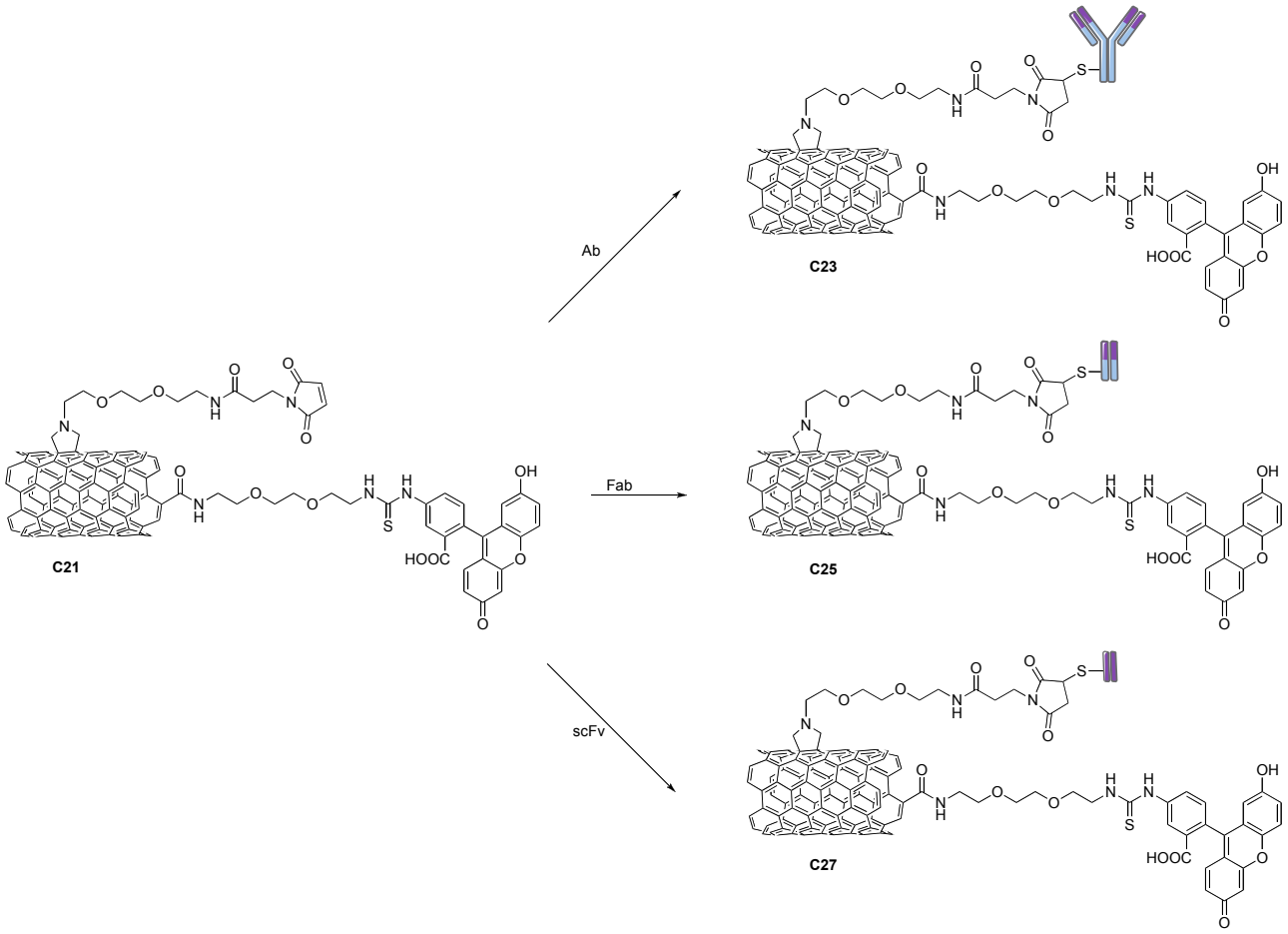

Schéma 4: Fonctionnalisation des nanotubes FITC-MWCNTs-maléimide (**C21**) avec l'anticorps (**C23**) ou ses fragments (**C25** et **C27**). Note: les mêmes réactions ont été répétées aussi avec les nanotubes DTPA-MWCNTs-maléimide (**C22**).

Les études de pénétration cellulaire ont montré que tous les conjugués sont internalisés dans les cellules, ce qui confirme que la faible internalisation des conjugués mono-fonctionnalisés Ab-CNT était certainement due à la faible dispersibilité du premier type de nanotubes utilisé. Les conjugués ont été efficacement internalisés par la lignée cellulaire de cancer du sein (MCF-7) dans laquelle l'antigène MUC1 est surexprimé. Toutefois, des expériences complémentaires sont en cours pour étudier et comprendre le rôle de l'anticorps dans le processus d'internalisation et de ciblage des cellules tumorales. De plus, la réduction de la taille de la protéine liée aux nanotubes a permis aux conjugués préparés à partir des nanotubes moins solubles (Nanocyl) d'être internalisés dans les cellules. La taille du conjugué MWCNT-protéine joue donc également un rôle très important dans le processus d'internalisation.

Ces résultats encourageants nous ont amenés à développer un conjugué thérapeutique. Nous avons utilisé le fragment VHH (*Variable domain of the Heavy chain of Heavy-chain antibodies*) d'une immunoglobuline différente de hCTM01 qui fait partie de la famille des anticorps composés uniquement de la chaîne lourde (*heavy-chain antibodies*) et présents dans le sérum de camélidés

[Hamers-Casterman, C., *et al*. 1993; Harmsen, M. M., *et al*. 2007]. Ce VHH présente à la fois une capacité de ciblage de la protéine β-caténine et une activité thérapeutique contre cette protéine. La surexpression ou des mutations de cette protéine sont impliquées dans plusieurs maladies telles que le cancer colorectal, le cancer du sein ou la leucémie [Gehrke, I., *et al*. 2009; El Wakil, A., *et al.* 2011].

La caractérisation physico-chimique du conjugué VHH-MWCNTs a permis de déterminer la quantité de VHH introduit et de confirmer qu'après liaison aux nanotubes la capacité de reconnaître l'antigène est bien conservée. Des études biologiques sont en cours pour évaluer la capacité du conjugué VHH-MWCNT à être internalisé dans les cellules, mais aussi pour tester ses propriétés thérapeutiques.

IV: Etudes pharmacocinétiques et toxicologiques

Afin d'utiliser les conjugués à base de nanotubes et d'anticorps (ou de ses fragments) à des fins biomédicales, nous avons évalué leurs profils pharmacocinétiques et toxicologiques.

En particulier, la distribution dans les tissus et les paramètres pharmacocinétiques des différents conjugués ont été déterminés grâce à la détection des rayons gamma émis par le radioisotope ^{111}In chélaté aux nanotubes fonctionnalisés avec le DTPA. Ce radionucléide a été choisi pour son temps de demi-vie (67,5 heures) particulièrement adéquat pour évaluer la biodistribution des nanotubes pendant de courtes périodes. En collaboration avec le groupe du Prof. Kostas Kostarelos à Londres, nous avons chélaté le radionucléide ^{111}In avec le DTPA lié aux nanotubes. Ensuite, nous avons injecté aux souris les différents conjugués radiomarqués, acquis des images de l'animal entier par technique SPECT/CT (tomographie computée à émission de photon unique) et évalué la distribution dans les organes.

Les résultats ont montré que les nanotubes fonctionnalisés ont tendance à être répartis surtout dans les organes du système réticulo-endothélial (*i.e*. le foie et la rate) et les poumons. Des différences dans les profils de biodistribution liées au diamètre des nanotubes ont été observées telles qu'une accumulation majeure dans les poumons et dans les reins pour les nanotubes ayant un diamètre plus petit et moins de défauts (Nanocyl). Par contre, la taille de la protéine liée n'induit pas de modifications importantes de la distribution des conjugués dans les organes.

Au sein de notre équipe, nous avons aussi évalué la cytotoxicité potentielle des différents conjugués sur deux lignées cellulaires du système immunitaire (*i.e.* macrophages et splénocytes). Nous avons comparé le comportement des conjugués avec celui des immunoglobulines seules (Ab, Fab et scFv) et des nanotubes fonctionnalisés sans les immunoglobulines. La viabilité cellulaire a

été évaluée après une incubation de 24 heures par cytométrie en flux ou par détection de l'enzyme lactate déshydrogénase (LDH). Nous avons constaté un faible effet cytotoxique des conjugués utilisés comme précurseurs (sans immunoglobuline) à une concentration de 100 µg/mL. Au contraire, les conjugués MWCNT-protéine ou les protéines seules n'induisent aucun effet toxique. Ces résultats nous ont permis de confirmer que la fonctionnalisation chimique des nanotubes augmente leur biocompatibilité et donc leurs possibles applications dans le domaine de la nanomédicine.

Par ailleurs les nanotubes fonctionnalisés avec le DTPA ont également été marqués avec le radioisotope ^{153}Gd (temps de demi-vie de 240 jours) et des études ultérieures sur leurs effets à long terme sont en cours.

V: Conclusions

Lors de ce travail de thèse, je me suis intéressée à la fonctionnalisation des nanotubes de carbone avec des anticorps, ainsi qu'à leurs applications potentielles dans le domaine biomédical, pour développer une stratégie de thérapie contre le cancer.

La fonctionnalisation chimique nous a permis d'accroître le degré de dispersion des nanotubes dans les milieux physiologiques ainsi que leur biocompatibilité comme l'ont montré les études toxicologiques effectuées sur les cellules du système immunitaire.

Nous avons démontré la possibilité de fonctionnaliser soit la paroi, soit les pointes des nanotubes avec un anticorps de ciblage des cellules tumorales (anticorps anti-MUC1) qui, une fois lié aux nanotubes, conserve son activité de reconnaissance de l'antigène.

Ces études préliminaires de mono-fonctionnalisation des nanotubes de carbone avec l'immunoglobuline anti-MUC1 nous ont amenés ensuite à la préparation de nanotubes doublement fonctionnalisés. Nous avons combiné une réaction de cycloaddition 1,3-dipolaire et une réaction d'amidation, ce qui nous a permis d'introduire des amines sur la paroi et aux extrémités des nanotubes. En particulier, nous avons fonctionnalisé les amines aux pointes avec des sondes pour l'imagerie pour permettre de localiser les nanotubes dans les cellules par microscopie confocale à balayage laser ou dans les animaux (souris) par tomographie computée à émission de photon unique. La paroi a été derivatisée avec l'anticorps ou ses fragments (Fab et scFv) pour le ciblage des cellules tumorales.

Les études biologiques *in vitro* et *in vivo* nous ont permis d'évaluer le rôle joué par les différents paramètres tels que la taille de la protéine, la morphologie et le diamètre des nanotubes

dans les processus d'internalisation dans les cellules et de distribution dans les organes. Des études complémentaires sont actuellement en cours pour déterminer le rôle de la protéine dans le processus d'internalisation.

Ces résultats nous ont amenés au développement d'un conjugué thérapeutique par couplage des nanotubes avec un fragment d'un anticorps à chaîne lourde (VHH) qui présente des propriétés de ciblage ainsi que des propriétés thérapeutiques. La stratégie de synthèse de ce conjugué a également reposé sur la double fonctionnalisation des nanotubes afin de réaliser les études biologiques telles que l'internalisation dans les cellules, l'évaluation de l'activité thérapeutique ainsi que la biodistribution (actuellement en cours).

Les résultats obtenus au cours de ce travail de thèse sont encourageants quant à l'utilisation des nanotubes pour la délivrance de molécules biologiquement actives afin de développer une thérapie ciblée contre le cancer. Ces études représentent une nouvelle avancée dans le domaine de la nanomédicine car nous avons démontré que les nanotubes peuvent transporter efficacement des anticorps dans les cellules sans causer d'effets toxiques (à court-terme) tout en gardant l'activité biologique de la protéine liée. Si les résultats biologiques confirment la conservation, voire l'augmentation de l'activité thérapeutique du VHH couplé aux nanotubes, nous envisagerons des études plus approfondies pour ce traitement innovant du cancer. En conclusion, étant donné que le système hybride nanotubes-anticorps peut représenter une nouvelle stratégie dans le cadre de la thérapie oncologique, nous espérons que les travaux présentés dans cette thèse puissent stimuler de nouvelles études dans ce domaine.

Chapter I: Introduction

Elemental carbon exists in different natural allotropes, such as amorphous carbon, diamond and graphite (Figure I.1). Diamond and graphite consist of extended networks of sp^3- and sp^2-hybridized carbon atoms, respectively. Both forms show unique physical properties such as hardness, thermal conductivity, lubrication behavior or electrical conductivity. Diamond and graphite have represented the only known allotropes of carbon for a long time. In 1985, Kroto and co-workers observed for the first time fullerenes [Kroto, H. W., *et al*. 1985]. Since then a large family of synthetic carbon allotropes has been discovered. This family includes carbon nanotubes (CNTs) described at atomic level in 1991 [Iijima, S., 1991] and graphene, a single layer of graphite, discovered in 2004 [Novoselov, K. S., *et al.* 2004].

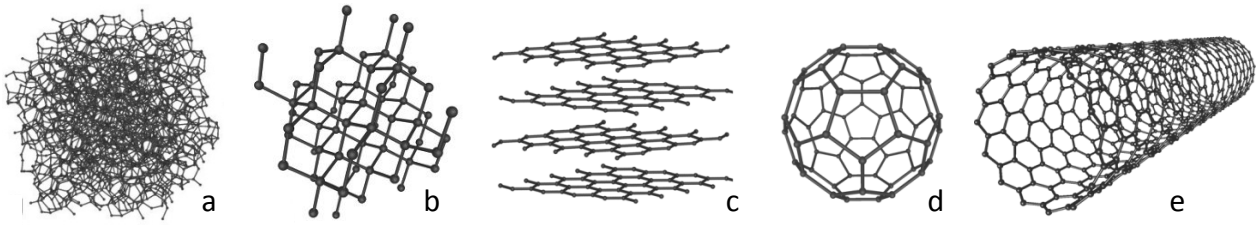

Figure I.1: Molecular structure of five carbon allotropes: a) amorphous carbon; b) diamond; c) graphite; d) fullerene; e) single-walled carbon nanotube.

Carbon nanotubes are constituted of cylinders of graphene sheets opened or closed at the extremities. CNTs can be either composed by a single plane of graphene (single-walled carbon nanotubes, SWCNTs) or by multiple concentric layers (multi-walled carbon nanotubes, MWCNTs). They have diameters in the nanometer range, while their lengths can reach several micrometers. This material offers very interesting mechanical, optical, electronic and magnetic properties [Jorio, A., *et al*. 2008], which have attracted interest in many research fields. CNTs find applications in materials science [Byrne, M. T., *et al*. 2010], nanoelectronics or in photovoltaic devices [Bottari, G., *et al*. 2010]. The properties of carbon nanotubes stimulated also their applications in the biomedical field as substrates for tissue regeneration [Saito, N., *et al*. 2009] or as new drug delivery systems [Ménard-Moyon, C., *et al*. 2010a].

I.1 Structure, Synthesis and Properties of Carbon Nanotubes

I.1.1 Structure of Carbon Nanotubes

CNTs are considered as sheets of graphene coiled into seamless hollow cylinders. The exact structure of a nanotube depends on the different angles and curvatures in which a graphene sheet can be rolled into a tube (Figure I.2). The circumference of a CNT can be described by a vector, called chiral vector $\vec{C}_h$. The value of this vector is determined by a pair of integers (m, n). The chiral angle (θ) defines the wrapping angle of graphene sheet [Iijima, S., *et al*. 1993].

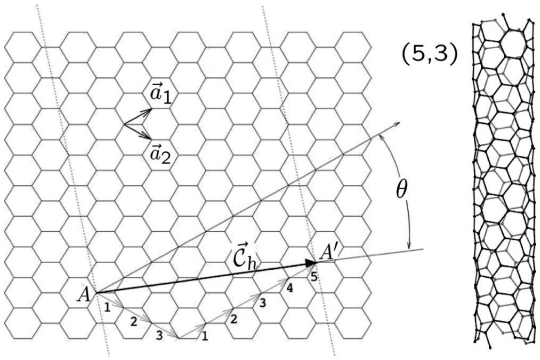

Figure I.2: Graphene honeycomb network with lattice vector a_1 and a_2. The chiral vector $\vec{C}_h = ma_1 + na_2$ represents the possible wrapping of the two-dimensional graphene sheet into a tubular form. The direction perpendicular to $\vec{C}_h$ is the tube axis. In the present example, a (5,3) nanotube is under construction and the resulting tube is illustrated on the right. Reproduced from Charlier, J. C., *et al*. 2007.

Depending on the values of the indices (m, n) and of the chiral angle, we can discriminate CNTs into three forms (Figure I.3):

- armchair: n=m≠0, θ=30° (the tube axis is perpendicular to C-C bonds)
- zigzag: n≠0, m=0, θ=0° (the tube axis is parallel to the C-C bonds)
- chiral: n≠m≠0, 0°<θ<30°

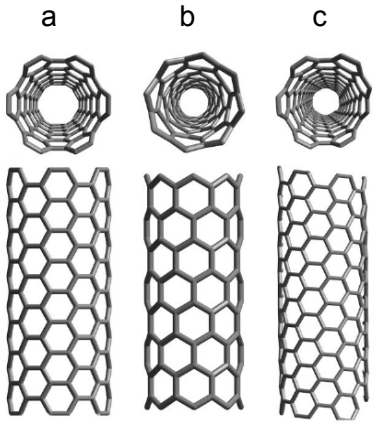

Figure I.3: Molecular models of SWCNTs exhibiting different chiralities: a) armchair arrangement; b) zig-zag configuration; c) chiral conformation. Reproduced from Terrones, M., 2003.

Depending on the number of the graphene layers from which a single nanotube is composed, CNTs are classified as single-walled carbon nanotubes or multi-walled carbon nanotubes. SWCNTs have diameters of ~1 nm and lengths of a few micrometers. MWCNTs have much larger diameters until ~100 nm, due to the presence of multiple layers of graphene [Haddon, R. C., 2002].

I.1.2 Synthesis of Carbon Nanotubes

Since the discovery of nanotubes, several techniques have been explored for their production. The most widely used methods to produce nanotubes are:

- electric arc discharge
- laser ablation
- chemical vapor deposition (CVD)

The first two methods belong to the family of high temperature route, in which carbon is vaporized from graphite and rearrange into a tubular shape forming CNTs. The process needs high temperatures as graphite sublimates at 3200°C. Chemical vapor deposition route is a medium temperature route as it needs lower temperatures (700-1000°C). In this case the carbon source is a carbon-containing molecule in a gas state.

I.1.2.1 Electric Arc Discharge

Electric arc discharge is one of the first methods used to produce CNTs [Iijima, S. 1991]. The arc discharge method employs two graphite electrodes (6-12 mm in diameter) that are separated by a short distance (1-4 mm) inside a chamber filled with an inert gas. A current of about 50-100 A is passed through the electrodes and carbon atoms are ejected from the positive electrode and deposited on the negative electrode (Figure I.4).

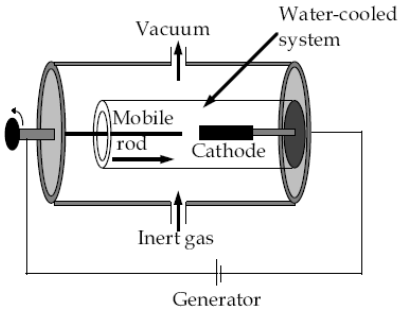

Figure I.4: Schematic representation of the electric arc discharge apparatus. Reproduced from Journet, C., *et al.* 1998.

Carbon is vaporized from the graphite anode in form of crystallites, which generates small carbon clusters that rearrange into carbon nanotubes. The limiting factor for high yield MWCNTs is the presence of graphite crystallites that do not rearrange into the tubular form [Dervishi, E., *et al*. 2009]. Metallic nanoparticles such as Fe, Co or Ni are used to catalyze the SWCNT growth in the arc discharge method [Journet, C., *et al*. 1997]. MWCNTs produced by the arc discharge method have fewer structural defects (due to high growth temperature) and better electrical, thermal and mechanical properties than the nanotubes produced by medium temperature techniques (CVD).

I.1.2.2 Laser Ablation

In 1995, the group led by Smalley introduced a very promising approach to produce CNTs, called the laser ablation method [Guo, T., *et al*. 1995]. A powerful laser is used to ablate a carbon source in a hot helium (He) or argon (Ar) atmosphere. As the graphite source inside a furnace is heated up at about 1200°C, a pulsed laser beam incident on the target starts evaporating carbon from the graphite. The carrier gas sweeps the carbon atoms from the high-temperature zone to a cold copper collector on which they condense into nanotubes (Figure I.5).

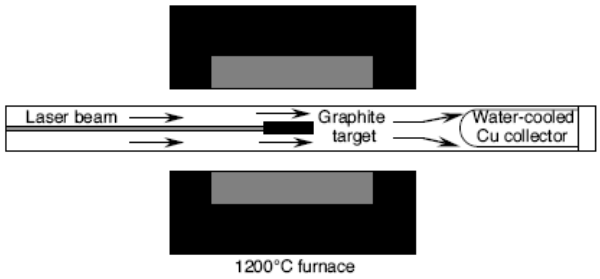

Figure I.5: Schematic representation of the oven laser ablation apparatus. Reproduced from Journet, C., *et al.* 1998.

In order to generate SWCNTs using the laser ablation technique, it is necessary to impregnate the graphite source with transition metal catalysts [Terrones, M., 2003]. The morphology and the properties of CNTs are highly influenced by many different parameters such as light intensity, furnace temperature, type of hydrocarbon and carrier gas, as well as the flow rate of different gases [Meyyappan, M., 2005]. Unfortunately, the laser ablation technique is very expensive because it involves high-purity graphite rods and high-power lasers [Terrones, M., 2003].

I.1.2.3 Chemical Vapor Deposition

The chemical vapor deposition route has become the most common way to produce nanotubes at a relatively low cost, as this approach offers the possibility to scale-up the synthesis for large scale production of CNTs. It is the most common method used at industrial level. In this case the hydrocarbon source is heated at temperatures between 700° and 1000°C inside a quartz tube in the presence of catalytic systems (Figure I.6).

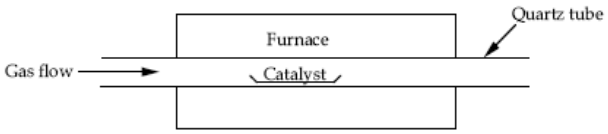

Figure I.6: Schematic representation of the experimental setup used for the catalytic decomposition of hydrocarbons. Reproduced from Journet, C., *et al.* 1998.

CNTs are produced from the thermal decomposition of the carbon-containing gas molecules on the catalytic systems. The catalyst provides nucleation sites for the nanotube growth (Figure I.7) [Dresselhaus, M. S., *et al*. 2001]. At high temperatures, once the hydrocarbon decomposes into hydrogen and carbon, carbon atoms dissolve and diffuse into the metal surface and rearrange themselves into a network containing hexagons of carbon atoms and finally precipitate in the form of CNTs. Once the metal surface is covered by amorphous carbon and its surface is "poisoned," the carbon atoms cannot come in contact with the metal catalyst, which results in the termination of the CNT growth [Dervishi, E., *et al*. 2009].

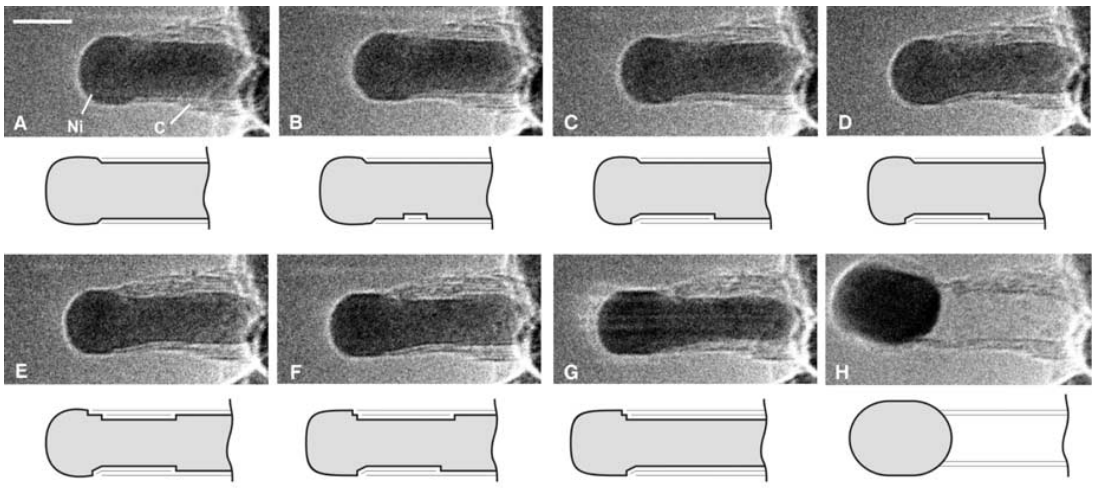

Figure I.7: Image sequence of a growing carbon nanotube. Images A–H illustrate the elongation/contraction process. Drawings are included to guide the eye in locating the positions of mono-atomic Ni step edges at the C–Ni interface. The images are acquired *in situ* with CH_4:H_2 = 1:1 at a total pressure of 2.1 mbar with the sample heated to 536°C. All images are obtained with a rate of 2 frames s^{-1}. Scale bar, 5 nm. Reproduction from Helveg, S., *et al*. 2004.

The hydrocarbon source exploited in the CVD method can be in gas state such as acetylene, methane, and ethylene, in liquid state such as benzene, alcohol, and hexane, or in solid state such as camphor, naphthalene, and many more [Kumar, M., *et al*. 2010]. The catalytic system is composed of metal catalysts such as Fe, Co, Ni, or Mo and a support such as MgO, $CaCO_3$, Al_2O_3, or Si to increase the specific surface area of the catalyst [Terrones, M., 2003]. It has been shown theoretically and experimentally that the diameter of the CNTs is closely related to the diameter of the metal nanoparticles. Small metal catalysts yield CNTs with a small diameter and larger diameter CNTs are grown on top of large metal nanoparticles [Dervishi, E., *et al*. 2007]. An advantage of the CVD method is that it enables the deposition of CNTs on pre-designed lithographic structures, producing ordered arrays of CNTs. The CVD method is also used to grow vertically aligned CNTs, which can be used in applications such as flat panel displays [Dervishi, E., *et al*. 2009].

I.I.3 Properties of Carbon Nanotubes

The properties of CNTs depend on their structure, such as the diameter, chirality and degree of graphitization. CNTs show high aspect ratio, high tensile strength, large surface area, low mass density, high heat conductivity and versatile electronic properties [Dresselhaus, M. S., *et al.* 2001].

The electronic properties of CNTs change in correspondence to their diameter and chirality. Especially for SWCNTs the electronic behavior varies from metallic (one-third of the SWCNTs) to semiconducting (two-thirds of the SWCNTs). CNTs possess higher electrical conductivity than copper due to their low resistance [Dai, H., *et al*. 1996]. As electrons are conducted without being scattered, carbon nanotubes conduct electrons without dissipating energy as heat (ballistic transport). The electrical properties of CNTs can be modulated by introducing dopant atoms in the carbon lattice. For example, boron or nitrogen can increase the electrical conductivity of MWCNTs and SWCNTs of an order of magnitude [Terrones, M., 2003].

The mechanical properties of CNTs are also very remarkable. CNTs present extraordinary Young's modulus (1 TPa) and tensile strength (50 GPa) [Dresselhaus, M. S., *et al*. 2001]. The Young's modulus measures the stiffness of a material and the tensile strength is a measure of the amount of stress needed to pull a material apart. CNTs are about hundred times stronger and six times lighter than steel. Their elastic response to deformation is also very astonishing as CNTs can be twisted or bent severely without breaking.

I.2 Chemical Functionalization

The unique properties of CNTs offer a wide range of opportunities and applications in many fields [Schnorr, J. M., *et al.* 2011], which spans from materials science (field emitters, photovoltaic devices or in composite reinforcement) [Byrne, M. T., *et al*. 2010] to biomedical applications (substrates for tissue regeneration [Saito, N., *et al*. 2009] or drug delivery systems [Lu, F., *et al*. 2009; Ménard-Moyon, C., *et al*. 2010a]). However, raw carbon nanotubes contain impurities as by-product carbonaceous species and residues from the catalysts used to produce CNTs. Moreover, they are highly hydrophobic and insoluble in all solvents due to the strong van der Waals interactions that hold them together to form bundles. To overcome these drawbacks, CNTs can undergo chemical functionalization [Tasis, D., *et al.* 2006; Singh, P., *et al*. 2009; Karousis, N., *et al.* 2010] to enhance their solubility and to purify the pristine material.

The main approaches to functionalize CNTs can be distinguished in two groups:

- covalent bonding of chemical moieties through reactions on the conjugated skeleton of CNTs (examples are approaches A and B in Figure I.8)
- non-covalent interactions of various molecules with the nanotube surface (for example functionalization C and D in Figure I.8).

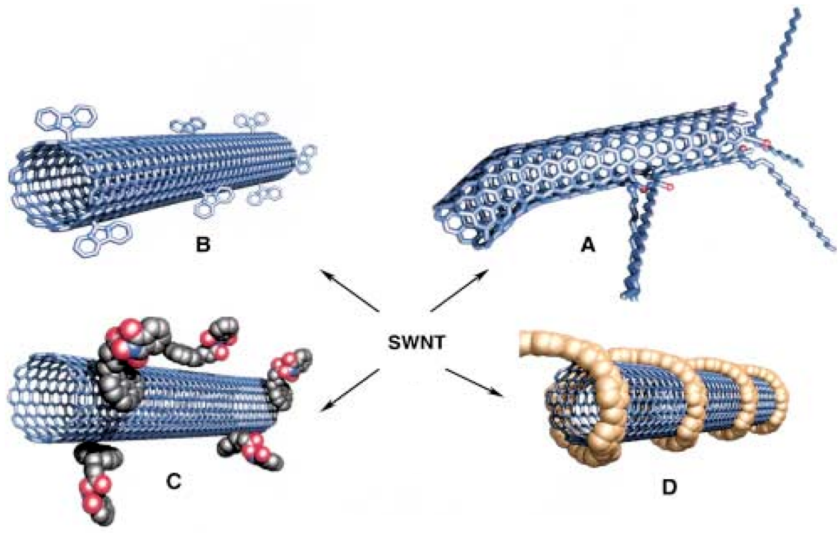

Figure I.8: Different possibilities for functionalization of SWCNTs. A) defect-group functionalization; B) covalent sidewall functionalization; C) non-covalent functionalization with molecules through π-stacking; D) non-covalent functionalization with polymers. Reproduction from Hirsch, A. 2002.

The covalent functionalization of CNTs allows to attach functional groups either to the tube ends or onto their sidewall. The covalent approach is widely exploited as it offers the possibility to obtain chemically stable conjugates. The most common example of this type of functionalization is the oxidation reaction of CNTs with acids, such as nitric acid and sulfuric acid. This reaction

generates nanotubes containing carboxylic functions that are easier to disperse in water. However, the covalent functionalization generates the rehybridation of sp^2 carbon atoms to sp^3, which perturbs the electronic network and the structure of nanotubes causing the loss of their electrical and mechanical properties.

The non-covalent functionalization approach offers the main advantage that it does not affect the lattice of the nanotubes. Adsorption or wrapping of polynuclear aromatic compounds, surfactants, polymers or biomolecules reduces the surface hydrophobicity *via* π-π interactions or van der Waals forces. For example, surfactants can adsorb onto the nanotube surface by interaction of the hydrophobic part of the molecules with the nanotube surface, while the hydrophilic part interacts with the solvent allowing disruption of CNT bundles.

I.2.1 Covalent Functionalization

Various covalent organic reactions have been applied to functionalize the nanotube surface. They can be divided into two main classes:

- coupling reactions exploiting oxidized defect sites (amidation and esterification of carboxylic groups)
- addition reactions onto the conjugated skeleton of CNTs

I.2.1.1 Amidation and Esterification

Amidation and esterification reactions represent a highly exploited approach to functionalize oxidized carbon nanotubes, obtained by sonication of the raw material in a mixture of nitric and sulfuric acids or by heating the pristine material in hydrogen peroxide and nitric acid [Liu, J., *et al.* 1998; Samorì, C., *et al.* 2010a]. These treatments afford purified, short and open carbon nanotubes, bearing oxygenated functions (mainly carboxylic groups). These reactive groups can be further derivatized with alcohols or amines to give esters or amides, respectively. Prato and co-workers employed scanning tunneling microscopy (STM) (Figure I.9) to prove that the covalent functionalization of oxidized SWCNTs with alkyl amines takes place mainly at the tips of the tubes, where are located the majority of carboxylic acid groups [Bonifazi, D., *et al*. 2006].

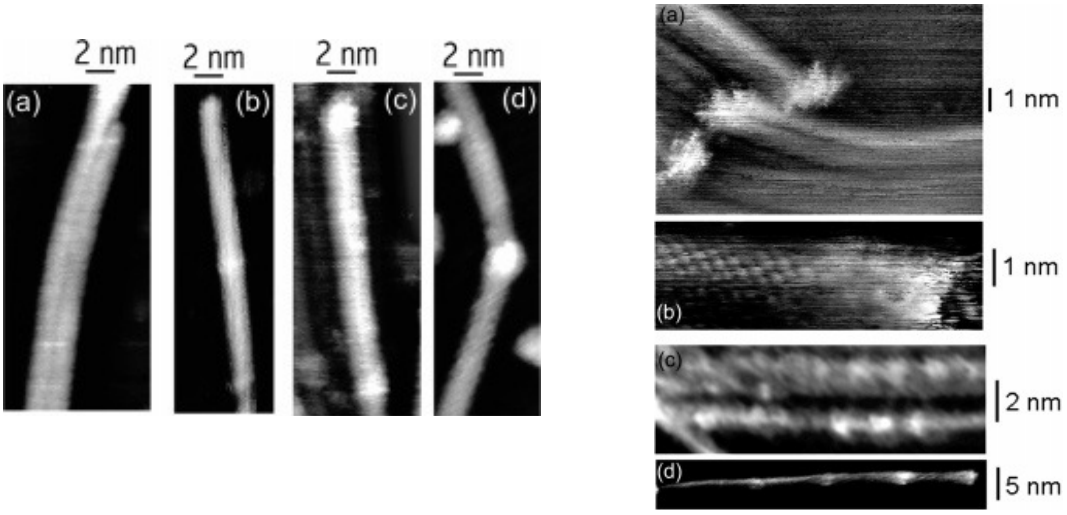

Figure I.9: STM images of oxidized SWCNTs showing both regular tubes (a) and tubes bearing some irregularities at the ends or/and on the sidewall (b)-(d). STM images of the nanotube terminations (a and b) and of the lumps on the sidewall (c and d) of functionalized nanotubes after amidation reaction with 1-octylamine. Reproduction from Bonifazi, D., *et al.* 2006.

The coupling of the carboxyl groups with amines or alcohols can be carried out *via* standard methods, using acyl chloride or carbodiimide-activate intermediates (Scheme I.1).

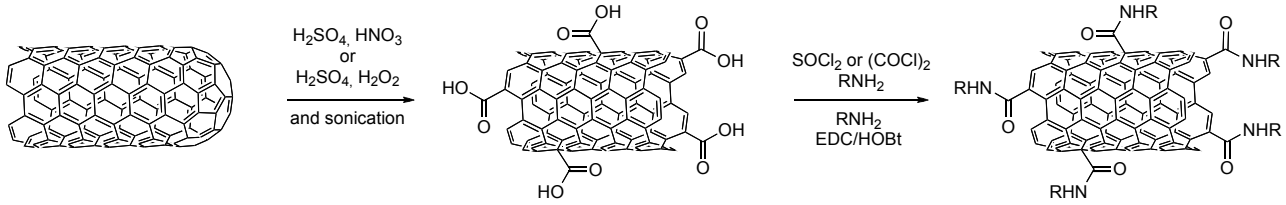

Scheme I.1: Covalent functionalization of CNTs following amidation reaction of carboxylic acid groups.

In 1999 the group of Haddon reported the amidation reaction between shortened SWCNTs and octadecylamine *via* the use of thionyl chloride. The amine acts as solubilizing agent and renders the nanotubes soluble in various organic solvents [Hamon, M. A., *et al.* 1999]. Carbon nanotubes have been functionalized with biomolecules such as peptides and proteins by amidation using *N*-hydroxy succinimide (NHS) or 1-hydroxy-benzotriazole (HOBt) in the presence of carbodiimide [usually *N-N'*-dicyclohexylcarbodiimide (DCC) or 1-ethyl-3-(3-dimethylaminopropyl) carbodiimide (EDC)] [Jiang, K., *et al*. 2004].

Esterification of carboxylic groups was also proposed as alternative functionalization to enhance the solubility of the carbon nanotubes in organic solvents. For example, porphyrin units were attached to CNTs *via* esterification reaction to obtain a donor-acceptor complex [Li, H., *et al*. 2004; Baskaran, D., *et al*. 2005].

I.2.1.2 Addition Reactions

The functionalization of the sidewall of CNTs is more difficult to achieve and requires highly reactive species, like carbenes, nitrenes or radicals. The chemical reactivity of the CNT sidewall is profoundly altered by the presence of defects such as vacancies or pentagon-heptagon pairs (Stone-Wales defects) and results in a locally enhanced chemical reactivity of the graphitic structure. Another parameter that increases the reactivity of the CNT surface is the curvature degree: as the curvature increases the addition reactions are more favorable.

I.2.1.2.a Electrophilic Additions

CNTs can be functionalized by electrophilic additions, such as Friedel-Craft acylation. Tessonnier *et al*. have demonstrated that tertiary amines can be introduced on MWCNTs by a deprotonation–carbometalation reaction in the presence of butyl lithium followed by an electrophilic substitution with bromo derivatives. This procedure is simpler and faster than the classical oxidation–amidation route and leads to CNTs with a high number of easily accessible basic groups, used as catalysts in the synthesis of biodiesel [Tessonnier, J.-P. *et al*. 2009]. Friedel-Craft acylation (Scheme I.2) has been reported by Balaban *et al*. under different reaction conditions to afford polyacylated materials with improved solubility properties in organic solvents [Balaban, T. S., *et al*. 2006].

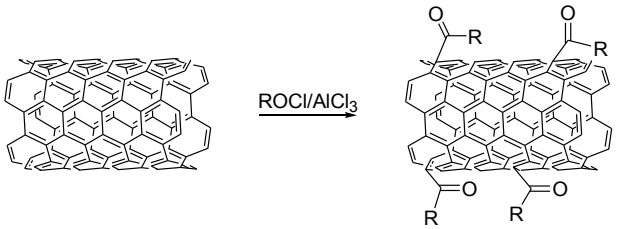

Scheme I.2: Functionalization of CNTs by Friedel-Craft acylation.

I.2.1.2.b Nucleophilic Additions

Nucleophilic addition of nitrenes on the nanotube surface was first described by the group of Hirsch, using alkyl azidoformates as precursor [Holzinger, M., *et al*. 2001]. After thermal-induced N_2 extrusion, nitrene addition resulted in the formation of alkoxycarbonylaziridino-SWCNT adducts (Scheme I.3). By varying the side chain of the nitrene precursor the solubility of the adducts can be modulated in different solvents.

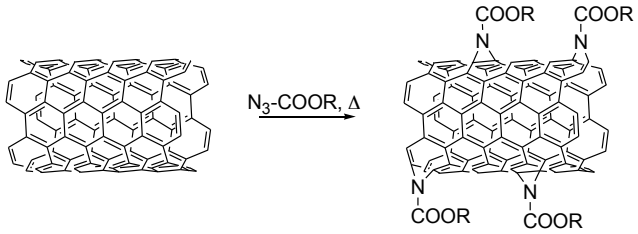

Scheme I.3: Nitrene addition on carbon nanotubes.

Another approach for the functionalization of CNTs with nitrenes relies on azide photochemistry [Moghaddam, M. J., *et al*. 2004]. The photoactive molecule azidothymidine (AZT) led to the formation of nitrenes by photolysis, which added to the carbon nanotube lattice to form aziridine adducts. DNA oligonucleotides were then synthesized *in situ* from the introduced aziridothymidine groups to produce water-soluble DNA-CNT constructs. The presence of DNA on the nanotubes was confirmed by TEM after hybridization with a complementary DNA strand, bound to gold nanoparticles. The attachment of DNA to CNTs is particularly interesting for integration of CNTs into electronic devices such as chips or sensors.

I.2.1.2.c Cycloaddition Reactions

Cycloaddition reactions, including 1,3-dipolar and Diels-Alder cycloadditions, have been widely exploited for the covalent functionalization of CNTs. The 1,3-dipolar cycloaddition of azomethine ylides generated *in situ* by thermal condensation of aldehydes and α-amino acids generates pyrrolidine rings fused to the C-C bonds of CNTs (Scheme I.4). First reported in 2002 to render CNTs soluble in water [Georgakilas, V., *et al*. 2002], this reaction still attracts the interest of a great number of scientists. The main advantages of this reaction are the high efficiency on different substrates (oxidized SWCNTs, pristine SWCNTs and MWCNTs) and the possibility to obtain wide range of diverse functionalized conjugates by varying the functional groups on the aldehyde or the side chain of the α-amino acid [Rubio, N., *et al*. 2010]. Examples of functionalization of CNTs through the 1,3-dipolar cycloaddition route include the covalent linkage of electron donor molecules (*i.e.* ferrocene) [Guldi, D. M., *et al.* 2003] or biomolecules (peptide, proteins or drugs) [Bianco, A., *et al.* 2005a; Prato, M., *et al*. 2008] to afford hybrid material that find applications in photovoltaics or nanomedicine, respectively. Recently, Brunetti *et al*. reported an alternative approach using microwaves to functionalize SWCNTs by employing aziridines as alternative starting materials to generate the azomethine ylide (Scheme I.4) [Brunetti, F. G., *et al*. 2007].

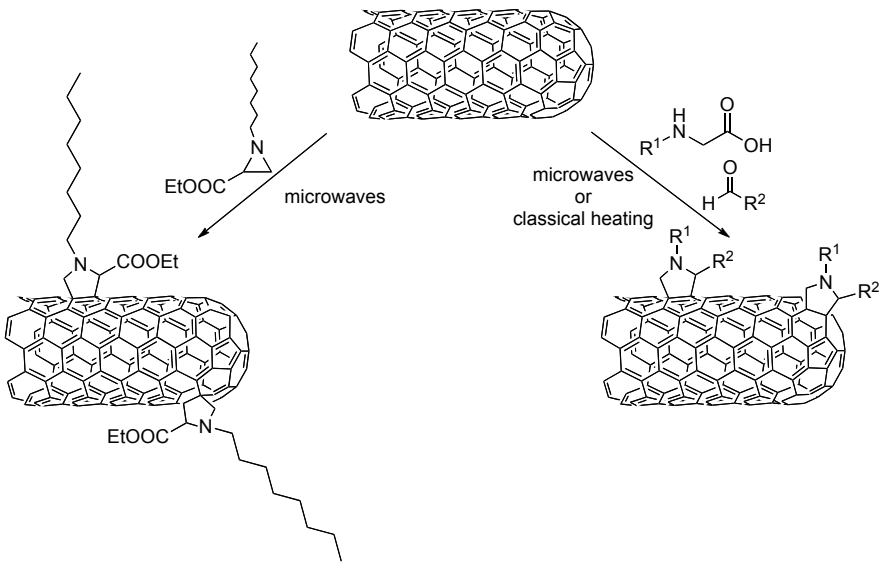

Scheme I.4: 1,3-dipolar cycloaddition of carbon nanotubes.

The Diels-Alder reaction is also known to take place on the sidewall of CNTs. Langa and co-workers reported Diels-Alder cycloaddition onto short nanotubes in the presence of *o*-quinodimethane generated *in situ* from the corresponding 4,5-benzo-1,2-oxathiin-2-oxide derivative under microwave irradiation (Scheme I.5) [Delgado, J. L., *et al*. 2004].

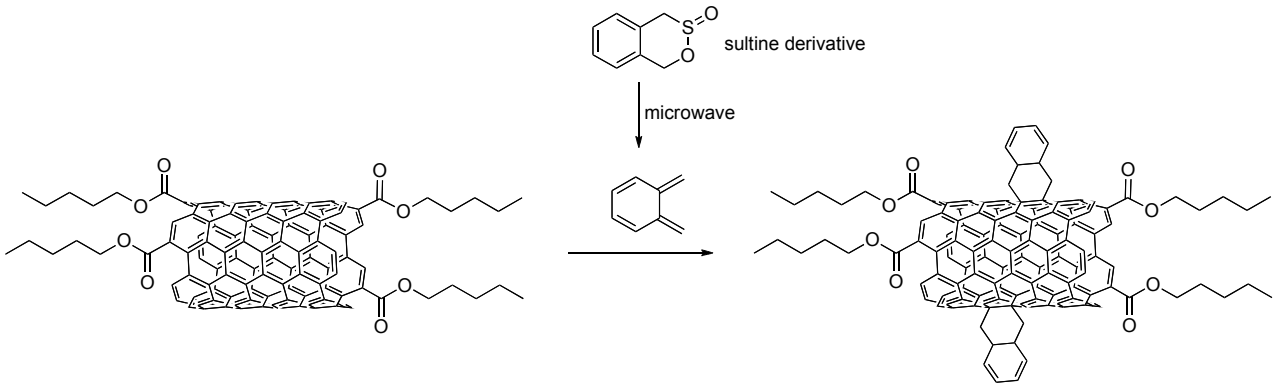

Scheme I.5: Diels-Alder cycloaddition reaction to SWCNTs.

I.2.1.2.d Radical Additions

Functionalization of CNTs with radicals is one of the most investigated strategy to modify their surface and enhance their solubility. First proposed by Tour and co-workers, the use of aryl diazonium salts is one of the most versatile addition reactions, widely explored to obtain different conjugates. As shown in Scheme I.6 different conditions have been developed. The aryl radical can be generated *via* electrochemical reduction of a preformed diazonium salt prepared using as precursor an aniline derivative and $NOBF_4$ [Bahr, J. L., *et al*. 2001a]. The diazonium salt can also

be generated *in situ* from the corresponding aniline using alkyl nitrite in a mixture of 1,2-dichlorobenzene and acetonitrile (Bahr, J. L., *et al*. 2001b) or in solvent-free conditions [Dyke, C. A., *et al*. 2003]. Triazene compounds were also investigated as stable precursors to diazonium salts for functionalizing nanotubes in aqueous media [Hudson, J. L., *et al.* 2006]. An environmentally friendly approach was also proposed. SWCNTs were ground with a pestle in a mortar for few minutes with aryldiazonium salts in the presence of K_2CO_3 and ionic liquids [Price, B. K., *et al*. 2005]. CNTs functionalized by diazonium chemistry have been used as starting materials for further modifications. In this context, water soluble 4-carboxyphenyl modified SWCNTs were functionalized with a nitrilotriacetic ligand that can complex nickel for directing the reversible self-assembly of polyhistidine tagged proteins onto the nanotube surface at controlled orientation [Graff, R. A., *et al*. 2008].

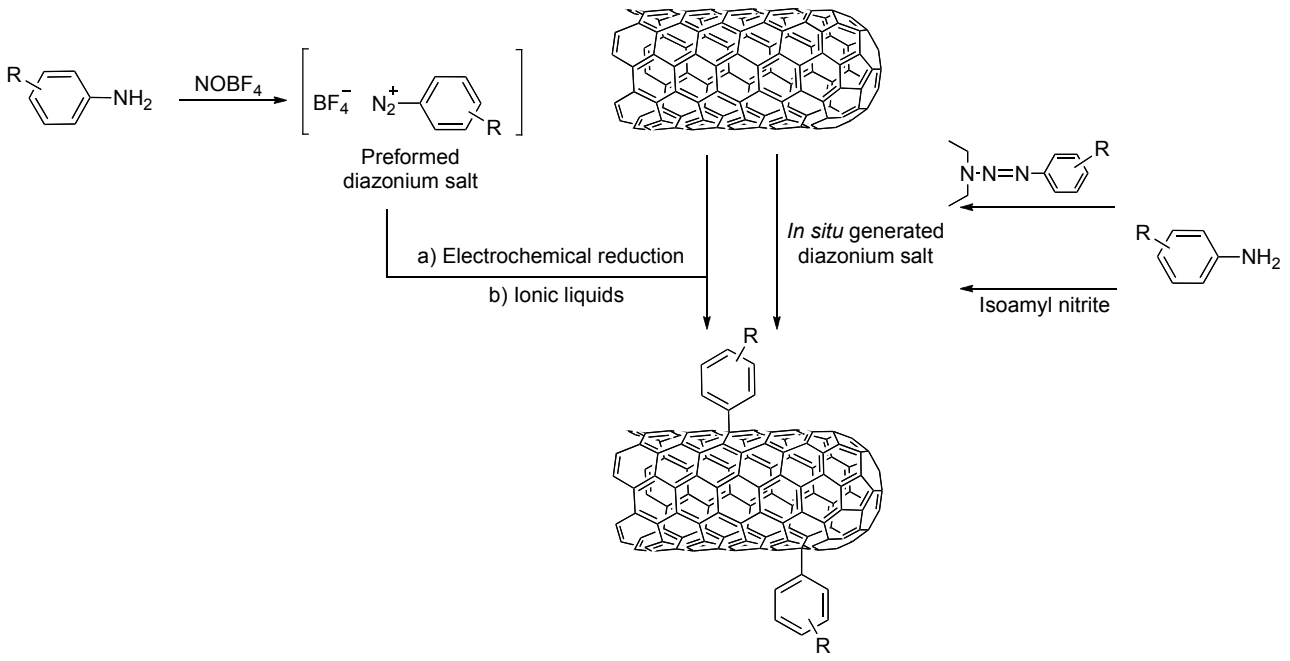

Scheme I.6: Functionalization of carbon nanotubes using diazonium salts under different conditions.

Besides the diazonium route, several other techniques that involve thermal or photochemical radical additions were studied. Billups and co-workers reported the reaction of SWCNTs with organic peroxides in the presence of alkyl halides [Ying, Y., *et al*. 2003]. Finally, alkyl groups can be introduced using lithium in liquid ammonia or lithium naphthalenide in tetrahydrofuran [Borondics, F., *et al.* 2007]. These reduction reactions generate carbanionic CNTs that are easily alkylated with alkyl halides.

I.2.1.2.e Multi-functionalization of Carbon Nanotubes

The multi-functionalization of carbon nanotubes is of particular interest for the development of multimodal CNT-based platforms (Scheme I.7). One of the first examples of double functionalization of carbon nanotubes was reported in 2006 by our group. In this study MWCNTs were covalently functionalized with two different moieties using double 1,3-dipolar cycloaddition. The amino acids used as precursors of azomethine ylides were protected at the amino functions with two orthogonal groups that, after selective deprotection, were further functionalized with a drug and a fluorescent probe [Pastorin, G., *et al*. 2006]. Analogously, the combination of an oxidative treatment to generate oxidized CNTs followed by 1,3-dipolar cycloaddition allows also to obtain double functionalized CNTs. In a work conducted in our laboratory, Samorì *et al*. used this approach to introduce a therapeutic agent onto the sidewall and a fluorescent probe at the tips [Samorì, C., *et al*. 2010b].

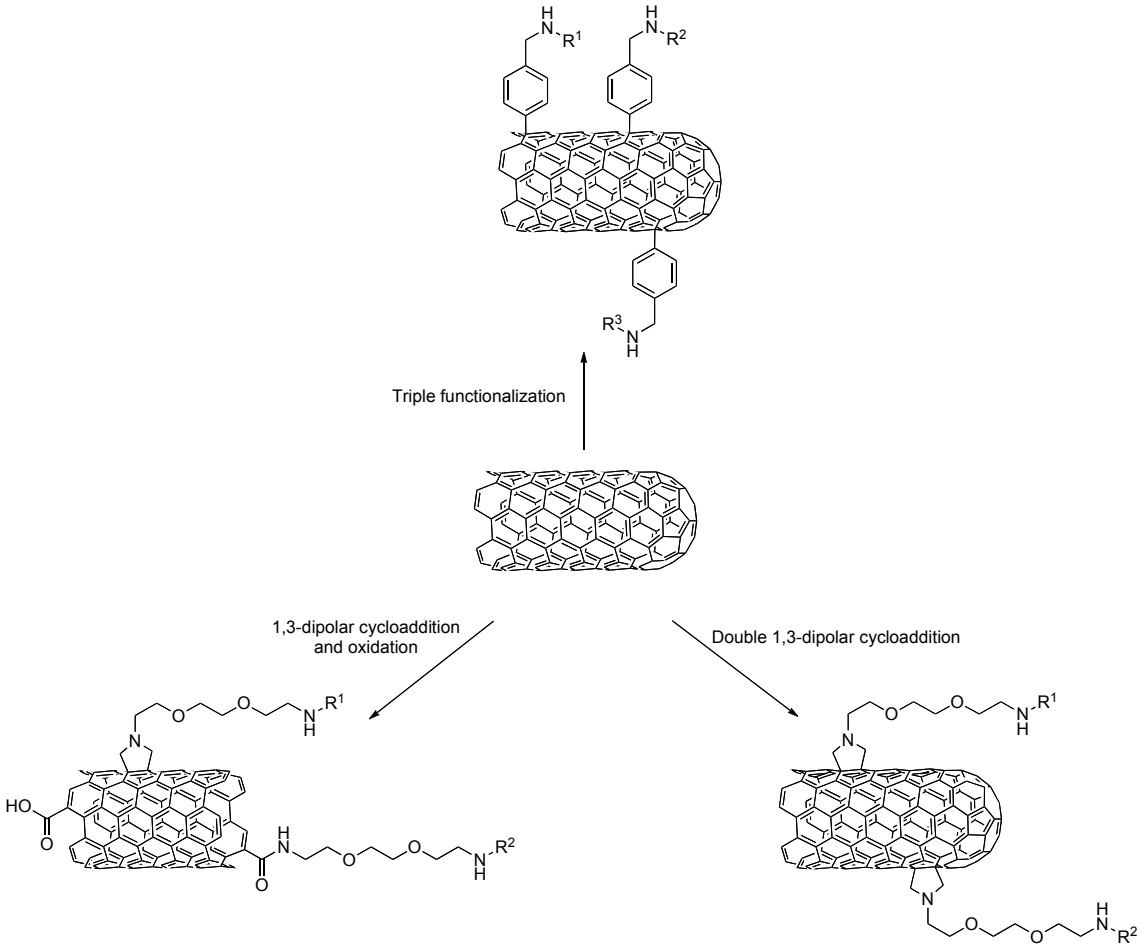

Scheme I.7: Examples of multi-functionalization of carbon nanotubes.

More recently, a triple functionalization strategy was developed in our group. This reaction allows introducing three different molecules in one step by addition of a mixture of aryl diazonium

salts generated *in situ*. The amine functions bear three quasi-orthogonal groups that can be selectively cleaved and further derivatized with the molecule of interest [Ménard-Moyon, C., *et al*. 2011]. This covalent strategy presents several advantages as it offers a better control during the functionalization process and avoids the presence of molecules simply adsorbed onto the CNT sidewall that can lead to constructs with poor chemical stability, as proposed by McFadden and co-workers [Heister, E., *et al*. 2009].

I.2.2 Non-covalent Interactions

Non-covalent functionalization of CNTs is a simple method to solubilize CNTs without perturbing the nanotube structure. Solubilization can be carried out by coating nanotubes with amphiphilic molecules such as surfactants: the hydrophilic part interacts with the solvent and the hydrophobic moiety with the surface of carbon nanotubes. Various surfactants have been used, including charged surfactants as sodium dodecyl sulfate (SDS) or neutral such as Triton [Wang, H., *et al*. 2004]. Due to their high critical micelle concentrations, these surfactants are stable only at high concentrations and this hinders the use of this method for biological applications. Indeed the excess of surfactant can cause cell membrane lysis or protein denaturation [Dong, L., *et al*. 2008].

Aromatic molecules can also disperse CNTs in aqueous or organic media depending on the presence of a hydrophilic or hydrophobic moiety, respectively. Pyrene-based derivatives are the most used compounds to disperse CNTs, taking advantage of the π-π interactions between pyrene and the graphitic surface of the CNTs [Karousis, N., *et al*. 2010].

An alternative approach is the non-covalent wrapping by various species of polymers. Thanks to the exceptional physical properties of nanotubes, nanotube-polymer composites have potential applications in aerospace science as lightweight robust material or in biology as biosensors. The main issues related to the fabrication of nanotube-polymer composites concern the homogeneous dispersion of the tubes in the matrix and the formation of strong interactions between the two components. To address these problems, several strategies have been developed. They involve physical mixing in solution, *in situ* polymerization of monomers in the presence of nanotubes and surfactant-assisted processing of composites [Tasis, D., *et al*. 2006].

Beside these approaches, biomolecules (proteins, carbohydrates, nucleic acids or phospholipids) have been explored as efficient solubilizers. The interactions with biomolecules are important to integrate CNTs in biological environment or to generate bioactive CNTs. Proteins have a high affinity with the CNT sidewall due to hydrophobic interactions between the exterior CNT surface and hydrophobic regions within the protein structure. Lysozyme, bovine serum albumin,

hemoglobin but also synthetic oligopeptides are able to suspend CNT bundles. Atomic force microscope (AFM) images confirmed this ability that depends on various factors such as pH or density of aromatic residues in the primary peptide sequence [Karousis, N., *et al*. 2010]. Similar to proteins, nucleic acids [Zheng, M., *et al*. 2003] could be immobilized on carbon nanotubes by simple adsorption to impart aqueous solubility (Figure I.10) but also to obtain new constructs useful in electrical circuits, for molecular sensing applications or therapeutic delivery.

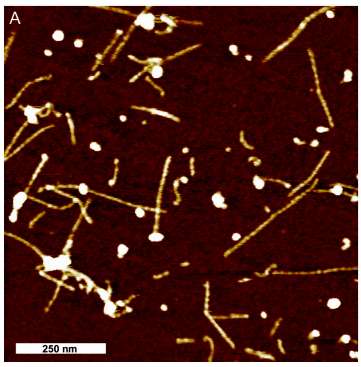

Figure I.10: AFM image of CNTs wrapped with $(GT)_{30}$ oligonucleotide (5-nm scale). Reproduction from Campbell, J. F. *et al*. 2008.

To make CNTs soluble in aqueous media, polysaccharides such as chitosan, alginic acid, cyclodextrins or starch can also be used. For example, Akins and co-workers used chitosan to disperse SWCNTs in water and separate smaller diameter tubes from larger diameter tubes, after sedimentation. This simple and efficient process is based on the fact that narrower tubes are better dispersed and wrapped by chitosan than larger ones [Yang, H., *et al*. 2006]. CNT-polysaccharide hybrids were also successfully used as electrochemical sensors of glucose [Gorityala, B. K., *et al*. 2010]. Finally, phospholipid derivatives can also be assembled onto the CNT sidewall. This class of coating molecules offers several advantages like biocompatibility as phospholipids are the major component of the cell membranes. Moreover, these molecules present low critical micelle concentrations, thus the coating is stable also in absence of excess of surfactant. CNTs functionalized with phospholipids have been used as drug delivery systems or optical probes [Liu, Z., *et al*. 2009a].

I.2.3 Endohedral Functionalization

A fascinating way to functionalize carbon nanotubes is by filling their cavity with guest molecules. Indeed the hollow cavity offers enough space to store molecules and confine them in a quasi-1D array.

Several researchers reported on the encapsulation of C_{60} and higher fullerenes producing the

so-called “peapod” structures [Karousis, N., *et al*. 2010]. The fullerene-filled nanotubes have been characterized by several spectroscopy techniques and studied mainly for their optical and electronic transport properties [Husu, H., *et al.* 2008]. More recently, other organic molecules such as dyes were encapsulated and photoluminescence spectra indicated an energy transfer from the dye to the SWCNTs [Yanagi, K., *et al*. 2007].

Inorganic substances can also be entrapped inside CNTs. For example, SWCNTs were filled with iodine salts (NaI or $Na^{125}I$) and used as *in vivo* radiotracers to localize and image SWCNTs administered to mice [Hong, S. Y., *et al*. 2010]. Endohedral functionalization of SWCNTs with cisplatin was reported by Tripisciano *et al.* This approach offers the possibility to protect the drug from photodegradation and external reactive species, avoiding rapid drug decomposition. The resulting conjugate was then coated with PEG-lipid surfactant and its activity tested on prostate cancer cells, showing a dose-dependent cytotoxicity [Tripisciano, C., *et al*. 2009].

I.3 Toxicity and Biodegradation of Carbon Nanotubes

I.3.1 Toxicity of Carbon Nanotubes

Carbon nanotubes can be used as scaffold for biomolecule immobilization, allowing subsequent applications in biology and medicine. Indeed, CNTs have been exploited as component in biosensors, optical probes [Lu, F., *et al*. 2009], delivery system for bioactive molecules [Ménard-Moyon, C., *et al*. 2010a] or substrate for tissue regeneration [Saito, N., *et al*. 2009]. The interest and advances of using CNTs in biomedicine have raised concerns about biosafety and promoted the study of the toxicological properties of carbon nanotubes. Therefore, a large number of studies (*in vitro* and *in vivo*) have been performed to explore the potential toxic effects of carbon nanotubes.

In vitro studies conducted by different groups showed no toxicity of CNTs if properly functionalized. In our laboratory we studied the impact of water-soluble carbon nanotubes functionalized by 1,3-dipolar cycloaddition on primary immune cells and showed that these functionalized CNTs were not cytotoxic [Dumortier, H., *et al*. 2006]. On the other hand, Ramesh and co-workers studied the impact of pristine MWCNTs on rat lung epithelial cells, showing induction of oxidative stress and stimulation of apoptosis signalling pathway through caspase activation [Ravichandran, P., *et al*. 2009]. These results confirmed the initial *in vivo* studies on the toxicity of raw carbon nanotubes when intratracheally instilled into animals, inducing inflammation and fibrotic reactions [Lam, C. W., *et al*. 2004; Shvedova, A. A., *et al*. 2005]. In contrast to these reports, Cherukuri *et al*. did not observe acute toxicity of surfactant-dispersed (Pluronic F108)

pristine SWCNTs intravenously administered to rabbits [Cherukuri, P., *et al.* 2006]. Recently, Yan and co-workers showed that repeated intravenous injections of water-soluble multi-walled carbon nanotubes into male mice caused reversible testis damage without affecting fertility [Bai, Y., *et al*. 2010]. Therefore, in this moment the toxicity appears to be dependent on several factors, such as experimental protocols, surface functionalization, administration route, CNT dimension (diameter and length) as well as CNT purity. Indeed, CNTs without proper functionalization have highly hydrophobic surface that may adsorb protein or biological species via π-π stacking and induce various cell responses like inflammation [Salvador-Morales, C., *et al*. 2008]. Other parameters may also contribute to the observed toxicity of CNTs *in vitro*. For example, non biomimetic coatings or excess of surfactant used to solubilize carbon nanotubes are known to be highly toxic to cells [Dong, L., *et al*. 2008]. It has also been shown that the purity of the sample plays an important role. The catalysts present in pristine CNTs can induce apoptosis/necrosis of different cell lines [Plata, D. L., *et al*. 2008] or immunological responses in mice, such as changes in interleukin levels [Koyama, S., *et al*. 2009]. In addition, the experimental protocols employed to assess toxicity should be carefully designed and performed. Indeed, carbon nanotubes can interfere with assay reagents employed in the toxicity tests, giving false-positive results [Wörle-Knirsch, J. M. *et al*. 2006; Casey, A., *et al*. 2007]. Finally, the type and degree of chemical functionalization are considered critical parameters in determining tissue accumulation and related toxic responses. Since the persistence into organs is commonly associated with long-term risks, elimination of CNTs through excretion or biodegradation pathways is actively studied. Coated nanotubes tend to accumulate in the liver and be slowly eliminated [Liu, Z., *et al*. 2007a]. On the contrary, highly covalently functionalized carbon nanotubes are rapidly eliminated *via* urinary excretion as demonstrated in our laboratory (Figure I.11) [Singh, R., *et al*. 2006; Lacerda, L., *et al*. 2008a].

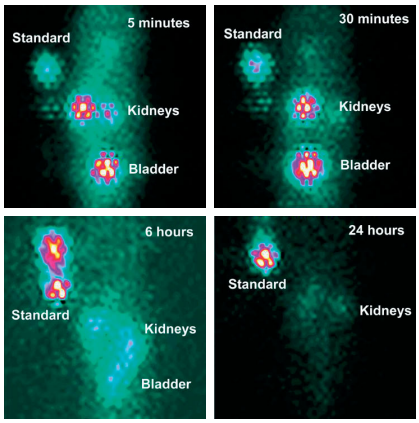

Figure I.11: Images of whole body distribution of [^{111}In]DTPA-MWCNTs in rats after 5 min, 30 min, 6 h, and 24 h post-injection. Reproduction from Lacerda, L. *et al.* 2008a.

I.3.2 Biodegradation of Carbon Nanotubes

Although considered biocompatible after functionalization, carbon nanotubes are still perceived with skepticism as their degradability is still not fully proved. Very recently, some research groups were interested on the possibility of the biodegradation of carbon nanotubes. It has been demonstrated that single-walled carbon nanotubes can be biodegraded by exogenous and endogenous enzymes or by fluids mimicking phagolysosome content. Star and colleagues studied the degradation of carboxylated SWCNTs induced by the catalytic activity of horseradish peroxidase (HRP) in the presence of low concentration of hydrogen peroxide. In 10 days nearly all the nanotubes were degraded. This finding was further supported by a detailed analysis of the enzymatic degradation [Allen, B. L., *et al*. 2008]. Oxidized aromatic fragments were detected during the nanotube degradation, which eventually evolved to carbon dioxide [Allen, B. L., *et al*. 2009]. SWCNTs can be also degraded inside cells such as neutrophils and macrophages by action of myeloperoxidase [Kagan, V. E., *et al*. 2010]. This result has important implications on the inflammatory responses induced by inhaled CNTs and to a wider extent on their use as vehicle for drug delivery and targeted therapies. *In vitro* evaluation of biodegradation of SWCNTs in mild physiological environment (mimicking phagolysosomal conditions) showed a clear dependence on the CNT functionalization. The presence of carboxylic functions and defects on the graphitic surface likely offers the site of interaction with the oxidative agents that are responsible for the degradation [Liu, X., *et al*. 2010]. In this context, our group was interested in a comparative study of the biodegradation of both oxidized SWCNTs and MWCNTs under different oxidative conditions. HRP or an enzyme-free buffer (phagosolysosomal simulant fluid, PSF) were used to degrade CNTs, derived from different commercial sources and presenting therefore different dimensions and morphology (Figure I.12).

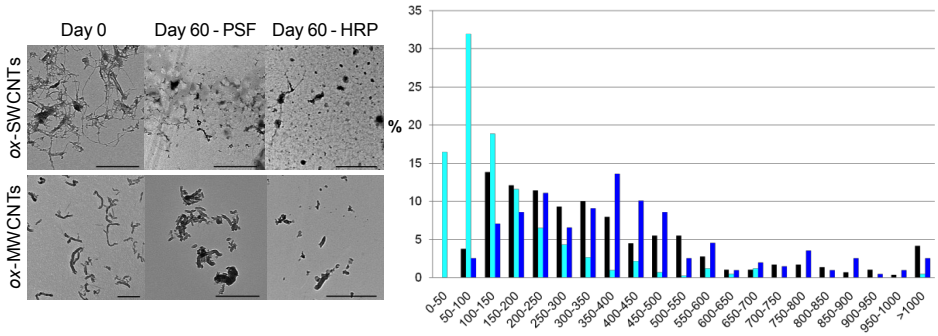

Figure I.12: TEM images of oxidized SWCNTs (top) and oxidized MWCNTs (bottom) during the degradation process (left). The samples were observed after 60 days in different oxidizing conditions (PSF, phagolysosomal condition; HRP, horseradish peroxidase condition) and compared to the starting material. Scale bars correspond to 500 nm. Statistical distribution of the length of the oxidized MWCNTs at the end of the degradation process (60 days). Blue bars correspond to the starting material. Black and cyan bars correspond to the PSF and HRP treatment, respectively. Reproduced from Russier, J., *et al*. 2011.

In both conditions, oxidized SWCNTs are rapidly degraded, especially when using HRP. It has been demonstrated that also MWCNTs are highly degraded, although not to completeness when treated with horseradish peroxidase in the presence of hydrogen peroxide. Distribution of lengths showed that nanotubes were significantly shortened in comparison to the pristine material. In particular, it was observed a higher degree of degradation for MWCNTs showing a higher presence of defect sites and a higher amount of carboxylic acids at the surface [Russier, J., *et al.* 2011; Zhao, Y. *et al*. 2011]. Based on these findings, the mechanism of degradation is likely a combination of two processes: layer-by-layer exfoliation and shortening. All these results underline that the biodegradability depends on the characteristics of the starting material (presence of existing structural defects) and on the type and degree of chemical functionalization.

I.4 Bioapplications of CNTs

Bioapplications of CNTs comprise a broad research field spanning over the use of nanotubes as biosensing devices, drug delivery systems, substrates for tissue regeneration and bioimaging probes [Ménard-Moyon, C. *et al*. 2010b; Schnorr, J. M., *et al.* 2011].

I.4.1 Biosensors

Several groups exploited carbon nanotubes to develop both electrochemical sensors and field effect transistor (FET) [Balasubramanian, K., *et al*. 2008]. The integration of carbon nanotubes into electrical devices offers several advantages over conventional methods. Indeed, CNTs offer peculiar electrical properties able to detect even small charge changes in the surrounding environment. In addition, SWCNTs have a diameter comparable in size to many biomacromolecules to assure size-compatibility between the sensor and the analyte. A number of sensing mechanisms have been proposed to achieve more and more low detection limits and miniaturized devices.

The detection of proteins, antibody-antigen interactions, glucose, DNA or other biomolecules can be achieved *via* electrochemical, electrical or optical mechanisms [Lei, J., *et al*. 2010]. For example, Hu and co-workers developed a label-free DNA biosensor based on the intrinsic electroactivity of DNA. This biosensor was fabricated with an aligned array of SWCNTs able to immobilize a single stranded DNA (ssDNA) probe. Once the hybridization recognition of the target DNA strand took place, a change in the current response occurred. The outstanding merits of this label-free sensor are the possibility to reuse it more than 3000 times and the detection limit

of 20 nM for the targeted strand [Zhang, X. Z., *et al*. 2009]. Similarly, a label-free approach has been employed by Star *et al*. to detect DNA immobilization and hybridization, reaching a detection limit of 1 pM upon addition of Mg^{2+}. In this study SWCNTs were used in a FET configuration [Star, A., *et al*. 2006]. Owing to the extremely high sensitivity and fast response time, also other groups were interested in the fabrication of SWCNT-based FET devices. Examples include the use of antibodies or synthetic oligonucleotides as specific targeting agents [Kauffman, D. R., *et al*. 2008]. Future researches will improve the fabrication of devices with complex arrays of SWCNTs. Recently, Heller *et al*. proposed a multiplexed biosensor based on different types of SWCNTs. This DNA-based sensor allowed identification of different class of molecules (alkylating agents and reactive oxygen species) at the same time. The sensing mechanism is based on a change in the near-IR photoluminescence of SWCNTs due to a damage in the DNA conformation induced by the genotoxins [Heller, D. A., *et al*. 2009].

Finally, another issue is the connection of these nanoelectronic devices to living cells for probing responses in living systems. Only few works are present in the literature. For example, Shao *et al*. reported a single nanotube field effect transistor array, functionalized with specific antibodies, which exhibits highly sensitive and selective sensing of live, intact breast cancer cells (MCF7 and BT474) in human blood [Shao, N., *et al*. 2008].

I.4.2 Carbon Nanotubes for Scaffold Materials in Tissue Regeneration

Carbon nanotubes have attracted particular attention in the design of new scaffold material for use in tissue regeneration to stimulate cellular growth. Several research groups were interested in the development of CNT-based biomaterials due to their superior characteristics over conventional biomaterials. Indeed, CNTs can add strength and flexibility to the implants thanks to their unique mechanical properties. Nanotubes can be combined with collagen, the most commonly used scaffold material to provide structural reinforcement [MacDonald, R. A., *et al*. 2005; Cao, Y., *et al*. 2007]. Due to the immunogenic risks associated with collagen-based material, the researchers focused on the development of a new class of nanocomposite for tissue engineering, *i.e*. CNT-polymer complexes. Examples include material containing CNTs and polylactic acid (PLA) [McCullen, S. D., *et al*. 2007] or chitosan (CHI) [Abarrategi, A., *et al*. 2008] to obtain biocompatible scaffolds for cell culture growth. Both complexes showed satisfactory results for cell adhesion, viability and proliferation onto the external surface of the biomaterials.

CNTs can be used also for bone tissue regeneration. Reports indicate that CNTs promote the proliferation of osteoblastic cells *in vitro* [Zanello, L. P., *et al*. 2006]. Usui *et al*. were interested in

the bone tissue compatibility of CNTs and their ability to stimulate bone formation *in vivo* [Usui, Y., *et al*. 2008]. MWCNTs showed good biocompatibility and when implanted into dorsal muscle of mice accelerated the formation of new bone in response to recombinant human bone morphogenetic protein-2 (rhBMP-2).

Recently, Pastorin and co-workers evaluated the ability of PEGylated MWCNTs to influence human mesenchymal stem cells (hMSCs) proliferation, morphology and differentiation into osteoblasts [Nayak, T. R., *et al*. 2010]. Results indicated that the homogeneous layer of functionalized nanotubes is not toxic and that the cell differentiation occurred even in the absence of biochemical inducing agent, such as BMP-2 protein (Figure I.13).

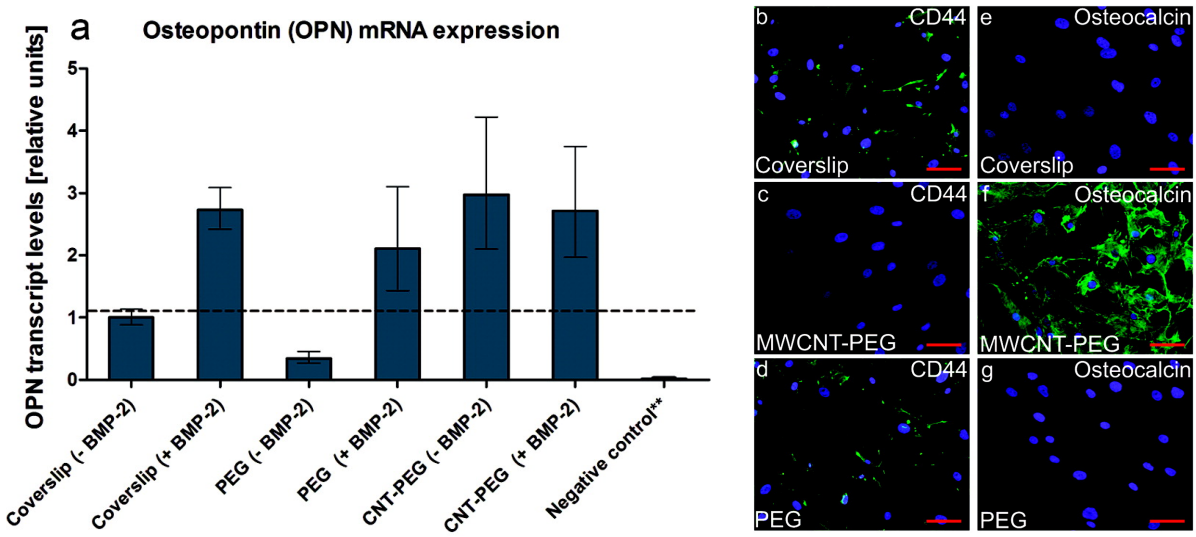

Figure I.13: a) qPCR (quantitative real time polymerase chain reaction) analysis of relative expression levels of osteopontin (early biomarker for osteogenesis) for hMSCs cultured on different types of substrates and osteoinduced with osteogenic media with and without BMP-2 for 14 days. b-g) Immunofluorescence image of cells subjected to osteoinduction without BMP-2. Only PEG-coated MWCNTs (c-f) support shows the absence of green fluorescence for CD44 (protein marker for hMSCs) and the presence of green fluorescence for osteocalcin (protein marker for osteoblasts); nucleus staining (blue fluorescence) was performed using 4′,6-diamidino-2-phenylindole (DAPI). Scale bar: 100 µm. Reproduction from Nayak, T. R., *et al.* 2010.

CNTs have been applied in several areas of nerve tissue engineering owing to their physical properties such as electrical conductivity, flexibility and textile strength. In 2000 Mattson *et al*. first reported the use of CNTs coated with a bioactive molecule (4-hydroxynonenal) as substrate for nerve cell growth and as probe of neuronal functions at nanometer scale [Mattson, M. P. *et al.* 2000]. Recent reports confirmed these results on the ability of nanotubes to sustain and promote neuronal electrical activity [Hu, H., *et al*. 2004; Lovat, V., *et al*. 2005; Galvan-Garcia, P., *et al.* 2007] but the way in which they affect neuronal growth, differentiation and long-term survival is still poorly understood. Using different techniques, Ballerini and co-workers showed that nanotubes

improve the responsiveness of neurons by forming tight contacts with the cell membranes that might favor electrical shortcuts between the different compartments of the neuron [Cellot, G., *et al.* 2009]. In this context, in our laboratory a series of CNT-peptide conjugates was developed for integration into innovative microsystems for nerve reparation. In this study MWCNTs were covalently functionalized with two different cell-adhesion-promoting peptides and their biocompatibility was assessed for different cell lines including neuronal cells. CNT-peptide conjugates did not alter the morphology, viability and basic functions of neurons confirming the possibility of applying functionalized carbon nanotubes as new self-assembling nerve "bridges" [Gaillard, C., *et al*. 2009].

I.4.3 Use of Carbon Nanotubes for Cancer Therapy

CNT-based constructs have been explored for applications in the field of oncology by a number of research groups. CNTs can be used as delivery systems for drugs and genes as well as tools for hyperthermia therapy.

A drug delivery system is designed to improve the pharmacological and therapeutic profile of a drug molecule. It is aimed to solve problems associated with the free drug such as poor solubility, limited bioavailability, unfavorable pharmacokinetics, lack of selectivity and healthy tissue damage. Current drug delivery systems include liposomes [Abu Lila, A. S., *et al*. 2010], virus-based systems [Steinmetz, N. F. 2010], polymers and dendrimers [Cheng, Y., *et al.* 2011]. There are several factors that either contribute or limit the biomedical applications of these drug delivery systems. Liposomes, for example, show excellent biocompatibility but suffer from physical instability in solution due to their amphiphilic nature. Dendrimers present as main advantage a high dimensional control but tend to be cytotoxic [Jain, K., *et al.* 2010]. Viral-based devices might undergo quick mutations which can lead unspecific toxicity and undesirable effects [Thomas, C. E., *et al*. 2003].

Carbon nanotubes are promising drug delivery systems, in particular after the demonstration that functionalized nanotubes are able to enter cells without causing cytotoxic effects [Kam, N. W. S., *et al*. 2004; Pantarotto, D., *et al*. 2004a]. As illustrate in Figure I.14, two main mechanisms of cellular uptake have been described and include phagocytosis/endocytosis processes [Kam, N. W. S., *et al*. 2004; Kam, N. W. S., *et al*. 2006] and energy-independent diffusion ("nanoneedle" mechanism) [Bianco, A. *et al*. 2005b; Kostarelos, K. *et al*. 2007].

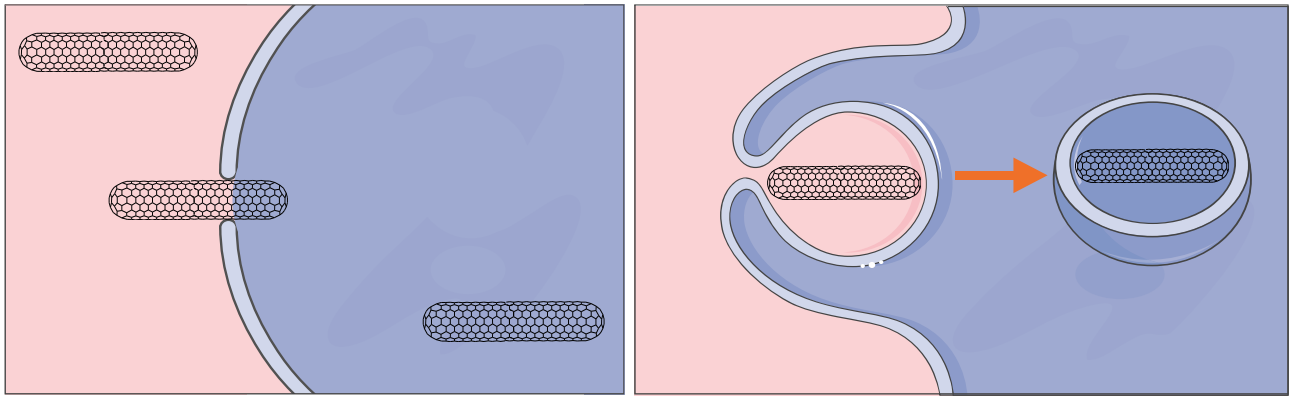

Figure I.14: The "nanoneedle" mechanism (left) and endocytotic (right) cellular internalization mechanism.

Differences in cell internalization may depend on the functionalization and size of the CNTs. Direct cytoplasmic translocation by insertion/diffusion is based on the findings that functionalized carbon nanotubes can enter cells also under-energy inhibiting conditions [Kostarelos, K., *et al*. 2007]. Indeed, the cylindrical shape and high aspect ratio of functionalized CNTs can allow their penetration by a spontaneous mechanism similar to a "nanoneedle" as reported experimentally [Pantarotto, D., *et al.* 2004b] and theoretically simulated [Lopez, C. F., *et al*. 2004].

Internalization by endocytosis/phagocytosis pathways as reported by Dai and co-workers have been mainly described for supramolecular complexes formed between proteins [Kam, N. W. S., *et al.* 2005a] or single stranded oligonucleotides and CNTs [Kam, N. W. S., *et al.* 2006], exhibiting therefore a bigger size than carbon nanotubes derivatized *via* covalent functionalization. This has been observed also for other supramolecular complexes formed between biological macromolecules and nanoparticles, such as polymer-DNA constructs [Van der Aa, M. A. *et al.* 2007].

I.4.3.1 Carbon Nanotubes as Drug Delivery Systems

Several groups used CNTs as efficient carriers to deliver chemotherapeutic drugs inside cells thus improving their pharmacological profiles. For example, CNTs were conjugated with several anticancer agents to improve the efficacy of these therapeutically active molecules [Ménard-Moyon, C., *et al*. 2010a]. In our laboratory we studied the cytotoxic activity of methotrexate (MTX) covalently tethered to MWCNTs *via* different cleavable linkers against breast cancer (MCF-7) cells. We showed enhanced cytotoxic activity when the drug is conjugated to the nanotubes *via* an enzyme-sensitive peptide linker [Samorì, C., *et al*. 2010b].

Wu *et al*. conjugated 10-hydroxycamptothecin (HCPT) to MWCNTs through a cleavable ester linkage and obtained a construct showing better antitumor activity than the clinical

formulation both *in vitro* and *in vivo*. After conjugation, HCPT showed increased water solubility, long circulation in the blood and high drug accumulation in the tumor site [Wu, W., *et al*. 2009].

Drugs can be also conjugated to CNTs by the formation of supramolecular complexes via π-π and/or hydrophobic interactions. Dai and co-workers loaded doxorubicin (DOX) on the surface of PEGylated SWCNTs achieving a remarkable high loading thanks to the high surface area of SWCNTs. The release of the drug is pH dependent and is favored in tumor environment owing to the acidic pH. The conjugate showed high efficiency in killing malignant glioblastoma (U87MG) cells and overall lower toxicity compared to free doxorubicin [Liu, Z., *et al*. 2007b]. These encouraging *in vitro* results opened the door to *in vivo* studies [Liu, Z., *et al*. 2009b]. DOX-conjugates were injected in mice bearing Raji lymphoma xenografts. Mice treated with DOX-SWCNTs exhibited tumor regression and reduced mortality compared to mice treated with the free drug. The improvement is owing to the prolonged circulation in blood due to the presence of PEG coating, which allows repeated transit of drug conjugates through tumor vessels and increased tumor uptake by the EPR (enhanced permeability and retention) effect.

In addition to passive tumor targeting relying on the EPR effect, active *in vivo* tumor targeting has been achieved by conjugating peptides, small molecules (folate) or antibodies to nanotubes (Figure I.15). Usually, cancer cells overexpress some tumor-associated antigen receptors that can be used as target to deliver antineoplastic agents only into tumors. A combination of CNTs and targeting agents may solve a long-standing problem in cancer chemotherapy: the lack of tumor-specific treatments.

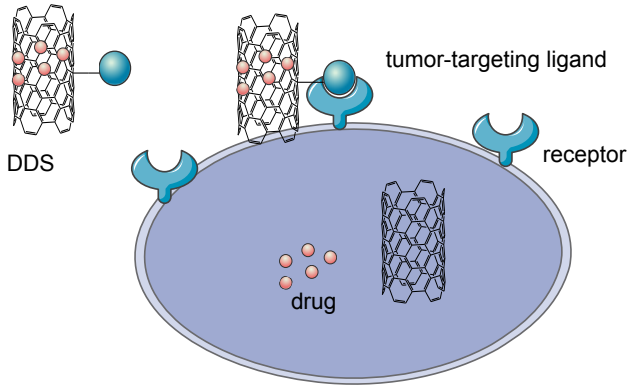

Figure I.15: CNT-based tumor targeting drug delivery system (DDS): CNTs, drug and tumor-targeting ligands. When DDS is administered, it can recognize specific receptor on the surface of cancer cells and cross the cell membrane. Reproduction from Ji, S. R., *et al*. 2010.

Possible protein targets are receptors of various growth factors. For example, SWCNTs were functionalized with epidermal growth factor (EGF) and cisplatin to kill selectively squamous cancer cells. *In vivo* studies confirmed an enhanced decrease in tumor volume in mice treated with SWCNTs-EGF-cisplatin relative to non-targeted construct [Bhirde, A. A. *et al*. 2009]. In another

study carried out by Ruggiero *et al*. SWCNTs were covalently modified with the chelating agent DOTA (1,4,7,10-tetraazacyclododecane-1,4,7,10-tetraacetic acid) or DFO (desferrioxamine B) for complexing therapeutic or imaging radionuclides, respectively. An antibody, targeting the monomeric vascular endothelial-cadherin (VE-cad) epitope expressed in the tumor irregular vessels was then coupled to CNTs obtaining a multifunctional hybrid. The constructs showed specific tumor accumulation and a good therapeutic efficacy [Ruggiero, A., *et al*. 2010a].

I.4.3.2 Hyperthermia Therapy

Hyperthermia therapy is an alternative solution for cancer treatment. CNTs absorb radiation in the near-infrared (NIR) region and convert efficiently the absorbed energy into heat. This intrinsic property of CNTs can be used to optically stimulate nanotubes and cause cell death because of excessive local heating. Moreover, human tissue and biological fluids are relatively transparent to near-infrared light allowing deep tissue penetration of light up to several centimeters in thick tissue and blood. Therefore, hyperthermia therapy using NIR light is promising for *in vivo* biomedical applications. Specificity is also necessary for constructs used in thermal ablation of cancer cells. Recently, SWCNTs were dispersed by ultrasonication in chitosan, which was covalently conjugated with CD133 monoclonal antibody to target cancer stem-like cells ($CD133^+$) in glioblastoma, a common brain tumor in adults suffering from a low efficacy of usual chemotherapy treatment. Results showed that only $CD133^+$ cells were targeted by the conjugate and eradicated both *in vitro* and *in vivo* [Wang, C. H. *et al*. 2011]. Other molecules used as target for cancer therapy are folic acid [Kam, N. W. S., *et al*. 2005b] or proteins, like CD22 expressed in human lymphoma [Marches, R., *et al*. 2009] or HER2 overexpressed in breast tumor [Xiao, Y., *et al*. 2009].

I.4.3.3 Gene Therapy

A new powerful way to treat cancer is offered by the gene therapy and RNA interference (RNAi). The advantages of these therapies lie in their high affinity and specificity to the target sites but the main obstacle to their application is related with the development of a delivery system able to cross the cell membrane and hamper degradation of genes by enzymes [Lacerda, L. *et al*. 2008b]. In a pioneer study conducted in our laboratory, Pantarotto *et al*. demonstrated that carbon nanotubes can be used as novel non-viral gene delivery vector for plasmid DNA (p-DNA) [Pantarotto, D., *et al*. 2004b]. The presence of amino groups on the CNT surface allowed the condensation of pDNA

to form a supramolecular complex. Moreover, pDNA-CNT construct did not exert any cytotoxic effect. Nanotubes represent an alternative to other gene delivery vectors like dendrimers or liposomes that show pronounced toxicity while they achieve very effective DNA delivery. In one of the first study Yang and co-workers conjugated small interfering RNA (siRNA) to ammonium functionalized-SWCNTs and specifically targeted murine telomerase reverse transcriptase (mTERT) expression. The mTERT-siRNA:SWCNT complex successfully entered three cultured murine tumor cell lines, silenced the expression of the targeted gene, inhibited cell proliferation and promoted tumor suppression both *in vitro* and *in vivo* [Zhang, Z. H., *et al*. 2006].

Hu and co-workers used polyamidoamide dendrimers modified-CNTs to increase the amount and delivery efficiency of the carried genes. The resulting antisense oligonucleotides (asODN)-CNT conjugate entered tumor cells and inhibited their growth in a time- and dose-dependent manner [Pan, B., *et al*. 2009].

Recently, in a comparative study amino-functionalized MWCNTs and cationic liposomes were used to complex toxic siRNA sequence (siTOX) and evaluate the ability of these constructs to treat lung cancer *in vivo*. As shown in Figure I.16, only MWCNT-siRNA complex can cause cell death through apoptosis cascade. The data obtained in this study illustrate the capacity of functionalized CNTs to cross the plasma membrane much more efficiently compared to cationic liposomes and in the case of local administration directly at the disease site to achieve advantages in therapeutic activity. Carbon-nanotube-mediated delivery of siRNA led therefore to successful and statistically significant suppression of tumor volume, followed by a concomitant prolongation of survival of animals [Podesta, J. E., *et al*. 2009].

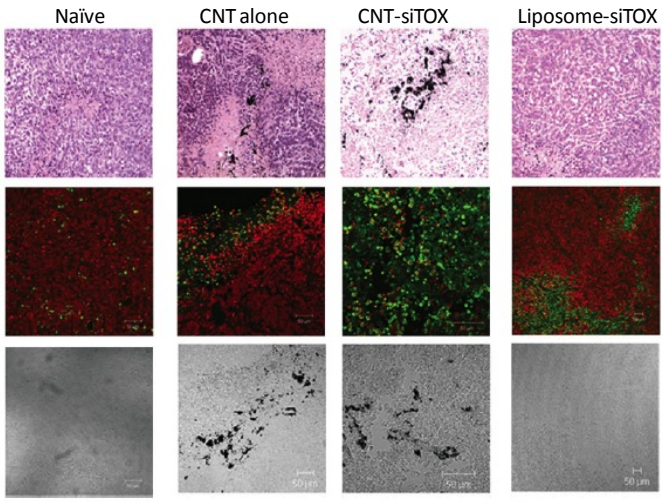

Figure I.16: MWCNT-NH_3^+:siTOX complexes induced tumor apoptosis of human Calu6 xenograft tumors. Heamatoxylin and eosin staining was performed (first row) or terminal deoxynucleotidyl transferase mediated dUTP nick end labeling (TUNEL) and propidium iodide (PI) nuclear counterstain were used to identify apoptotic (green) cells from the total cell population (red, second row). Phase images of corresponding fields of view for TUNEL/PI are shown in the last row to indicate MWCNT-NH_3^+ localization. Reproduction from Podesta, J. E., *et al*. 2009.

I.5 Bioimaging with Functionalized Carbon Nanotubes and Assessment of their *in vivo* Biodistribution

I.5.1 Bioimaging with Functionalized Carbon Nanotubes

The rapid advance in carbon nanotube applications in the field of nanomedicine has raised concerns about their biodistribution and their pharmacological profile *in vivo*. In living body carbon is one of the most abundant element, therefore, it is difficult to trace *in vivo* the small amount of carbon in the form of carbon nanotubes. In recent years several techniques have been used to study the biodistribution of both pristine and functionalized carbon nanotubes. These techniques include indirect detection relying on isotope labeling (radio- and stable isotopes) and direct detection based on intrinsic physical properties of carbon nanotubes. Exploiting these properties such as near-IR or UV-Vis photoluminescence, Raman scattering and photoacoustic signal, carbon nanotubes represent also a new material in the field of imaging for biological systems [Kostarelos, K. et *al*. 2009; Hong, H., *et al*. 2009].

The near-IR photoluminescence (800-1600 nm) was first demonstrated in 2002 by the group led by Smalley [O'Connell, M. J., *et al*. 2002] and it is useful for biological imaging as tissue are nearly transparent in this range of wavelengths. Dai and co-workers used semiconducting SWCNTs as near-IR fluorescent tag for cell imaging and for selective probing of cell surface receptor [Welsher, K., *et al*. 2008]. The nanotubes were non-covalently functionalized with phospholipid-polyethyleneglycol (PL-PEG) surfactant bearing amino groups that were further derivatized with two antibodies, recognizing CD20 cell surface receptor on B-cells and HER2/neu receptor on breast cancer cells. The results showed preservation of near-IR photoluminescence after antibody conjugation and probed sensitive and selective detection of interactions between the nanotubes and the living cells.

Lacerda *et al*. exploited the intrinsic UV-Vis fluorescence of SWCNTs-NH_3^+ prepared by 1,3-dipolar cycloaddition to visualize the interactions between nanotubes and human caucasian lung carcinoma A549 cells (Figure I.17). The authors observed intracellular localization of CNTs without affecting the cellular viability [Lacerda, L., *et al*. 2007]. This was the first report on the visible fluorescence imaging of CNTs in cells without the need of a fluorescent tag.

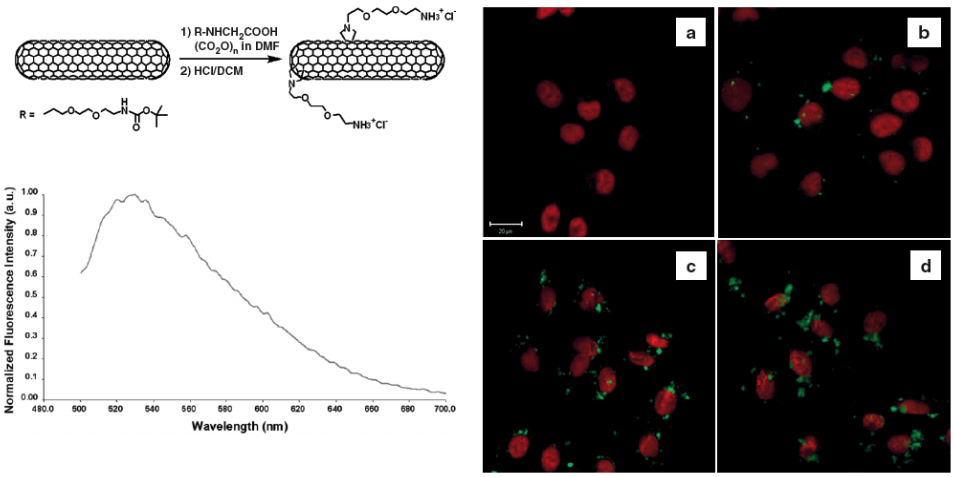

Figure I.17: Fluorescence spectrum of an aqueous solution of SWCNTs-NH_3^+ (150 µg/mL) excited at 488 nm (left); confocal images of A549 cells incubated for 2h with different doses of SWCNTs-NH_3^+ (green). a) A549 cells alone. b) 5 µg SWCNTs-NH_3^+. c) 25 µg SWCNTs-NH_3^+. d) 50 µg SWCNTs-NH_3^+. Cellular nuclei are counterstained red by using propidium iodide (PI). Scale bar: 20 nm (right). Reproduction from Lacerda, L., *et al*. 2007.

Due to the limitations of fluorescence imaging (poor resolution, low tissue penetration and medium sensitivity), SWCNTs are not suitable for *in vivo* imaging. Other techniques, such as photoacoustic tomography or Raman scattering, are more promising.

For example, photoacoustic tomography (PAT), in which sound is generated as a result of local heating by the absorption of a laser light, offers deeper tissue penetration and high spatial resolution. De la Zerda *et al*. used RGD-conjugated SWCNTs as contrast agent for photoacoustic molecular imaging of cancer in mice [de la Zerda, A., *et al*. 2008]. Intravenously administered to tumor-bearing mice, targeted SWCNTs showed eight times greater photoacoustic signal in the tumor than non-targeted SWCNTs (Figure I.18).

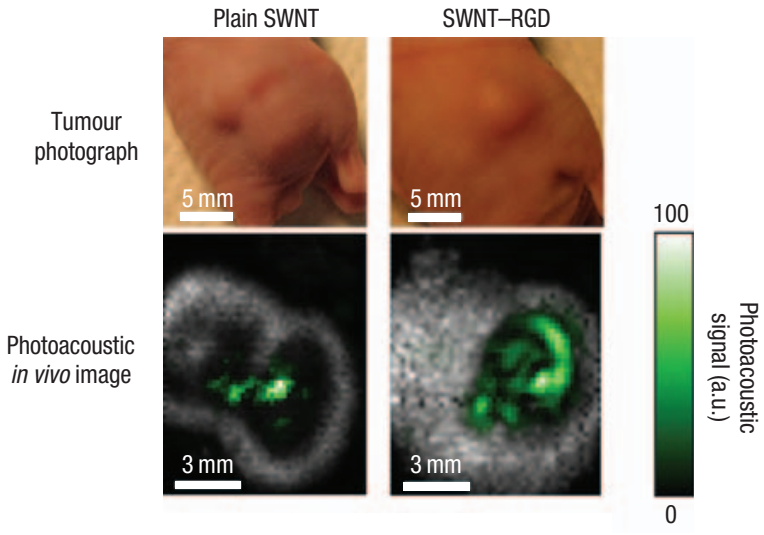

Figure I.18: Photographs of the tumors in mice and the corresponding photoacoustic images, shown as horizontal slices through the tumors. Reproduction from de la Zerda, A. *et al*. 2008.

SWCNTs exhibt also distinctive Raman scattering signals that are suitable for imaging purposes. Dai and co-workers reported the use of Raman spectroscopy to track nanotubes in animals or organs for long periods without the concerns of label falling off or decay over the time [Liu, Z., *et al*. 2008a]. The same group prepared SWCNTs with different isotope composition (^{12}C, $^{12/13}$C and ^{13}C). These CNTs exhibited shifted G-band peaks (at 1590, 1544, and 1528 cm^{-1}) and were used as multicolor contrast agents for multiplexed Raman imaging. Three types of cells were incubated with the three Raman color SWCNTs previously functionalized with various targeting ligands (Heceptin, Erbitux and RGD peptide) to obtain confocal Raman spectroscopy images. The images clearly identified the three cell types, each labeled by a distinct Raman signal. This demonstrated the ability of multiplexed cell identification/imaging by SWCNTs with different isotope compositions, for simultaneously probing and imaging of several biological species [Liu, Z., *et al*. 2008b].

Finally, carbon nanotubes can serve as carriers for radioisotopes for radionuclide-based imaging techniques. Lacerda *et al*. reported the biodistribution of MWCNTs covalently functionalized with a chelating agent (diethylene triamine pentaacetic acid, DTPA) and labeled with the radioisotope ^{111}In [Lacerda, L., *et al*. 2008b]. Alternatively, the radioprobe (^{125}I) was encapsulated inside the SWCNT cavity and the biodistribution profile monitored [Hong, S.Y., *et al.* 2010]. In both studies, the radionuclide was tracked using micro-SPECT (single-photon emission computed tomography). This technique provides non-invasive and panoramic images of the distribution of radioisotope in the body (Figure I.19). Micro-SPECT presents also other advantages such as widely use in the clinic, no tissue penetration limit and high sensitivity.

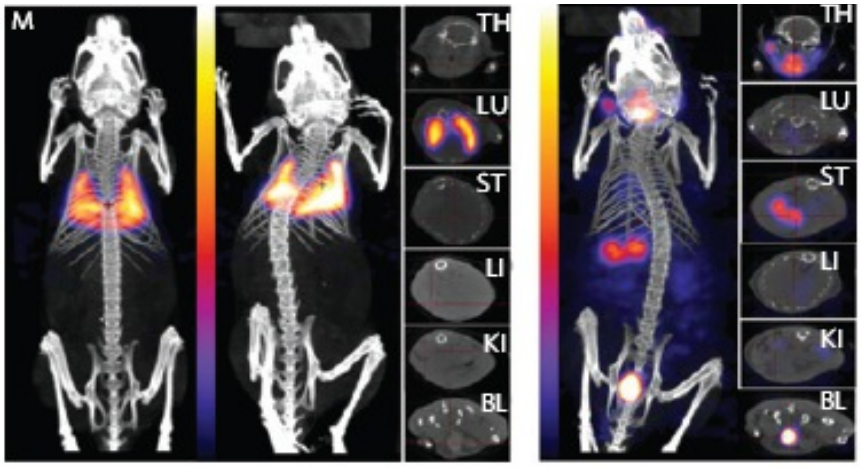

Figure I.19: Whole-body SPECT/CT imaging of ^{125}I encapsulated inside SWCNTs (50 µg and 250 µg, left side) or Na^{125}I (right side). Cross-sections of the thyroid (TH), lung (LU), stomach (ST), liver (LI), kidney (KI) and bladder (BL) are shown. Reproduction from Hong, S. Y., *et al*. 2010.

I.5.2 *In vivo* biodistribution

In recent years, a number of *in vivo* biodistribution and pharmacokinetic studies have been carried out by different groups using both indirect or direct tracking methodologies.

The isotope method was the first one used to describe the distribution profile of ^{125}I labeled SWCNTs. The radioisotope was introduced on the surface of pristine SWCNTs through the formation of covalent bond between C and I. The authors found a rapid distribution throughout the body, except for the brain. The nanotubes were finally excreted via urines and feces [Wang, H. F., *et al*. 2004]. Yang *et al*. acquired data on pristine SWCNTs using ^{13}C enriched skeleton. In this case the ^{13}C amount is quantified by measuring the $^{13}C/^{12}C$ ratio by isotope ratio mass spectrometry (IRMS). This indirect technique offers several advantages: the nature of the CNTs is maintained and the stability of the skeleton labeling is suitable also for long-term distribution studies. In this case, pristine nanotubes were cleared from the blood stream quickly and accumulated mainly in lung, liver and spleen [Yang, S. T., *et a*l. 2007].

a) Pristine SWCNTs
^{13}C-SWCNTs

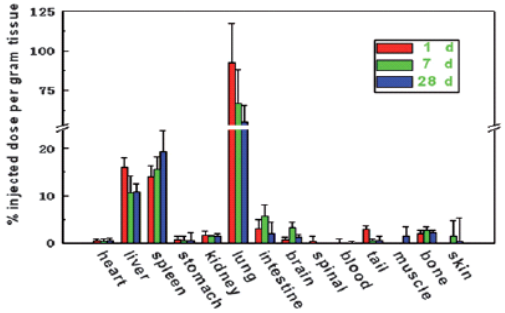

b) Hydroxyl-functionalized SWCNTs
^{125}I-SWCNTs

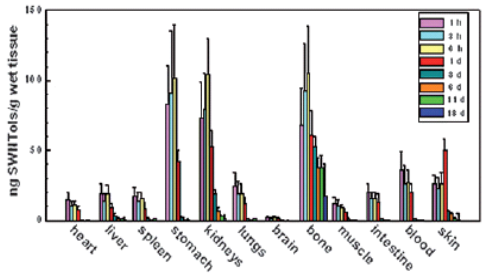

c) PEG-functionalized SWCNTs
^{13}C-SWCNTs-PEG

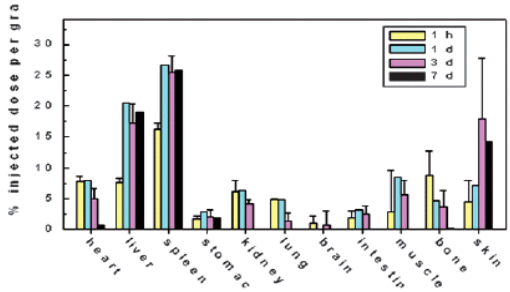

Figure I.20: Comparisons between biodistribution of pristine and functionalized CNTs in mice. a) biodistribution of pristine SWCNTs (^{13}C-SWCNTs) in mice at different time points post-exposure [Reproduction from Yang, S. T., *et al.* 2007]; b) biodistribution histogram of ^{125}I-SWCNTs-OH in mice at eight different time intervals [Reproduction from Wang, H. F., *et al.* 2004]; c) time-dependent biodistribution of PEG-SWCNTs in mice post-exposure at a dose of 2.4 mg SWCNTs equivalent/kg body weight [Reproduction from Yang, S. T., *et al.* 2008].

As shown in Figure I.20, the functionalization affects significantly the biodistribution profile. Surface functionalization by polymers or other molecules improves the dispersibility in water and avoids protein nonspecific binding, resulting in a prolonged blood circulation time and reduced reticuloendothelial system (RES) uptake. The group of Dai studied the influence of PEG coating on the biodistribution profile of SWCNTs. A long and branched PEG chain increases the blood circulation time to 7 h, suggesting low rapid RES uptake. This was confirmed by Raman measurements showing lower hepatic uptake for $PEG_{7000\ branched}$/PL SWCNTs (30% ID (injected dose)/g) than PEG_{2000}/PL SWCNTs (70% ID/g). SWCNTs were then excreted through the biliar and renal pathway [Liu, Z., *et al*. 2008a]. This feature is very suitable in drug delivery application as long circulation times and low RES uptake enable a better targeting of disease tissues [Liu, Z. *et al*. 2008c]. Similar results were obtained by Yang *et al*. studying the pharmacokinetic behavior of covalently PEGylated SWCNTs [Yang, S. T., *et al*. 2008].

CNTs modified with amino groups and labeled with ^{111}In showed rapid clearance from the blood (3 h) and excretion through the renal route without retention in any RES organs [Singh, R. *et al*. 2006]. McDevitt *et al*. confirmed the rapid clearance from blood stream of DOTA (1,4,7,10-tetraazacyclododecane-1,4,7,10-tetraacetic acid) functionalized SWCNTs and labeled with ^{86}Y and ^{111}In. After intravenous injection, these conjugates localized mainly in the spleen (14.3% ID/g) and liver (17.8% ID/g) and were slowly excreted from these organs. In this study the authors compared also the effect of the administration route on the distribution profile of ^{86}Y-DOTA-SWCNTs. If intraperitoneally administered they showed less RES uptake [McDevitt, M. R., *et al*. 2007].

The above mentioned studies used radiolabeling techniques that suffer from decreasing or losing in activity over time due to decay or dissociation of the label. Therefore, Cherukury *et al*. used near-IR fluorescence of individual SWCNTs to monitor directly the biodistribution in rabbits. Results indicated that blood proteins displaced the nanotube coating (Pluronic F108) quickly and the blood clearance was about 1 h. Twenty-four hours after intravenous injection CNTs were mainly found in liver [Cherukury, P., *et al.* 2006].

Taken together, these data are very important to guide the applications of carbon nanotubes in biomedical field in the near future. However, these results suggest that many factors influence the behavior of nanotubes *in vivo* (size, functionalization, administration route, animal model *etc*.) and render the comparison between the different studies difficult.

I.6 Conclusions

Carbon nanotubes, with their unique properties, are considered a suited nanomaterial for applications in the biomedical field. Chemical functionalization represents a powerful way to overcome drawbacks related to CNTs, such as insolubility in aqueous media and poor biocompatibility of the pristine material. Furthermore, surface functionalization enables conjugation of various molecules to develop new hybrid materials for various applications, such as delivery systems for drugs or genes in cancer therapy, scaffold materials for tissue regeneration or bioimaging probes.

The applications of CNTs as nanomedicine tools, triggered by the findings that nanotubes are able to cross cellular membranes in a non-invasive way, raised concerns about their toxicity and long-term fate. *In vitro* and *in vivo* studies highlighted that toxicity depends on several factors such as morphology (size, length, presence of structural defect sites), type and degree of functionalization and administration route. Moreover, recent studies demonstrated that carbon nanotubes can be degraded by oxidative enzymes in biological milieu, reinforcing the optimism for future development of CNTs in biology and medicine.

I.7 Objects of the Thesis

In this thesis, I focused my interest on the development and synthesis of antibody-CNT (Ab-CNT) conjugates as new CNT-based targeted cancer therapeutics. The nanotubes are used as drug delivery system whereas the antibody is the targeting moiety to cancer cells. Although antibodies represent nowadays promising targeting agents for cancer cells, their application is still little explored. In this context, we developed different strategies to couple an antibody to carbon nanotubes. Complementary techniques were used to fully characterize the mono-functionalized constructs (Chapter II).

The third chapter describes the synthesis of a second generation of Ab-CNT conjugates, formed by i) the antibody or fragments of the antibody and ii) a fluorescent or radioactive probe. Wide interest is given to the physico-chemical characterization of the Ab-CNT conjugates and to the assessment of their biological activity. Results from *in vitro* studies showing the mechanism of cellular internalization and toxicity are also presented. Based on these findings, we also developed a therapeutic tool by conjugating CNTs and a fragment of the antibody showing concomitant targeting and therapeutic features towards cancer cells. The new construct was characterized by different techniques and biological studies on its therapeutic activity are ongoing.

The fourth chapter presents results from toxicological and *in vivo* studies, in particular the biodistribution profile of the different constructs, obtained in collaboration with the group led by Prof. Kostas Kostarelos.

The last chapter describes the chemical and biological experimental procedures followed to functionalize CNTs and to perform biological studies.

Finally, references are reported for all chapters at the end of the thesis in alphabetical order.

Chapter II: Mono-functionalization of CNTs with Antibodies or Tracking Probes

The aim of this study was the design and synthesis of antibody-CNT (Ab-CNT) conjugates for applications as new nanomedicine tools, in particular in cancer therapy. In this context, we exploited the ability of carbon nanotubes to easily cross cell membranes [Kam, N. W. S. *et al*. 2004; Pantarotto, D., *et al*. 2004a] to deliver a targeting or therapeutic antibody inside cells. Antibodies represent nowadays promising oncological therapeutics as they display high selectivity and potency towards their target (antigen) [Weiner, L. M., *et al*. 2010]. This therapy displays the main limitation that it can be used only towards extracellular targets due to low aptitude of antibodies to traverse the plasma membrane [Begent, R. H., *et al.* 1996]. The conjugation to CNTs was therefore aimed to circumvent this limit and extend the application of antibody-based therapy to intracellular targets. The first part of this study was focused on the design and synthesis of a hybrid model able to target cancer cells. We conjugated MWCNTs to an antibody showing only targeting activity. In the second part we expanded the study to the preparation of CNT-based constructs with a fragment of the antibody showing therapeutic activity.

Before using nanotubes for specific applications in the nanomedicine domain, functionalization is required to overcome the high hydrophobicity and to enhance their biocompatibility [Tasis, D., *et al*. 2006; Singh, P., *et al*. 2009; Karousis, N., *et al*. 2010]. Indeed, the raw CNTs present some impurities such as amorphous carbon or catalytic particles. A common way to purify CNTs relies on an oxidative treatment. This method also allows obtaining oxidized CNTs containing carboxylic functions mainly located at the tips, which can be further modified to introduce functional groups [Bonifazi, D., *et al*. 2006]. The second strategy we followed was the sidewall functionalization of the tubes using the 1,3-dipolar cycloaddition route. This reaction first developed for fullerene functionalization can also be used to obtain water-dispersible CNTs [Georgakilas, V., *et al*. 2002a].

These functionalized CNTs (*f*-CNTs) were used as starting material to conjugate the selected monoclonal antibody to the tubes, either at the ends or onto the sidewall. These Ab-MWCNT conjugates and their precursors were then fully characterized using complementary techniques.

II.1 Oxidation of Carbon Nanotubes

During my Thesis I worked with MWCNTs produced by the catalytic carbon vapor deposition (Nanocyl, Belgium). The pristine sample has an average diameter of 9.5 nm and a mean length of 1.5 μm.

To obtain oxidized MWCNTs (ox-MWCNTs), the pristine material was first dispersed in a mixture of nitric and sulfuric acids by sonication for 24 hours (Scheme II.1).

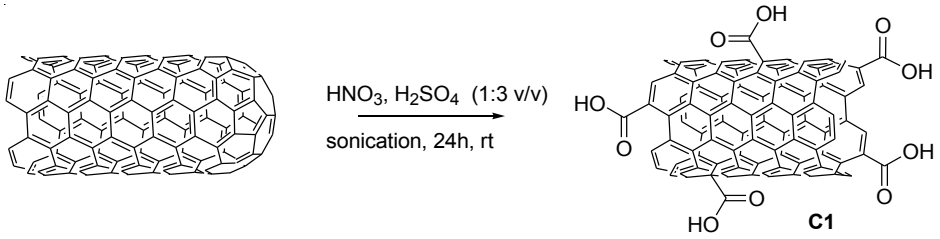

Scheme II.1: Synthesis of oxidized MWCNTs.

Then the ox-MWCNTs (**C1**) were washed several times until pH became neutral and dried. The ox-MWCNTs were observed by transmission electron microscopy (TEM). The images show that the treatment does not induce a morphological change in the tubular structure of the nanotubes but it induces a disruption of the nanotube aggregates (Figure II.1).

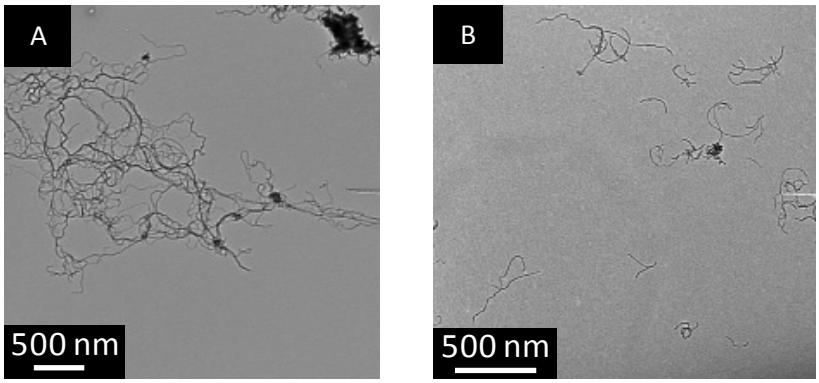

Figure II.1: TEM images of pristine MWCNTs (A) produced by Nanocyl and oxidized MWCNTs (B).

This oxidation process affords shortened CNTs compared to the pristine material as it is conducted under the effect of ultrasounds. A statistical analysis of individualized MWCNTs from TEM images gives a mean length value of around 400 nm (Figure II. 2).

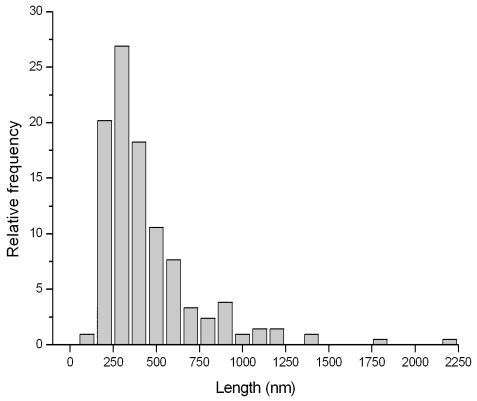

Figure II.2: Length distribution of ox-MWCNTs obtained from 208 measurements.

The presence of oxygen-containing moieties and their quantification was assessed by different techniques. Thermogravimetric analysis (TGA) was used to calculate the degree of functionalization of ox-MWCNTs. This technique is based on the thermal decomposition of the surface groups under inert atmosphere, while the pristine material is stable up to 800°C, thus inducing no significant weight loss. Ox-MWCNTs showed an increased weight loss (8.7% at 500°C), which corresponds to the release of the carboxylic groups from the nanotube surface. This was confirmed by TGA coupled with mass spectrometric analysis: the detection of CO_2 can be attributed mainly to the decomposition of COOH moieties.

In addition to TGA, we used argentometric titration to determine the level of functionalization of ox-MWCNTs [Samorì, C., *et al.* 2010a]. Already applied to other types of nanoparticles [Castaldello, A., *et al*. 2006], we have extended this technique to the direct titration of COOH groups on ox-MWCNTs **C1**. First, the silver salt of ox-MWCNTs **C2'** was prepared by quantitative ion exchange between Na^+ and Ag^+. The silver salt was then protonated using an aqueous solution of HCl. The chloride ion in excess was then titrated using an aqueous solution of $AgNO_3$ as titrant (Scheme II.2).

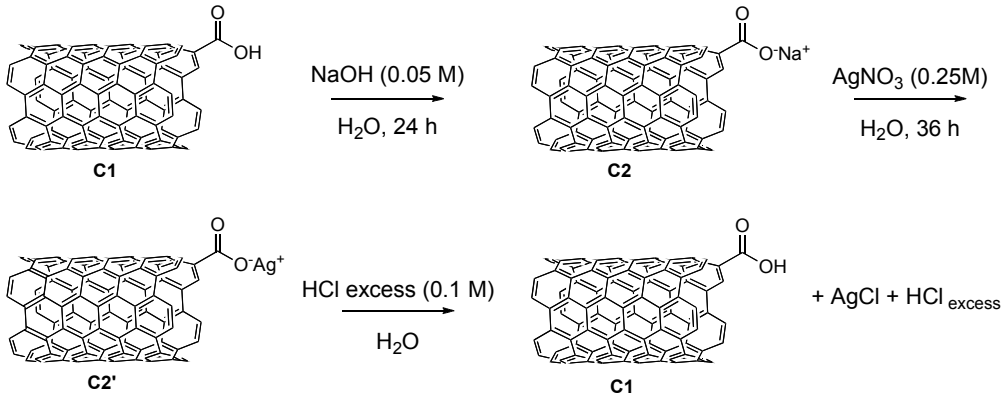

Scheme II.2: Preparation of the silver salt of ox-MWCNTs.

The loading of carboxyl groups, estimated from the equivalence point, corresponded to 1.70 mmol per gram of ox-MWCNTs (Figure II.3). This value is consistent with TGA results, where

8.7% of weight loss corresponds to 1.98 mmol per gram of tubes. The loading values obtained by the two techniques are in good agreement which suggests that both techniques are suitable and reliable when applied to the determination of the number functional moieties present on the nanotube surface.

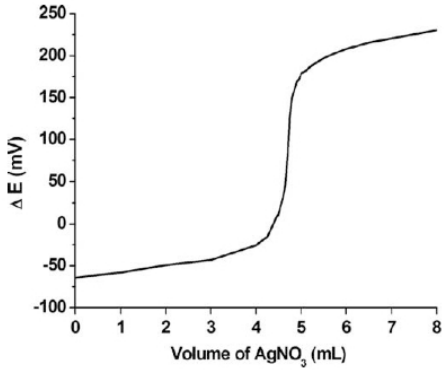

Figure II.3: Argentometric titration curve of ox-MWCNTs.

II.2 Functionalization of Carbon Nanotubes by 1,3-Dipolar Cycloaddition

The 1,3-dipolar cycloaddition of azomethine ylides is one of the most powerful methods used to functionalize carbon nanotubes. This reaction was first applied to incorporate various solubilizing moieties on the fullerene surface [Maggini, M., *et al*. 1993]. This method is based on the condensation of an aldehyde or a ketone and an α-amino acid to generate *in situ* the azomethine ylide by thermally induced decarboxylation. This reaction leads to the introduction of pyrrolidine rings at the hexagon-hexagon junction of fullerene (Scheme II.3).

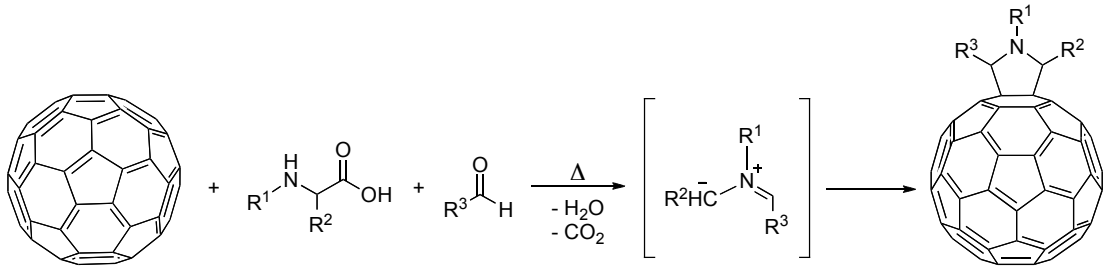

Scheme II.3: 1,3-dipolar cycloaddition of azomethine ylides to C_{60} fullerene.

The electrophilicity and the curved surface of fullerene are factors that promote the reaction with the azomethine ylide. Moreover, this reaction is very versatile as the three groups R^1, R^2 and R^3 can be further derivatized with various functional groups to tailor the solubility properties of the fullerene adducts.

Carbon nanotubes present a structure analogous to fullerene. This promoted the study on the possibility to apply the 1,3-dipolar cycloaddition to the functionalization of carbon nanotubes [Georgakilas, V., *et al.* 2002b]. Indeed, computational calculations also confirmed the feasibility of this reaction as it has a barrier height of only 3.4 kcal/mol and it is exothermic by 39.3 kcal/mol [Lu, X., *et al*. 2003].

Based on the published results on fullerenes [Prato, M., 1997; Da Ros, T., *et al*. 1999; Kordatos, K., *et al*. 2001], we chose, as substituent R^1 on the nitrogen of glycine, a modified tri-ethylene glycol chain to impart water dispersibility to carbon nanotubes. The α-amino acid **3** was prepared as shown in Scheme II.4, using as starting material the commercially available diaminotriethylene glycol. The synthesis of the α-amino acid **3** was carried out by mono-protecting the amino group with the acid labile *tert*-butyloxycarbonyl (Boc) protecting group (**1**). Then, the addition of benzyl bromoacetate afforded the protected α-amino acid **2**. By catalytic hydrogenolysis we obtained the desired α-amino acid **3**. The final compound and the intermediates were characterized by NMR spectroscopy and FT-IR.

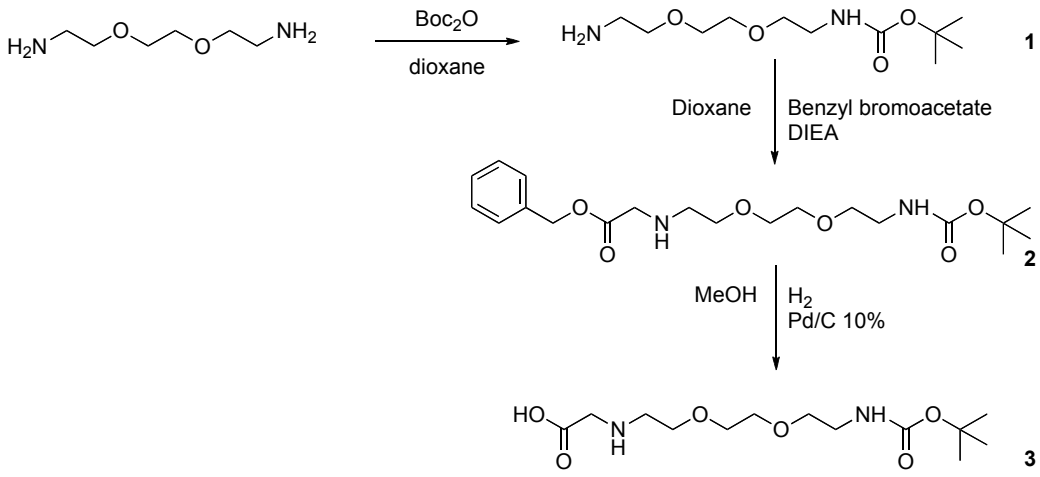

Scheme II.4: Synthesis of the α-amino acid **3**.

In the presence of paraformaldehyde, the as-prepared α-amino acid **3** generates *in situ* the azomethine ylide intermediate that attacks the graphitic surface of the CNTs. As shown in Scheme II.5, ox-MWCNTs **C1** were suspended in DMF by sonication in a water bath and a mixture of α-amino acid **3** and paraformaldehyde was then added in portions, while the reaction mixture was heated at 115°C. After cleavage of the Boc protecting groups using HCl in dioxane, the number of the ammonium groups was determined by UV-Vis spectroscopy using the Kaiser test, yielding a loading value of 110 μmol/g. The Kaiser test is a colorimetric test which is commonly used in peptide synthesis for the qualitative and quantitative determination of amine functions [Kaiser, E.,

et al. 1970; Sarin, V. K., *et al.* 1981; Samorì, C., *et al*. 2010a]. This test is based on the reaction of amine functions with ninhydrine, leading to the formation of a chromophoric compound whose concentration can be determined using UV-Vis absorbance spectroscopy (maximum at 570 nm).

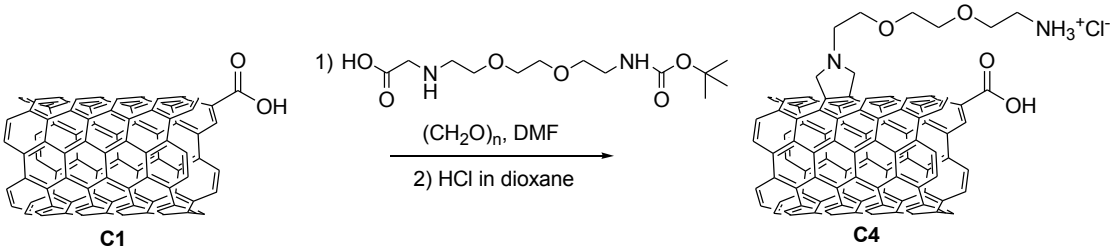

Scheme II.5: 1,3-dipolar cycloaddition and subsequent cleavage of the Boc protecting groups on ox-MWCNTs.

The functionalized MWCNTs **C4** were characterized by TEM, confirming that the surface of the ammonium-functionalized CNTs **C4** was intact. TGA showed an increased weight loss for CNTs functionalized *via* 1,3 dipolar cycloaddition compared to ox-MWCNTs (Figure II.4).

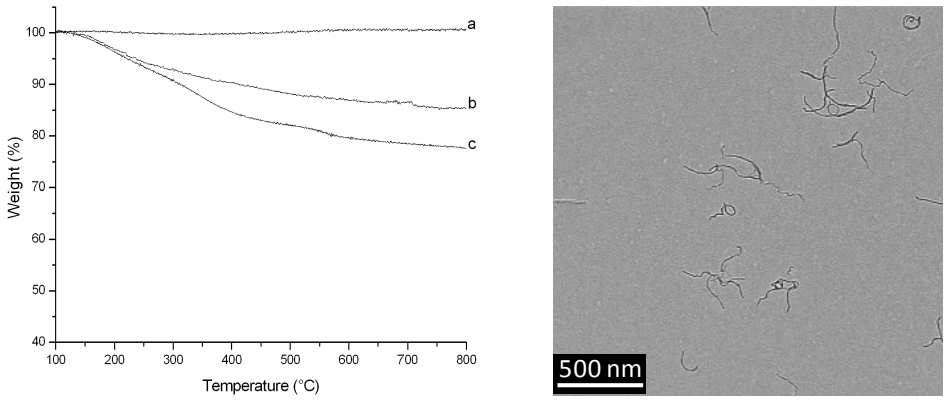

Figure II.4: Thermogravimetric profiles of pristine MWCNTs (a), ox-MWCNTs **C1** (b) and ammonium-functionalized MWCNTs **C4** (c), (left); TEM image of ammonium-functionalized MWCNTs **C4** (right).

The 1,3-dipolar cycloaddition allowed us to obtain MWCNTs easily dispersible in organic solvents and water. Moreover, the amines introduced onto the sidewall of carbon nanotubes can be further derivatized to couple the antibodies or other molecules of interest.

II.3 Labeling of Carbon Nanotubes

Amino-functionalized carbon nanotubes were labeled with an imaging probe (fluorescent probe or radioisotope). The labeling was necessary for *in vitro* and *in vivo* studies to follow the trafficking of CNTs inside cells or the biodistribution profile in animals. Fluorescein was chosen for *in vitro* experiments because of the possibility to track fluorescently labeled CNTs by fluorescence microscopy techniques. Indeed, it is possible to study the molecular trafficking inside cells thanks to the colocalization of CNTs and different cell organelles stained by other fluorescent probes.

Radioactive-labeling was used to perform *in vivo* studies to assess the biodistribution of the different CNT-based constructs (see Chapter IV).

We functionalized MWCNTs with fluorescein isothiocyanate (FITC) in DMF in the presence of *N,N*-diisopropylethylamine (DIEA) to afford the fluorescently labeled MWCNTs **C5** (Scheme II.6). The Kaiser test performed on MWCNTs **C5** corresponded to 30 µmol of NH_2 per gram of nanotubes (yield: 75%), thus the loading of FITC was 90 µmol per gram of CNTs. This result indicated that the reaction was not quantitative probably due to the sterical hindrance of the amine functions.

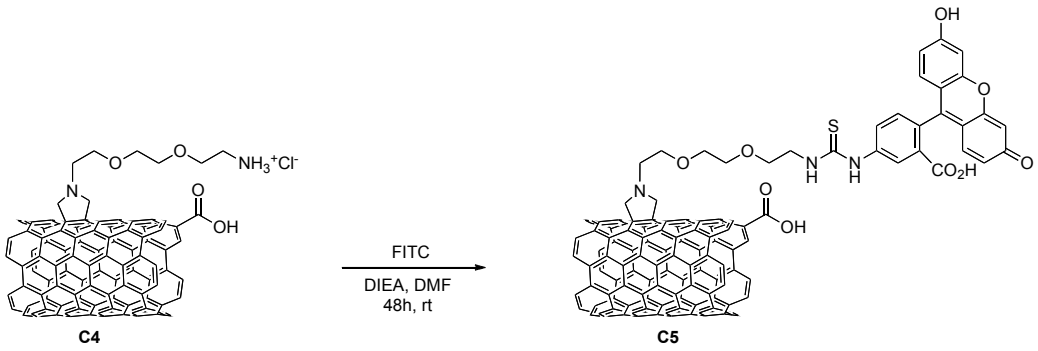

Scheme II.6: Sidewall functionalization of MWCNTs with FITC.

Alternatively, we introduced fluorescein at the nanotube tips (Scheme II.7). For this purpose, the carboxylic acid functions were converted to acyl chlorides by heating the oxidized nanotubes in neat oxalyl chloride for 24h. After evaporation of the reagent, the reaction with the Boc-monoprotected diamino triethyleneglycol **1** resulted in the formation of the corresponding amide. The Boc protecting group was then removed using HCl in dioxane to yield ammonium-functionalized MWCNTs **C7**. Fluorescein isothiocyanate reacted with MWCNTs **C7** to yield fluorescently labeled *f*-MWCNTs **C8**. The quantitative Kaiser test decreased from 390 µmol/g to 90 µmol/g (yield: 77%), indicating that the loading of FITC was 300 µmol/g.

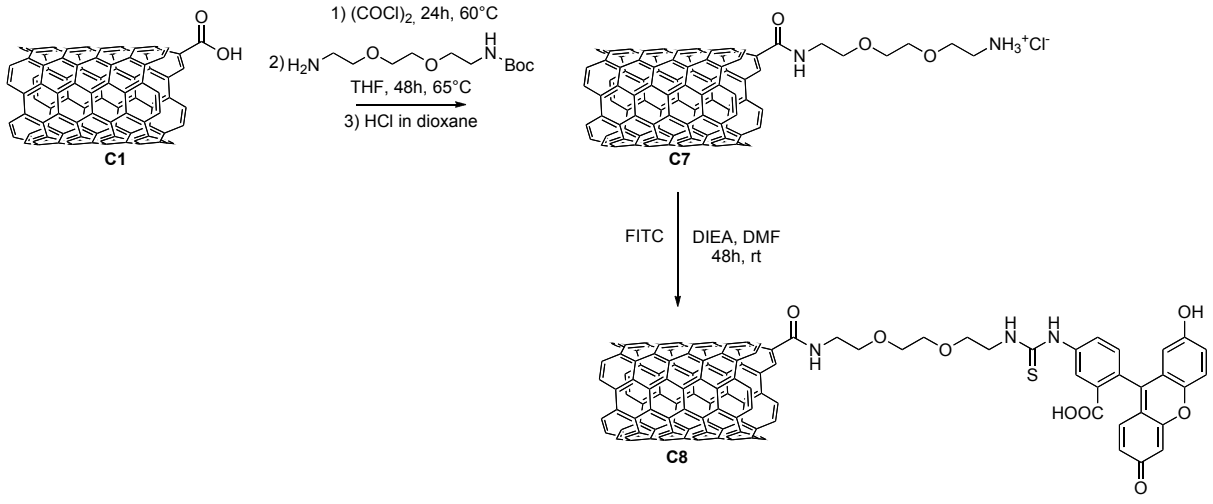

Scheme II.7: Tips functionalization of MWCNTs with FITC.

In order to perform *in vivo* studies, we decided to derivatize ammonium-functionalized MWCNTs with diethylenetriaminepentaacetic acid (DTPA). Indeed, this chelating agent allows the complexation of different radiometals (*e.g.* ^{111}In and ^{153}Gd) that are commonly used in biodistribution studies. In this context, *f*-MWCNTs **C4** were reacted with DTPA dianhydride (Scheme II.8). The dianhydride form of DTPA readily reacted with amino groups present on the nanotube sidewall to afford *f*-MWCNTs **C9**. The quantitative Kaiser test was used to assess the number of free amino groups, yielding 20 μmol/g (yield: 85%, loading DTPA: 100 μmol/g). Finally, the *f*-CNTs **C9** reacted with $^{111}InCl_3$ to form the desired complex. The labeling step was performed in London by the group of Prof. Kostas Kostarelos.

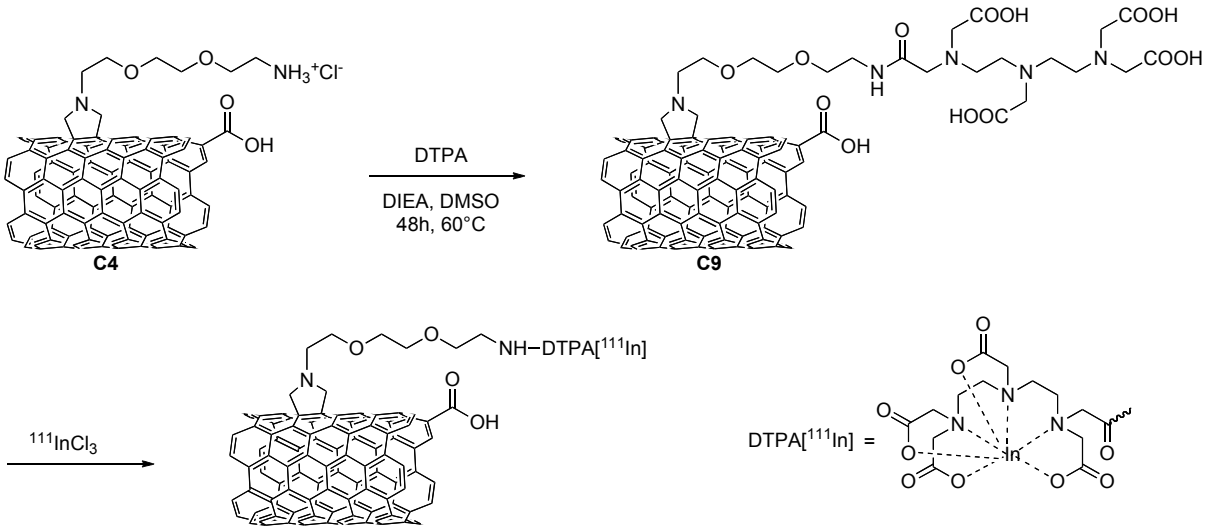

Scheme II.8: Synthesis of ^{111}In-labeled MWCNTs.

Following the same protocol we prepared MWCNTs functionalized with DTPA at the tips **C10** (Figure II.5) using as starting material MWCNTs **C7** (yield: 92%, loading DTPA: 360 μmol/g).

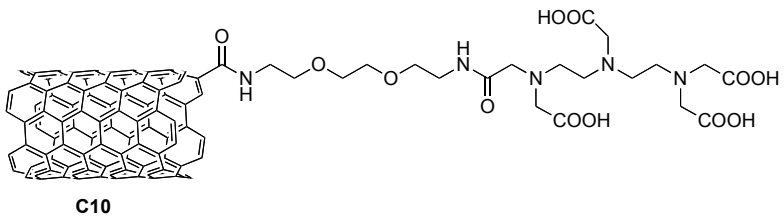

Figure II.5: Structure of *f*-MWCNTs **C10**.

II.4 Coupling of the Antibody to Carbon Nanotubes

The first step in the preparation of targeting monoclonal antibody-CNTs for further applications in cancer therapy consisted on the selection of the antibody hCTM01 anti-MUC1 immunoglobulin G (IgG). MUC1 or polymorphic epithelial mucin (PEM) is the best characterized protein belonging to the mucin family [Hattrup, C. L., *et al*. 2008]. These proteins are high molecular weight glycoproteins, which are involved in the protection and lubrication of healthy cells. Mucins can be categorized into two classes: secretory mucins and membrane-bound mucins (Figure II.6). The secretory mucins lack the transmembrane domain and are directly secreted into the extracellular space. MUC1 belongs to the membrane-bound mucin class [Hattrup, C. L., *et al*. 2008]. As shown in Figure II.6, the core of mucins is dominated by a large extracellular domain, called variable number tandem repeat (VNTR) region. The tandem repeat domain in the center of MUC1 is flanked by the N-terminal sequence and by the more extended C-terminal portion. This region comprises the transmembrane region and a cytoplasmatic tail, which has been proposed to be involved in cell signaling events [Singh, P. K., *et al*. 2006].

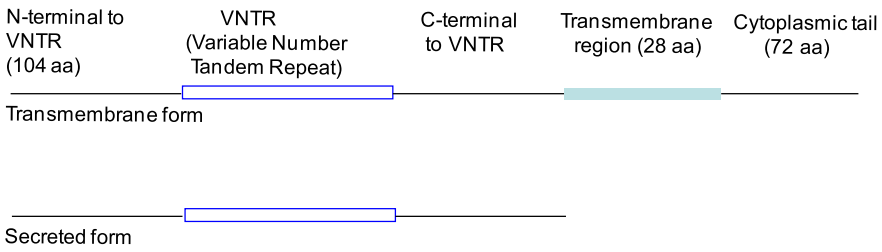

Figure II.6: Schematic representations of membrane-bound mucin (top) and secretory mucin (bottom).

MUC1 aberrant overexpression is often associated with breast and other carcinomas [Niv, Y., 2008]. MUC1 is therefore a potential target for anticancer therapy. The Ab-CNT conjugates will exploit the cell-penetrating properties of nanotubes and the targeting properties of the bound antibody.

The preparation of anti-MUC1-CNT conjugates is therefore aimed at building a hybrid model able to target tumor cells [Venturelli, E., *et al*. 2011]. In order to synthetize the carbon nanotube-antibody conjugates, two types of connection between the CNTs and the antibody can be used: non-covalent interaction and covalent bonding. So far, several research groups have used non-covalent interactions to immobilize immunoglobulins on carbon nanotubes [Chakravarty, P., *et al*. 2008; Ou, Z., *et al*. 2009; Wang, C.-H., *et al.* 2011]. However, non-covalent conjugates may display lack of selectivity and insufficient stability. On the contrary, a covalent bonding can offer a good

stability and a better selectivity due to its capability to control the location of the biomolecule. Therefore, we synthesized Ab-MWCNT conjugates using two different covalent approaches. The antibody was conjugated to CNTs either at the tips or onto the sidewall of the nanotubes. This methodology enabled us to evaluate the best position for the conjugation of the antibody, in terms of preservation of biological activity and feasibility of the synthesis. The second advantage is the possibility to prepare doubly functionalized CNTs containing a functional group at the tips and another on the sidewall. One functional group could be used for the binding of the antibody and the other for the insertion of an imaging probe.

II.4.1 Tip Functionalization of Carbon Nanotubes with the Antibody

In the first of our conjugation strategy (Scheme II.9), the Ab was introduced principally at the functionalized ends of the CNTs by peptide coupling between the carboxylic functions of ox-MWCNTs **C1** and the amino groups of the basic amino acid side chains (i.e. lysine) available on the Ab. In addition, Ab binding is likely to occur at any defects on the CNT sidewall.

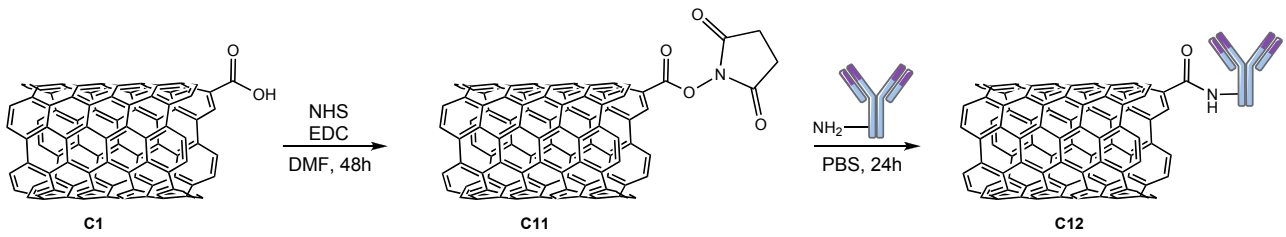

Scheme II.9: Preparation of Ab-MWCNT conjugate **C12** *via* diimide-activated amidation process.

Amidation is one of the most used method to conjugate biomolecules to other materials by direct coupling of carboxylic acid groups to amine functions on proteins using generally EDC as coupling agent. However, an important drawback of this reaction is the undesirable side reaction of intermolecular coupling of antibodies, because of the presence of both carboxylic acids and amines on the surface of the biomolecule. This problem was circumvented by using a two-step process where carboxylic acid groups were first converted to highly reactive esters **C11** (*N*-hydroxysuccinimidyl esters, NHS) *via* diimide-activation (Scheme II.9). The esters reacted then with the amine groups of the antibody. This process guarantees homogeneous attachment of biomolecules onto carbon nanotubes, avoiding the undesirable side reaction of intermolecular conjugation.

II.4.2 Sidewall Functionalization of Carbon Nanotubes with the Antibody

As an alternative to the direct conjugation of Ab to the carboxylic groups of ox-MWCNTs, we covalently linked the Ab to the sidewall of CNTs using selective chemical ligation via addition of the thiolated Ab to maleimide groups introduced onto ammonium-functionalized CNTs (Scheme II.10).

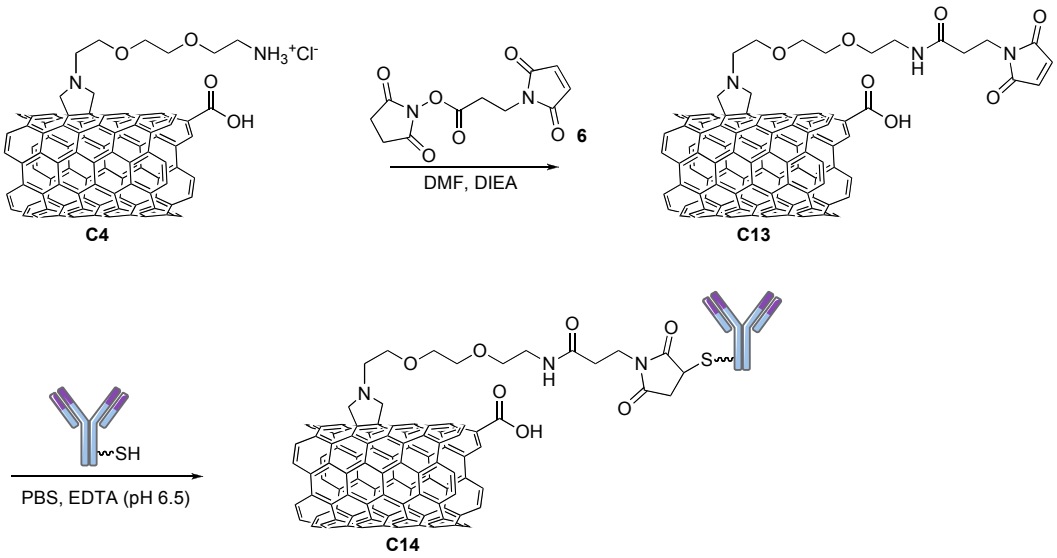

Scheme II.10: Preparation of Ab-MWCNT conjugate **C14** by maleimide/thiol coupling.

The ammonium functions at the end of the triethylene glycol chain on the pyrrolidine ring were derivatized using the heterobifunctional cross-linker 3-maleimidopropionic NHS ester **6**. NHS reacted first with the primary amines on the sidewall of CNTs **C4** to form amide bonds, leading to maleimido-MWCNTs **C13**. These conjugates were characterized by Kaiser test to determine the amount of maleimido functions (85 µmol/g). The maleimide group allows the covalent conjugation of sulfhydryl-containing molecules to form stable thioether bonds. Because of the absence of cysteine amino acid residues with free thiol groups within the anti-MUC1 sequence, we generated thiol moieties on the antibody using Traut's reagent (2-iminothiolane) (Scheme II.11) [Traut, R. R., *et al*. 1973; Jue, R., *et al*. 1978].

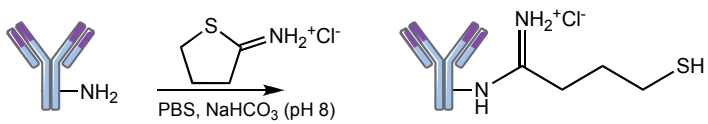

Scheme II.11: Thiolation of the antibody by Traut's reagent.

The amount of reactive thiol groups was determined by Ellman's assay [Ellman, G. L. 1959] using UV-Vis spectroscopy. The thiolated-antibody was then conjugated to CNTs **C13**. All coupling reactions between the CNTs and the Ab were monitored by UV-Vis spectroscopy. The

absorbance at 280 nm (due to the side chains of the aromatic amino acids present in the antibody) of the supernatant of the reaction mixture decreased as the antibody bound to the nanotubes (Figure II.7).

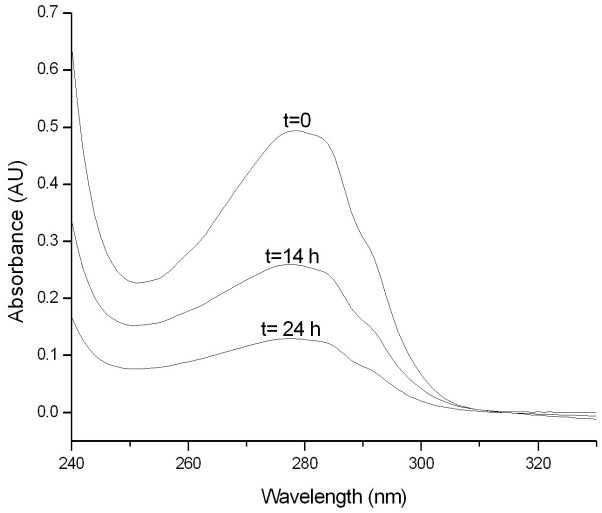

Figure II.7: UV-Vis spectra of the supernatant of aliquots of the coupling reaction (sidewall functionalization) between MWCNTs and Ab, which show the decrease of the absorption peak at 280 nm with time.

At specified time points an aliquot of the reaction mixture was centrifuged at high speed (16000 g) and the supernatant was collected. The centrifugation process allowed to separate the solution containing the unreacted antibody (in the supernatant) from CNTs, which were collected as a black precipitate. This was necessary to avoid the interference of the nanotubes in the UV spectrum because of their strong absorbance.

After the reaction, the remaining free Ab or the Ab simply adsorbed on the sidewall of the tubes was eliminated by washing cycles with PBS and a final dialysis against PBS.

II.5 Characterization of the Ab-Carbon Nanotube Conjugates

We used complementary techniques to prove the successful covalent immobilization of the antibody on CNTs by the two strategies. Although a direct visualization of the Ab on the nanotubes was not possible by TEM due to its low contrast in comparison to CNTs, TEM images of Ab-MWCNT conjugates **C12** and **C14** show that the morphological structure of the nanotubes was not affected by the conditions used for the IgG coupling reaction (Figure II.8).

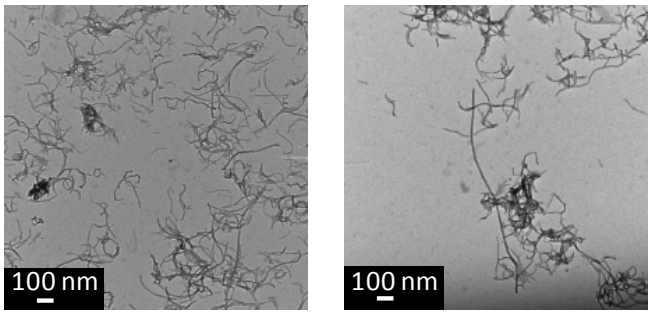

Figure II.8: TEM images of Ab-MWCNT conjugate **C12** (left) and Ab-MWCNT conjugate **C14** (right).

Thermogravimetric analysis was used to evaluate the degree of functionalization of the Ab-MWCNT conjugates. Figure II.9 shows the weight loss observed when the CNT constructs underwent thermal decomposition under inert atmosphere. The thermogravimetric analyses permitted us to estimate the amount of IgG bound to the CNTs (at 500°C), by comparison with the thermogravimetric profile of their precursors. We could calculate a loading of 35% in weight of Ab with respect to the Ab-MWCNT conjugate **C12** and 22% of Ab with respect to the Ab-MWCNT conjugate **C14**. These values were in agreement with the decrease of Ab concentration in the supernatant following reaction between CNTs and Ab (Figure II.7). The loading calculated by TGA, if expressed in molarity, corresponds to concentrations in the range of 2 to 3.3 µmol of Ab per gram of CNTs.

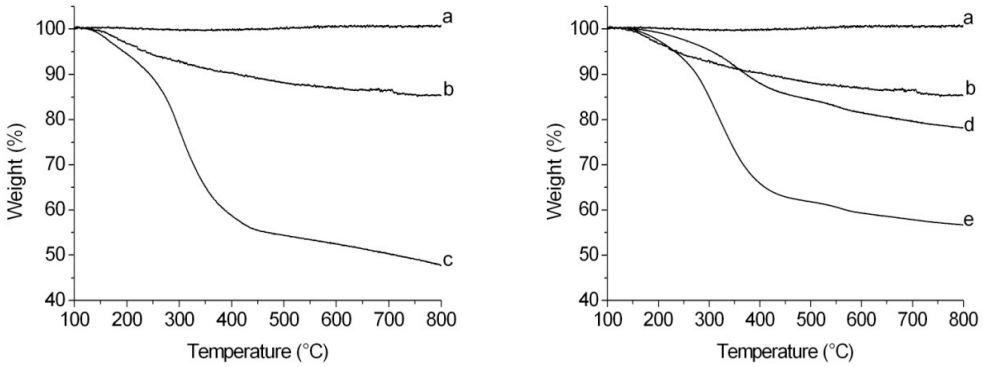

Figure II.9: TGA profiles of pristine MWCNTs (a), ox-MWCNTs **C1** (b), Ab-MWCNT conjugate **C12** (c), maleimido-functionalised MWCNTs **C13** (d) and Ab-MWCNT conjugate **C14** (e).

Gel electrophoresis analysis under both non-reducing and reducing conditions was then used to show covalent binding between CNTs and the Ab. The free antibody (150 kDa) was used as a reference in the analysis (Figure II.10, lane 1). As displayed in Figure II.10 (lanes 2 and 3), no MWCNTs entered in the gel and no Ab was detected under non-reducing conditions, confirming that the Ab was not simply adsorbed on the surface of the CNTs but firmly bound to them, thus remaining in the loading well. Under reducing conditions a pattern of two bands appeared, due to

the heavy chains (~50 kDa) and the light chains (~25 kDa) of the Ab. These results suggest that the antibody was intact after conjugation with the CNTs.

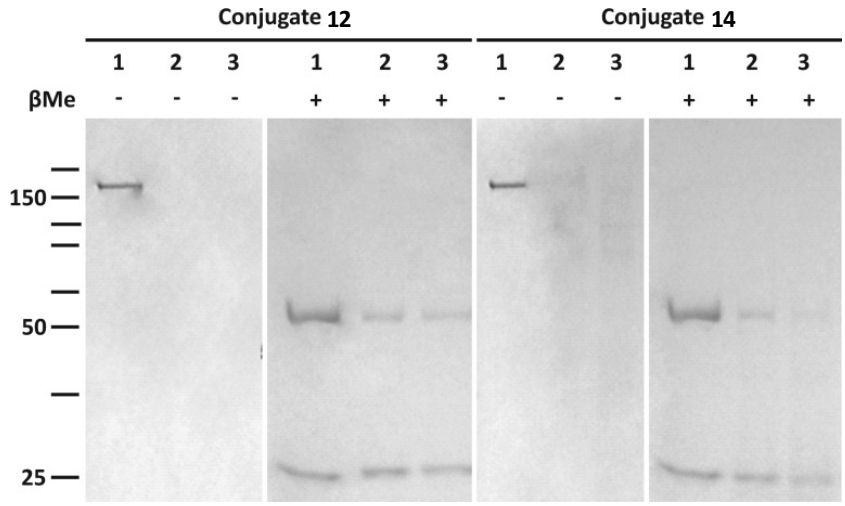

Figure II.10: Gel electrophoresis of Ab-MWCNT conjugate **C12** (left) and **C14** (right) and under non-reducing conditions (-βMe, β-mercaptoethanol) and reducing conditions (+βMe) Lane 1: Ab reference; lane 2: Ab-MWCNT conjugate before dialysis; lane 3: Ab-MWCNT conjugate after dialysis.

For the Ab-MWCNT **C14** we also performed microscopic analysis by immunostaining. This technique allowed us to localize the antibody on the MWCNT sidewall by TEM. After depositing the conjugate **C14** on the TEM grid, we incubated it with a biotinylated goat-anti-human IgG and then with a goat anti-biotin IgG coupled to colloidal gold nanoparticles (6 nm in diameter). We clearly observed the gold nanoparticles only on the sidewall of the nanotubes functionalized with the Ab (Figure II.11A). A control TEM grid was prepared by depositing ammonium-functionalized MWCNTs **C4**, used as starting material (Figure II.11B). In this case, as expected, no gold nanoparticles were bound to the nanotube surface.

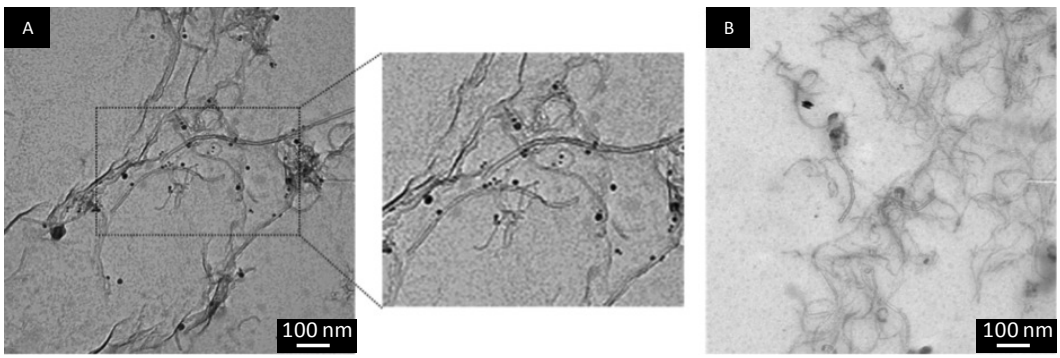

Figure II.11: TEM images of Ab-MWCNT conjugate **C14** (A) and ammonium-functionalized MWCNTs **C4** (B) after labeling with gold nanoparticles.

II.6 Molecular Recognition Analysis

The biological affinity of the coupled antibody towards its antigen was assessed by surface plasmon resonance (SPR). This technique allows the measurement of the biospecific interaction between the antibody and its antigen in real time. The principle is to immobilize the antigen on a sensor chip surface while the antibody is allowed to continuously flow over this surface. The interaction is then detected by surface plasmon resonance, registered and presented as a sensorgram (Figure II.12). The registered sensorgram offers the possibility to calculate the kinetic parameters for the interaction, *i.e.* the association and dissociation rate constants (k_a and k_d, respectively). All SPR measurements presented in the manuscript were performed in collaboration with Dr. O. Chaloin.

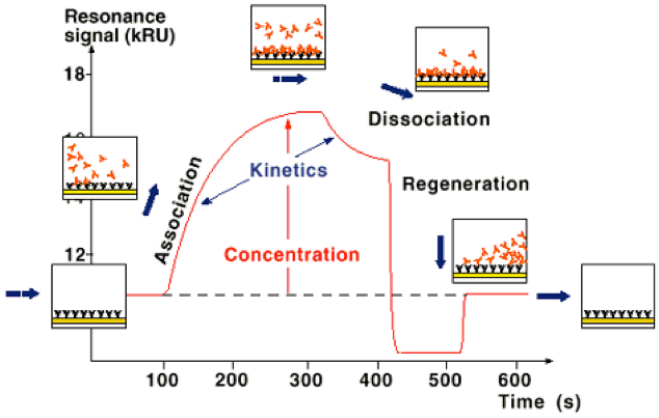

Figure II.12: Sensorgram showing the interaction between the analyte and the ligand.

To determine the biological activity of the Ab-CNT conjugates, we performed the synthesis of its antigen and registered the sensorgrams of the native antibody, the thiolated antibody, the *f*-CNTs (both oxidized- and ammonium-functionalized CNTs) and the CNT-Ab conjugates **C12** and **C14**.

The antigen sequence ^{296}HGVTSAPDTRPAPGSTAPPA^{315} corresponds to the 20-mer sequence composing the variable number tandem repeat (VNTR) region of the MUC1 protein [Gendler, S. J., *et al.* 1990]. To immobilize the peptide on the chip surface, we exploited a bioaffinity approach based on the streptavidin-biotin interaction. The bicyclic ring on the biotin interacts with streptavidin, giving one of the strongest known non-covalent interaction ($K_D = 4 \cdot 10^{-14}$ M). In our case, streptavidin molecules were bound onto the dextran-coated chip by activation with EDC/NHS whereas biotin was introduced on the antigen sequence. In particular, we introduced at the *N*-terminal part of the peptide sequence a lysine residue that contains a molecule of biotin in its side chain. The antigen peptide was prepared by solid phase peptide synthesis by Dr. J.-P. Briand

and characterized by HPLC (high pressure liquid chromatography) and mass spectrometry (Figure II.13).

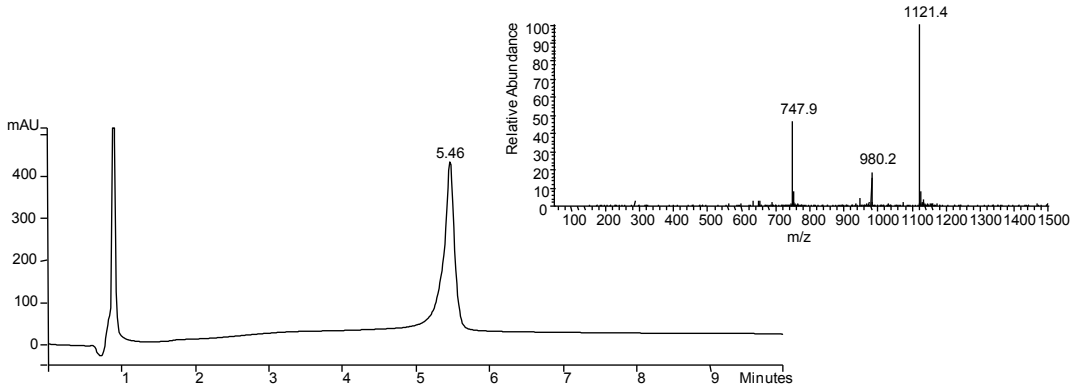

Figure II.13: HPLC chromatogram and mass spectrum (*m/z*: calcd 2241.5) of antigen sequence (peptide MUC1, ^{296}HGVTSAPDTRPAPGSTAPPA^{315}).

By using a similar approach, we prepared a "scrambled" antigen. Indeed, we synthesized a second peptide with the same number and type of amino acids but placed at different positions in the peptide sequence. The "scrambled" antigen (APHADPSTPGAPSVTPRTAG) was similarly characterized by HPLC and mass spectrometry (Figure II.14). This sequence enabled us to evaluate the non-specific component of the binding.

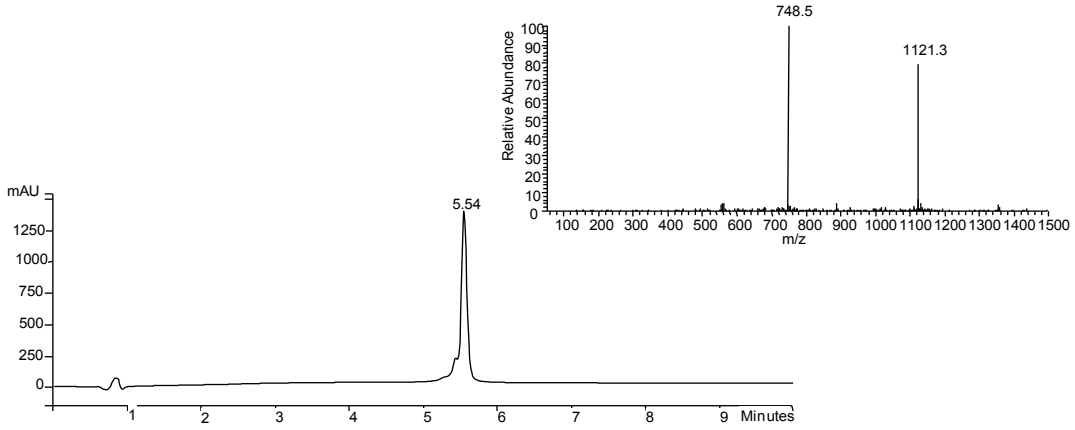

Figure II.14: HPLC chromatogram and mass spectrum (*m/z*: calcd 2241.5) of scrambled antigen (peptide scrambled MUC1, APHADPSTPGAPSVTPRTAG).

As showing in Figure II.15, the antibody recognized only the antigen (curve a) while the binding between "scrambled" antigen and the antibody (curve b) due to non-specific interactions was very weak. The strength of the binding (affinity) is determined by the equilibrium dissociation constant K_D (K_D=k_d/k_a). The value measured for this interaction was K_D = (1.65 ± 0.23) × 10^{-8} M, typical of the antigen/antibody interaction (Altschuh, D., *et al*. 1992).

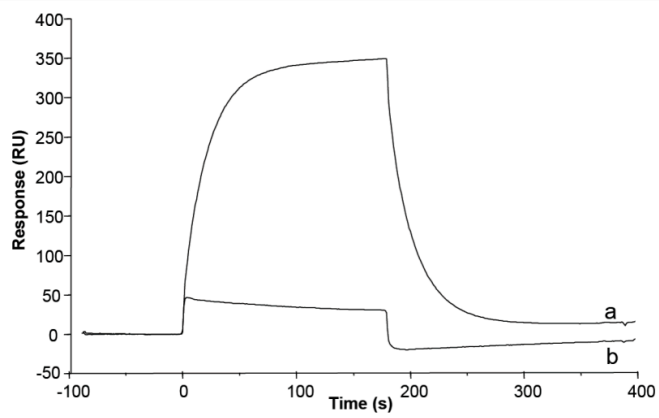

Figure II.15: Sensorgrams showing specific binding between antigen and antibody (a) and non-specific binding (b) between scrambled antigen and antibody.

The biological affinity of the thiolated antibody was then examined. We found that the introduction of free thiol groups did not alter the biological properties of the native antibody ($K_D \sim 10^{-8}$ M). We also performed control experiments using ox-MWCNTs and ammonium-functionalized CNTs to rule out non-specific binding between the antigen and the nanotubes. Finally, we assessed the interaction of the Ab-MWCNT constructs **C12** and **C14** with the antigen (Figure II.16).

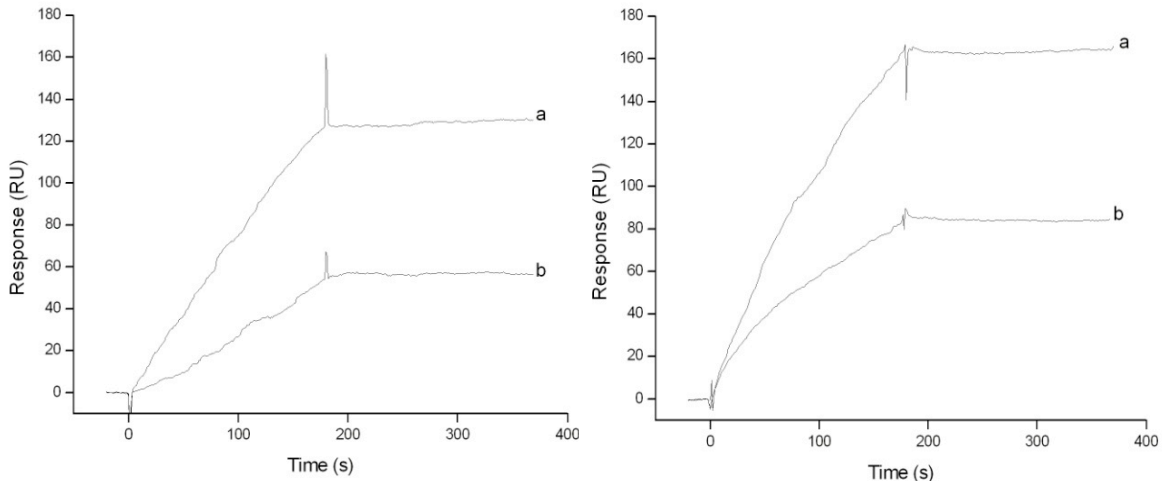

Figure II.16: Sensorgrams showing the binding of Ab-MWCNT conjugates **C12** (left) and **C14** (right) with the antigen. Concentrations were 100 (a) and 25 (b) µg/mL.

All conjugates were able to recognize the antigen on the sensor chip, however it was not possible with the CNT-Ab constructs to obtain quantitative binding information from the SPR, for two main reasons: 1) a precise molecular weight for CNTs (being heterogeneous material) cannot be determined, therefore K_D values could not be obtained from the sensorgrams; 2) Ab attachment onto the conjugates is likely to be unevenly distributed along the nanotubes, that may affect their antigen binding capacity. Based on the results obtained, covalent attachment of Ab onto CNTs does not seem to affect their recognition capacity, demonstrating that the conjugates can be used to

specifically target cancer cells over-expressing MUC1 receptors. As it has been recently demonstrated using a different system, the kinetic parameters of ligand-receptor interaction could be taken as indicative of the potential biological *in vitro* and *in vivo* activity of the analyzed construct [Pavet, V., *et al.* 2010]. The detailed characterization of the Ab-MWCNT conjugates performed using TGA, TEM, gel electrophoresis and SPR confirmed that Ab was covalently bound and biologically functional once onto the nanotubes, illustrated by the highly preserved antigen binding capacity for all conjugates.

II.7 Antibody-Carbon Nanotube Cell Biology

A fundamental aspect related to the development of new therapeutics based on Ab-CNT conjugates is the evaluation of their interaction with different cell lines. In particular, in collaboration with the group led by Prof. Kostas Kostarelos in London, we studied the cytotoxicity and the *in vitro* cellular uptake of the conjugates and their precursors. Moreover, we were interested in the assessment of the capacity of our constructs to specifically target cancer cells over-expressing the antigen MUC1 and to evaluate the cellular trafficking within the different cell compartments.

The first step in the evaluation of the cellular uptake of the Ab-CNT conjugates consisted in the study of cell biology of the antibody alone. Breast cancer (MCF-7) and lung cancer (Calu6) cell lines were used to detect the capacity of the antibody to be internalized. These two cell lines were chosen because MCF-7 cells overexpress the antigen MUC1 whereas Calu6 are MUC1 negative cells. The cellular uptake was evaluated by confocal laser scanning microscopy, after labeling the antibody with a fluorescent probe (AlexaFluor® 488). As shown in Figure II.17, only MCF-7 cells were able to internalize the antibody. On the contrary, Calu6 cells did not internalize the antibody. These results confirmed the specificity of the selected antibody towards the antigen MUC1.

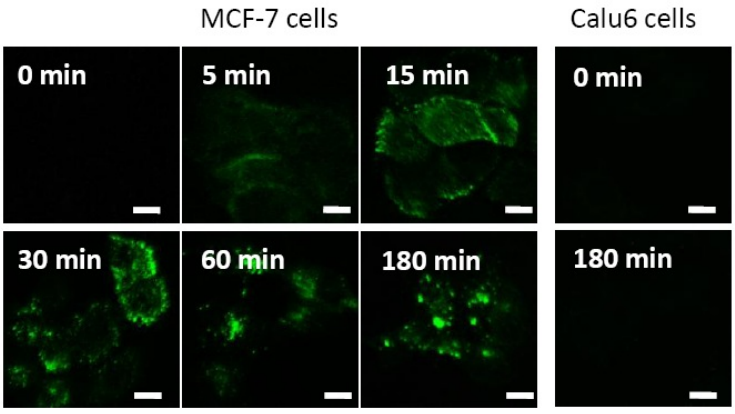

Figure II.17: Confocal microscope images of the cellular uptake of hCTM01 IgG in MCF-7 and Calu6 cells at different time points. Scale bar: 10 μm.

To understand the cellular uptake mechanism of the antibody, MCF-7 cells were treated with specific pathway inhibitors, such as low temperature or energy-depleted conditions. The results, obtained in the laboratory in London, suggested a clathrin-dependent endocytosis pathway. In general, endocytosis can be divided into two broad categories: phagocytosis (the uptake of large particles) and pinocytosis (the uptake of fluids and solutes) [Sahay, G., *et al.* 2010]. Pinocytosis can be further classified as clathrin-dependent endocytosis (CDE) and clathrin-independent endocytosis (CIE). In clathrin-dependent endocytosis, the ligand is recognized by a plasma membrane receptor and the complex receptor-ligand is then internalized through a clathrin-coated vesicle. Within cells the clathrin coating is eliminated and the vesicles fuse with the early endosomes where they are sorted to late endosomes/lysosomes for degradation, to trans-Golgi network or to the recycling endosomes to be transported back to plasma membrane [Grant, B. D., *et al.* 2009].

Before studying the cellular uptake, we investigated the cytotoxic effects of the carbon nanotube conjugate **C12**, the antibody and the ox-MWCNTs **C1** on both cell lines (Figure II.18).

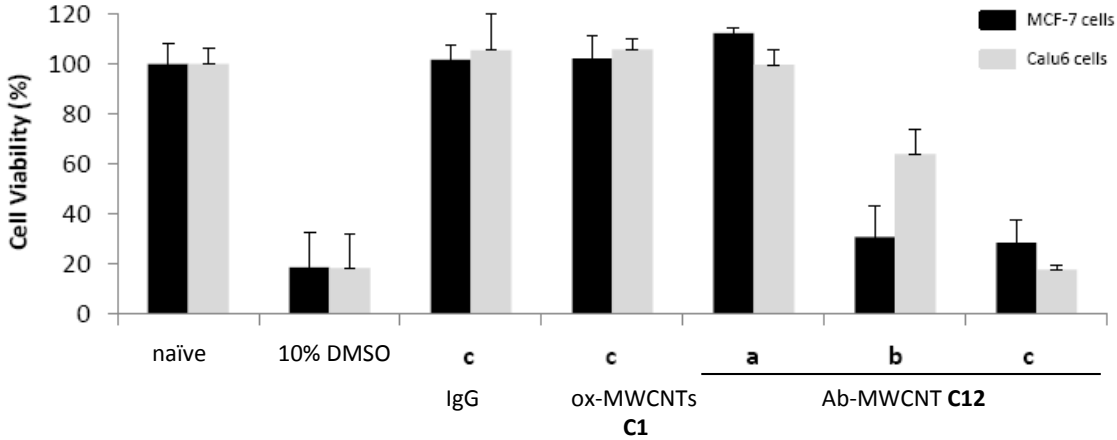

Figure II.18: *In vitro* cytotoxicity of Ab-MWCNT **C12** in MCF-7 and Calu6 cells after 24 hours incubation at different concentrations. **a**) at CNT concentration of 10 µg/mL; **b)** at CNT concentration of 50 µg/mL; **c)** at CNT concentration of 100 µg/mL, equals to IgG concentration of 50 µg/mL. 10% DMSO was used as a positive control for cytotoxicity.

In these experiments carbon nanotubes were dispersed in PBS at a concentration of 500 µg/mL and further diluted in cell culture medium to final concentration of 10, 50 and 100 µg/mL. MCF-7 and Calu6 cells were then incubated for 24 hours and the cytotoxicity evaluated by lactate dehydrogenase (LDH) assay. LDH is a soluble cytosolic enzyme that is released into the culture medium following loss of membrane integrity resulting from cell death (apoptosis or necrosis). LDH activity, therefore, can be used as an indicator of cell membrane integrity and serves as a general means to assess cytotoxicity resulting from chemical compounds or environmental toxic factors. LDH assay measures LDH activity present in the culture medium using a coupled two-step reaction. In the first step, LDH catalyzes the reduction of NAD^+ to NADH by oxidation of lactate to pyruvate. In the second step of the reaction, pyruvate reacts with a tetrazolium salt to give a highly-

colored water-soluble dye (formazan), which is detected spectrophotometrically. We observed a cytotoxic effect only for CNT-Ab **C12** conjugate at high concentrations (50 and 100 µg/mL). This is probably due to aggregation phenomena of the nanotube conjugates.

Based on these results, we then studied the cellular uptake at concentrations up to 10 µg/mL by confocal microscopy and flow cytometry. Because of the absence of a fluorescence probe, the antibody alone (used as control) and the conjugate **C12** were visualized by staining with a fluorescently-labeled secondary antibody (anti-human Cy3). We analyzed the cell fluorescence at different time points (1 hour, 3 hours and 24 hours) and at two concentrations (10 µg/mL and 2 µg/mL) for both cell lines, as displayed in the diagrams in Figure II.19.

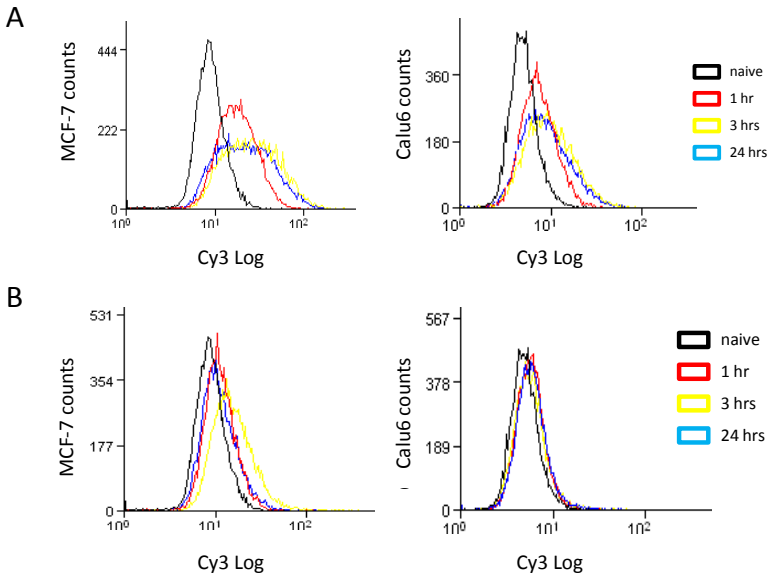

Figure II.19: Cellular uptake of Ab-MWCNTs **C12**. Flow cytometry of the cellular uptake of Ab-MWCNTs **C12** in MCF-7 and Calu6 cells up to 24 hours incubation at different CNT concentrations [10 µg/mL (A) and 2 µg/mL (B)].

Experiments with CNT untreated cells were performed as control and represented by the black curves in Figure II.19. The different colors of the curves correspond to the different time points: red for 1 hour, yellow for 3 hours and blue for 24 hours. The fluorescence intensity inside MCF-7 cells is stronger than the control and varies with the time. On the contrary, the fluorescence intensity for MUC1 negative cells is less significant and tends to be constant with time. These results show that the Ab-MWCNTs **C12** is mainly bound and/or uptaken by MCF-7 cells. We repeated the study at a concentration of 2 µg/mL (Figure II.19B). In this case the non specific binding to Calu6 cells was absent, confirming the selectivity of the conjugate for MUC1 positive cells. However, the interaction with MCF-7 cells is also reduced although not completely abolished.

To further define the uptake mechanism, MCF-7 and Calu6 cells were incubated with Ab-MWCNTs **C12** at concentration of 10 µg/mL and observed using confocal microscope (Figure II.20).

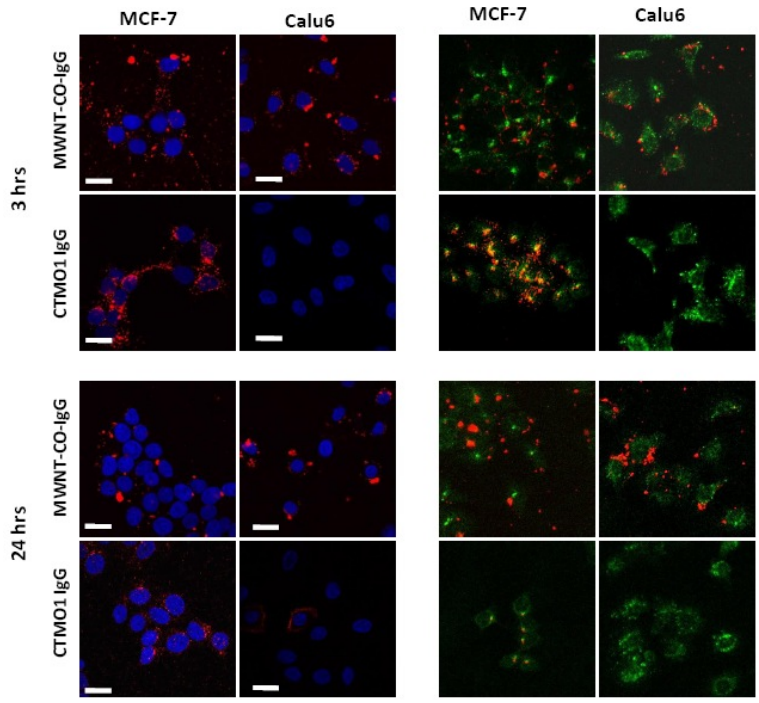

Figure II.20: Cellular uptake of Ab-MWCNTs **C12**. Confocal microscopy images of the cellular uptake of Ab-MWCNTs **C12** in MCF-7 and Calu6 cells at CNT concentration of 10 µg/mL after 3 hours or 24 hours of incubation. IgG alone or the construct **C12** were visualized by staining the antibody using anti-human Cy3 (red), nucleus were visualized by staining with DAPI (blue) and early endosomes were visualized by staining with anti-EEA (anti-early endosome antigen, green). Scale bar: 20 µm.

After treatment with the conjugate or the antibody alone for 3 or 24 hours, the cells were washed and stained with DAPI, a blue-fluorescent dye for nuclei. Antibody alone and the conjugate Ab-MWCNT **C12** were visualized by staining with a red secondary antibody (anti-human Cy3). As shown in Figure II.20, the uptake of the antibody alone was limited only to MUC1 positive cell lines (MCF-7) and after 3 hours it tends to localize into the cytoplasm. For the conjugate **C12**, we observed that the cellular uptake was less intense and had a punctate pattern. Moreover, the construct was internalized not only by the MUC1 positive cell lines but to a lesser extent in Calu6 cells, confirming the flow cytometry results.

To differentiate between endosome-dependent (endocytosis) or membrane permeation ("nanoneedle") uptake mechanisms, cells were treated with anti-EEA, a green marker for early endosomes. The resulting images of this treatment showed that the antibody alone and endosomes colocalize to produce yellow staining only in MCF-7 cells, suggesting receptor-mediated endocytosis. On the contrary, for the construct **C12** we did not observe colocalization. This is probably due to the fact that the construct is likely localized at the level of the plasma membrane.

These findings were further investigated by incubating MCF-7 and Calu6 cells with Ab-MWCNTs **C12** at a concentration of 2 µg/mL and by observing the internalization at different time points up to 3 hours (Figure II.21).

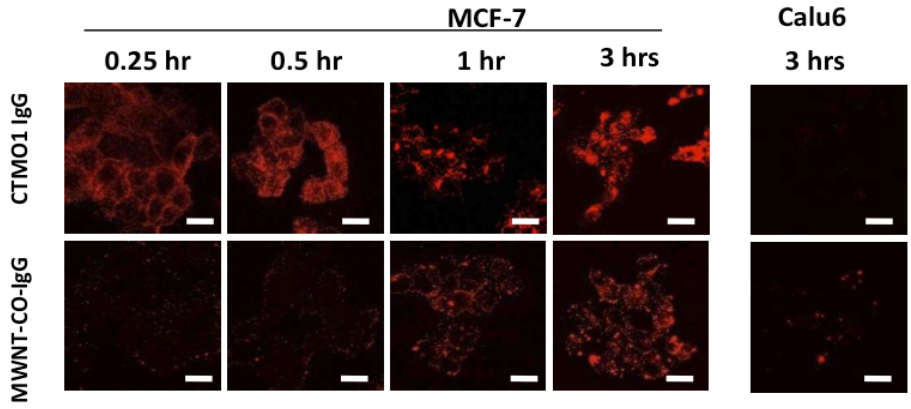

Figure II.21: Cellular uptake of Ab-MWCNTs **C12**. Confocal microscopy images of the cellular uptake of Ab-MWCNTs **C12** in MCF-7 and Calu6 cells at CNT concentration of 2 µg/mL at different time points. IgG alone or the construct **C12** were visualized by staining the antibody using anti-human Cy3 (red). Scale bar: 20 µm.

After treatment with red-fluorescent secondary antibody anti-human Cy3, the observation of the cells revealed that the uptake was more rapid for the antibody alone than for the construct **C12**. Initial uptake of the antibody alone appeared localized at the level of the plasma membrane but after 30 minutes the antibody accumulated diffusely in the cytoplasm. The Ab-MWCNTs were internalized only after 3 hours and they were mainly retained at the level of the cellular membrane.

This result is probably related to dispersibility issues of MWCNTs produced by Nanocyl. Indeed, it was not possible to perform cell biology studies for the other Ab-MWCNT conjugate **C14** due to the low dispersibility of the material. Another critical point that can be taken into account to explain the reduced uptake is the big size of the Ab-MWCNT conjugate.

In view of these initial results and to overcome the low intracellular uptake of the Ab-CNT conjugate, we decided therefore to prepare two new series of conjugates (see Chapter III). To circumvent the dispersibility issues, a first series of conjugates was prepared by changing the type of MWCNTs and using as starting material MWCNTs produced by another company (NanoAmor). These nanotubes present a different aspect ratio and morphology compared to Nanocyl material. Table II.1 displays the characteristics of both MWCNTs after oxidation.

Table II.1: Characteristics of both types of ox-MWCNTs.

Entry	Diameter/nm	Functional groups (COOH)/mmol g^{-1}	Weight loss (%)
ox-MWCNTs (Nanocyl)	9.5	1.9	8.7
ox-MWCNTs (NanoAmor)	20-30	1.7	7.3

Carbon nanotubes from NanoAmor have a diameter ranging from 20 to 30 nm, while Nanocyl sample has a narrower diameter (9.5 nm). Analysis of TEM images of ox-MWCNTs afforded a mean length value of around 400 nm for both materials. However, length distribution is larger for NanoAmor's sample (Figure II.22).

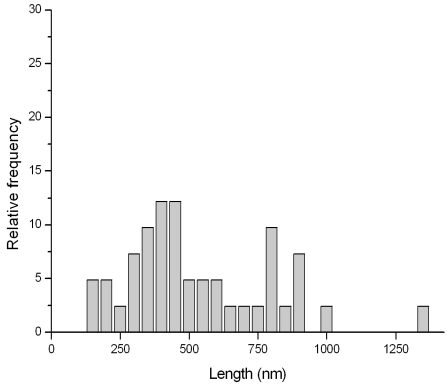

Figure II.22: Length distribution of ox-MWCNTs produced by NanoAmor obtained from 165 measurements. For comparison with ox-MWCNTs from Nanocyl see Figure II.2.

Their morphology is also different as MWCNTs from NanoAmor appear less regular and more distorted (Figure II.23). All these factors seem to contribute to the higher dispersibility observed for NanoAmor ox-MWCNTs.

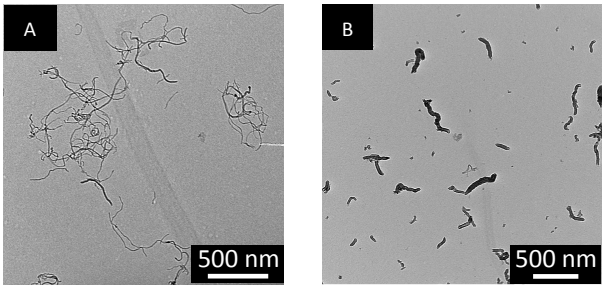

Figure II.23: TEM images of oxidized MWCNTs produced by Nanocyl (A) and by NanoAmor (B).

To overcome the critical point of the big size of the conjugate Ab-CNT, we decided to reduce its size by preparing a second series of conjugates where the size of the bound protein varied. In particular, two fragments of the antibody such as the fragment antigen binding (Fab) and the single chain variable fragment (scFv) were bound to MWCNTs, produced by Nanocyl and NanoAmor. The synthesis and characterization of these new series of conjugates are discussed in the next chapter.

II.8 Conclusions

Functionalization of carbon nanotubes represents a versatile approach to prepare new hybrid material. After oxidation treatment and subsequent amidation reaction or 1,3 dipolar cycloaddition, MWCNTs were derivatized with an antibody or an imaging probe (fluorescent probe or radioisotope).

Two strategies for the functionalization of MWCNTs with the antibody were developed. The antibody was covalently coupled either at the tips or onto the sidewall of CNTs. In the first strategy we used direct amidation reaction between the Ab and the carboxylic groups present at the tips of ox-MWCNTs. The second strategy allowed us to conjugate the Ab onto the sidewall of maleimido-functionalized CNTs *via* chemical ligation. The physico-chemical characterization of both constructs confirmed the presence of the Ab covalently bound to CNTs and the conservation of its biological activity. This was confirmed also by preliminary *in vitro* studies showing the ability of the hybrid material to bind the cells expressing the antigen (MUC1 protein).

Although both approaches were versatile, we decided to choose the 1,3-dipolar cycloaddition strategy for the preparation of a second generation of Ab-CNT constructs (see Chapter III). The 1,3-dipolar cycloaddition approach offers the advantage of freely available carboxylic functions mainly located at the tips of the nanotubes that can allow the conjugation of a second moiety to generate multifunctional systems. In this context the CNTs were functionalized on their sidewall with the antibody or a fragment of the antibody and an imaging probe at their tips.

Chapter III: Multi-functionalization of Carbon Nanotubes with Antibodies and Tracking Probes

Based on the results on the mono-functionalization of carbon nanotubes with the antibody, we decided to synthesize a second generation of Ab-CNT conjugates. The design of these constructs was aimed to combine an imaging probe and a targeting or therapeutic agent on the same CNT-based platform. We used the antibody anti-MUC1 or fragments of this antibody (Fab and scFv, Figure III.1) for their ability to target cancer cells. The Fab is the region on the Ab that binds to the antigen. It is composed of one constant and one variable domain of each of the heavy and the light chain and its size is 48 kDa (the entire Ab molecular weight is 150 kDa). The scFv is the smallest fragment (21 kDa) of the antibody still able to retain the same specificity of the full immunoglobulin towards the antigen.

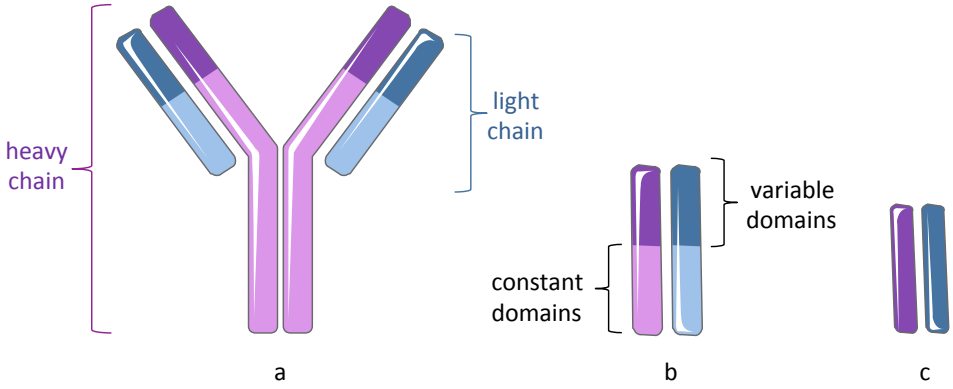

Figure III.1: Schematic representation of conventional antibody (a), Fab (b) and scFv (c).

In the frame of this project, we had the opportunity to develop also a therapeutic construct. Indeed, by binding a fragment of a different antibody (VHH, variable domain of the heavy chain of heavy-chain antibody) displaying simultaneous targeting and therapeutic activities, we obtained a therapeutic conjugate. In both cases, the presence of an imaging probe covalently bound to CNTs enabled us to directly image and localize CNTs in cancer cell lines or in animals by using confocal microscopy or micro-SPECT, respectively.

The suitable strategy to prepare these new constructs appeared to be the double functionalization approach. Indeed, the sidewall of carbon nanotubes could be derivatized with the immunoglobulin while the tips could be functionalized with the imaging probe (either fluorescein or DTPA). We thus exploited the combination of the 1,3-dipolar cycloaddition followed by an amidation reaction at the oxidized tips of MWCNTs.

Some synthetic strategies for the preparation of double functionalized carbon nanotubes with a therapeutic agent and an antibody have been already reported in the literature. For example, Kong

and co-workers functionalized non-covalently the surface of ox-MWCNTs with the recombinant ricin toxin A (RTA) and an anti-HER2 antibody. The complex displayed increased cellular uptake capability of this toxin and enhanced selectivity towards cancer cell lines overexpressing the antigen HER2 [Weng, X., *et al*. 2009]. Li *et al*. reported the preparation of a targeting therapeutic system by functionalization of ox-SWCNTs with an antibody *via* classical peptide coupling (amide bond formation) and physical adsorption of a drug (doxorubicin) onto the nanotube surface. This conjugate was selectively internalized by the multidrug resistant human leukemia (K562R) cells and the drug was rapidly released from the nanotube surface after exposure to near-IR radiation. Compared to the treatment with the free doxorubicin, the conjugate displayed increased therapeutic activity with an enhancement of cytotoxicity of 242% [Li, R., *et al*. 2010]. These approaches present however as limiting factor the presence of functionalities simply adsorbed onto the CNT surface. This may restrain the application of the obtained constructs for *in vivo* studies because these conjugates present a reduced stability. Indeed, the therapeutic or the targeting molecule can be desorbed or exchanged with serum proteins and other components present in biological fluids resulting in premature dissociation of the moiety from the delivery system.

To circumvent this limitation, the functionalities can be stably attached on the nanotube backbone through the formation of a covalent bonding. Ruggiero *et al*. reported the covalent functionalization of SWCNTs with a therapeutic radioisotope and the tumor neovasculature-targeting antibody E4G10. A fraction of the amine groups introduced by the 1,3-dipolar cycloaddition reaction were first reacted with a chelating agent of a radioactive probe and then a suitable linker for the antibody conjugation was conjugated to the remaining free ammonium groups [Ruggiero, A. *et al*. 2010a]. In another study, SWCNTs were simultaneously functionalized with a targeting agent for squamous cancer cells (epidermal growth factor) and cisplatin by simply mixing the two molecules of interest with carbodiimide-activated oxidized nanotubes [Bhirde, A. A., *et al*. 2009]. Although both approaches afforded constructs showing interesting therapeutic properties, these synthetic routes suffer from poor control over the entire functionalization process, especially on the control of the level of functionalization.

Compared to these strategies, our approach afforded the possibility to covalently double functionalize CNTs by conferring high chemical stability to the constructs and limiting at the same time the presence of adsorbed functionalities that could be released from the nanotube surface. Moreover, this strategy offers good control over the entire process as the two moieties are attached at non-competing positions.

III.1 Double Functionalization of Carbon Nanotubes

We prepared double functionalized carbon nanotubes using as starting material carbon nanotubes produced either from Nanocyl or NanoAmor. The nanotube-based constructs will be therefore categorized with letters **a** and **b** to denote Nanocyl and NanoAmor conjugates, respectively. Scheme III.1 shows the strategy followed to obtain double functionalized MWCNTs. Carbon nanotubes were derivatized by introduction of amine functions at the tips and onto the sidewall blocked by two orthogonal protecting groups, a phthalimide (Pht) moiety or a *tert*-butoxycarbonyl (Boc) group, respectively.

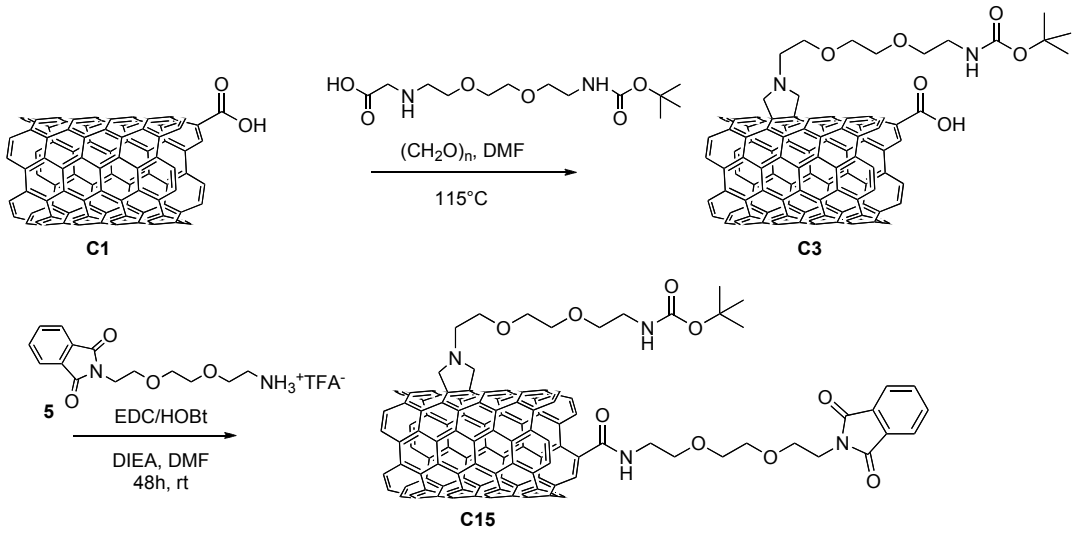

Scheme III.1: Preparation of doubly functionalized MWCNTs.

Pristine MWCNTs were first purified and shortened by oxidation reaction in acidic conditions, as reported in Chapter II. Subsequently, ox-MWCNTs were functionalized at the sidewall with ammonium groups through the 1,3-dipolar cycloaddition of *in situ* generated azomethine ylides. The number of amine functions was assessed by quantitative Kaiser test, after cleavage of the Boc protecting groups using HCl in dioxane on a small quantity of material. The loading values were 120 μmol/g (**a**) and 80 μmol/g (**b**).

The carboxylic acids were then converted to the corresponding amides through the coupling with the amine **5** bearing the Pht protecting group. The amine **5** was prepared by protecting the free amine function of Boc-monoprotected triethylene glycol **1** (Chapter II) with Pht group and subsequent Boc cleavage in acidic condition (trifluoroacetic acid in dichloromethane). Because of the presence of acid-labile Boc groups onto the sidewall, the amidation reaction was carried out *via* a carbodiimide-activated approach. Indeed, the activation with oxalyl chloride as described in Chapter II would lead to the simultaneous Boc deprotection, as HCl would be generated during the

reaction. The selective cleavage of the phthalimide group of *f*-MWCNTs **C15** was achieved by using hydrazine in ethanol (Scheme III.2). The Kaiser test was performed to determine the amount of NH_2 functions introduced by amidation. The loading values were found 180 µmol per gram of nanotubes (**C16a**) and 120 µmol per gram of nanotubes (**C16b**).

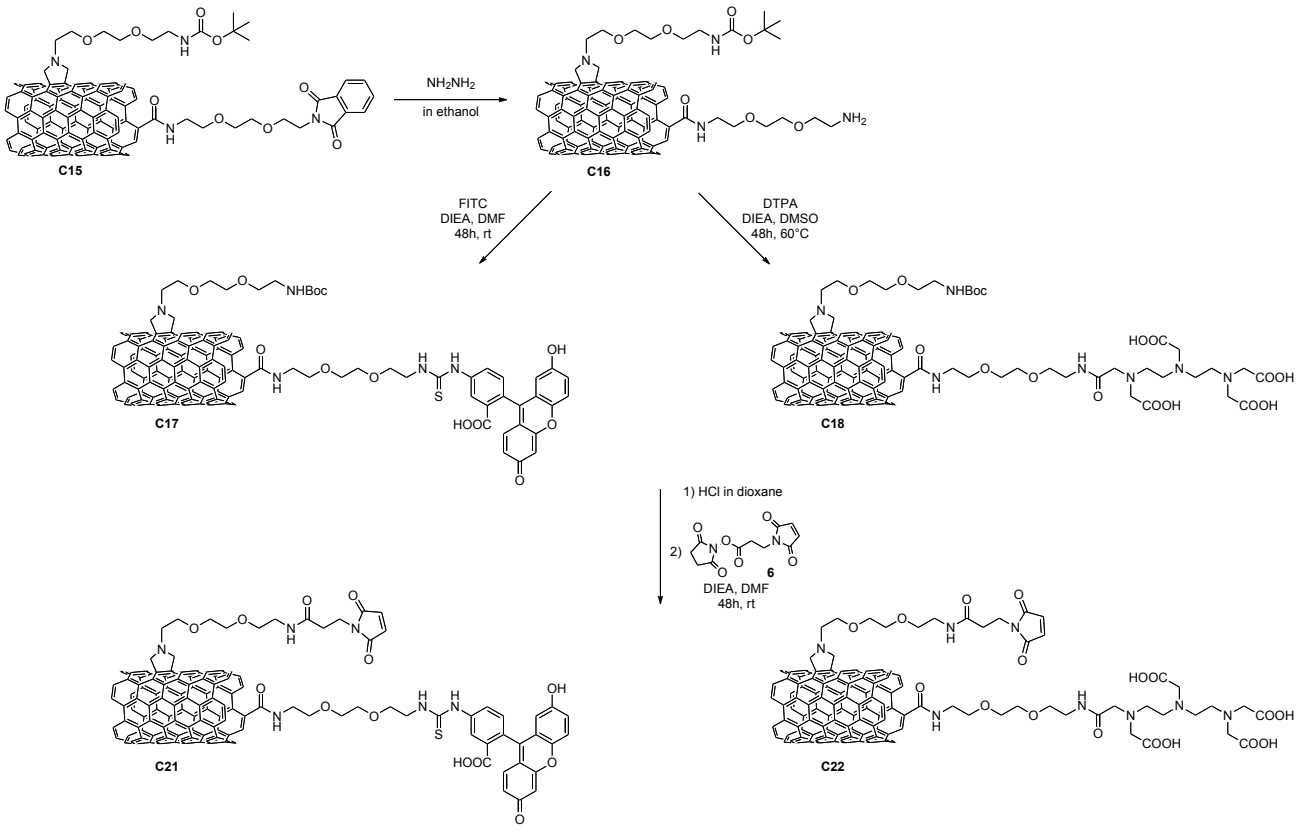

Scheme III.2: Preparation of *f*-MWCNTs **C21** and **C22**.

After removal of the phthalimide groups (**C16**), either DTPA or FITC were coupled to the free amine functions to allow subsequent *in vivo* or *in vitro* studies, respectively. The loadings of the imaging probes on *f*-MWCNTs **C17** and **C18** were determined by Kaiser test. Afterwards, the Boc groups were removed by acid treatment and the amines onto the sidewall were derivatized with the heterobifunctional crosslinker **6** to give **C21** and **C22**, as displayed in Scheme III.2. **C21** and **C22** were characterized by Kaiser test to determine the loading of the maleimido moieties introduced. Tables III.1 and III.2 summarize the loading values obtained for conjugates **C21** and **C22**, respectively.

Table III.1: Loading values for conjugate FITC-MWCNT-maleimide **C21**.

Entry	FITC loading µmol/g	Maleimide loading µmol/g
f-MWCNT **C21a** Nanocyl	110 (yield: 60%)	90 (yield: 75%)
f-MWCNT **C21b** NanoAmor	60 (yield: 50%)	40 (yield: 50%)

Table III.2: Loading values for conjugate DTPA-MWCNT-maleimide **C22**.

Entry	DTPA loading µmol/g	Maleimide loading µmol/g
f-MWCNT **C22a** Nanocyl	140 (yield: 77%)	90 (yield: 75%)
f-MWCNT **C22b** NanoAmor	75 (yield: 63%)	30 (yield: 38%)

We observed an overall decrease of the different loadings for conjugates prepared using NanoAmor MWCNTs as starting material. This is probably related to the presence of higher carbon content per gram of material. Indeed, these nanotubes have a bigger diameter and more internal layers than Nanocyl MWCNTs that cannot be functionalized as the reaction occurs only on the outer layer.

Finally, *f*-MWCNTs **C21** and **C22** were coupled to the Ab, Fab or scFv. For clarity reasons, in Scheme III.3 the preparation of FITC-derivatized CNTs **C23**, **C25** and **C27** is shown while the corresponding DTPA-derivatized conjugates **C24**, **C26** and **C28** are not displayed.

Before coupling the antibody to *f*-MWCNTs **C21** or **C22**, we introduced free thiol groups using Traut's reagent, as already described in Chapter II.

Fab and scFv could be directly conjugated to the CNTs as they contain exposed thiols. However, in solution these SH functions easily oxidize to form disulfide bridges, giving the corresponding dimer of the protein. Prior to coupling Fab or scFv, we performed a reduction step by incubating the protein with a mild reductant (2-mercaptoethylamine). A parameter that is important to control is the incubation time. This parameter was determined by varying the incubation time and evaluating the concentration of the dimer still present by gel electrophoresis. By this procedure we determined that two hours was the optimal incubation time to use. The band of the dimer disappeared while the monomer was still intact. Indeed, no other minor bands appeared in the electrophoresis gel that could be due to over-reduction of the protein.

After two hours the reduction reaction was stopped and the reductant was eliminated by buffer exchange. Once the dimers were reduced, the Fab or the scFv were immediately coupled to the CNTs.

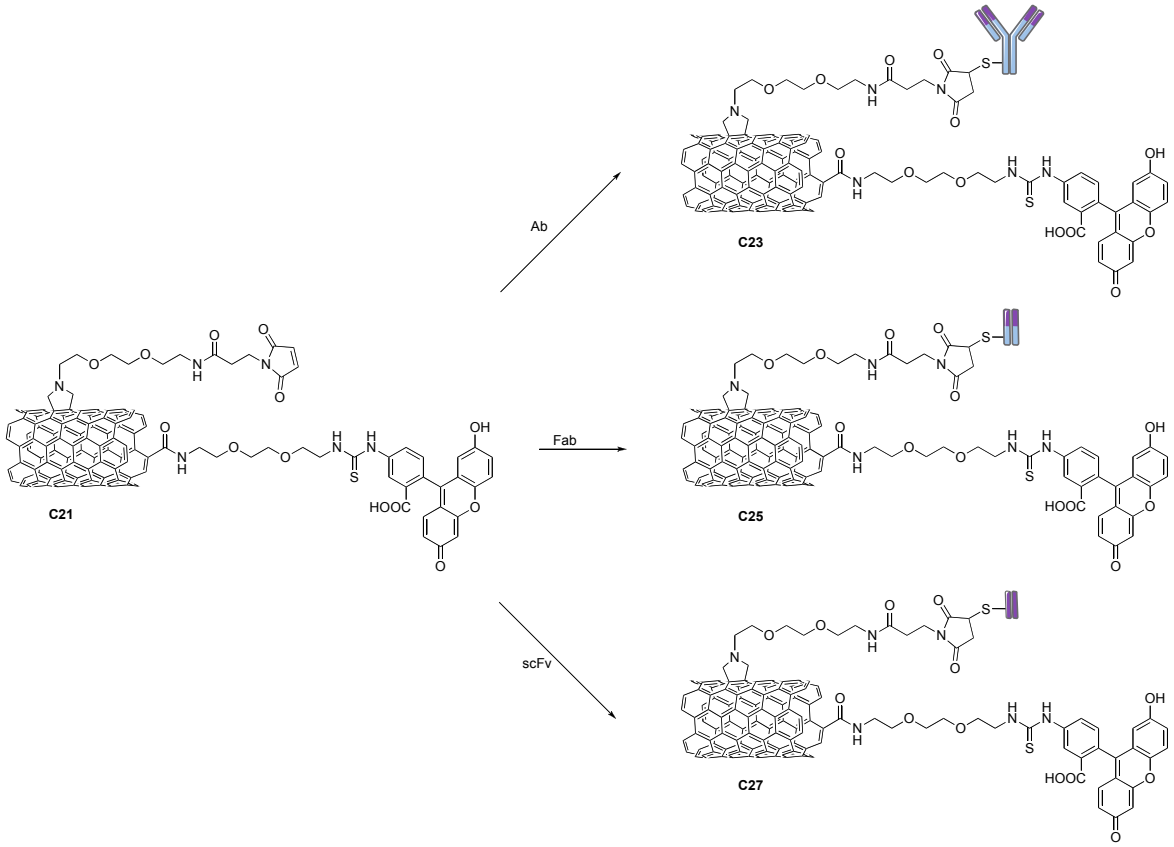

Scheme III.3: Double functionalization of *f*-MWCNTs **C21** with the antibody or its fragments (Fab and scFv).

The obtained double functionalized CNTs were fully characterized by different techniques including transmission electron microscopy, thermogravimetric analysis, gel electrophoresis and surface plasmon resonance.

TEM was used to confirm that the morphology of the constructs after each functionalization step was intact (Figure III.2).

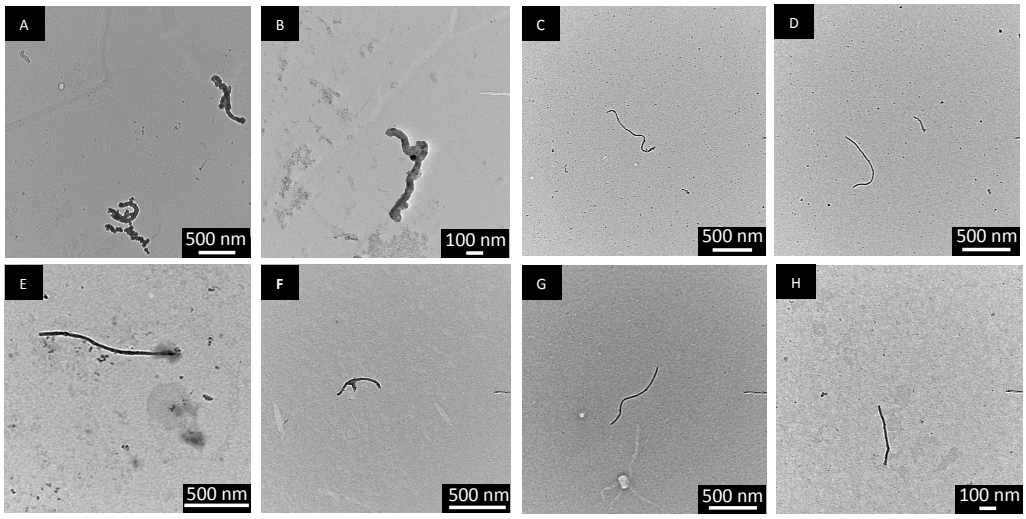

Figure III.2: TEM images of Ab-MWCNTs-FITC **C23b** (A), Ab-MWCNTs-DTPA **C24b** (B), Ab-MWCNTs-FITC **C23a** (C), Ab-MWCNTs-DTPA **C24a** (D), Fab-MWCNTs-FITC **C25a** (E), Fab-MWCNTs-DTPA **C26a** (F), scFv-MWCNTs-FITC **C27a** (G) and scFv-MWCNTs-DTPA **C28a** (H).

TGA was used to determine the loading of the conjugated proteins by comparing the weight loss of the final conjugates to their precursors (Figure III.3 and Figure III.4).

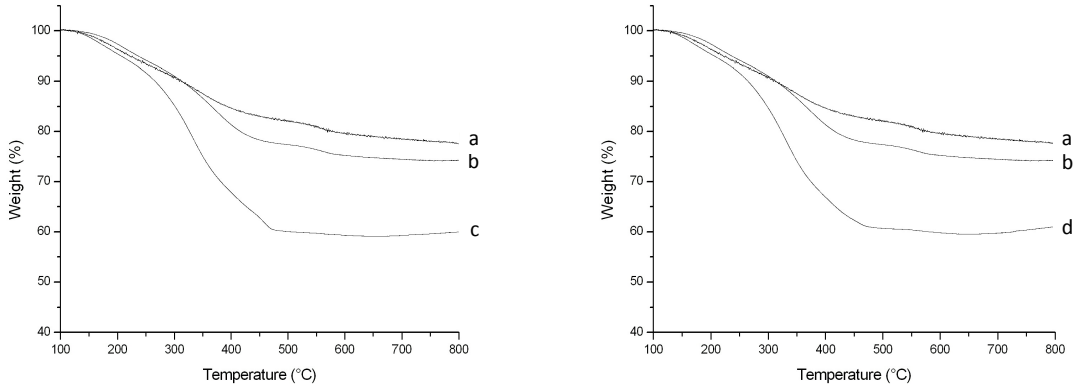

Figure III.3: TGA profiles of mono-functionalized MWCNTs **C3a** (a), double functionalized MWCNTs **C15a** (b), Ab-MWCNTs-FITC **C23a** (c) and Ab-MWCNTs-DTPA **C24a** (d).

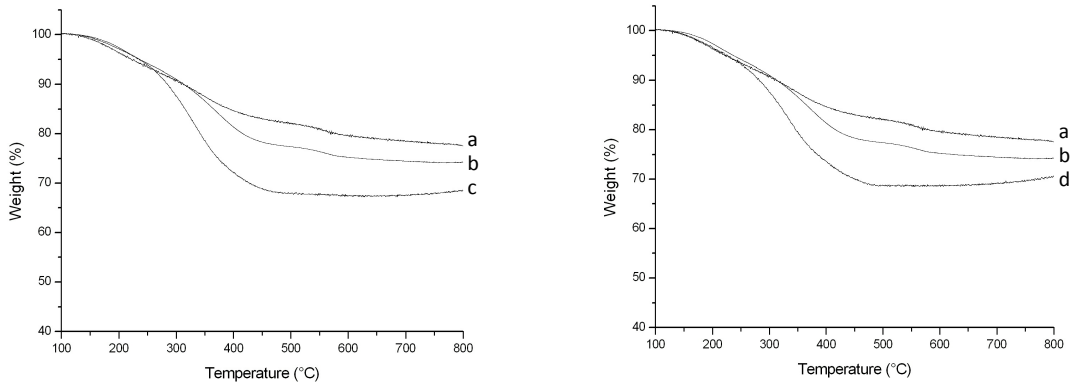

Figure III.4: TGA profiles of mono-functionalized MWCNTs **C3a** (a), double functionalized MWCNTs **C15a** (b), Fab-MWCNTs-FITC **C25a** (c) and scFv-MWCNTs-FITC **C27a** (d).

The loading of bound antibody or its fragments calculated by TGA and expressed in molarity are summarized in Table III.3.

Table III.3: Loading values for antibody or its fragments.

Entry	Antibody (µmol/g)	Fab (µmol/g)	scFv (µmol/g)
f-MWCNTs Nanocyl (**a**)	1.3	3	3.6
f-MWCNTs NanoAmor (**b**)	0.6	2.9	–

Note: the conjugates scFv-MWCNTs-DTPA and scFv-MWCNTs-FITC starting from NanoAmor MWCNTs were not synthesized.

The gel electrophoresis analysis confirmed the formation of a covalent bonding between the proteins and the CNTs. For conjugates **C23** and **C24**, the free antibody was used as reference (lane 1 in Figure III.5) in the analysis, conducted both under reducing and non-reducing conditions. As displayed in the Figure III.5, no antibody was detected in non-reducing conditions, proving the

formation of a covalent bond between the immunoglobulin and the CNTs (lanes 2 and 3). The gel conducted under reducing conditions confirmed that the protein bound to CNTs was intact.

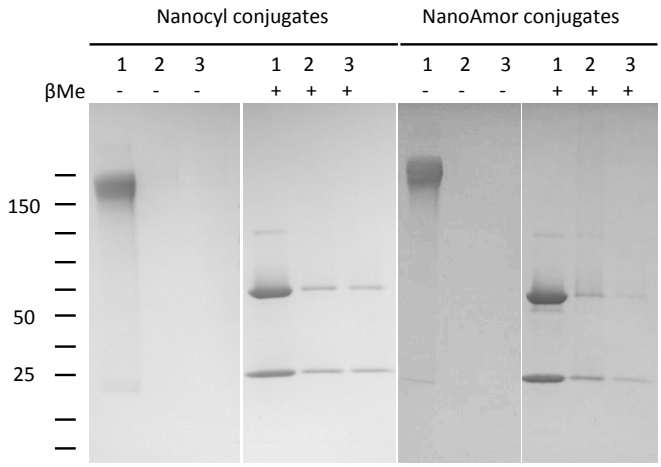

Figure III.5: Gel electrophoresis of Nanocyl conjugates **C23a** and **C24a** under non-reducing conditions (-βMe, β-mercaptoethanol) and reducing conditions (+βMe) (left); gel electrophoresis of NanoAmor conjugate **C23b** and **C24b** under non-reducing conditions (-βMe) and in reducing conditions (+βMe) (right). Lane 1: Ab reference; lane 2: Ab-MWCNT-FITC **C23** conjugate; lane 3: Ab-MWCNT-DTPA **C24** conjugate.

Figure III.6 displays the results obtained for Fab-MWCNT constructs. The gel electrophoresis analysis confirms the formation of a covalent bonding for both Fab-MWCNT-FITC **C25** (**a** and **b**) conjugate and for Fab-MWCNT-DTPA **C26a** construct. The protein is not denatured, as confirmed by the analysis conducted under reducing conditions.

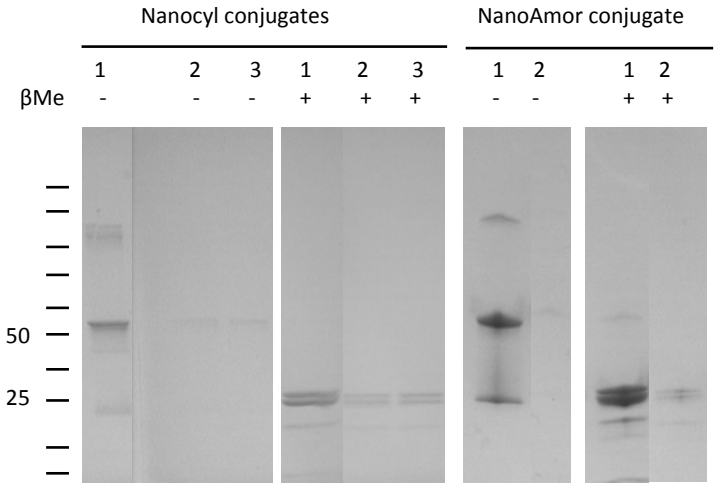

Figure III.6: Gel electrophoresis of Nanocyl conjugates **C25a** and **C26a** under non-reducing conditions (-βMe, β-mercaptoethanol) and reducing conditions (+βMe) (left); gel electrophoresis of NanoAmor conjugate **C25b** under non-reducing conditions (-βMe) and in reducing conditions (+βMe) (right). Lane 1: Fab reference; lane 2: Fab-MWCNT-FITC **C25** conjugate; lane 3: Fab-MWCNT-DTPA **C26** conjugate.

For the scFv-MWCNT conjugates **C27a** and **C28a** we obtained similar results, indicating covalent binding and intact protein after the conjugation (Figure III.7).

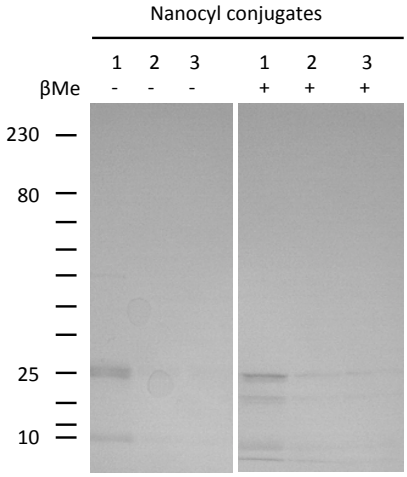

Figure III.7: Gel electrophoresis of Nanocyl conjugates **C27** and **C28** under non-reducing conditions (-βMe, β-mercaptoethanol) and reducing conditions (+βMe); Lane 1: scFv reference; lane 2: scFv-MWCNT-FITC **C27a** conjugate; lane 3: scFv-MWCNT-DTPA **C28a** conjugate.

Finally, we studied the functional activity of the Ab, Fab and scFv coupled to MWCNTs by surface plasmon resonance. As described in Chapter II, the antigen was bound to the chip and the different conjugates were analyzed to assess if the recognition capability is maintained after the conjugation to CNTs. Figure III.8 displays the results obtained for the new Ab-MWCNT conjugates **C23a** and **C24a**. Both conjugates were able to recognize the antigen on the sensor chip.

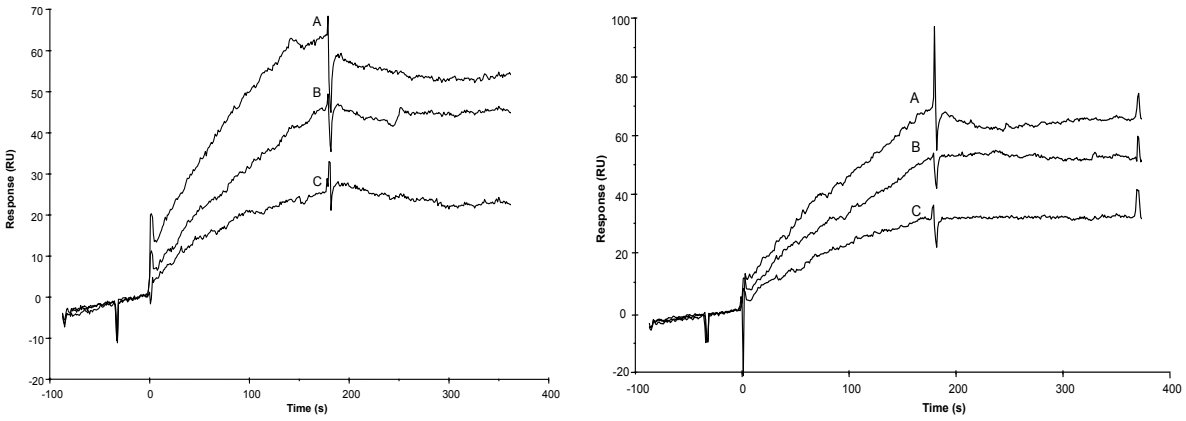

Figure III.8: Sensorgrams showing the binding of Ab-MWCNT-FITC **C23a** (left) and Ab-MWCNT-DTPA **C24a** (right) conjugates with the antigen. Concentrations 100 (A), 50 (B) and 25 (C) μg mL^{-1}.

Similar results were obtained for the conjugates **C23b** and **C24b** (Figure III.9). The lower registered response is probably related to the lower content of protein in these conjugates (0.6 μmol/g for NanoAmor conjugates whereas Nanocyl conjugates contain 1.3 μmol/g).

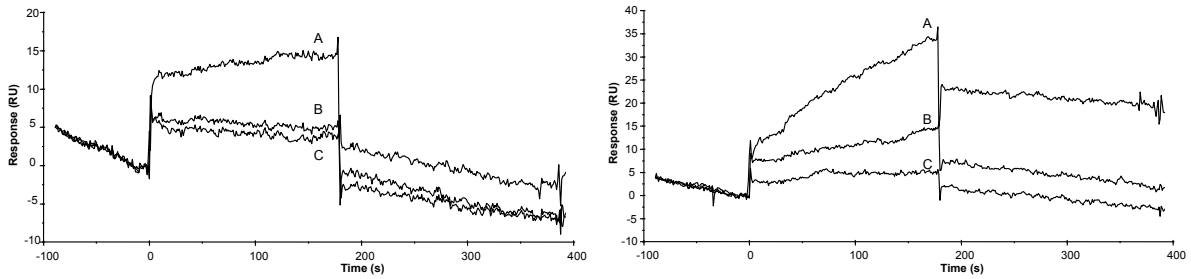

Figure III.9: Sensorgrams showing the binding of Ab-MWCNT-FITC **C23b** (left) and Ab-MWCNT-DTPA **C24b** (right) conjugates with the antigen. Concentrations 100 (A), 50 (B) and 25 (C) μg/mL.

Before determining the ability of the conjugates Fab-MWCNTs and scFv-MWCNTs to bind to the antigen, we assessed the interaction between the protein alone and the antigen. We determined for both proteins the corresponding equilibrium constant K_D. Figure III.10 shows the registered sensorgrams at different concentrations for the fragment antigen binding and the single chain variable fragment.

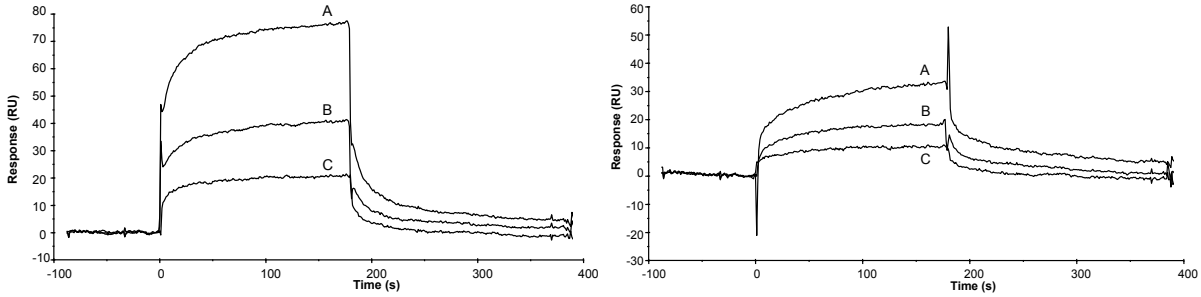

Figure III.10: Sensorgrams showing the binding of Fab (left) and scFv (right) with the antigen. Concentrations for Fab 400 (A), 200 (B) and 100 (C) nM. Concentrations for the scFv 660 (A), 330 (B) and 165 (C) nM.

The determined K_D is equal to $2.4 \cdot 10^{-8}$ M for Fab and to $2.3 \cdot 10^{-7}$ M for scFv. This finding may suggest that scFv has a lower binding affinity to the antigen than the antibody ($1.65 \cdot 10^{-8}$ M) whereas the antigen binding fragment shows the same affinity displayed by the full immunoglobulin. This result is more likely related to the fact that the antibody presents a higher avidity towards the antigen than the scFv. Indeed, this fragment has only one binding site for the antigen while the antibody displays two binding sites. The SPR technique allows to determine an affinity constant and therefore the avidity parameter cannot be taken into account in the determination of the K_D.

As displayed in Figures III.11 and III.12, also the Fab-MWCNT conjugates maintained the ability to bind to the antigen.

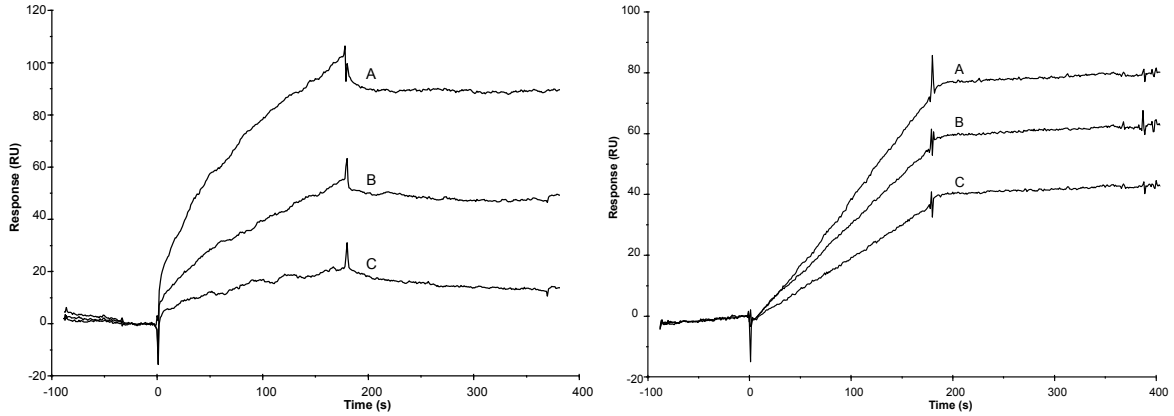

Figure III.11: Sensorgrams showing the binding of Fab-MWCNT-FITC **C25a** (left) and **C25b** (right) conjugates with the antigen. Concentrations 100 (A), 50 (B) and 25 (C) µg/mL.

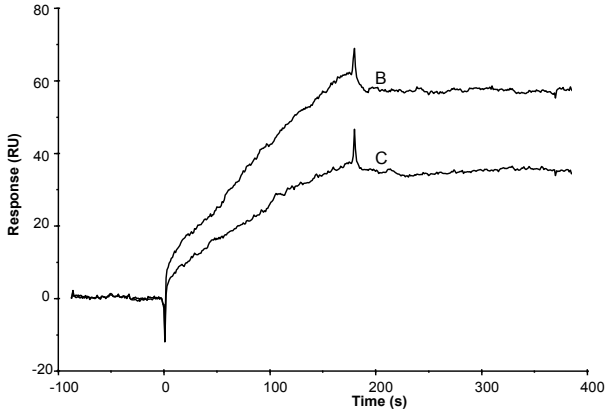

Figure III.12: Sensorgrams showing the binding of Fab-MWCNT-DTPA **C26a** conjugate with the antigen. Concentrations 50 (B) and 25 (C) µg/mL. Note: Due to aggregation phenomena at 100 µg/mL, we did not perform the analysis at that concentration.

The scFv-MWCNT conjugates showed lower signal intensity, confirming the lower response towards the antigen as already showed for the protein alone (Figure III.13).

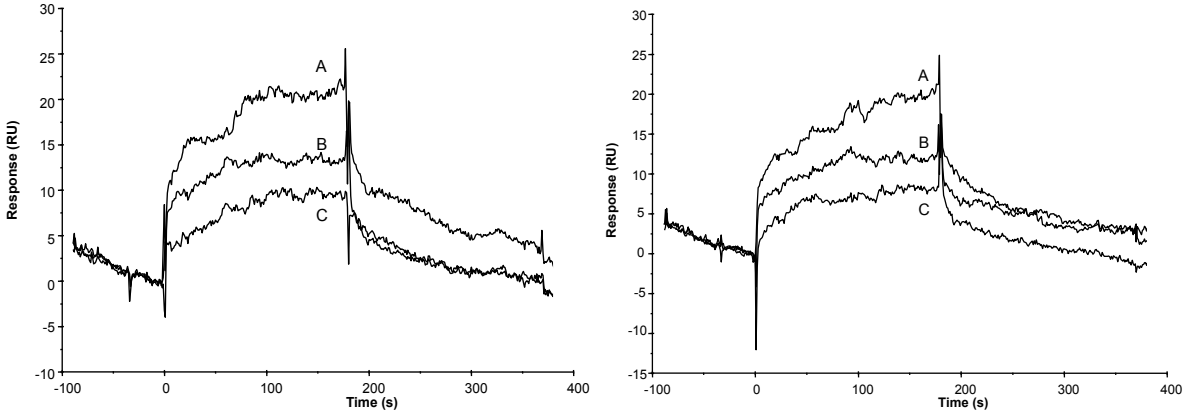

Figure III.13: Sensorgrams showing the binding of scFv-MWCNT-FITC **C27a** (left) and scFv-MWCNT-DTPA **C28a** (right) conjugates with the antigen. Concentrations 100 (A), 50 (B) and 25 (C) µg/mL.

Taken together, these results suggest that the ability of the antibody and its fragments (Fab and scFv) to recognize the antigen is not affected by the conjugation to CNTs. Moreover,

differences in morphology and aspect ratio of the MWCNTs did not affect this ability. Differences in the registered intensity are more likely related to the different amounts of protein introduced (as determined by TGA). However, as explained in Chapter II it is not possible with the CNT-based constructs to obtain quantitative binding information and determine an affinity constant as CNTs are a heterogeneous material without a precise molecular weight.

III.2 Double Functionalized Carbon Nanotube Cell Biology

Confocal microscopy was used to study the cell biology of selected conjugates. These experiments were conducted in London in collaboration with the group of Prof. Kostas Kostarelos. Cellular uptake, intracellular localization and trafficking mechanism were evaluated using MCF-7 (antigen-positive) and Calu6 (antigen-negative) cell lines. In Figure III.14 we report the images obtained after incubation of both cell lines with the Ab-MWCNT-FITC construct **C23b** at a different temperatures (37°C and 4°C).

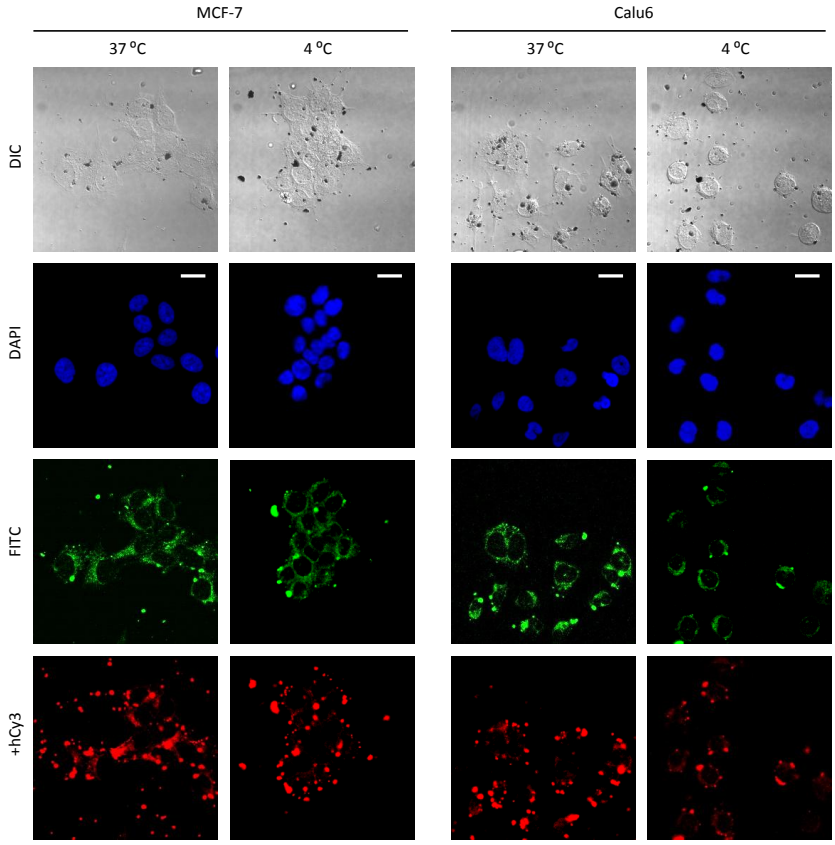

Figure III.14: Cellular uptake of Ab-MWCNT-FITC **C23b**. Top panels depict differential interference contrast (DIC) images. Second row images depict nucleus (stained with DAPI, blue). Third row images depict **C23b** construct (FITC, green). Bottom panels depict bound antibody in **C23b** conjugate, visualized by staining using anti-human Cy3 (red). Scale bar: 20 μm.

After incubation for 3 hours with **C23b** conjugate, cells were washed and stained with DAPI to visualize cells nucleus (blue signal). Antibody bound to MWCNTs was stained by using anti-human Cy3 (secondary antibody, red). In addition, thanks to the presence of FITC covalently bound to **C23b**, we were able to visualize directly the MWCNTs (green signal).

Differential interference contrast (DIC) images illustrate that the cell morphology is not altered by the presence of carbon nanotubes. As shown in Figure III.14, the construct **C23b** was internalized both in MCF-7 and in Calu6 cells. To differentiate between endocytosis (energy-dependent) and membrane permeation (energy-independent) mechanisms, cells were incubated with CNTs at 4°C. Also under energy-inhibiting conditions, CNTs **C23b** were internalized but to a lesser extent. This finding suggests the possibility of an energy-independent mechanism for the cellular uptake, based on passive diffusion ("nanoneedle" mechanism). Once the antibody is bound to carbon nanotubes, it seems that its targeting ability to discriminate between the cells expressing or not the antigen is less significant. To prove the relevance of the CNT role on the internalization process, it would be therefore useful to co-culture the two cell lines to verify if there is a preference for cells expressing the antigen.

To further define the cellular internalization mechanism, cells were treated with a marker for endosomes (EEA-1, blue signal in Figure III.15), responsible for internalization *via* endocytosis.

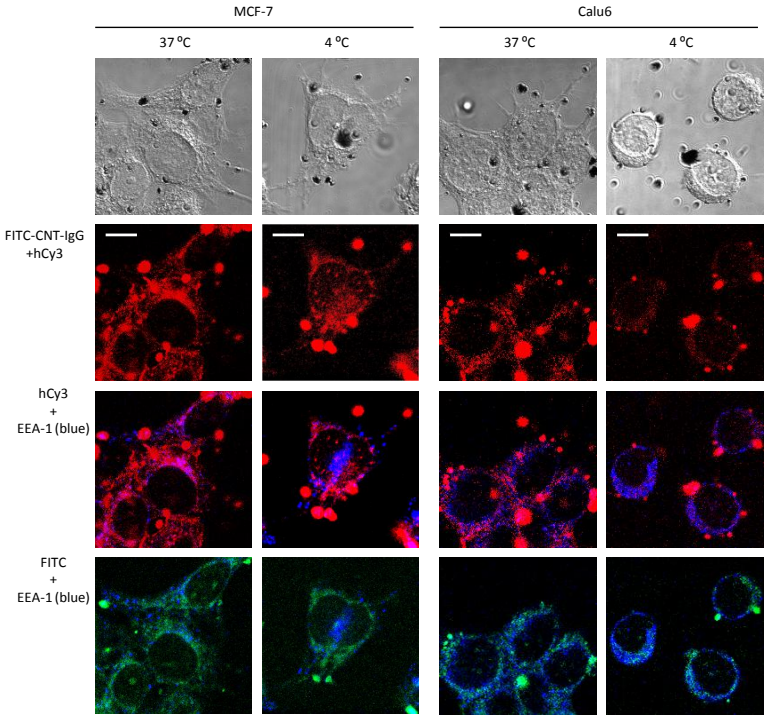

Figure III.15: Cellular uptake of Ab-MWCNT-FITC **C23b** in MCF-7 and Calu6 cell lines at different temperatures. Top panels depict DIC images. Second row images depict bound antibody in **C23b** conjugate (stained with Cy3, red). Third row images depict bound antibody in **C23b** construct (red) and endosomes (stained with EEA-1, blue). Bottom panels depict **C23b** conjugate (FITC, green) and endosomes (blue). Scale bar: 20 µm.

At 37°C, we observed that CNTs **C23b** (red) and endosomes (blue) partly colocalize to produce pink staining, suggesting endosome-mediated pathway contributing in the internalization in MCF-7 cells. At 4°C or in Calu6 cells, CNTs did not colocalize with endosomes and are mainly in the cytoplasm. This finding suggests that the conjugate **C23b** was internalized *via* a mixed mechanism. Under energy-inhibiting condition or in antigen-negative cell line (Calu6), the construct was internalized by permeation mechanism whereas in MCF-7 cells the internalization was also antigen-mediated.

We performed cellular uptake studies also for Fab-CNT-FITC **C25a** and scFv-CNT-FITC **C27a** constructs at 37°C (Figure III.16).

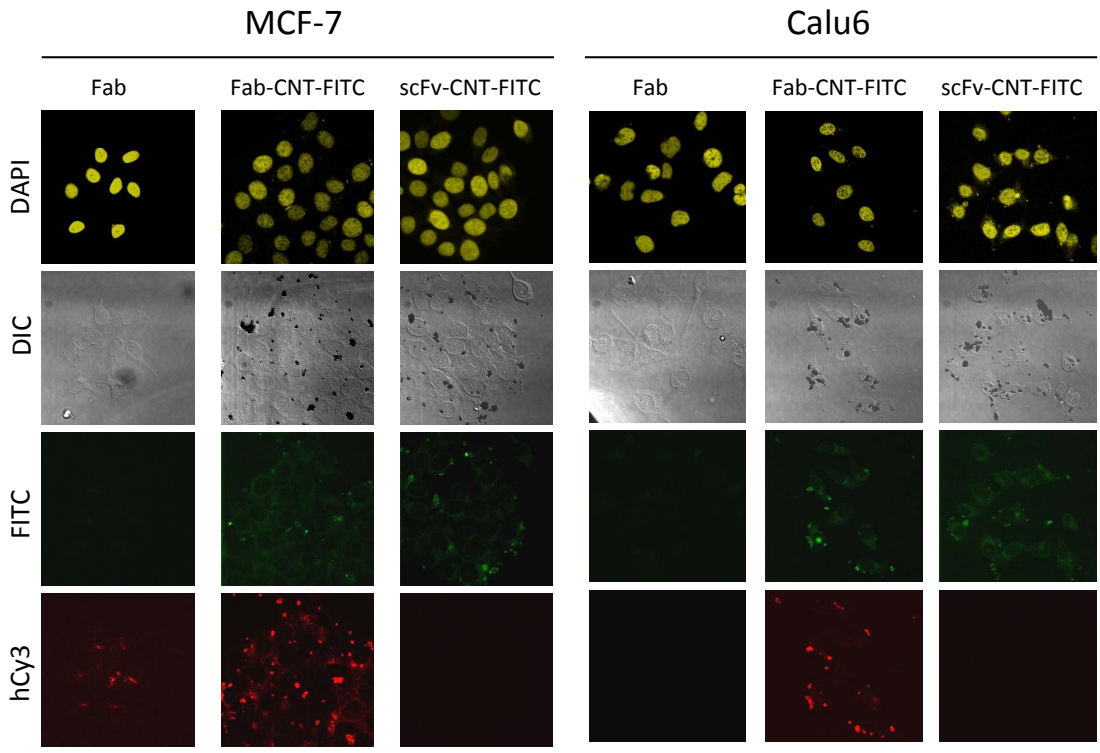

Figure III.16: Cellular uptake of Fab-MWCNT-FITC **C25a** and scFv-MWCNTs-FITC **C27a** in MCF-7 and Calu6 cell lines at 37°C. Top panel images depict nucleus (DAPI, yellow). Second row images depict DIC images. Third row images depict **C25a** and **C27a** conjugates (FITC, green). Bottom panel images depict Fab (stained with hCy3, red).

Cells were incubated with CNTs for 3 hours, washed and the nuclei stained with DAPI (yellow signal in Figures III.16 and III.17). CNTs were visualized thanks to the presence of FITC (green) and Fab was stained with the secondary antibody anti-human Cy3 (red). This marker did not stain scFv because hCy3 binds to the constant region of the proteins and the scFv is only composed of variable domains.

DIC images confirmed that CNTs **C25a** and **C27a** did not alter the morphology of the cells, as observed before for the entire antibody-construct. At 37°C, both cell lines internalized the conjugates without remarkable differences, suggesting mainly an uptake mechanism *via* permeation

(Figure III.16). To further confirm this possibility, we studied the internalization also at 4°C (Figure III.17).

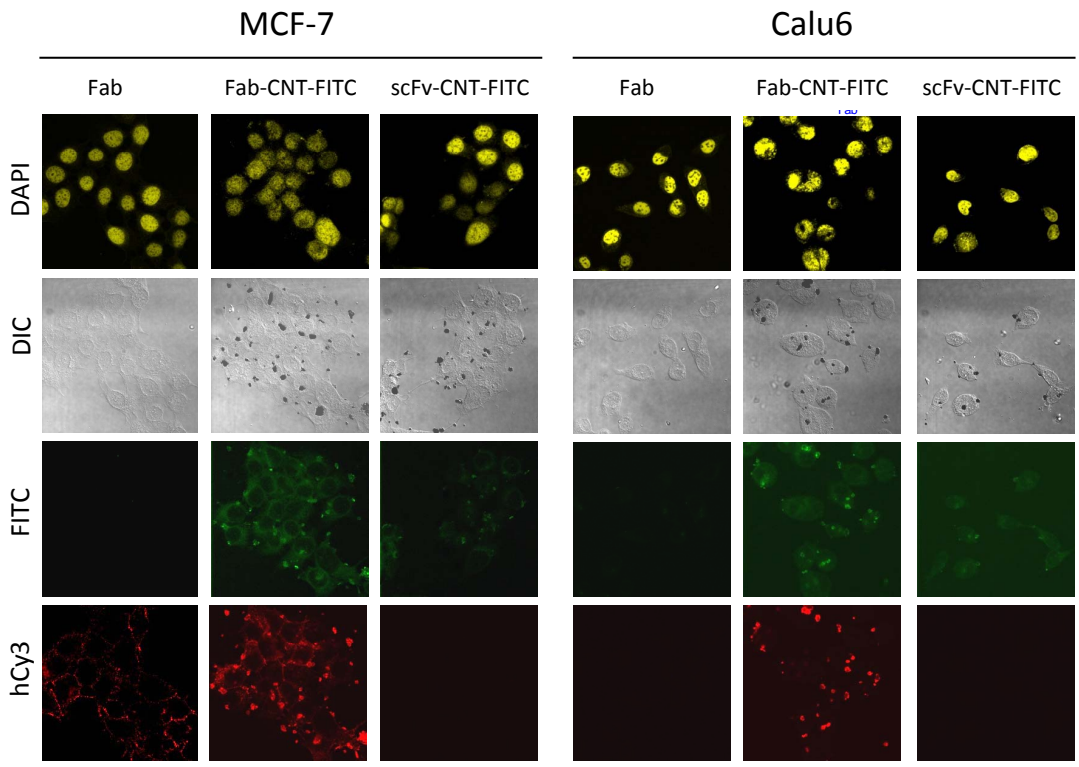

Figure III.17: Cellular uptake of Fab-MWCNT-FITC **C25a** and scFv-MWCNTs-FITC **C27a** in MCF-7 and Calu6 cell lines at 4°C. Top panel images depict nucleus (DAPI, yellow). Second row images depict DIC images. Third row images depict **C25a** and **C27a** conjugates (FITC, green). Bottom panel images depict Fab (stained with hCy3, red).

Both conjugates were internalized also under energy-inhibiting conditions in both cell lines. These findings suggest that the internalization of scFv-MWCNTs-FITC and Fab-MWCNTs-FITC occurs mainly through passive diffusion.

In vitro experiments confirmed that the approaches developed to overcome the low cellular uptake displayed by the mono-functionalized Ab-CNT **C12** were successful. By changing the type of MWCNTs, we increased the dispersibility of the material and therefore the conjugate **C23b** was efficiently internalized by MCF-7 cell line. The *in vitro* results demonstrated also that the reduction of the size of the construct was another important parameter to improve the internalization of the construct. Indeed, by varying the size of the bound protein also the second series of constructs prepared starting from Nanocyl material was effectively internalized.

SPR and *in vitro* studies demonstrated the conservation of the biological activity of the antibody or its fragments once bound to the carbon nanotubes. This finding encouraged us to

develop a therapeutic construct by conjugating a therapeutic fragment of the antibody (VHH) able to both target and kill cancer cells.

III.3 Functionalization of Carbon Nanotubes with a Therapeutic Antibody

The application of carbon nanotubes as drug delivery system is widely documented (Ménard-Moyon, C., *et al*. 2010a). We decided to exploit this property by coupling to *f*-MWCNTs (NanoAmor) a therapeutic intrabody, provided by UCB (UK). To achieve this goal, the strategy was based on the double functionalization approach described above. In particular, the CNT sidewall was functionalized with the intrabody while the tips were derivatized with the imaging probes.

The intrabody belongs to the family of single-domain antibody fragment (VHH). These proteins are antibody-derived therapeutic proteins based on the structural and functional properties of naturally occurring heavy-chain antibodies (Figure III.18).

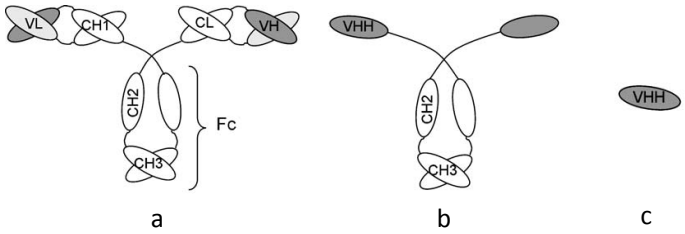

Figure III.18: Schematic representations of a conventional immunoglobulin (a), heavy chain antibody (b) and VHH (c). VL: variable domains derived from the light chains; VH: variable domains from heavy chains; CL: constant domains from light chains; CH: constant domains from heavy chains. Reproduction from Harmsen, M. M., *et al.* 2007.

The intrabodies technology was developed after the discovery that camelidae (camels and llamas) possess fully functional antibodies that lack light chains [Hamers-Casterman, C., *et al*. 1993]. These heavy-chain antibodies contain a single variable domain (VHH) and two constant domains (CH2 and CH3), as illustrated in Figure III.18. The isolated VHH domain is a perfectly stable polypeptide harboring the full antigen-binding capacity of the original heavy-chain antibody. Intrabodies present typical antibodies advantages, such as high affinity for the target and low inherent toxicity [van der Linden, R. H., *et al*. 1999; Muyldermans, S., 2001]. Moreover, they are generally very stable [Ewert, S., *et al.* 2002] and are easy to manufacture [Harmsen, M. M., *et al.* 2007]. Intrabodies display relatively high sequence homology to human heavy chain variable domains (between 80% and 90%) limiting the risk of immunogenicity [Harmsen, M. M., *et al*. 2007]. Starting from a VHH scaffold, our partner in this project, UCB, prepared a therapeutic

intrabody able to target selectively the protein β-catenin implicated in the endogenous Wnt signaling pathway.

The Wnt signaling pathway regulates cell fate determination, proliferation, migration and gene expression during embryogenesis and early development. In adults, Wnt signaling regulates epithelial cell proliferation and hematopoiesis [Angers, S., *et al*. 2009]. Overexpession or mutations of β-catenin (member of Wnt pathway) are associated with several diseases including leukemia, colon-rectal cancer and multiple myeloma [El Wakil, A. *et al.* 2011; Gehrke, I., *et al.* 2009].

The most widely accepted model of Wnt/β-catenin signaling pathway is illustrated in Figure III.19.

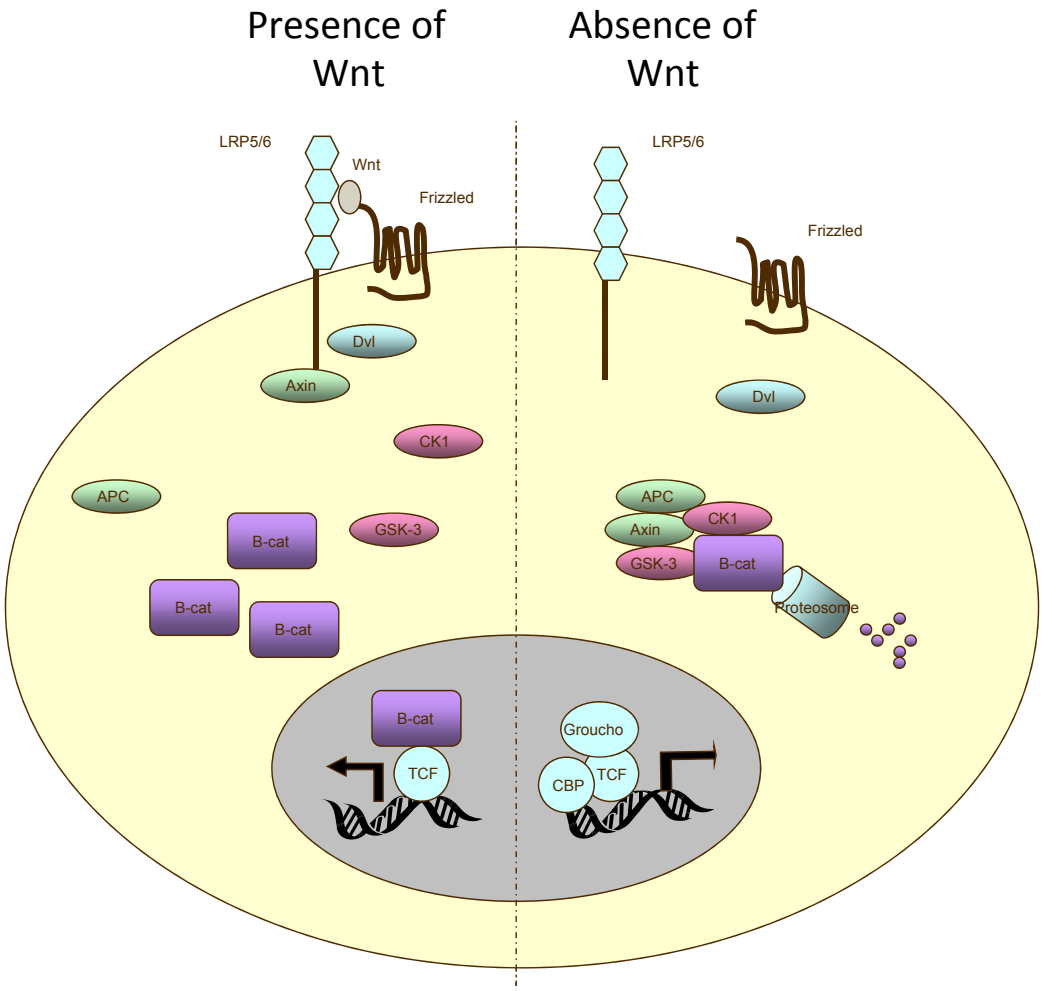

Figure III.19: The canonical Wnt/β-catenin signaling pathway.

In the absence of Wnt (a glycoprotein), β-catenin present in the Axin complex is phosphorylated by casein kinase 1 (CK1) and glycogen synthase kinase-3 (GSK-3) and subsequently degraded by proteosomes. This continual elimination of β-catenin by the action of the Axin complex keeps its level low, preventing the gene expression. The Wnt/β-catenin pathway is activated when a Wnt ligand binds to cell-surface frizzled receptors. This triggers a series of events

that culminate with the cytosolic accumulation of β-catenin and its translocation in the nucleus, where it stimulates the expression of Wnt target genes [El Wakil, A. *et al.* 2011; Lucero, O. M., *et al.* 2010].

Two VHH proteins were synthetized by UCB: one with a therapeutic activity (VHH_T, molecular weight 16 kDa) and one without activity (VHH_C, molecular weight 17 kDa), used as control. VHH_T is able to target and hinder the transcriptional activity of the β-catenin thus blocking the expression of tumor-associated genes.

Both proteins present in their structure free thiol groups that we used to couple both proteins to *f*-MWCNTs **C21b** (FITC-MWCNT-maleimide). As control, we coupled only the protein VHH_C to MWCNTs **C22b** (DTPA-MWCNT-maleimide) in order to perform *in vivo* studies. We followed the same protocol used to couple the antibody to carbon nanotubes *via* the maleimide/thiol approach. For this purpose, CNTs were dispersed in an aqueous solution of the protein at pH 6.5. The reaction was followed by UV-Vis spectroscopy, monitoring the decrease of the protein concentration over time. Finally, the final constructs were washed by multiple centrifugation/sonication cycles in phosphate saline buffer (pH 7.4) and by dialysis against PBS.

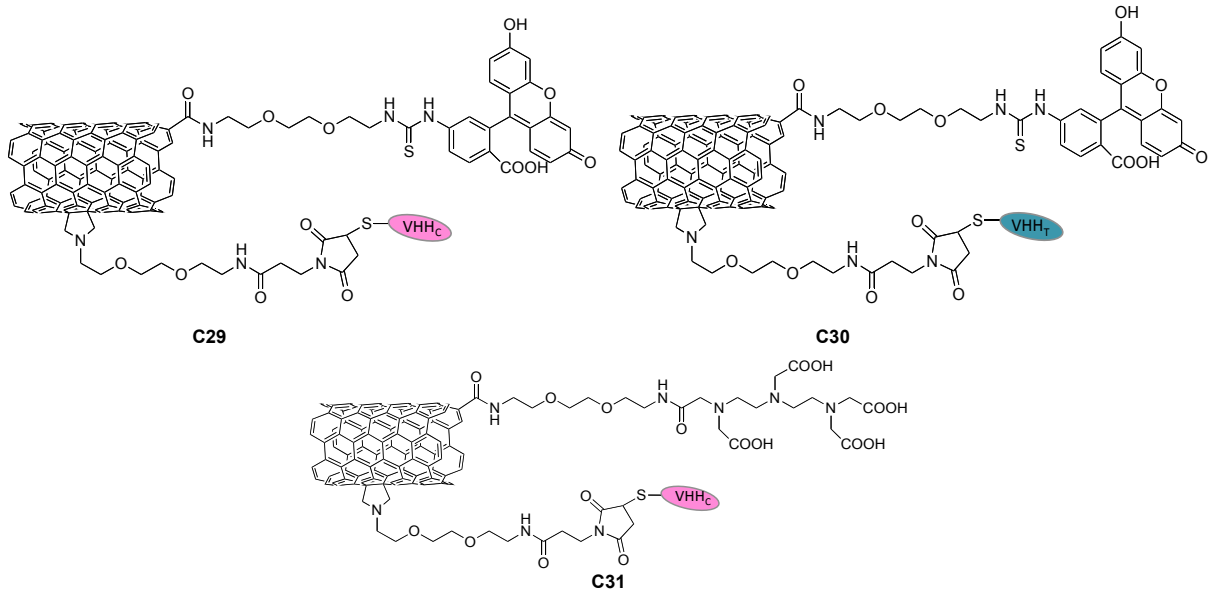

Figure III.20: Structures of double functionalized MWCNTs with the therapeutic VHH (VHH_T) or the control VHH (VHH_C) and imaging probes.

The final conjugates (Figure III.20) were characterized by transmission electron microscopy, thermogravimetric analysis, gel electrophoresis and surface plasmon resonance.

TEM images (Figure III.21) confirmed that the morphology of the CNT-VHH conjugates is not altered after the functionalization.

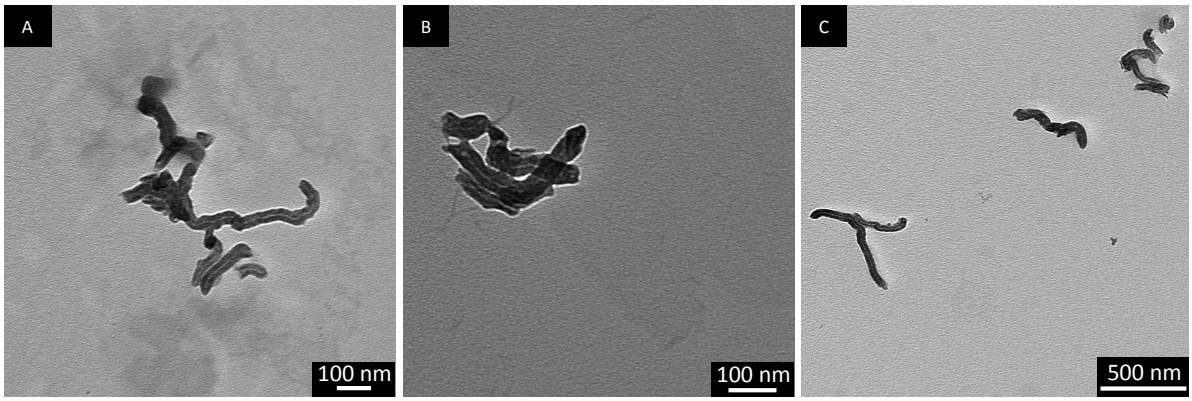

Figure III.21: TEM images of VHH_C-CNT-FITC **C29b** (A), VHH_T-CNT-FITC **C30b** (B) and VHH_C-CNT-DTPA **C31b**.

The VHH loadings were determined by TGA by comparison of the weight loss of the final constructs with their precursors. The loading was 15 µmol per gram of CNTs for both intrabodies.

Gel electrophoresis analysis under non-reducing conditions confirmed the presence of adsorbed proteins onto the surface of carbon nanotubes (Figure III.22) contrary to what we observed for Ab-MWCNT, Fab-MWCNT and scFv-MWCNT conjugates. We tried several conditions to remove the adsorbed VHHs, such as prolonged dialysis in PBS or washings with a solution at high ionic strength (3M $MgCl_2$ in water) but these attempts were not successful.

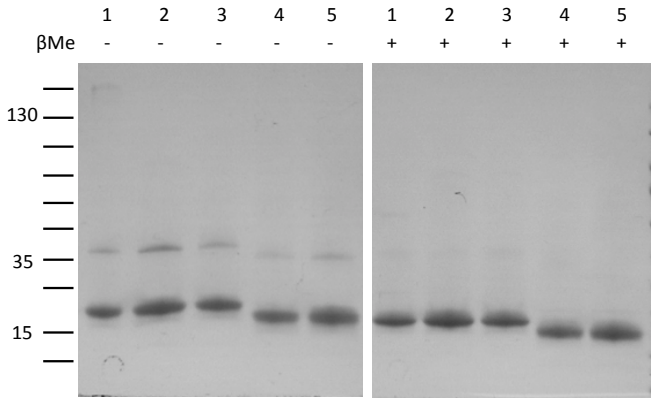

Figure III.22: Gel electrophoresis of VHH-MWCNT conjugates under non-reducing conditions (-βMe, β-mercaptoethanol) and reducing conditions (+βMe). Lane 1: VHH_C-CNT-DTPA **C31b**; lane 2: VHH_C reference; lane 3: VHH_C-CNT-FITC **C29b**; lane 4: VHH_T-CNT-FITC **C30b**; lane 5: VHH_T reference.

We therefore decided to incubate the VHH_C-CNT-FITC conjugate **C29b** in mice serum for 3 hours at 37°C. This experiment allowed us to evaluate the stability of the conjugate by simulating what could happen once the conjugate is injected in mice for *in vivo* studies. For this purpose, we decided to use the Western blot technique. It is an analytical technique used to detect a specific protein in a mixture of proteins (as in serum). Proteins were first separated by gel electrophoresis and then were transferred to a membrane (nitrocellulose), where they were detected using an antibody specific to the target protein. In our case, we used an anti-His tag antibody to detect the

protein VHH_C, as a polyhistidine-tag (His tag) motif of six histidine residues is present in the peptide sequence of VHH_C.

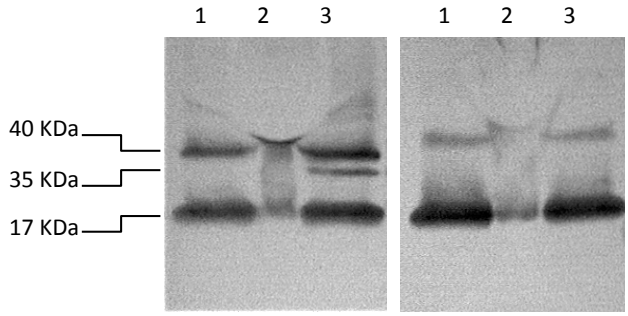

Figure III.23: Western blot of VHH_C-CNT-FITC **C29b** under non-reducing conditions (left) and reducing conditions (right). Lane 1: VHH_C reference; lane 2 VHH_C-CNT-FITC **C29b** in serum; lane 3 VHH_C-CNT-FITC **C29b** after incubation in serum and washing in PBS.

The free VHH_C was used as a reference in the Western blot analysis (Figure III.23 lane 1) and under non-reducing condition a pattern of two bands appeared, due to the dimer (around 40 KDa) and the monomer (17 KDa) of the protein VHH_C. After incubation in serum of VHH_C-MWCNTs-FITC **C29b** and washing in PBS (Figure III.23, lane 3), a similar pattern appeared confirming that the protein is intact after incubation in serum. Under reducing conditions, only the band of the monomer was detected as the minor band of the dimer was reduced. In addition, the Western Blot analysis confirmed that incubation in serum for 3 hours did not affect the stability of the VHH-CNT construct. Indeed, no minor bands due to the denaturation of the protein were observed.

Finally, we performed surface plasmon resonance studies to assess the conservation of the biological activity of the VHH protein after conjugation to CNTs. We injected the VHH proteins alone or the VHH-CNT constructs on a sensor chip previously functionalized with the antigen β-catenin, provided by UCB. We exploited the same approach based on the streptavidin-biotin interaction. As described in Chapter II, the antigen contains a biotin molecule in its peptide sequence while the chip is derivatized with streptavidin.

The registered sensorgrams confirmed that only the therapeutic VHH was able to recognize the antigen (Figure III.24) whereas the control intrabody showed non-specific interaction (Figure III.25). We determined the equilibrium constant by repeating the analysis at different VHH concentrations and we obtained a value equal to $5.9 \cdot 10^{-9}$ M, indicating the high affinity of the intrabody towards the β-catenin protein.

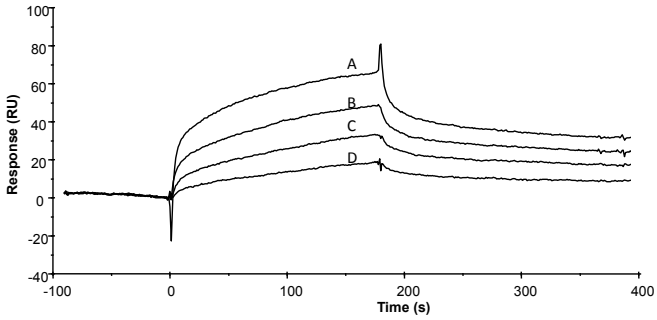

Figure III.24: Sensorgrams showing the specific binding of therapeutic VHH_T with the antigen β-catenin at different concentrations [A: 55 nM; B: 28 nM; C: 14 nM; D: 7 nM].

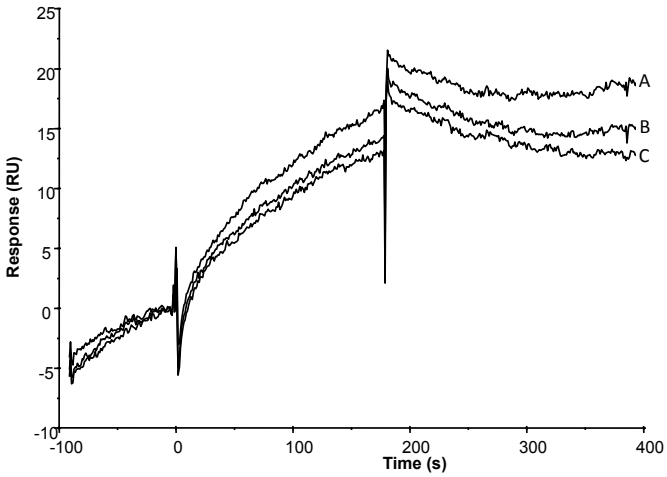

Figure III.25: Sensorgrams showing the non specific binding of control VHH_C with the antigen β-catenin at different concentrations [A: 7 µM; B: 3.5 µM; C: 1.7 µM].

Similarly, only the VHH_T-MWCNT-FITC construct was able to target specifically the antigen (Figure III.26), while the VHH_C-MWCNT-FITC conjugate showed no binding to the chip (Figure III.27).

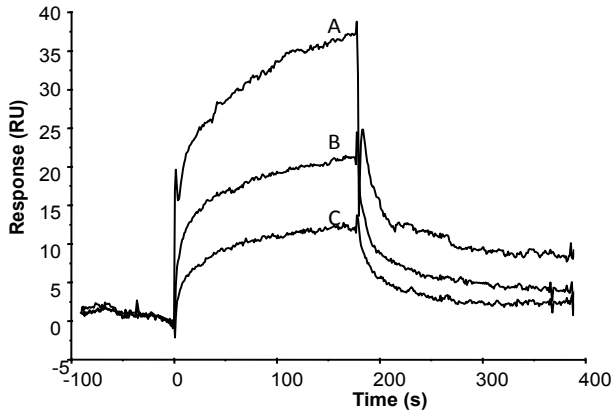

Figure III.26: Sensorgrams showing the binding of VHH_T-CNT-FITC **C30b** with the antigen β-catenin at different concentrations [A: 100 µg/mL; B: 50 µg/mL; C: 25 µg/mL].

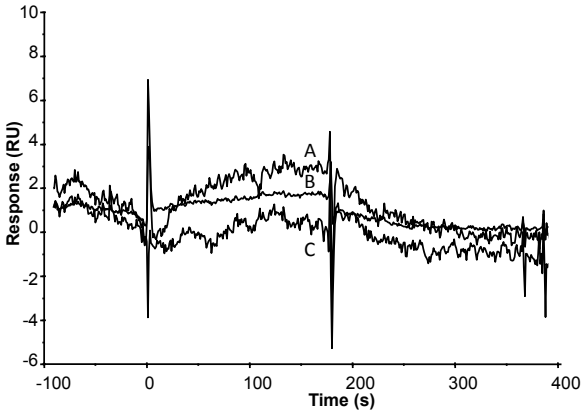

Figure III.27: Sensorgrams showing the binding of VHH_C-CNT-FITC **C29b** with the antigen β-catenin at different concentrations [A: 100 µg/mL; B: 50 µg/mL; C: 25 µg/mL].

The SPR analysis confirmed again that the conjugation to CNTs did not affect the affinity of the intrabody to its antigen.

In collaboration with the group of Prof. Kostas Kostarelos, *in vitro* and *in vivo* studies are currently conducted on the VHH-CNT conjugates.

III.4 Conclusions

Double functionalization of carbon nanotubes was achieved by sidewall functionalization *via* 1,3-dipolar cycloaddition and tips derivatization with amidation reaction. This approach allowed us to obtain multifunctional systems by introducing onto the sidewall the antibody or a fragment of this antibody and at the tips a tracking probe. The characterization of these constructs by complementary techniques confirmed the presence of the proteins and the conservation of their biological activity.

In vitro cellular uptake studies showed the presence of a mixed mechanism for the internalization of functionalized MWCNTs: passive diffusion and the antigen-mediated endocytosis. The construct Ab-MWCNT-FITC **C23b** was mainly uptaken through antigen-mediated endocytosis while Fab-MWCNT-FITC **C25a** and scFv-MWCNT-FITC **C27a** conjugates were mainly internalized *via* diffusive mechanism. These findings are probably related to different parameters, such as the size, the affinity and avidity of the protein towards the antigen (as summarized in Table III.4).

Table III.4: Characteristics of different proteins used in this study.

Entry	Molecular weight (KDa)	Size (nm)[a]	K_D (M)[b]
Ab	150	15	$1.6 \cdot 10^{-8}$
Fab	48	7.5	$2.4 \cdot 10^{-8}$
scFv	21	4	$2.3 \cdot 10^{-7}$
VHH_C	17	4	-
VHH_T	16	4	$5.9 \cdot 10^{-9}$

[a] The size of the proteins was assessed by a molecular modeling software (PyMol) and compared to data present in the literature. [b] Determined by SPR analysis.

The antibody presents greater size and avidity than its fragments. These features may be responsible for a reduction of the diffusive mechanism as the Ab-CNT conjugate present a big size and in the structure of the antibody there are two sites for the binding to the antigen. Fab and scFv are smaller proteins and therefore they show a reduced ability to mediate the internalization *via* the antigen-dependent pathway. However, these data confirmed that antibodies could be used as effective targeting agents to deliver carbon nanotubes in cancer cells by reducing the cellular uptake by antigen-negative cell lines.

In this context, we expanded the study to the preparation of constructs displaying both targeting and therapeutic activity by binding a intrabody (VHH). Physico-chemical characterization was carried out to determine the amount of bound protein and to confirm the preservation of recognition ability towards the antigen β-catenin. Cell biology experiments are currently performed and further biological studies are ongoing to evaluate the therapeutic activity of the VHH bound to CNTs.

Chapter IV: Pharmacokinetic and Toxicological Studies

Fundamental aspects related to the development of a novel system for biomedical applications concern the evaluation of its pharmacological and toxicological characteristics.

The pharmacological behavior is highly dependent on several parameters such as the tissue distribution, pharmacokinetics, blood circulation half-life and body excretion kinetics. Moreover, the pharmacokinetic studies of covalently functionalized SWCNTs [Singh, R., *et al*. 2006; Ruggiero, A., *et al*. 2010b] and MWCNTs [Lacerda, L., *et al*. 2008a] have reported a short blood half-life circulation (1-3h) and a limited tissue accumulation (liver, spleen and kidneys) and renal excretion. On the contrary, non-covalently functionalized CNTs tend to be slowly eliminated by the hepatobiliary route [Liu, Z., *et al*. 2008a].

In this study, the biodistribution and pharmacokinetics were conveniently evaluated through detection of gamma radiation emitted by the radionuclide ^{111}In. In collaboration with the group of Prof. Kostas Kostarelos in London, we performed the complexation of the radioisotope with the chelating agent DTPA, covalently attached onto the nanotube surface. Then SPECT/CT technique enabled us to obtain 3D images of the whole body of the animals and to evaluate the pharmacokinetic profile.

To further explore the use of Ab-CNT constructs as therapeutic or biomedical tools, another important parameter to evaluate is their toxicological profile. These studies were conducted in our team in collaboration with Dr. J. Russier. In particular, we assessed the potential cytotoxicity towards different cell lines belonging to the immune system such as macrophages and splenocytes. The cell viability was evaluated using two different tests. This process allowed us to validate the results by excluding the possible interference of carbon nanotubes with the assay reagents employed in the toxicity test.

IV.1 Pharmacokinetic Studies

In order to perform the *in vivo* pharmacokinetics and imaging studies, MWCNTs were functionalized with DTPA and the constructs labeled with ^{111}In (see Scheme II.8, page 56). This radioisotope was chosen for its optimal half-life decay (67.5 h) which allows monitoring the CNT biodistribution for short periods and because the chelating agent DTPA rapidly chelates [^{111}In] with high thermodynamic equilibrium constant [Jasanada, F., *et al.* 1996]. MWCNTs bearing the DTPA moieties were reacted with $^{111}InCl_3$ to form the radio-conjugates.

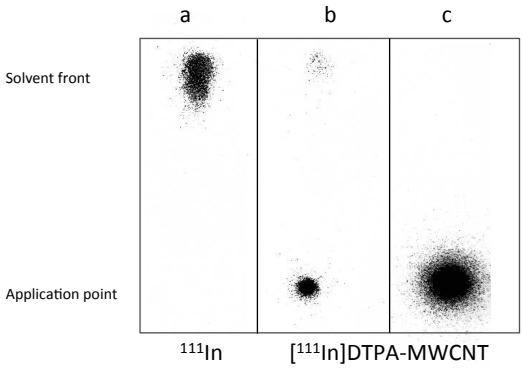

Figure IV.1: Images of the TLC strips; lane a: free ^{111}In; lane b: [^{111}In]DTPA-MWCNT complex before washing; lane c: [^{111}In]DTPA-MWCNT complex after washing.

The labeling yield was determined by spotting the constructs in TLC plates (Figure IV.1). The mobile phase was chosen in order to have the construct at the application point while the free isotope was able to migrate at the solvent front. The labeled conjugates were then washed several times by centrifugation/sonication procedure in order to eliminate the indium present in free form and the purity of the material was assessed by TLC analysis (lane c in Figure IV.1). Before injecting the complex in animals, the stability of [^{111}In]DTPA-MWCNTs was checked by incubating the complex for 24 hours in serum at 37°C. As expected, the labeling of the [^{111}In]DTPA-MWCNT constructs proved to be stable under these conditions.

Each group of animals (n=3-4) was administered with 50 μg of [^{111}In]DTPA-MWCNT constructs which contained approximately 5-6 MBq. SPECT/CT imaging was carried out immediately after tail vein injection of the complex, after 4 hours and 24 hours (Figure IV.2).

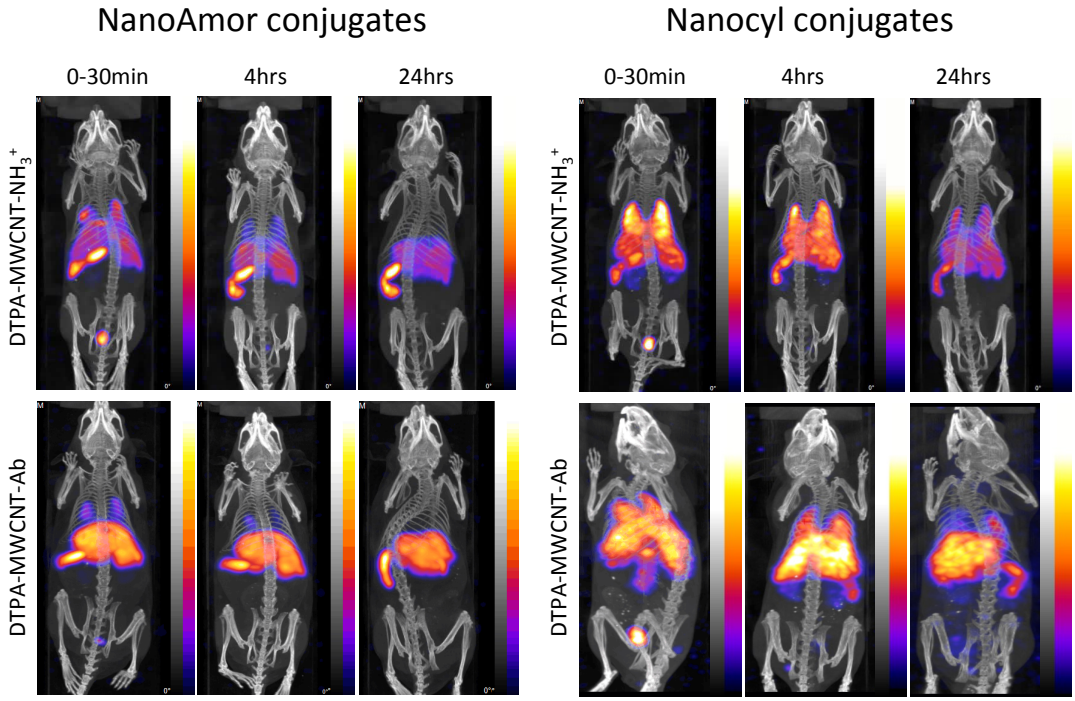

Figure IV.2: Whole-animal SPECT/CT imaging which was carried out immediately after tail-vein injection, after 4h and 24h post-injection of the precursor DTPA-MWCNT-NH_3^+ (**C19**) and the conjugate DTPA-MWCNT-Ab (**C24**).

3D reconstruction by SPECT/CT of the whole animal for [^{111}In]DTPA-MWCNT-NH_3^+ NanoAmor precursor **C19b** displayed accumulation in the liver, spleen and lung. SPECT/CT imaging of the functionalized [^{111}In]DTPA-MWCNTs-Ab **C24b** showed similar tissue accumulation predominantly in the liver, spleen and lung. Signals were also detected in the bladder (at 30 minutes) likely due to early excretion of the highly individualized and short nanotube fraction. Imaging at later time points (4 hours and 24 hours) showed mainly liver and spleen accumulation with reduced signal in the lung and completely abolished in the bladder.

The analysis of SPECT/CT images obtained after injection of Nanocyl constructs (**C19a** and **C24a**) revealed that these conjugates present a different tissue distribution profile. Indeed, Nanocyl constructs showed more accumulation in lung and kidney than NanoAmor material. This is probably related to the morphology of the material as these nanotubes present a thinner diameter (9.5 nm) than NanoAmor MWCNTs (20-30 nm).

To assess the organ biodistribution and blood-clearance profile, we carried out a more quantitative study by measuring the radioactivity in the organs by direct gamma counting. The mice were therefore sacrificed after 24 hours, the organs were harvested and weighted and the radioactivity was measured by gamma scintigraphy techniques. The results were expressed as percentage of injected dose per gram of tissue (%ID/g) (Figure IV.3).

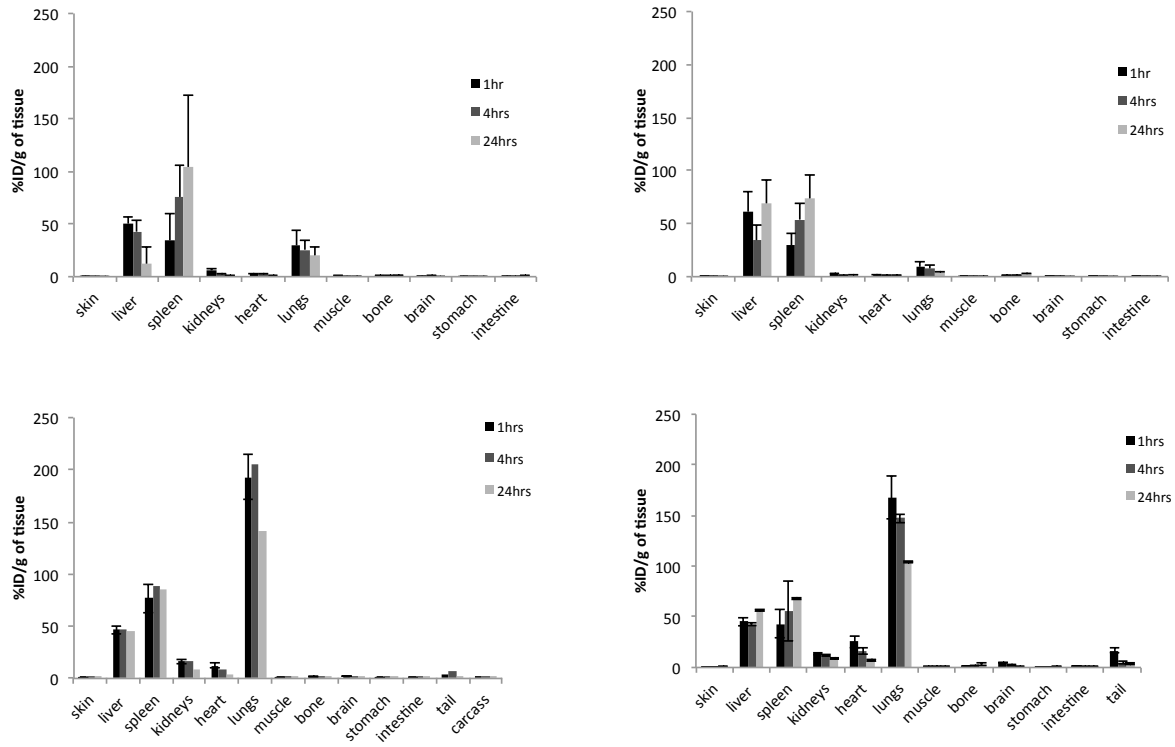

Figure IV.3: Tissue biodistribution profile of the precursor DTPA-MWCNT-NH_3^+ **C19b** (top panel, left) and the conjugate DTPA-MWCNT-Ab **C24b** (top panel, right) and the precursor DTPA-MWCNT-NH_3^+ **C19a** (bottom panel, left) and the conjugate DTPA-MWCNT-Ab **C24a** (bottom panel, right).

For NanoAmor conjugates gamma counting indicated liver, spleen and lung accumulation. In particular, the precursor **C19b** accumulated mainly in the spleen while the DTPA-MWCNT-Ab **C24b** distributed in liver and spleen. Nanocyl construct DTPA-MWCNT-Ab **C24a** and its precursor accumulated mostly in liver, spleen and lungs. All these results are consistent with the SPECT/CT data.

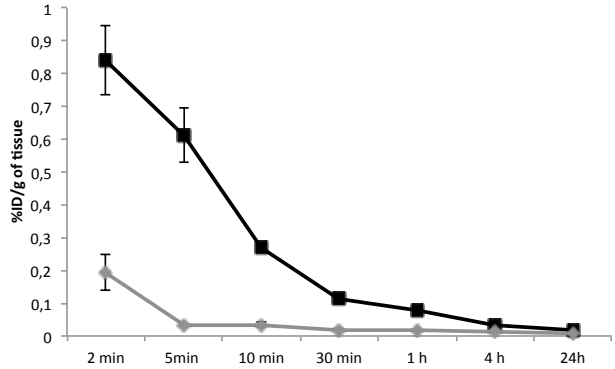

Figure IV.4: Blood clearance profile of the precursor DTPA-MWCNT-NH_3^+ **C19b** (black curve), the conjugate DTPA-MWCNT-Ab **C24b** (grey curve).

As shown in Figure IV.4, negligible percentages of the injected dose were detected in blood after administration owing to rapid organ accumulation. By comparing the biodistribution curves of NanoAmor conjugates, the antibody conjugation modified the distribution profile by further reducing the blood half-life and increasing the liver accumulation.

These data are in agreement to a previous reported biodistribution profile of antibody-functionalized SWCNTs, displaying mainly liver, spleen and kidney accumulation [McDevitt, M. R., *et al*. 2007].

The *in vivo* imaging studies were performed also for the conjugates DTPA-MWCNT-Fab **C26a** and DTPA-MWCNT-scFv **C28a** and compared to their precursor DTPA-MWCNT-NH_3^+ **C19a**. These experiments were aimed to investigate if the biodistribution profiles are affected by the size of the bound protein.

The analysis of SPECT/CT images obtained immediately after tail-vein injection and after 4 hours and 24 hours revealed that also in this case Nanocyl material accumulated mainly in lungs, liver, spleen and kidneys. By comparing images of Fab- or scFv-constructs, we did not observe evident differences induced by the variation of the size of the protein.

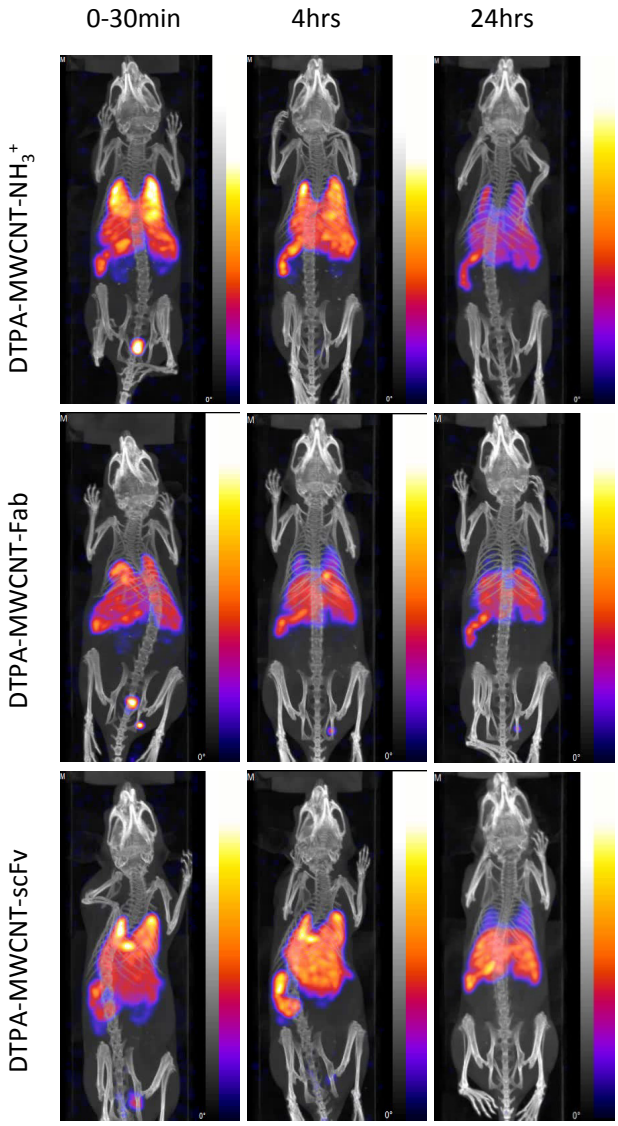

Figure IV.5: Whole-animal SPECT/CT imaging which was carried out immediately after tail-vein injection, after 4h and 24h post-injection of the precursor DTPA-MWCNT-NH_3^+ (**C19a**), the conjugate DTPA-MWCNT-Fab (**C26a**) and the conjugate DTPA-MWCNT-scFv (**C28a**).

Quantitative studies by gamma counting are currently ongoing to further understand how the different parameters such as morphology, functionalization degree and size of the bound protein could affect the tissue distribution profile.

IV.2 Toxicological Studies

In order to evaluate the potential application of carbon nanotubes in the nanomedicine domain, we explored their effects on cell viability using cells from the immune system (*i.e.* splenocytes and macrophages). The cell viability was assessed using LDH assay, as described in Chapter II or by flow cytometry using propidium iodide (PI) staining.

The PI flow cytometric test is widely used for the evaluation of apoptotic cells. It is based on the principle that dead cells are characterized by DNA fragmentation and consequent loss of nuclear DNA content. The use of PI, which is capable of binding and labeling DNA makes possible to obtain a precise evaluation of cellular DNA content and therefore identification of dead cells. PI does not stain viable cells because these cells maintain plasma membrane integrity and therefore are not permeable to PI [Vermes, I., *et al.* 1995].

We compared the cell viability after incubation with the proteins alone (IgG, Fab and scFv), the conjugates used as precursors (ox-MWCNTs **C1**, amino-functionalized MWCNTs **C4** and double functionalized MWCNTs **C16'**, corresponding to **C16** after Boc protecting group cleavage) and the CNT-based constructs:

- Ab-MWCNT **C12** and **C14** (tips and sidewall functionalization);
- FITC-MWCNT-Ab **C23**, FITC-MWCNT-Fab **C25** and FITC-MWCNT-scFv **C27**;
- DTPA-MWCNT-Ab **C24**, DTPA-MWCNT-Fab **C26** and DTPA-MWCNT-scFv **C28**.

The conjugates were dispersed by sonication in water or PBS at concentration of 500 µg/mL and further diluted in cell culture medium at final concentrations of 1, 10 and 100 µg/mL. After an incubation of 24 hours for both cell lines, the cell viability was evaluated by LDH assay. The results are displayed in the Figures IV.6 and IV.7.

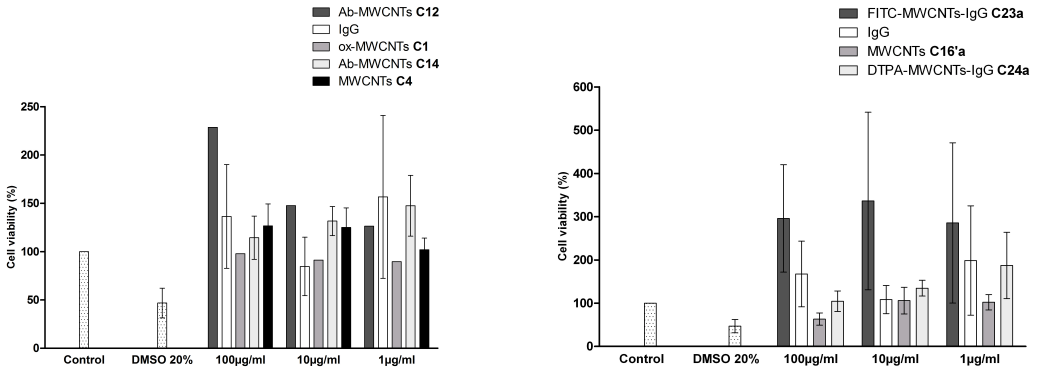

Figure IV.6: Cell viability of splenocytes in the presence of mono-functionalized MWCNTs (left) or double functionalized MWCNTs (right) and antibody alone (IgG) at different concentrations.

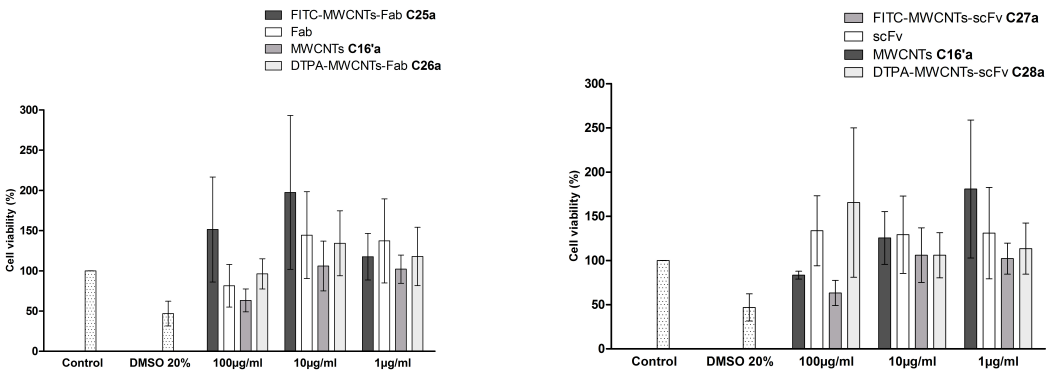

Figure IV.7: Cell viability of splenocytes in the presence of double-functionalized MWCNTs (**a**) or Fab (left) and double-functionalized MWCNTs (**a**) or scFv (right) at different concentrations.

We observed a cytotoxic effect only for the constructs **C16'a** at 100 µg/mL as the cell viability decreased at 60%, compared to non-treated cells (control). Overall, MWCNTs conjugated to proteins are not cytotoxic.

We repeated these experiments also for CNT-based constructs prepared starting from NanoAmor MWCNTs. The results are illustrated in Figure IV.8.

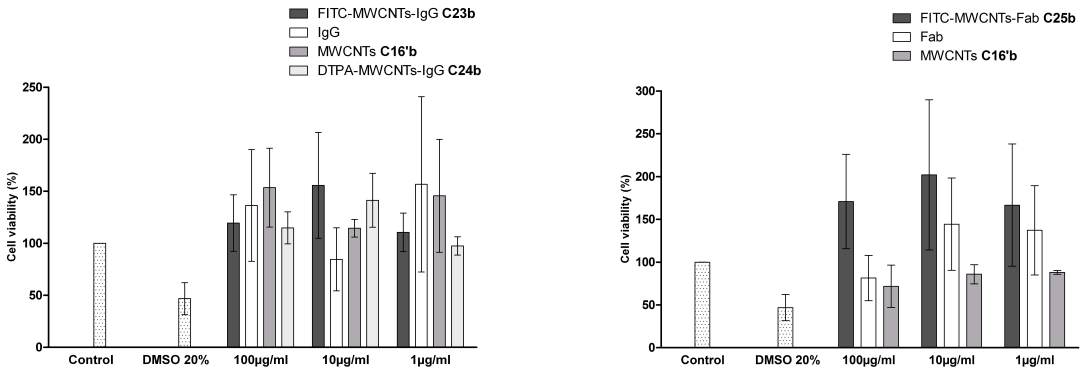

Figure IV.8: Cell viability of splenocytes in the presence of double-functionalized MWCNTs (**b**) and IgG (left) or double-functionalized MWCNTs (**b**) and Fab (right) at different concentrations.

We observed a low cytotoxic effect for FITC-MWCNT-Ab **C23b** at 100 µg/mL as the percentage of live cells decreased to 80%. Overall, changes in morphology or aspect ratio did not induce significant cytotoxic effects.

To have an additional test and to exclude the possibility that carbon nanotubes interfered with LDH assay, we also performed cytometric PI test at the same range of concentrations. As expected, the results were comparable to that of LDH assay and no significant cytotoxicity was observed.

Finally, we assessed the cell viability using a different cell line (macrophages) and no cytotoxic effects were observed, as already determined for splenocytes.

Taken together, these results confirm that functionalization makes carbon nanotube biocompatible as already observed in our laboratory on primary immune cells [Dumortier, H., *et al*. 2006].

IV.3 Conclusions

The results reported in this Chapter illustrate the absence of toxicity of Ab-CNT constructs or limited toxicity for their precursors towards cells of the immune system. These findings confirm

that the chemical functionalization of carbon nanotubes enhances their biocompatibity and support the possibility to use CNT-based conjugates for biomedical applications.

As already observed for Ab-SWCNT conjugates by Scheinberg and co-workers, pharmacokinetic studies showed tissue accumulation in spleen, liver and lung. Differences in biodistribution profiles related to morphological features of carbon nanotubes were observed, such as increased lung and kidney accumulation for MWCNTs with smaller diameter (Nanocyl). On the contrary, changes in the size of the bound protein did not induce any significant modification in the tissue accumulation profiles.

Given the promising observations obtained in this study, further investigation to assess long-term toxicological responses and pharmacokinetic profiles (*i.e.* using ^{153}Gd as radioisotope) are currently ongoing.

Chapter V: Conclusions and Perspectives

Carbon nanotubes represent an interesting material that have been stimulating applications in several fields, including electronics, materials science and nanotechnology. Recently, the potential applications of carbon nanotubes in the biomedical field have been also explored, thus contributing to the development of novel nanomedicines based on advanced nanomaterials.

In this context, we were interested in developing a tumor-specific therapy by conjugating the antibodies to CNTs. A targeted therapy offers several advantages over a classical treatment such as improvements in the therapeutic and pharmacological profiles. Indeed, the presence of a targeting agent can promote the delivery of the therapeutic agent towards cancer cells, thus limiting the cellular damage of healthy cells. Immunoglobulins represent nowadays promising oncological therapeutics but they suffer from a limited aptitude to traverse the plasma membrane. We circumvented this drawback by conjugating antibodies to carbon nanotubes used as delivery system. We exploited the proven ability of carbon nanotubes to cross cell membranes in a non-invasive way to deliver antibodies inside cells.

In the first part of this study we focused on the preparation of a hybrid model able to target cancer cells. We chose an antibody showing targeting properties towards carcinomas such as breast or colorectal cancer overexpressing the protein MUC1 (antigen).

The first step in the preparation of these conjugates was the functionalization of carbon nanotubes by using a covalent strategy, in particular the 1,3-dipolar cycloaddition of azomethine ylides. This reaction allowed to increase the dispersibility of the material both in organic solvents and in aqueous solutions and it introduced reactive groups (amines) onto the sidewall of the nanotubes. Then, we designed two approaches to conjugate the protein to carbon nanotubes. The first strategy was based on the formation of a peptide bond between the free amines present on the surface of the antibody and the carboxylic groups introduced by oxidation of pristine CNTs. The second approach exploited a chemical selective ligation reaction between thiol groups introduced in the antibody sequence and maleimide moieties grafted onto the sidewall of carbon nanotubes by derivatization of the amino groups.

Both conjugates were characterized by complementary techniques (transmission electron microscopy, thermogravimetric analysis, gel electrophoresis and surface plasmon resonance) to investigate the morphology of the carbon nanotube-based conjugates and the biological activity of the bound antibody and to assess the level of functionalization. SPR analysis confirmed that once bound to carbon nanotubes the antibody is still able to recognize its antigen. Further *in vitro*

experiments showed the tendency of the conjugate to target cells overexpressing the antigen more selectively but the ability of the constructs to be internalized was quite limited.

These preliminary results aimed us to develop a second generation of Ab-CNT conjugates in order to overcome the low intracellular uptake that could be due to the size of the Ab-CNT conjugate and/or its low dispersibility. Using a double functionalization approach, we prepared two series of conjugates. The first series of constructs was synthetized using as starting material a different type of MWCNTs, produced by NanoAmor, which displays a better degree of dispersibility. In the second series of conjugates, we conjugated fragments (Fab and scFv) of the antibody in order to decrease the size of the construct.

Double functionalization of carbon nanotubes was achieved by sidewall functionalization *via* 1,3-dipolar cycloaddition and tip derivatization with amidation reaction. This approach allowed us to obtain multifunctional systems by introducing onto the sidewall the antibody or a fragment of this antibody and at the tips an imaging probe. The presence of fluorescein or a chelating agent for radioisotopes (DTPA) allowed us to perform *in vitro* and *in vivo* studies, respectively, and directly localize carbon nanotubes in cells or animals.

The complete characterization of each construct confirmed the presence of the proteins covalently bound to the nanotubes and their ability to recognize the antigen. *In vitro* studies confirmed the effective cellular internalization of these constructs, proving that the approaches developed to overcome the low uptake were successful. Moreover, we determined that the uptake mechanism is a mixed pathway based both on passive diffusion ("nanoneedle" mechanism) and active antigen-mediated endocytosis. However, complementary studies to further define and prove the relevant role of the antibody to discriminate between cell lines overexpressing or not the antigen will be performed.

The pharmacokinetic profile assessed by *in vivo* studies using ^{111}In-radiolabeled MWCNTs (half-life of ^{111}In: 67.5 hours) showed marked dependence on the morphology of the nanotubes. Indeed, we observed an increased accumulation of MWCNT conjugates in lungs and kidneys for Nanocyl constructs whereas NanoAmor conjugates distributed mainly in liver and spleen. *In vivo* studies did not display significant variations in tissue accumulation when varying the size of the protein in the construct. In order to investigate the long-term pharmacokinetic profile, studies using a different radioisotope (^{153}Gd, half-life: 240 days) are currently ongoing.

In order to use Ab-CNT conjugates as biomedical tools, we analyzed also their toxicological profile towards cell lines of the immune system. We assessed the potential toxicity through two cell viability tests and both assays confirmed that once functionalized the carbon nanotubes are not

toxic. Further studies are currently conducted to determine the possible toxicological and immunological responses *in vivo*.

The obtained results encouraged us to expand this project by developing a therapeutic construct. We coupled a intrabody (fragment of a heavy-chain antibody) displaying both targeting and therapeutic activity by blocking the activity of the protein β-catenin. Indeed, overexpession or mutations of this protein are associated with several diseases including leukemia, colon-rectal cancer and multiple myeloma. Before performing the coupling step, we prepared a doubly functionalized CNT where the amines onto the sidewall were used for the conjugation of the VHH, while the amino groups at the tips were derivatized with the imaging probe.

Characterization by SPR confirmed that the bound intrabody recognized the antigen (β-catenin). However, the gel electrophoresis analysis showed the presence of both adsorbed and covalently bound intrabody. Further analysis through western blot technique confirmed that the intrabody-CNT conjugate is stable in serum without displaying premature release of the protein from the CNTs. This has encouraged us to use the intrabody-CNT conjugate for *in vitro* and *in vivo* studies. We are currently assessing the cellular internalization and therapeutic activity as well as the *in vivo* tissue distribution.

In conclusion, these studies confirm the potential application of carbon nanotubes as delivery system. Indeed, we proved the ability of CNTs to deliver antibodies inside cells to perform a tumor-specific therapy. Indeed, the biological activity of the antibody is not affected by conjugation to carbon nanotubes. Moreover, the different CNT conjugates did not show any short-term toxicological effects. If the conservation or hopefully the enhancement of the therapeutic activity of the intrabody is proven, the Ab-CNT hybrid systems could represent in the future a new oncology treatment option.

Chapter VI: Experimental Part

VI.1 General Indications

VI.1.1 Chemicals and Solvents

VI.1.1.1 Chemicals

Chemicals were used without any further purification. Different suppliers were selected.

CHEMICAL	SUPPLIER
MWCNTs (NC3100; 9.5 nm diameter, 1.5 μm length, 95+ % purity; batch no. 171119)	Nanocyl (Belgium)
MWCNTs (20-30 nm diameter, 10-30 μm length, 95% purity; batch no. 1240 XH)	Nanostructured and Amorphous Materials Inc (USA)
HOBt Di-*tert*-butyl dicarbonate Fmoc-Gly-MPPA(Wang)-Resin	PolyPeptide Laboratories
Paraformaldehyde 1,8-diamino-3,6-dioxaoctane Benzyl bromoacetate Ninhydrine Phenol Triethylamine DIEA BOP EDC NHS Fluorescein isothiocyanate DTPA dianhydride 2-mercaptoethylamine 2-iminothiolane-HCl (Traut reagent) 5,5'-dithiobis-2-nitrobenzoic acid (Ellman reagent) HCl in dioxane (4 M)	SIGMA-ALDRICH
Pd/C 10%	ACROS

CHEMICAL	SUPPLIER
Fmoc protected amino acids	SENN CHEMICALS
2-chloro-trityl-chloride resin	CBL

VI.1.1.2 Solvents

All solvents used for synthesis were analytical grade. When anhydrous conditions were required, solvents such as THF and CH_2Cl_2 were dehydrated using specific dehydrating agents or high quality commercial solvents and treated with molecular sieves (porosity 4Å) were used (DMF, DMSO). THF anhydrous was obtained by reflux on Na/benzophenone and CH_2Cl_2 by refluxing on CaH_2. Water was purified using a Millipore filter system MilliQ®.

VI.1.2 Characterization Methods

VI.1.2.1 Nuclear Magnetic Resonance

NMR spectra were recorded in $CDCl_3$ using a Brucker DPX 300 spectrometer equipped with a 5 mm $^{13}C/^{1}H$ probe for both proton (300 MHz) and carbon (75 MHz). The peak values are given as ppm (δ), using the tetramethylsilane or the residual deuterated solvent proton as reference.

VI.1.2.2 Transmission Electron Microscopy

Transmission electron microscopy (TEM) was performed on a Hitachi 600 microscope with an accelerating voltage of 75 kV. Pictures were taken using a CCD high-resolution camera AMT.
The samples were dispersed in water or ethanol by sonication, deposited on a carbon-coated copper TEM grid and dried. TEM images were recorded at the RIO Microscopy Facility Platform of Esplanade Campus (Strasbourg, France).

VI.1.2.3 Thermogravimetric Analysis

The thermogravimetric analysis were performed using TGA Q500 TA instrument with a ramp of 10°C min^{-1} under N_2 using a flow rate of 60 mL min^{-1} from 100 to 900°C.

VI.1.2.4 UV-Vis Spectroscopy

UV-Vis spectra were recorded using a Varian Cary5000 spectrophotometer between 200 and 800 nm.

VI.1.2.5 Chromatography

The reactions were monitored by thin-layer chromatography (TLC) on silica gel (F_{254} Merck) and the products were visualized by ultraviolet light and/or on ninhydrin spray followed by heating. Chromatographic purifications were done with silica gel (Merck Kieselgel 60, 40-60 μm, 230-400 mesh ASTM) in standard column.

HPLC analyses were performed on a Varian ProStar 240 instrument, equipped with a ProStar 410 autosampler and a ProStar 330 PDA detector, using a Macherey-Nagel Nucleodur 100-3 C_{18} column. Gradient: 5-65% B in 10 min. Eluents: A: H_2O + 0.1% TFA; B: MeCN + 0.08% TFA.

VI.1.2.6 Quantitative Kaiser Test

Three solutions were prepared separately:

• 10 g of phenol dissolved in 20 mL of ethanol (solution I)

• 2 mL of KCN 1 mM (aqueous solution) dissolved in 98 mL of pyridine (solution II)

• 1.0 g of ninhydrin dissolved in 20 mL of ethanol (solution III)

An amount of approximately 200-300 μg of free amino CNT conjugates was carefully weighted in a test tube and the following solutions are carefully added in this order: 75 μL of solution I, 100 μL of solution II and 75 μL of solution III. As blank solution, the three solutions were mixed in a test tube without CNTs. The test tube was sonicated in water bath for 3 min, heated at 120°C for 5 min and then removed, 4.75 mL of 60% ethanol were added immediately for a final volume of 5 mL. The tube was then mixed to render the violet colour homogeneous.

A UV/Vis cuvette was filled with the blank solution (pale yellow) to collect the baseline. The absorbance of each sample was measured at 570 nm. The calculation of the amine loading is made using the Equation VI.1. The result is expressed as micromole of amino group per gram of material. A series of at least three to five measurements are necessary to reduce the standard deviation.

Equation VI.1: CNT loading calculation.

$$\mu mol / g = \frac{[Abs_{sample} - Abs_{blank}] \cdot dilution\ (mL) \cdot 10^6}{Molar\ extinction\ coefficient \cdot sample\ weight(mg)}$$

Where dilution is equal to 5 mL and molar extinction coefficient to 15000 M^{-1} cm^{-1}.

VI.1.2.7 Argentometric Titration

These experiments were performed by Dr. Marco Ballestri at Istituto CNR per la Sintesi Organica e Fotoreattività ‘‘I.S.O.F.’’, Bologna (Italy).

The concentration of Cl^- ions in aqueous solutions of ox-MWCNTs **C1a** was measured by argentometric titration using as electrode an INGOLD Ag 4805-s7/120 combination silver and

conducted on a Mettler Toledo Seven Multi. Several titrations were performed using different quantities of f-MWCNTs. To have a good reproducibility it is necessary to use 20–30 mg. The potentiometric titration was carried out using an aqueous solution of $AgNO_3$ (0.0506 M). The $AgNO_3$ solution was previously standardized with NaCl standard solution (0.019 M). The titration was carried out in high ionic strength conditions by adding 25 mL of 1.0 M KNO_3 aqueous solution to the mixture and adjusting the pH to 1 with H_2SO_4. The loading was calculated from the Equation VI.2.

Equation VI.2: ox-MWCNT loading calculation.

$$Loading\ (mmol/g) = \frac{V(Eq.P.)(mL)\cdot[AgNO_3](mmol/mL)}{sample\ weight(g)}$$

Where V (Eq.P.) is the volume of $AgNO_3$ titration solution at the equivalent point, [$AgNO_3$] is the molarity of $AgNO_3$, while sample weight is the weight of the sample that is titrated.

The equivalence point was found by a drawing method. First, two parallel tangent lines with the same slope to the titration curve were drawn before and after a large potential change. Next, a third parallel line was drawn at the same distance from the two parallel lines. The intersection between the titration curve and the third parallel line gave the equivalent point. The loading value is an average of three titrations performed for each batch [Samorì, C., *et al.* 2010b].

VI.1.2.8 Surface Plasmon Resonance

These experiments were conducted with the help of Dr. O. Chaloin in our group in Strasbourg.

Surface plasmon resonance measurements were performed on the BIACORE 3000 system. The sensor chip CM5, surfactant P20, amine coupling kit containing *N*-hydroxysuccinimide (NHS) and 1-(3-dimethylaminopropyl)-3-ethylcarbodiimide hydrochloride (EDC·HCl), were purchased from BIACORE (Uppsala, Sweden) and streptavidin from Sigma-Aldrich. All biosensor assays were performed with Hepes-buffered saline (HBS-EP) as running buffer (10 mM Hepes, 150 mM sodium acetate, 3 mM magnesium acetate, 0.005% surfactant P20, pH 7.4). The different compounds were dissolved in the running buffer. The surface of a sensor CM5 chip was activated by EDC/NHS. Immobilisation of streptavidin was performed by injection onto the activated surface with 35 µL of streptavidin (100 $\mu g \cdot mL^{-1}$ in formate buffer, pH 4.3), which gave a signal of approximately 5000 RU, followed by 20 µL of ethanolamine hydrochloride (pH 8.5) to saturate the free activated sites of the matrix. Biotinylated MUC1 peptide and scrambled MUC1 peptide (1 µM in Hepes buffer) were allowed to interact with streptavidin until a response of 700 RU was obtained. Similarly, β-catenin (0.2 µM in Hepes buffer) was allowed to interact with streptavidin until a response of 3000 RU was obtained. All binding experiments were carried out at 25°C with a constant flow rate of 20

$\mu L \cdot min^{-1}$. Different concentrations of proteins alone (Ab, Fab, scFv or VHH_T and VHH_C) or CNT-based conjugates were injected for 3 min, followed by a dissociation phase of 3 min. The sensor chip surface was regenerated after each experiment by injection of 10 µL of 10 mM HCl. The kinetic parameters (k_a, k_d and K_D) were calculated using the BIAeval 4.1 software. Global analysis was performed using the simple Langmuir binding model. The specific binding profiles were obtained after subtracting the response signal from the peptide control. Fitting to each model was considered based on the reduced chi square and randomness of residue distribution. The K_D SD (standard deviation) value was calculated from the k_a SD and the k_d SD given by the fitting to the Langmuir binding model on BIAeval software.

VI.1.2.9 Gel Electrophoresis

These experiments were conducted with the help of Dr. C. Smulski in our group in Strasbourg.
Gel electrophoresis was performed using a Novex® 8-16% Tris-Glycine gel (Invitrogen, Carlsbad, California) or a Mini-PROTEAN® TGX™ 4-15% Tris-Glycine gel (Bio-Rad Laboratories, Hercules, California) and run under non-reducing and reducing conditions (5% β-mercaptoethanol). The gels were stained with Coomassie blue.

VI.1.2.10 Western Blot Analysis

This experiment was conducted with the help of Dr. C. Smulski in our group in Strasbourg.
VHH_C-MWCNTs-FITC **C30b** conjugate was incubated for 3 h in mice serum or as control in PBS at 37°C. After incubation in serum, the construct was washed three times with PBS. The CNT-based conjugates were deposited in a 4-15% Tris-Glycine gel and the protein bound to CNTs separated by gel electrophoresis and electrotransferred onto nitrocellulose membrane. The membrane was blocked with 5% skim milk in PBS + 0.1 % Tween 20 (50 mL) overnight (4°C). To detect the protein VHH_C, the membrane was incubated 60 min with anti-His tag horseradish peroxidase conjugate (Sigma) and washed four times with PBS + 0.1 % Tween 20 and once with PBS (each step: 5 minutes, room temperature, gentle shaking). The membrane was incubated with dextran sulfate 1% in buffer citrate and the protein was revealed *via* TMB chromogenic reaction.

VI.2 Chemical Synthesis

VI.2.1 Synthesis of the Amino Acid Derivative

Synthesis of {2-[2-(2-amino-ethoxy)-ethoxy]-ethyl}-carbamic acid *tert*-butyl ester (1)

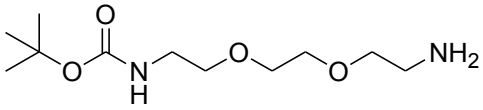

To a solution of 2,2'-(ethylene-dioxy)bis(ethylamine) (50.6 g, 341 mmol) in 1,4-dioxane (200 mL) was added a solution of Boc_2O (7.35 g, 34 mmol) in 1,4-dioxane (120 mL), dropwise over a period of 5 h. The reaction mixture was stirred overnight at room temperature. The solvent was removed under reduced pressure and the residue dissolved in DCM (100 mL), washed with water (3x150 mL), dried (Na_2SO_4) and evaporated. The final product was purified by flash chromatography in DCM/MeOH 9:1.

$C_{11}H_{24}N_2O_4$ (MW 248.32), yield: 2.82 g (11 mmol, 33%).

^{1}H NMR (300 MHz, $CDCl_3$): δ 1.43 (s, 9 H), 2.03 (s, 2 H), 2.84-3.59 (m, 12 H), 5.21 (bs, 1 H).

^{13}C NMR (75 MHz, $CDCl_3$): δ 28.27, 40.16, 41.51, 70.04, 73.14, 78.83, 155.92.

Synthesis of {2-[2-(2-benzyloxycarbonylamino-ethoxy)-ethoxy]-ethyl}-carbamic acid *tert*-butyl ester (2)

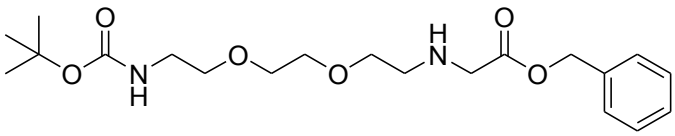

To a solution of compound **1** (2.8 g, 11 mmol) in 1,4-dioxane (60 mL) cooled to 0°C, was added a solution of benzyl-bromoacetate (0.5 mL, 3.4 mmol) in 1,4-dioxane (30 mL), dropwise over a period of 2 h. The reaction mixture was allowed to reach room temperature and was stirred overnight. The solvent was removed under reduced pressure and the residue dissolved in DCM (50 mL), washed with water (3x100 mL), dried (Na_2SO_4) and evaporated. The final product was purified by flash chromatography in DCM/ MeOH 9.5:0.5.

$C_{20}H_{32}N_2O_6$ (MW 396.48), yield: 0.67 g (1.7 mmol, 52%).

^{1}H NMR (300 MHz, $CDCl_3$): δ 1.43 (s, 9 H), 1.99 (bs, 1 H), 2.80-3.61 (m, 14 H), 5.17 (s, 2 H), 5.21 (bs, 1 H), 7.35 (m, 5 H).

^{13}C NMR (75 MHz, $CDCl_3$): δ 28.42, 40.36, 48.67, 50.79, 66.55, 70.14, 70.23, 70.55, 79.10, 128.37, 128.59, 135.58, 156.03, 172.07.

Synthesis of {2-[2-(2-*tert*-butoxycarbonylamino-ethoxy)-ethoxy]-ethylamino}-acetic acid (3)

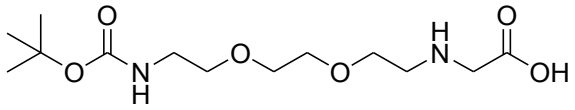

To a solution of compound **2** (0.67 g, 1.7 mmol) in methanol (20 mL) were added 70 mg of Pd/C (10%). The suspension was placed under H_2 atmosphere. The reaction mixture was stirred for 5 h at room temperature. The solution was filtered through a celite pad and the solvent was evaporated under reduced pressure.

$C_{13}H_{26}N_2O_6$ (MW 306.36), yield: 0.5 g (1.6 mmol, 93%).

^{1}H NMR (300 MHz, $CDCl_3$): δ 1.39 (s, 9 H), 3.20-3.78 (m, 14 H), 5.54 (s, 1 H), 6.23 (bs, 1 H), 8.21 (bs, 1 H).

^{13}C NMR (75 MHz, $CDCl_3$): δ 28.46, 40.35, 46.54, 50.02, 66.54, 70.04, 70.15, 70.29, 79.05, 156.14, 170.83.

VI.2.2. Other Organic Compounds

Synthesis of 2-{2-[2-(1,3-dioxo-1,3-dihydro-isoindol-2-yl)-ethoxy)-ethoxy]-ethyl}-carbamic acid *tert*-butyl ester (4)

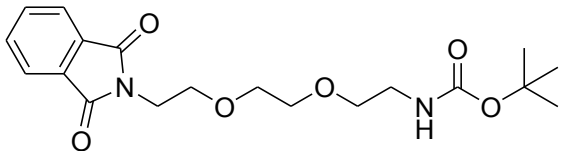

A solution of compound **1** (2 g, 8 mmol), mono-methylphthalate (1.44 g, 8 mmol), benzotriazole-1-yl-oxy-tris-(dimethylamino)-phosphonium hexafluorophosphate (BOP) (3.53 g, 8 mmol) and diisopropylethylamine (DIEA) (4 mL, 24 mmol) in CH_3CN (40 mL) was stirred at room temperature for 3 h. A solution of Na_2CO_3 (1.2 g, 11.52 mmol) in water (20 mL) was subsequently added and the reaction was stirred for 30 min at room temperature. The solvent was removed under reduced pressure. AcOEt was added and the solution was washed with saturated $NaHCO_3$, water, 1N $KHSO_4$ and water. The organic phase was dried with Na_2SO_4 and the solvent was evaporated. The product was obtained as an oil and used without further purifications.

$C_{19}H_{26}N_2O_6$ (MW 378.42), yield: 2.4 g (6.3 mmol, 80%).

^{1}H NMR (300 MHz, $CDCl_3$): δ 1.36 (s, 9 H), 3.20-3.60 (m, 12 H), 5.05 (bs, 1 H), 7.65 (dd, J = 3 Hz and 5 Hz, 2 H), 7.78 (dd, J = 3 Hz and 5 Hz, 2 H).

^{13}C NMR (75 MHz, $CDCl_3$): δ 28.39, 37.11, 40,31, 67.87, 69.86, 70.02, 70.21, 77.34, 79.01, 123.18, 132.05, 133.93, 155.94, 168.19.

Synthesis of 2-{2-[2-(2-amino-ethoxy)-ethoxy]-ethyl}-isoindole-1,3-dione (5)

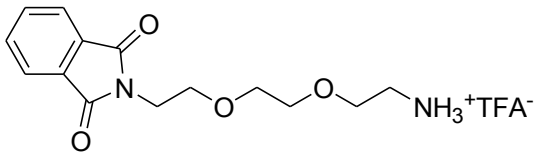

To the compound **4** (2.4 g, 6.3 mmol) was added a solution of TFA/CH_2Cl_2 (1:1 v/v). The reaction mixture was stirred at room temperature for 30 min. The solvent was removed under reduced pressure and the residue precipitated several times from DCM/Et_2O as trifluoroacetic acid salt.

$C_{16}H_{19}F_3N_2O_6$ (MW 392.33), yield: 1.95 g (4.9 mmol, 94 %).

^{1}H NMR (300 MHz, $CDCl_3$): δ 3.19-3.87 (m, 12 H), 7.75 (dd, *J* = 3 Hz and 5 Hz, 2 H), 7.81 (dd, *J* = 3 Hz and 5 Hz, 2 H), 8.04 (sb, 3 H).

^{13}C NMR (75 MHz, $CDCl_3$): δ 37.31, 39.68, 68.24, 68.51, 69.64, 70.05, 118.60, 123.37, 131.87, 134.17, 161.89, 168.57.

Synthesis of *N*-succimidyl 3-maleimidopropionate (6)

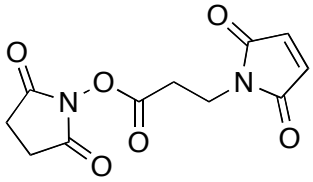

β-Alanine (0.91 g, 10 mmol) was added to a solution maleic anhydride (1.00 g, 10 mmol) in freshly degassed DMF (10 mL). The suspension was stirred for 1h after the amino acid has been dissolved. The resulting solution was cooled in an ice bath and NHS (1.44 g, 12.5 mmol) was added. After approximately 5 min, the ice bath was removed and the solution was stirred for 4 h. The resulting suspension was filtered to remove the precipitated dicyclohexylurea. The filtrate was dissolved in water and the ester extracted with DCM (3x50 mL). The organic phase was dried (Na_2SO_4) and the solvent has evaporated. The ester was precipitated from DCM/Et_2O.

$C_{10}H_{10}N_2O_6$ (MW 266.2), yield: 0.89g (3.3 mmol, 33%).

^{1}H NMR (300 MHz, $CDCl_3$): δ 2.81 (s, 4 H), 3.01 (t, *J* = 7 Hz, 2 H), 3.92 (t, *J* = 7 Hz, 2 H), 6.73 (s, 2H).

^{13}C NMR (75 MHz, $CDCl_3$): δ 25.56, 29.72, 33.04, 134.29, 166.02, 170.05.

Peptide Synthesis

The sequence of the antigen corresponding to the variable number tandem repeat (VNTR) region of MUC1 protein is ^{296}HGVTSAPDTRPAPGSTAPPA^{315}. An additional Lys(Biot) residue was added

to the *N*-terminal part of the antigen for immobilization to the SPR sensor chip. The synthesis of the antigen was performed on a 2-chlorotrityl-chloride resin, using a multichannel peptide synthesizer working on standard Fmoc/tBu chemistry. The synthesis of a scrambled control antigen (APHADPSTPGAPSVTPRTAG) was performed on a Fmoc-Gly-MPPA(Wang) resin using a multichannel peptide synthesizer working on standard Fmoc/tBu chemistry. An additional Lys(Biot) residue was added to the *N*-terminal part of the sequence for immobilization to the SPR sensor chip. Both peptides were purified by semi-preparative HPLC chromatography, characterized by HPLC chromatography and mass spectrometry.

HPLC (antigen): t_R 5.46 min.

HPLC (scrambled antigen): t_R 5.54 min.

MS (ESI, *m/z*) (calcd 2241.5): 1121.4 $[M+H]^{2+}$, 980.2 $[M-C_5H_8N_2OS]^{2+}$, 747.9 $[M+H]^{3+}$ antigen.

MS (ESI, *m/z*) (calcd 2241.5): 1121.2 $[M+H]^{2+}$, 747.9 $[M+H]^{3+}$ scrambled antigen.

VI.3 Mono-functionalization of Carbon Nanotubes

We prepared functionalized carbon nanotubes using as starting material carbon nanotubes produced either from Nanocyl or NanoAmor. Constructs will be therefore categorized with letters **a** and **b** to denote Nanocyl and NanoAmor conjugates, respectively.

Synthesis of Carbon Nanotubes C1

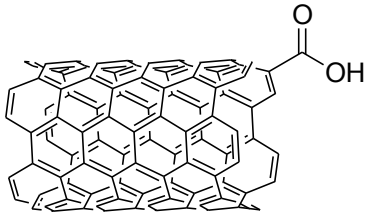

500 mg of MWCNTs were sonicated in a water bath (20 W, 40 kHz) for 24 h in 70 mL of sulfuric acid/nitric acid mixture (3:1 v/v, 98% and 65%, respectively) at room temperature. Deionized water was then carefully added and the oxidized MWCNTs (ox-MWCNTs) were filtered (Omnipore® PTFE membrane filtration, 0.45 μm), re-suspended in water, filtered again until the pH became neutral and dried. Yield: 84%.

Oxidized MWCNTs (ox-MWCNTs) were characterized by TEM and TGA.

Synthesis of Carbon Nanotubes C2 and C2'

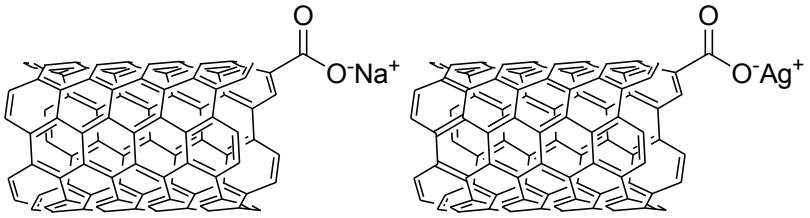

C2 **C2'**

To prepare the silver salt of ox-MWCNTs, ox-MWCNTs **C1a** were first stirred in a 0.05 M aqueous solution of NaOH under Ar atmosphere for 24 h. The resulting sodium salt **C2a** was filtered (PTFE membrane filtration, 0.45 µm) until pH became neutral. Treatment of sodium salt **C2a** with a 0.25 M aqueous solution of $AgNO_3$ for 36 h allowed complete exchange between Na^+ and Ag^+ cations. The silver salt **C2a'** was centrifuged to remove $AgNO_3$ in excess and subsequently dialyzed and lyophilized. Finally, the silver salt **C2a'** was dispersed in a 0.1 M aqueous solution of HCl (0.1 M FixAnal Normex purchased from Fluka).

Synthesis of Carbon Nanotubes C3

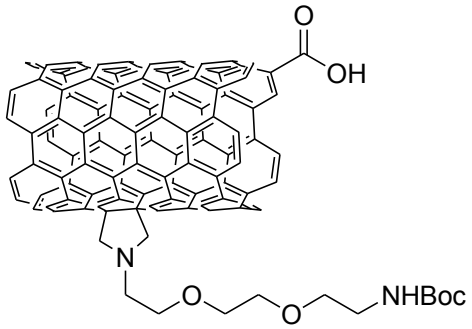

MWCNTs **C1** (100 mg) were suspended in 100 mL of DMF and sonicated in water bath for 20 min. A solution of amino acid **3** (5x100 mg) and paraformaldehyde (5x100 mg) in DMF were added by portions over 5 days (one addition per day). The reaction mixture was heated at 115°C. After cooling to room temperature, the suspension was filtered over a PTFE membrane (0.45 µm). The solid recovered on the filter was dispersed in DMF, sonicated for 15 min in a water bath and filtered over a PTFE membrane (0.45 µm). This sequence was repeated twice with DMF, methanol and diethyl ether. The resulting solid was dried under vacuum.

Synthesis of Carbon Nanotubes C4

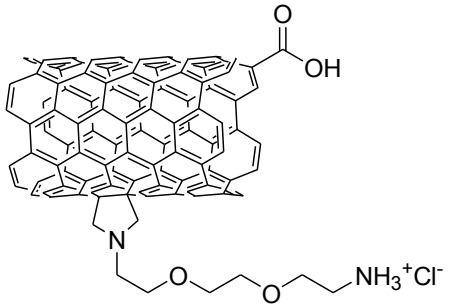

MWCNTs **C3** (50 mg) were suspended in a solution of HCl in dioxane (4 M, 7 mL) and sonicated in water bath for 20 min. The mixture was stirred overnight at room temperature and the product was filtered (PTFE membrane filtration, 0.45 μm). The solid recovered on the filter was dispersed in methanol, sonicated for 15 min in a water bath, and filtered over a PTFE membrane (0.45 μm). This sequence was repeated three times with methanol and twice with diethyl ether. The compound was dialyzed against water (Spectra/Por® dialysis membrane MWCO 12-14,000 Da) for 24-36 h and lyophilized.

Quantitative Kaiser test: 0.12 mmol of NH_2/g of CNTs (**a**); 0.08 mmol of NH_2/g of CNTs (**b**).

The compound was characterized by TEM and TGA.

Synthesis of Carbon Nanotubes C5

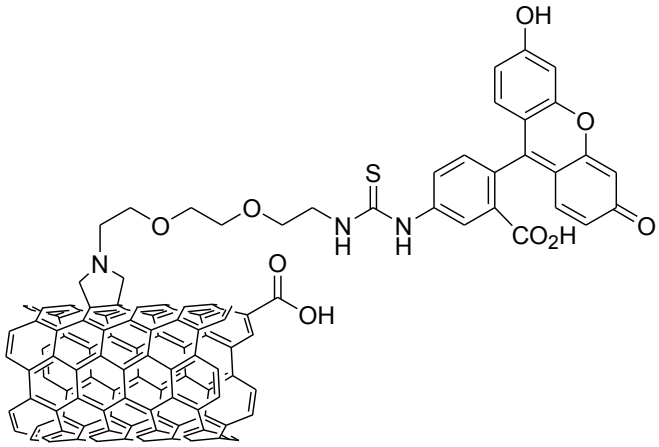

MWCNTs **C4a** (10 mg, 1.2 μmol corresponding to the amount of free NH_2 measured by quantitative Kaiser test) were solubilized in 2 mL of DMF and neutralized with DIEA. A solution of fluorescein isothiocyanate (FITC) (9 mg, 24 μmol) in 1 mL of DMF was added and the solution was stirred for 48 h at room temperature. The suspension was filtered (PTFE membrane filtration, 0.45 μm). The solid recovered on the filter was dispersed in DMF, sonicated for 15 min in a water bath, and filtered over a PTFE membrane (0.45 μm). This sequence was repeated twice with DMF, methanol and diethyl ether. The compound was dialyzed against water (dialysis membrane MWCO 12-14,000 Da) for 24-36 h and lyophilized. The amount of free amines was determined with the

Kaiser test: 30 µmol/g of CNTs. Hence, the amount of fluorescein functions was 90 µmol/g of CNTs. Yield: 75%.

MWCNTs **C5a** were characterized by TEM and TGA.

Synthesis of Carbon Nanotubes C6

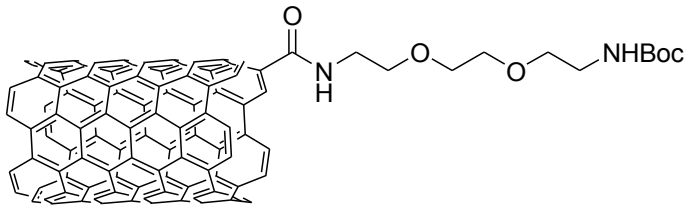

MWCNT **C1a** (50 mg) were suspended in 5 mL of oxalyl chloride, sonicated in a water bath for 20 min and the reaction mixture was heated at 60°C for 24 h. Oxalyl chloride was evaporated under vacuum and a solution of compound **3** (500 mg) in THF was added and the reaction mixture was heated at 65°C for 48 h. After cooling to room temperature, the suspension was filtered over a PTFE membrane (0.45 µm). The solid recovered on the filter was dispersed in DMF, sonicated for 15 min in a water bath and filtered over a PTFE membrane (0.45 µm). This sequence was repeated twice with DMF, methanol and diethyl ether. The resulting solid was dried under vacuum.

MWCNTs **C6a** was characterized by TEM and TGA.

Synthesis of Carbon Nanotubes C7

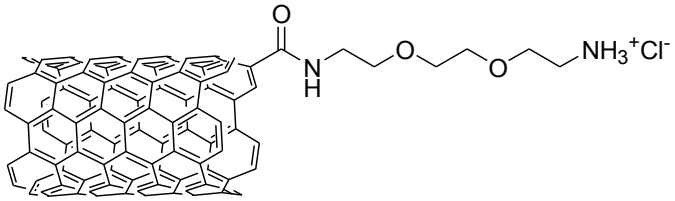

MWCNTs **C6a** (50 mg) were suspended in a solution of HCl in dioxane (4M, 7 mL) and sonicated in a water bath for 20 min. The mixture was stirred overnight at room temperature in the dark and the suspension was filtered (PTFE membrane filtration, 0.45 µm). The solid recovered on the filter was dispersed in methanol, sonicated for 15 min in a water bath and filtered over a PTFE membrane (0.45 µm). This sequence was repeated three times with methanol and twice with diethyl ether. The compound was dialyzed against water (dialysis membrane MWCO 12-14,000 Da) for 24-36h and lyophilized.

Quantitative Kaiser test: 0.39 mmol of NH_2/g of MWCNTs.

Synthesis of Carbon Nanotubes C8

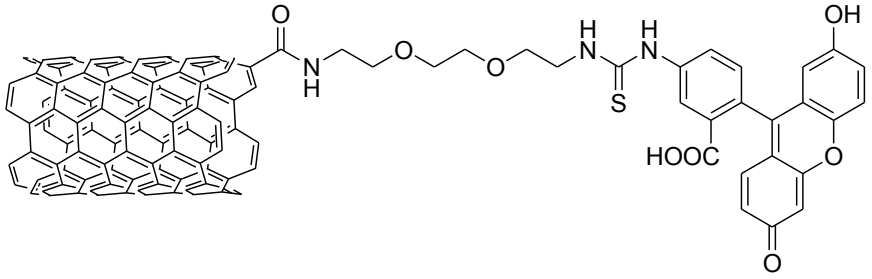

MWCNTs **C7a** (10 mg, 3.9 μmol of NH_2 functions) were solubilized in 2 mL of DMF and neutralized with DIEA. A solution of fluorescein isothiocyanate (FITC) (30 mg, 78 μmol) in 1 mL of DMF was added and the mixture was stirred for 48 h at room temperature in the dark. The suspension was filtered (PTFE membrane filtration, 0.45 μm). The solid recovered on the filter was dispersed in DMF, sonicated for 15 min in a water bath, and filtered over a PTFE membrane (0.45 μm). This sequence was repeated twice with DMF, methanol and diethyl ether. The compound was dialyzed against water (dialysis membrane MWCO 12-14,000 Da) for 24-36 h and lyophilized.
The amount of free amines was determined with the Kaiser test: 90 μmol/g of MWCNTs. Hence, the amount of fluorescein functions was 300 μmol/g of MWCNTs. Yield: 77%.
MWCNTs **C7a** were characterized by TEM and TGA.

Synthesis of Carbon Nanotubes C9

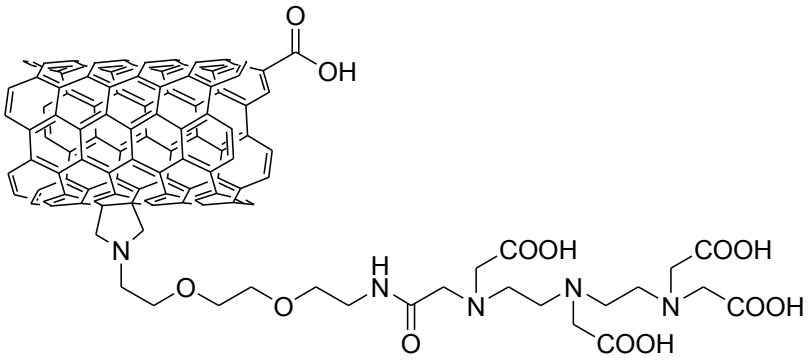

MWCNTs **C4a** (10 mg, 1.2 μmol of NH_2 functions) were solubilized in 2 mL of dry DMSO and neutralized with DIEA. A solution of diethylenetriaminepentaacetic acid (DTPA) dianhydride (15 mg, 40 μmol) in 1 mL of dry DMSO was added and the solution was stirred for 48 h at 60°C. After cooling to room temperature, the suspension was filtered over a PTFE membrane (0.45 μm). The solid recovered on the filter was dispersed in DMF, sonicated for 15 min in a water bath and filtered over a PTFE membrane (0.45 μm). This sequence was repeated twice with DMF, methanol and diethyl ether. The compound was dialyzed against water (dialysis membrane MWCO 12-14,000 Da) for 36 h and lyophilized. The amount of free amines was determined with the Kaiser test: 20 μmol/g of CNTs. Hence, the amount of DTPA functions was 100 μmol/g of CNTs. Yield: 85%.
MWCNTs **C9** were characterized by TEM and TGA.

Synthesis of Carbon Nanotubes C10

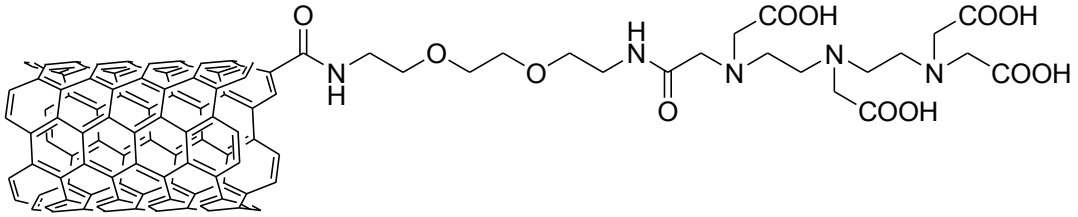

MWCNTs **C6a** (10 mg, 3.9 μmol of NH_2 functions) were solubilized in 2 mL of dry DMSO and neutralized with DIEA. A solution of DTPA dianhydride (15 mg, 40 μmol) in 1 mL of dry DMSO was added and the solution was stirred for 48 h at 60°C. After cooling to room temperature, the suspension was filtered over a PTFE membrane (0.45 μm). The solid recovered on the filter was dispersed in DMF, sonicated for 15 min in a water bath and filtered over a PTFE membrane (0.45 μm). This sequence was repeated twice with DMF, methanol and diethyl ether. The compound was dialyzed against water (dialysis membrane MWCO 12-14,000 Da) for 36 h and lyophilized. The amount of free amines was determined with the Kaiser test: 30 μmol/g of CNTs. Hence, the amount of DTPA functions was 360 μmol/g of CNTs. Yield: 92%.

MWCNTs **C10a** were characterized by TEM and TGA.

Synthesis of *N*-hydroxysuccinimide-functionalized Carbon Nanotubes C11

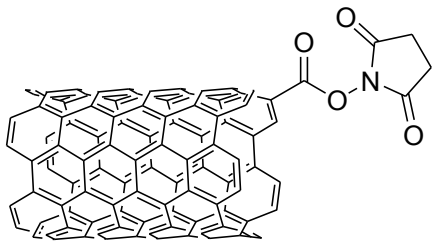

A suspension of 10 mg of **C1a** in DMF (5 mL) was sonicated in a water bath for 20 min. A solution of EDC·HCl (85 mg), NHS (52 mg) and DIEA (75 μL) in DMF (5 mL) was added and the reaction mixture was stirred for 24 h at room temperature under Ar. The suspension was filtered over a PTFE membrane (0.45 μm). The solid recovered on the filter was dispersed in DMF, sonicated for 15 min in a water bath and filtered over a PTFE membrane (0.45 μm). This sequence was repeated twice with DMF, isopropanol and diethyl ether. The resulting solid was dried under vacuum.

Synthesis of Antibody-functionalized Carbon Nanotubes C12

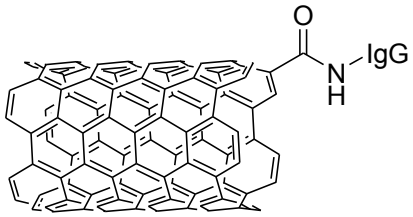

10 mg of **C11a** were dispersed in 20 mL of anti-MUC1 solution (3 μM) in PBS buffer (pH 7.4) and the mixture was shaken for 60 h at room temperature. The suspension was centrifuged and the precipitate was collected and washed thoroughly with PBS (pH 7.4) until there was no Ab detected in the supernatant by UV-Vis spectroscopy. Finally, the resulting Ab-MWCNT conjugate **C12** was dialyzed (dialysis membrane MWCO 300,000 Da) against PBS buffer (pH 7.4) for 24 h and stored at 4°C. The degree of functionalization was determined by TGA and was calculated as 3.3 μmol of Ab per gram of CNTs.

Synthesis of Maleimido-propionate Functionalized Carbon Nanotubes C13

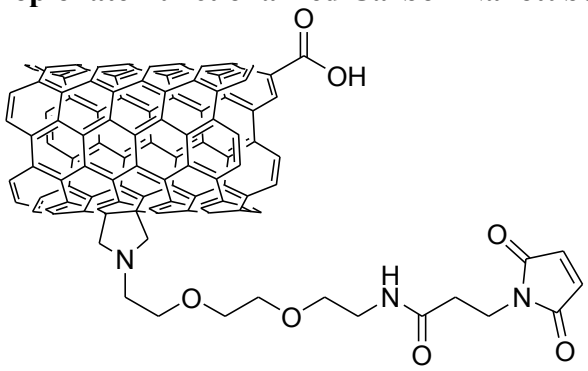

MWCNTs **C3a** (20 mg, 2.3 μmol of NH_2 loading) were suspended in DMF and neutralized with DIEA. *N*-succinimidyl-3-maleimidopropionate **6** (10 mg, 37 μmol) was dissolved in DMF and added to the solution with MWCNTs. The reaction was stirred for 48 h at room temperature. The suspension was filtered over a PTFE membrane (0.45 μm). The solid recovered on the filter was dispersed in DMF, sonicated for 15 min in a water bath and filtered over a PTFE membrane (0.45 μm). This sequence was repeated twice with DMF, methanol and diethyl ether. The resulting solid was dried under vacuum.

The amount of free amines was determined with the Kaiser test: 25 μmol/g of CNTs. Hence, the amount of maleimide functions was 85 μmol/g of CNTs. Yield: 77%.

Thiolation of the Antibody

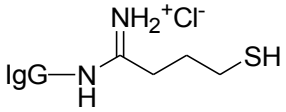

Reactive sulfhydryl groups were introduced onto the antibody by reaction with 2-iminothiolane-HCl (Traut's reagent). A freshly prepared solution of 2-iminothiolane (14 mM, 90 μL) in PBS buffer/5mM EDTA (pH increased to 8 with 1 M bicarbonate buffer) was added to the Ab solution (67 μM, 1 mL) in PBS buffer/5 mM EDTA (pH increased to 8 with 1 M bicarbonate buffer). The mixture was shaken for 1h at room temperature and the excess of 2-iminothiolane removed by dialysis (dialysis membrane MWCO 12-14,000 Da) against PBS buffer/4 mM EDTA (pH 6.5). The number of reactive thiol groups introduced was assessed by Ellman's essay.

Synthesis of Antibody-functionalized Carbon Nanotubes C14

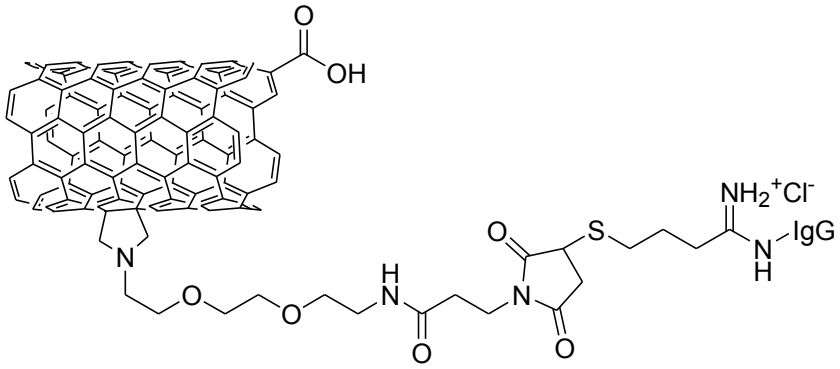

MWCNTs **C13a** (10 mg) were dispersed in 20 mL of thiolated Ab solution (2.7 μM) in PBS buffer (4mM EDTA, pH 6.5) and the mixture is shaken for 24 h at room temperature.

The MWCNTs-Ab conjugate was centrifuged and washed thoroughly with PBS buffer (pH 7.4), until there was no Ab detected in the supernatant by a UV-Vis spectrophotometer (Varian Cary 5000). The resulting conjugate was dialyzed (dialysis membrane MWCO 300,000 Da) against PBS buffer (pH 7.4) for 24 h and stored at 4°C. The degree of functionalization was determined by TGA and was calculated as 2 μmol of Ab per gram of CNTs.

VI.4 Multi-functionalization of Carbon Nanotubes

Synthesis of Carbon Nanotubes C15

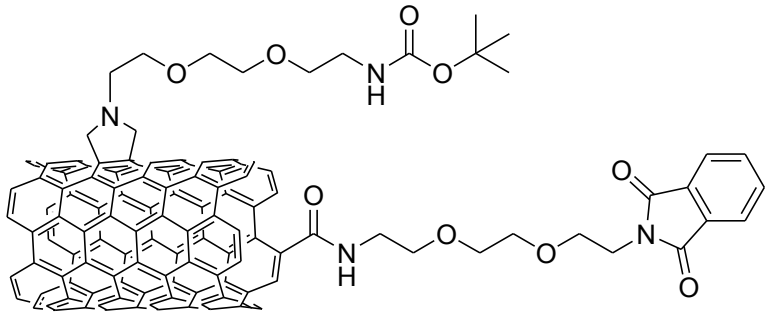

MWCNTs **C3** (50 mg) were suspended in dry DMF (5 mL). HOBt (67 mg, 496 μmol) and EDC (95 mg, 496 μmol) were added and the suspension was sonicated for 10 min. Amine **5** (200 mg, 510 μmol) and DIEA (150 μL) were dissolved in DMF (3 mL) and added to the reaction mixture. The reaction was stirred for 48 h at room temperature. The suspension was filtered over a PTFE membrane (0.45 μm). The solid recovered on the filter was dispersed in DMF, sonicated for 15 min in a water bath and filtered over a PTFE membrane (0.45 μm). This sequence was repeated twice with DMF, methanol and diethyl ether. The resulting solid was dried under vacuum.
MWCNTs **C15** were characterized by TEM and TGA.

Synthesis of Carbon Nanotubes C16 and C16'

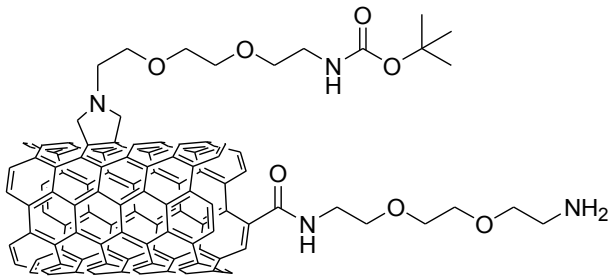

C16

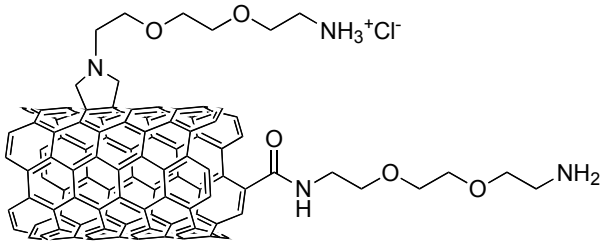

C16'

MWCNTs **C15** (40 mg) were suspended in a solution of hydrazine hydrate (120 μL) in ethanol (20 mL) and sonicated in water bath for 20 min. The mixture was stirred overnight at room temperature and the suspension was filtered over a PTFE membrane (0.45 μm). The solid recovered on the filter was dispersed in DMF, sonicated for 15 min in a water bath and filtered over a PTFE membrane (0.45 μm). This sequence was repeated twice with DMF, methanol and diethyl ether. The resulting solid was dried under vacuum. The compound was dialyzed against water (dialysis membrane MWCO 12-14,000 Da) for 24-36 h and lyophilized.
Quantitative Kaiser test: 0.18 mmol of NH_2/g of CNTs (**a**); 0.12 mmol of NH_2/g of CNTs (**b**).

To prepare MWCNTs **C16'**, MWCNTs **C16** (5 mg) were suspended in a solution of HCl in dioxane (4M, 5 mL) and sonicated in water bath for 20 min. The mixture was stirred overnight at room temperature and the suspension was filtered over a PTFE membrane (0.45 µm). The solid recovered on the filter was dispersed in methanol, sonicated for 15 min in a water bath and filtered over a PTFE membrane (0.45 µm). This sequence was repeated three times with methanol and twice with diethyl ether. The resulting solid was dried under vacuum.

Synthesis of Carbon Nanotubes C17

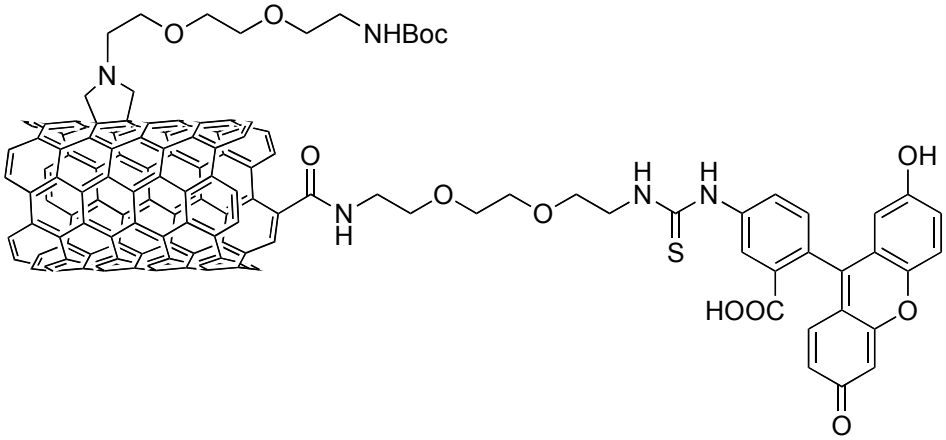

MWCNTs **C16** (20 mg, 3.6 µmol (**a**) and 2.4 µmol (**b**) of NH_2 functions) were solubilized in 6 mL of DMF and neutralized with DIEA. A solution of FITC (30 mg, 78 µmol) in 2 mL of DMF was added and the solution was stirred for 48 h at room temperature. The suspension was filtered over a PTFE membrane (0.45 µm). The solid recovered on the filter was dispersed in DMF, sonicated for 15 min in a water bath and filtered over a PTFE membrane (0.45 µm). This sequence was repeated twice with DMF, methanol and diethyl ether. The resulting solid was dried under vacuum.

The amount of free amines was determined with the Kaiser test: 70 µmol/g (**a**) and 60 µmol/g (**b**). Hence, the amount of fluorescein was 110 µmol/g of CNTs (**a**) and 60 µmol/g of CNTs (**b**). Yield: 60% (**a**) and 50% (**b**).

MWCNTs **C17** were characterized by TEM and TGA.

Synthesis of Carbon Nanotubes C18

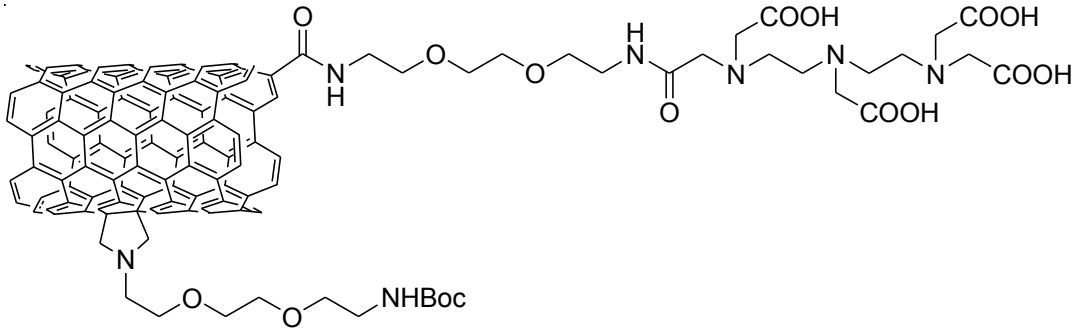

MWCNTs **C16** (20 mg, 3.6 µmol (**a**) and 2.4 µmol (**b**) of NH_2 functions) were solubilized in 3 mL of dry DMSO and neutralized with DIEA. A solution of DTPA dianhydride (28 mg, 78 µmol) in 1 mL of dry DMSO was added and the solution was stirred for 48 h at 60°C. After cooling to room temperature, the suspension was filtered over a PTFE membrane (0.45 µm). The solid recovered on the filter was dispersed in DMF, sonicated for 15 min in a water bath and filtered over a PTFE membrane (0.45 µm). This sequence was repeated twice with DMF, methanol and diethyl ether. The resulting solid was dried under vacuum. The amount of free amines was determined with the Kaiser test: 40 µmol/g of CNTs (**a**) and 45 µmol/g of CNTs (**b**). Hence, the amount of DTPA was 140 µmol/g of CNTs (**a**) and 75 µmol/g of CNTs (**b**). Yield: 77% (**a**) and 63% (**b**).
MWCNTs **C18** were characterized by TEM and TGA.

Synthesis of Carbon Nanotubes C19

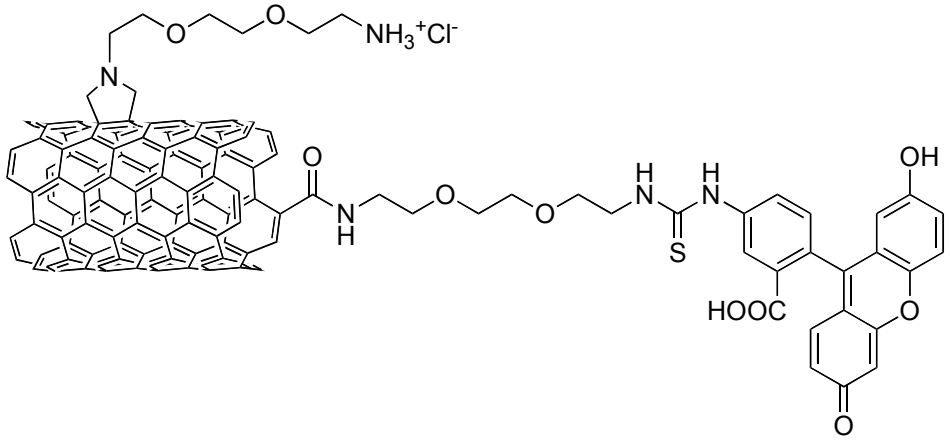

MWCNTs **C17** (20 mg) were suspended in a solution of HCl in dioxane (4M, 5 mL) and sonicated in water bath for 20 min. The mixture was stirred overnight at room temperature and the suspension was filtered over a PTFE membrane (0.45 µm). The solid recovered on the filter was dispersed in methanol, sonicated for 15 min in a water bath and filtered over a PTFE membrane (0.45 µm). This sequence was repeated three times with methanol and twice with diethyl ether. The resulting solid was dried under vacuum. The amount of free amines was determined with the Kaiser test: 120 µmol/g (**a**) and 80 µmol/g (**b**).

Synthesis of Carbon Nanotubes C20

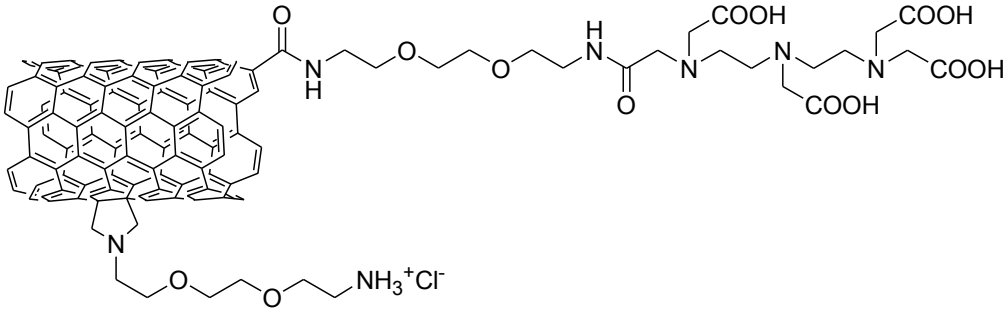

MWCNTs **C18** (20 mg) were suspended in a solution of HCl in dioxane (4 M, 5 mL) and sonicated in water bath for 20 min. The mixture was stirred overnight at room temperature and the suspension was filtered over a PTFE membrane (0.45 µm). The solid recovered on the filter was dispersed in methanol, sonicated for 15 min in a water bath and filtered over a PTFE membrane (0.45 µm). This sequence was repeated three times with methanol and twice with diethyl ether. The resulting solid was dried under vacuum. The amount of free amines was determined with the Kaiser test: 120 µmol/g of CNTs (**a**) and 80 µmol/g of CNTs (**b**).

Synthesis of Carbon Nanotubes C21

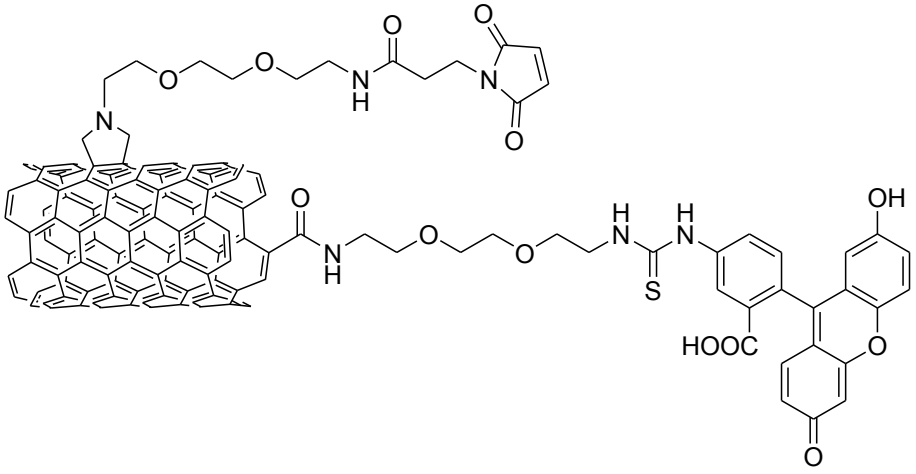

MWCNTs **C19** (15 mg; 1.8 µmol (**a**) and 1.2 µmol (**b**) of NH_2 functions) were suspended in DMF and neutralized with DIEA. *N*-succinimidyl-3-maleimidopropionate **6** (6 mg, 22 µmol) was dissolved in DMF and added to the dispersion of MWCNTs. The reaction was stirred for 48 h at room temperature. The suspension was filtered over a PTFE membrane (0.45 µm). The solid recovered on the filter was dispersed in DMF, sonicated for 15 min in a water bath and filtered over a PTFE membrane (0.45 µm). This sequence was repeated twice with DMF, methanol and diethyl ether. The resulting solid was dried under vacuum. The amount of free amines was determined with the Kaiser test: 30 µmol/g of CNTs (**a**) and 40 µmol/g of CNTs (**b**). Hence, the amount of maleimide was 90 µmol/g of CNTs (**a**) and 40 µmol/g of CNTs (**b**). Yield: 75% (**a**) and 50% (**b**).
MWCNTs **C21** were characterized by TEM and TGA.

Synthesis of Carbon Nanotubes C22

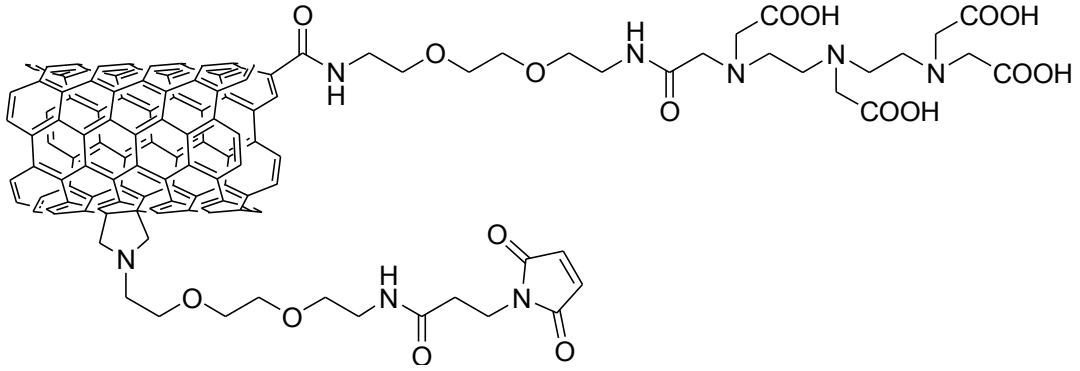

MWCNTs **C20** (15 mg; 1.8 μmol (**a**) and 1.2 μmol (**b**) of NH_2 functions) were suspended in DMF and neutralized with DIEA. *N*-succinimidyl-3-maleimidopropionate **6** (7 mg, 25 μmol) was dissolved in DMF and added to the dispersion of MWCNTs. The reaction was stirred for 48 h at room temperature. The suspension was filtered over a PTFE membrane (0.45 μm). The solid recovered on the filter was dispersed in DMF, sonicated for 15 min in a water bath and filtered over a PTFE membrane (0.45 μm). This sequence was repeated twice with DMF, methanol and diethyl ether. The resulting solid was dried under vacuum. The amount of free amines was determined with the Kaiser test: 30 μmol/g of CNTs (**a**) and 50 μmol/g of CNTs (**b**). Hence, the amount of maleimide functions was 90 μmol/g of CNTs (**a**) and 30 μmol/g of CNTs (**b**). Yield: 75% (**a**) and 38% (**b**).

MWCNTs **C22** were characterized by TEM and TGA.

Synthesis of Antibody-functionalized Carbon Nanotubes C23

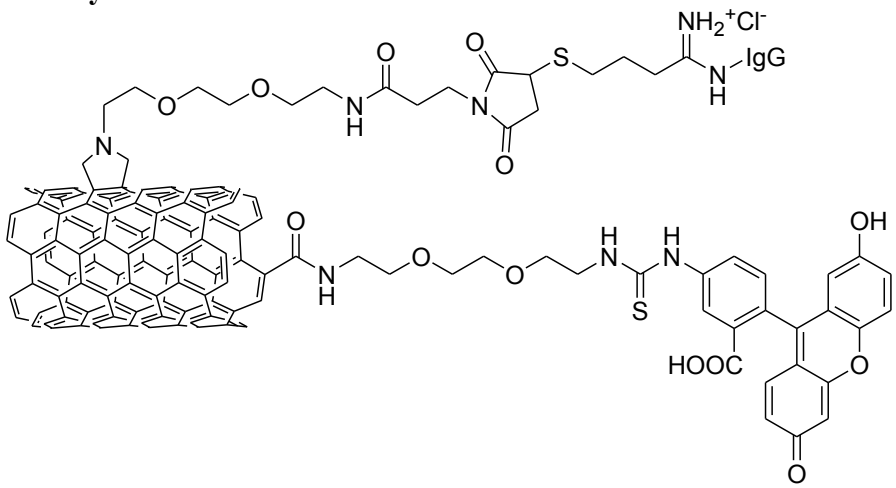

The maleimido-derivatized MWCNTs **C21** (7 mg) were dispersed in 14 mL of thiolated Ab solution (2.6 μM) in PBS buffer (4 mM EDTA, pH 6.5) and the mixture was shaken for 24 h at room temperature. The Ab-CNT conjugate was centrifuged and washed thoroughly with PBS buffer (pH 7.4) until there was no Ab detected in the supernatant by UV-Vis spectroscopy. Finally, the resulting Ab-CNT conjugate was dialyzed (dialysis membrane MWCO 300,000 Da) against PBS

buffer (pH 7.4) for 24 h and stored at 4°C. The degree of functionalization was determined by TGA and was calculated as 1.3 μmol (**a**) and 0.6 μmol (**b**) of Ab per gram of CNTs.
MWCNTs **C23** were characterized by TEM and TGA.

Synthesis of Antibody-functionalized Carbon Nanotubes C24

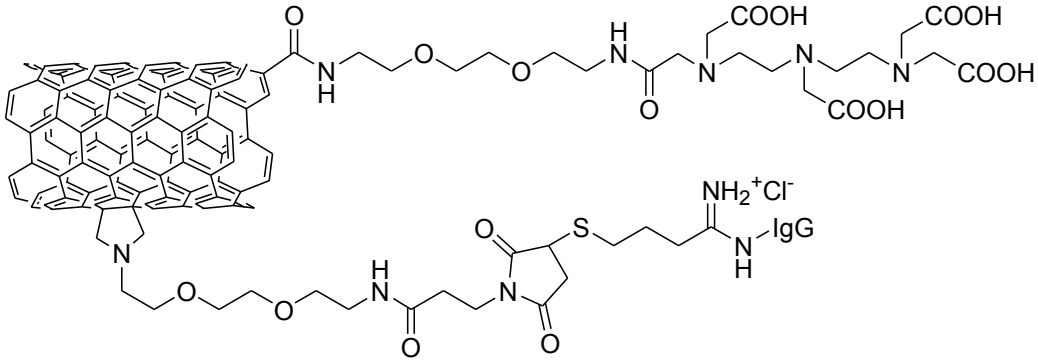

The maleimido-derivatized MWCNTs **C22** (6 mg) were dispersed in 12 mL of thiolated Ab solution (2.6 μM) in PBS buffer (4 mM EDTA, pH 6.5) and the mixture was shaken for 24 h at room temperature. The Ab-CNT conjugate was centrifuged and washed thoroughly with PBS buffer (pH 7.4) until there was no Ab detected in the supernatant by UV-Vis spectroscopy. Finally, the resulting Ab-CNT conjugate was dialyzed (dialysis membrane MWCO 300,000 Da) against PBS buffer (pH 7.4) for 24 h and stored at 4°C. The degree of functionalization was determined by TGA and was calculated as 1.3 μmol of Ab (**a**) and 0.6 μmol (**b**) per gram of CNTs.
MWCNTs **C24** were characterized by TEM and TGA.

Reduction of Fragment Antigen Binding (Fab)

A freshly prepared solution of 2-mercaptoethylamine (200 mM, 36 μL) in sodium acetate (50 mM) / EDTA (2 mM) buffer (pH 6) was added to the Fab solution (0.1 mM, 1.7 mL) in sodium acetate (50 mM) / EDTA (2 mM) buffer (pH 6). The mixture was shaken for 2 h at room temperature and subsequently the excess of 2-mercaptoethylamine was removed by buffer exchange into sodium acetate (50 mM)/ EDTA (2 mM) buffer (pH 6) using Sephadex^{TM} G25 Medium (PD10 desalting column). The number of free sulfhydryl groups introduced was assessed by Ellman's assay.

Synthesis of Fab-functionalized Carbon Nanotubes C25

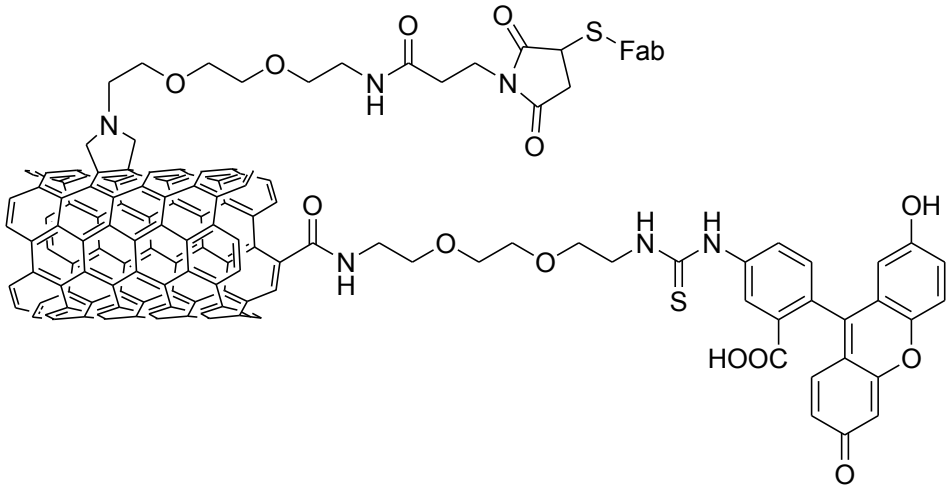

The maleimido-derivatized MWCNTs **C21** (6 mg) were dispersed in 12 mL of reduced Fab solution (5.4 μM) in PBS buffer (4mM EDTA, pH 6.5) and the mixture was shaken for 24h at room temperature. The Fab-CNT conjugate was centrifuged and washed thoroughly with PBS buffer (pH 7.4) until there was no Fab detected in the supernatant by UV-Vis spectroscopy. Finally, the resulting Fab-CNT conjugate was dialyzed (dialysis membrane MWCO 300,000 Da) against PBS buffer (pH 7.4) for 24 h and stored at 4°C. The degree of functionalization was determined by TGA and was calculated as 2.9 μmol of Fab (**a**) and 3.0 μmol (**b**) per gram of CNTs.
MWCNTs **C25** were characterized by TEM and TGA.

Synthesis of Fab-functionalized Carbon Nanotubes C26

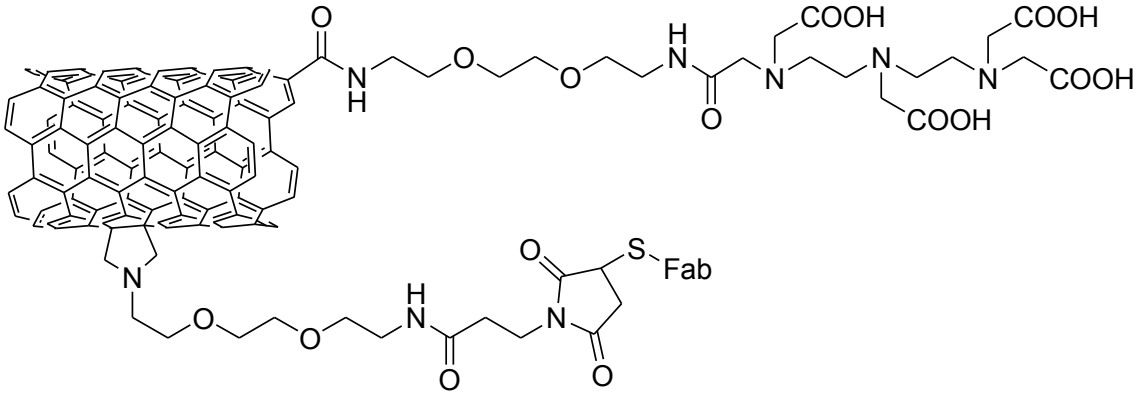

The maleimido-derivatized MWCNTs **C22** (6 mg) were dispersed in 12 mL of reduced Fab solution (5.4 μM) in PBS buffer (4 mM EDTA, pH 6.5) and the mixture was shaken for 24 h at room temperature. The Fab-CNT conjugate was centrifuged and washed thoroughly with PBS buffer (pH 7.4) until there was no Fab detected in the supernatant by UV-Vis spectroscopy. Finally, the resulting Fab-CNT conjugate was dialyzed (dialysis membrane MWCO 300,000 Da) against PBS

buffer (pH 7.4) for 24 h and stored at 4°C. The degree of functionalization was determined by TGA and was calculated as 2.9 μmol of Fab (**a**) per gram of CNTs.
MWCNTs **C26** were characterized by TEM and TGA.

Reduction of Single Variable Chain Fragment (scFv)

A freshly prepared solution of 2-mercaptoethylamine (200 mM, 75 μL) in sodium acetate (50 mM) / EDTA (2 mM) buffer (pH 6) was added to the scFv solution (22 μM, 7.5 mL) in sodium acetate (50 mM) / EDTA (2 mM) buffer (pH 6). The mixture was shaken for 2 h at room temperature and subsequently the excess of 2-mercaptoethylamine was removed by buffer exchange into sodium acetate (50 mM) / EDTA (2 mM) buffer (pH 6) using Sephadex™ G25 Medium (PD10 desalting column). The number of free sulfhydryl groups introduced was assessed by Ellman's assay.

Synthesis of scFv-functionalized Carbon Nanotubes C27

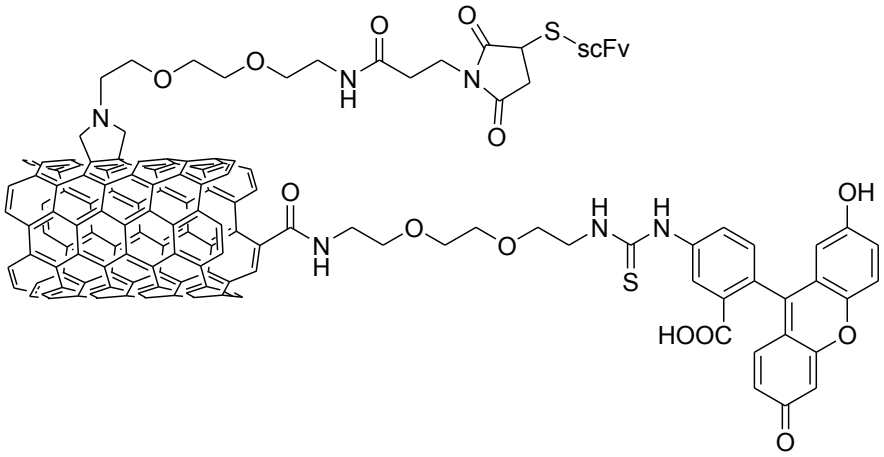

The maleimido-derivatized MWCNTs **C21** (6 mg) were dispersed in 12 mL of reduced scFv solution (5.3 μM) in PBS buffer (4 mM EDTA, pH 6.5) and the mixture was shaken for 24 h at room temperature. The scFv-CNT conjugate was centrifuged and washed thoroughly with PBS buffer (pH 7.4) until there was no scFv detected in the supernatant by UV-Vis spectroscopy. Finally, the resulting scFv-CNT conjugate was dialyzed (dialysis membrane MWCO 300,000 Da) against PBS buffer (pH 7.4) for 24 h and stored at 4°C. The degree of functionalization was determined by TGA and was calculated as 3.6 μmol of scFv (**a**) per gram of CNTs.
MWCNTs **C27** were characterized by TEM and TGA.

Synthesis of scFv-functionalized Carbon Nanotubes C28

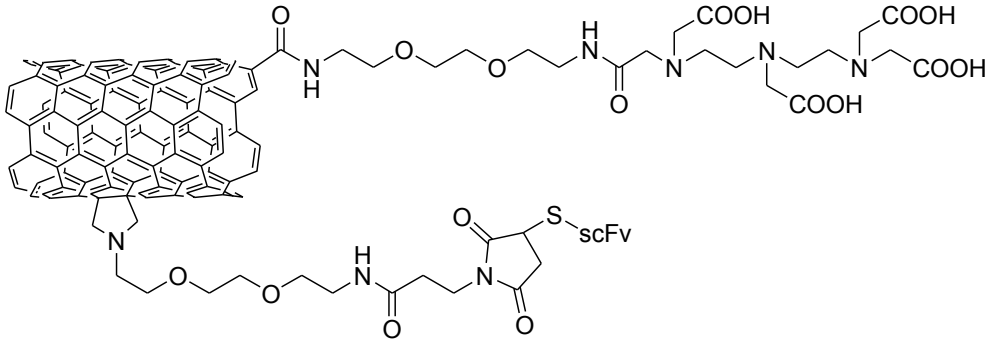

The maleimido-derivatized MWCNTs **C22** (6 mg) were dispersed in 12 mL of reduced scFv solution (5.3 μM) in PBS buffer (4mM EDTA, pH 6.5) and the mixture was shaken for 24 h at room temperature. The scFv-CNT conjugate was centrifuged and washed thoroughly with PBS buffer (pH 7.4) until there was no scFv detected in the supernatant by UV-Vis spectroscopy. Finally, the resulting scFv-CNT conjugate was dialyzed (dialysis membrane MWCO 300,000 Da) against PBS buffer (pH 7.4) for 24 h and stored at 4°C. The degree of functionalization was determined by TGA and was calculated as 3.6 μmol of scFv (**a**) per gram of CNTs.
MWCNTs **C28** were characterized by TEM and TGA.

Synthesis of VHH_C-functionalized Carbon Nanotubes C29

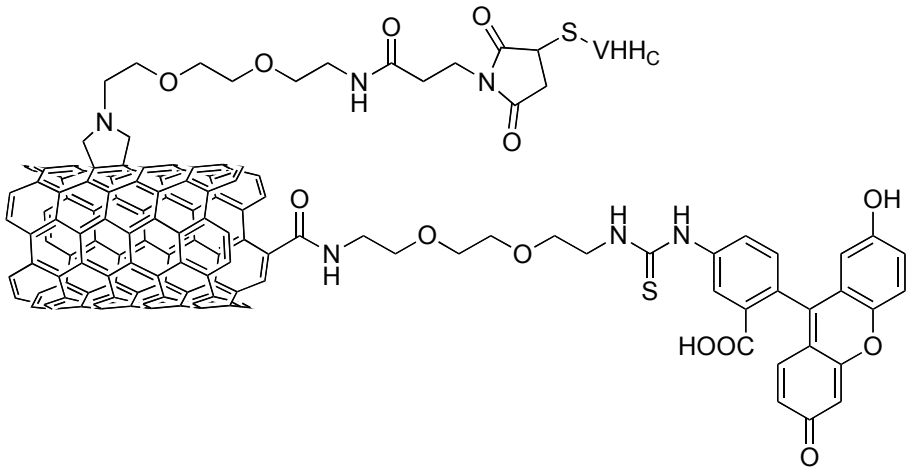

The maleimido-derivatized MWCNTs **C21b** (12 mg) were dispersed in 24 mL of VHH_C solution (23 μM) in PBS buffer (4 mM EDTA, pH 6.5) and the mixture was shaken for 6 h at room temperature. The VHH_C-CNT conjugate was centrifuged and washed thoroughly with PBS buffer (pH 7.4). Finally, the resulting VHH_C-CNT conjugate was dialyzed (dialysis membrane MWCO 300,000 Da) against PBS buffer (pH 7.4) for 48 h and stored at 4°C. The degree of functionalization was determined by TGA and was calculated as 15 μmol of scFv (**b**) per gram of CNTs.
MWCNTs **C29** were characterized by TEM and TGA.

Synthesis of VHH_T-functionalized Carbon Nanotubes C30

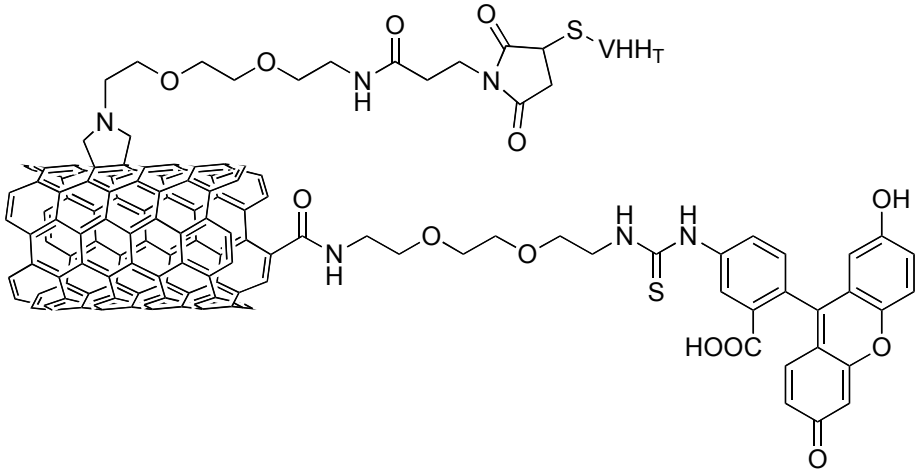

The maleimido-derivatized MWCNTs **C21b** (12 mg) were dispersed in 24 mL of VHH_T solution (18 μM) in PBS buffer (4 mM EDTA, pH 6.5) and the mixture was shaken for 6 h at room temperature. The VHH_T-CNT conjugate was centrifuged and washed thoroughly with PBS buffer (pH 7.4). Finally, the resulting VHH_T-CNT conjugate was dialyzed (dialysis membrane MWCO 300,000 Da) against PBS buffer (pH 7.4) for 48 h and stored at 4°C. The degree of functionalization was determined by TGA and was calculated as 15 μmol of VHH_T (**b**) per gram of CNTs.
MWCNTs **C30** were characterized by TEM and TGA.

Synthesis of VHH_C-functionalized Carbon Nanotubes C31

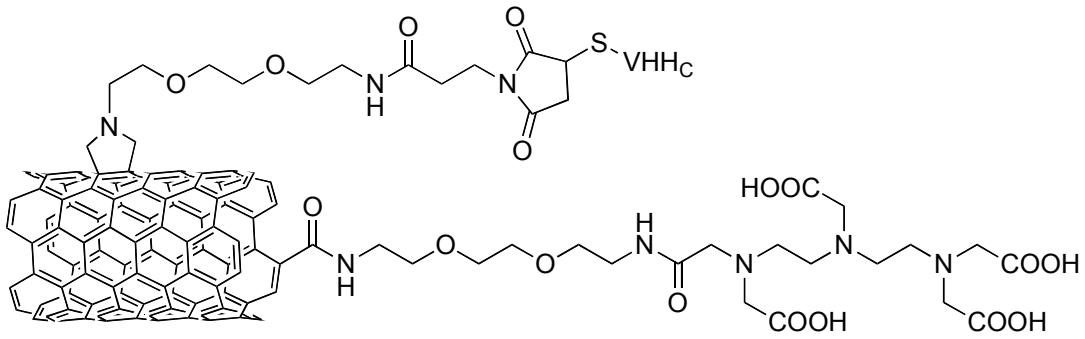

The maleimido-derivatized MWCNTs **C22b** (7 mg) were dispersed in 14 mL of VHH_C solution (23 μM) in PBS buffer (4 mM EDTA, pH 6.5) and the mixture was shaken for 6 h at room temperature. The VHH_C-CNT conjugate was centrifuged and washed thoroughly with PBS buffer (pH 7.4). Finally, the resulting VHH_C-CNT conjugate was dialyzed (dialysis membrane MWCO 300,000 Da) against PBS buffer (pH 7.4) for 48 h and stored at 4°C. The degree of functionalization was determined by TGA and was calculated as 15 μmol of VHH_C (**b**) per gram of CNTs.
MWCNTs **C31** were characterized by TEM and TGA.

VI.5 Biological Experimental Procedures

VI.5.1 Toxicological Studies

These experiments were conducted with the help of Dr. J. Russier from our group.

VI.5.1.1 Cells and Cell Culture

Splenocytes cells and mouse macrophages cell line (RAW 264.7) were obtained from American Type Culture Collection (ATCC). Both cellular types were cultured under controlled atmosphere (37°C, 5% CO_2) in RPMI 1640 supplemented with 10% heat inactivated fetal bovine serum (FBS) and 100 U/mL gentamycin. In addition, for the murine cell line, the culture medium contained β-mercaptoethanol (50 μM) and HEPES (20 mM). When confluency reached 70-80%, cells were trypsinized or detached with PBS/EDTA (2 mM) solution, respectively, and subcultured in T75 cm^2 flasks at a density of 50000 cells/mL. Before *in vitro* cytotoxicity assessments, cells were removed from the culture flasks, reseeded in 24 well plates (250000 and 450000 cells/well, respectively, in 500 μL complete medium) and allowed to adhere overnight. The media was then removed and replaced with 500 μL of fresh medium containing different concentrations of CNT-based conjugates. After 24 h of incubation, cells were harvested and processed for propidium iodide (PI) staining or intracellular lactate dehydrogenase (LDH) release evaluation.

VI.5.1.2 Cell Viability

PI is a fluorescent vital dye that stains DNA in cells that have lost their plasma membrane integrity (late stage of apoptosis or death). After treatment with CNT-based conjugates, the cells were collected, washed twice in PBS, resuspended in PBS-PI solution (1 μg/mL) and incubated at room temperature for 15-20 min. The fluorescence of 10000 individual cells was then measured by flow cytometry (FACS Calibur, Becton-Dickinson, USA) and data were analyzed using FlowJo software.

The content of the cytosolic LDH was also evaluated as an indicator of cellular viability/proliferation using the CytoTox 96® Non-Radioactive Cytotoxic Assay (Promega), following the manufacturer's instructions. Briefly, after the cells were washed and harvested, they were resuspended in 200 μL of the provided lysis solution, incubated 45 min at 37°C and centrifuged (5 min; 13400 g at 4°C). Then, 50 μL of cellular lysate was allowed to react with the equivalent volume of LDH substrate mix (30 min at room temperature protected from light), acetic acid (50 μL, 1 M) was added and absorbance was determined using a plate reader (λ=490 nm). In this case, the detected amount of LDH in the lysate is representative of the cells that survived the CNT-based conjugates subministration.

VI.5.2 *In Vitro* Studies

These experiments were performed in collaboration with the group of Prof. Kostas Kostarelos at the School of Pharmacy, University of London (UK).

VI.5.2.1 Cells and Cell Culture

MCF-7 cells or Calu6 cells were maintained and passaged in MEM medium or Advanced RPMI, respectively, supplemented with 10% FBS, 50 U/mL penicillin and 50 µg/mL streptomycin at 37°C in 5% CO_2. Cells were passaged to reach 80% confluency.

VI.5.2.2 Cellular Uptake Studies

In order to investigate the cellular internalization mechanism of *f*-MWCNTs by confocal laser scanning microscopy (CLSM), cells were washed with PBS and incubated with *f*-MWCNTs at 37°C in 5% CO_2 for 3h in serum-free media. To study the effect of the temperature on the cellular uptake of *f*-MWCNTs, cells were rinsed with PBS and pre-incubated at 4°C for 30 min in serum-free media, followed by incubation with *f*-MWCNTs in serum-free media for 3 h.

VI.5.2.3 Immunofluorescence

Cells were plated onto microscope glass coverslips at a density of 5,000 cells onto 24-well plate or onto glass-bottom petri-dishes at a density of 10000 cells and left to attach overnight. After treatment, cells were fixed in 4% PFA (paraformaldehyde) in PBS for 10 min at 37°C. Permeabilization was done using 1% Triton X-100 in PBS for 10 min at 4°C. Nonspecific binding was blocked using 4% normal goat serum and 3% bovine serum albumin in PBS (blocking buffer). Antibodies were diluted to their final concentration in the blocking buffer. For hCTM01 IgG staining, Cy3-conjugated goat anti-human IgG antibodies were applied for 2 h at room temperature. Then cells were washed five times for 5 min with PBS and followed with other staining if needed. For early endosome staining, anti-EEA-1 antibodies were applied for 2 h at room temperature. Cells were rinsed once in blocking buffer and three times for 5 min each with PBS, the secondary antibody was then applied for 2 h at room temperature. Finally, cells were washed five times for 5 min with PBS and mounted onto glass slides using Vectashield (Vector Laboratories Ltd, UK) as a mounting medium. Monolayers were examined for fluorescence using CLSM. In CLSM studies, fluorescence was visualized using a Zeiss LSM710 confocal microscope equipped with a 63X oil immersion objective (Carl Zeiss Inc., Thornwood, NY). DAPI, FITC, Cy3 and Cy5 were excited at 4% of 365, 2% of 488, 5% of 514 and 100% of 647 laser power, respectively.

VI.5.2.4 Flow Cytometry (FACS)

After incubation, cells were washed three times with ice-cold PBS in order to remove the excess and unbound CTMO1 IgG or *f*-MWCNT constructs. Then the cells were tripsinazed and collected in Eppendorfs. After centrifugation at 1,000 rmp for 5 min, the pellet was suspended in PBS and finally a minimum of 10,000 events were analyzed with a Cyan ADP flow cytometry (DakoCytomation).

VI.5.3 *In Vivo* Studies

These experiments were performed in collaboration with the group of Prof. Kostas Kostarelos at the School of Pharmacy, University of London (UK).

VI.5.3.1 Preparation of [^{111}In]DTPA-MWCNT

As a standard procedure, dispersions of DTPA-MWCNT (80μL-400μL of 250μg/mL) were diluted with an equal volume of 0.2 M ammonium acetate buffer pH 5.5, to which 2-20 MBq as indium chloride ($^{111}InCl_3$) was added. The indium was left to react with the DTPA-MWNT for 30 min at room temperature, after which the reaction was quenched by the addition of 0.1 M EDTA chelating solution (1/20 the reaction volume is added).

VI.5.3.2 Determination of Labeling Efficiency of [^{111}In]DTPA-MCWNT and Stability Studies in PBS and Serum

Aliquots of each final product were diluted five folds in PBS and then 1 μL spotted on silica gel impregnated glass fiber sheets (PALL Life Sciences, UK). The strips were developed with a mobile phase of 50 mM EDTA in 0.1 M ammonium acetate and allowed to dry before analysis. This was then developed and the autoradioactivity quantitatively counted using a Cyclone phosphor detector (Packard Biosciences, UK). The immobile spot on the TLC strips indicated the percentage of radiolabeled [^{111}In]DTPA-MWCNT conjugate , while the free ^{111}In or [^{111}In]DTPA were shown by the mobile spot. For checking for free DTPA contamination, the strips were developed with a mobile phase of 3.5% NH_3:MeOH (1:1) without quenching with EDTA. The mobile spot on the TLC strips indicated the percentage of free DTPA present in the DTPA-MWCNT mixture while precipitated ^{111}In or radiolabeled [^{111}In]DTPA-MWCNT conjugate remain at the application point, the absence of free DTPA in the mixture was confirmed.

To determine the stability of the labeled [^{111}In]DTPA-MWCNT, aliquots of each final product were diluted five folds either in PBS or mouse serum and then incubated at 37˚C over 24 h. At different

time-points (0 h, 1 h and 24 h), 1 µL of the aliquots was spotted on silica gel impregnated glass fiber sheets and then developed, and quantified as described above.

VI.5.3.3 Animals

Six- to eight-week-old BALB/c mice were obtained from Harlan (Oxfordshire, UK), allowed to acclimatize for 1 week and were kept in groups of 5 for the duration of the experiments and given food and water. All experiments were conducted with prior approval from the UK Home Office.

VI.5.3.4 Whole Body Imaging of [^{111}In]DTPA-MWCNT using Nano-SPECT/CT

Balb/C mice were anaesthetized by isofluorane inhalation. Each animal was injected via the tail vein injection with 250 µL containing 50 µg of [^{111}In]DTPA-MWCNT containing approximately 5-6 MBq. [^{111}In]EDTA was injected for comparison. Immediately after injection (t = 0.5 h) and at t = 3.5 h and t = 24 h, mice were imaged using the Nano-SPECT/CT scanner (Bioscan, USA). SPECT images were obtained in 16 projections over 40-60 min using a four-head scanner with 1.4 mm pinhole collimators. CT scans were taken at the end of each SPECT acquisition and all images were reconstructed with MEDISO software (Medical Imaging Systems). Fusion of SPECT and CT images was carried out using the PMOD software.

VI.5.3.5 Tissue Biodistribution of [^{111}In]DTPA-MWCNT

Animals (n=3-4) were injected with 250 µL containing 50 µg of [^{111}In]DTPA-MWCNT or [^{111}In]EDTA in 5% dextrose *via* tail vein injection. Twenty four hours after injection, mice were killed, and blood was collected. Heart, lungs, liver, spleen, kidneys, muscle and bone were sampled, each sample being weighed and counted on a Gamma Counter (Perkin Elmer, USA), together with a dilution of the injected dose with deadtime limit below 60%. The percentage injected dose (%ID) per gram tissue or the percentage injected dose per organ was calculated for each tissue.

A

Abarrategi A, Gutiérrez MC, Moreno-Vicente C, Hortigüela MJ, Ramos V, López-Lacomba JL, Ferrer ML, del Monte F. *Biomaterials.* (**2008**) 29, 94.

Abu Lila AS, Ishida T, Kiwada H. *Pharm. Res*. (**2010**) 27, 1171.

Adair JR, Hamann PR, Owens RJ, Baker TS, Lyons AH, Hinman LM, Menendez AT. *Anti-human milk fat globule humanised antibodies*. WO/**1993**/006231.

Allen BL, Kichambare PD, Gou P, Vlasova II, Kapralov AA, Konduru N, Kagan VE, Star A. *Nano Lett*. (**2008**) 8, 3899.

Allen BL, Kotchey GP, Chen Y, Yanamala NV, Klein-Seetharaman J, Kagan VE, Star A. *J. Am. Chem. Soc*. (**2009**) 131, 17194.

Altschuh D, Dubs MC, Weiss E, Zeder-Lutz G, Van Regenmortel MH. *Biochemistry* (**1992**) 31, 6298.

Angers S, Moon RT. *Nat. Rev. Mol. Cell Biol*. (**2009**) 10, 468.

B

Bacon R. *J. Appl. Phys*. (**1960**) 31, 283.

Bahr JL, Yang J, Kosynkin DV, Bronikowski M J, Smalley RE, Tour JM. *J. Am. Chem. Soc.* (**2001a**) 123, 6536.

Bahr JL, Tour JM. *Chem. Mater*. (**2001b**) 13, 3823.

Bai Y, Zhang Y, Zhang J, Mu Q, Zhang W, Butch ER, Snyder SE, Yan B. *Nat. Nanotechnol.* (**2010**) 5, 683.

Balaban TS, Balaban MC, Malik S, Hennrich F, Fischer R, Rosner H, Kappes MM. *Adv. Mater.* (**2006**) 18, 2763.

Balasubramanian K, Burghard M. *J. Mater. Chem.* (**2008)** 18, 3071.

Baskaran D, Mays JW, Zhang XP, Bratcher MS. *J. Am. Chem. Soc.* (**2005**) 127, 6916.
Begent RH, Verhaar MJ, Chester KA, Casey JL, Green AJ, Napier MP, Hope-Stone LD, Cushen N, Keep PA, Johnson CJ, Hawkins RE, Hilson AJ, Robson L. *Nat. Med*. (**1996)** 2, 979.

Bhirde AA, Patel V, Gavard J, Zhang G, Sousa AA, Masedunskas A, Leapman RD, Weigert R, Gutkind JS, Rusling JF. *ACS Nano* (**2009**) 3, 307.

Bianco A, Kostarelos K, Partidos CD, Prato M. *Chem. Commun*. (**2005a**) 571.

Bianco A, Kostarelos K, Prato M. *Curr. Opin. Chem. Biol*. (**2005b**) 9, 674.

Bonifazi D, Nacci C, Marega R, Campidelli S, Ceballos G, Modesti S, Meneghetti M, Prato M. *Nano Lett.* (**2006**) 6, 1408.

Borondics F, Jakab E, Pekker S. *J. Nanosci. Nanotechnol*. (**2007**) 7, 1551.

Bottari G, de la Torre G, Guldi DM, Torres T. *Chem. Rev*. (**2010**) 110, 6768.

Brunetti FG, Herrero MA, Muñoz Jde M, Giordani S, Díaz-Ortiz A, Filippone S, Ruaro G, Meneghetti M, Prato M, Vázquez E. *J. Am. Chem. Soc.* (**2007**) 129, 14580.

Byrne MT, Gun'ko YK, *Adv. Mater*. (**2010**) 22, 1672.

C

Campbell JF, Tessmer I, Thorp HH, Erie DA. *J. Am. Chem. Soc*. (**2008**) 130, 10648.

Cao Y, Zhou YM, Shan Y, Ju HX, Xue XJ. *J. Nanosci. Nanotechnol*. (**2007**) 7, 447.

Casey A, Herzog E, Davoren M, Lyng FM, Byrne HJ, Chambers G. *Carbon* (**2007**) 45, 1425.

Castaldello A, Brocca-Cofano E, Voltan R, Triulzi C, Altavilla G, Laus M, Sparnacci K, Ballestri M, Tondelli L, Fortini C, Gavioli R, Ensoli B, Caputo A. *Vaccine.* (**2006**) 24, 5655.

Cellot G, Cilia E, Cipollone S, Rancic V, Sucapane A, Giordani S, Gambazzi L, Markram H, Grandolfo M, Scaini D, Gelain F, Casalis L, Prato M, Giugliano M, Ballerini L. *Nat. Nanotechnol*. (**2009**) 4, 126.

Chakravarty P, Marches R, Zimmerman NS, Swafford AD, Bajaj P, Musselman IH, Pantano P, Draper RK, Vitetta ES. *Proc. Natl. Acad. Sci*. (**2008**) 105, 8697.

Charlier JC, Blase X, Roche S. *Rev. Mod. Phys*. (**2007**) 79, 677.

Chen RJ, Zhang Y, Wang D, Dai H. *J. Am. Chem. Soc*. (**2001**) 123, 3838.

Cheng Y, Zhao L, Li Y, Xu T. *Chem. Soc. Rev*. (**2011**) 40, 2673.

Cherukuri P, Gannon CJ, Leeuw TK, Schmidt HK, Smalley RE, Curley SA, Weisman RB. *Proc. Natl. Acad. Sci.* (**2006**) 103, 18882.

D

Da Ros T, Prato M. *Chem. Commun*. (**1999**) 663.

Dai H, Wong EW, Lieber CM. *Science* (**1996**) 272, 523.

De la Zerda A, Zavaleta C, Keren S, Vaithilingam S, Bodapati S, Liu Z, Levi J, Smith BR, Ma TJ, Oralkan O, Cheng Z, Chen X, Dai H, Khuri-Yakub BT, Gambhir SS. *Nat. Nanotechnol*. (**2008**) 3, 557.

Delgado JL, de la Cruz P, Langa F, Urbina A, Casado J, López Navarrete JT. *Chem. Commun*. (**2004**) 1734.

Dervishi E, Li Z, Biris AR, Lupu D, Trigwell S, Biris AS. *Chem. Mater*. (**2007**) 19, 179.

Dervishi E, Li Z, Xu Y, Saini V, Biris AR, Lupu D, Biris AS. *Part. Sci. Technol*. (**2009**) 27, 107.

Dong L, Joseph KL, Witkowski CM, Craig MM. *Nanotechnology* (**2008**) 19, 255702.

Dresselhaus MS, Dresselhaus G, Avouris P. *Carbon Nanotubes: Synthesis, Structure, Properties, and Applications*. (**2001**) Berlin: Springer.

Dumortier H, Lacotte S, Pastorin G, Marega R, Wu W, Bonifazi D, Briand JP, Prato M, Muller S, Bianco A. *Nano Lett*. (**2006**) 6, 1522.

Dyke CA, Tour JM. *J. Am. Chem. Soc*. (**2003**) 125, 1156.

E

Ellman GL, *Arch. Biochem. Biophys*. (**1959**) 82, 70.

El Wakil A, Lalli E. *Mol. Cell. Endocrinol*. (**2011)** 332, 32.

Ewert S, Cambillau C, Conrath K, Plückthun A. *Biochemistry* (**2002)** 41, 3628.

G

Gaillard C, Cellot G, Li S, Toma FM, Dumortier H, Spalluto G, Cacciari B, Prato M, Ballerini L, Bianco A. *Adv. Mater*. (**2009**) 21, 2903.

Galvan-Garcia P, Keefer EW, Yang F, Zhang M, Fang S, Zakhidov AA, Baughman RH, Romero MI. *J. Biomater. Sci. Polym. Ed.18* (**2007**) 18, 1245.

Gehrke I, Gandhirajan RK, Kreuzer KA. *Eur. J. Cancer* (**2009)** 45, 2759.

Gendler SJ, Lancaster CA, Taylor-Papadimitriou J, Duhig T, Peat N, Burchell J, Pemberton L, Lalani EN, Wilson D. *J. Biol. Chem*. (**1990**) 265, 15286.

Georgakilas V, Tagmatarchis N, Pantarotto D, Bianco A, Briand JP, Prato M. *Chem. Commun*. (**2002a**) 3050.

Georgakilas V, Kordatos K, Prato M, Guldi DM, Holzinger M, Hirsch A. *J. Am. Chem. Soc.* (**2002b**) 124, 760.

Gorityala BK, Ma J, Wang X, Chen P, Liu XW. *Chem. Soc. Rev*. (**2010**) 39, 2925.

Graff RA, Swanson TM, Strano MS. *Chem. Mater.* (**2008**) 20, 1824.

Grant BD, Donaldson JG. *Nat. Rev. Mol. Cell. Biol*. (**2009)** 10, 597.

Guldi DM, Marcaccio M, Paolucci D, Paolucci F, Tagmatarchis N, Tasis D, Vázquez E, Prato M. *Angew. Chem. Int. Ed*. (**2003**) 42, 4206.

Guo T, Nikolaev P, Rinzler AG, Tomanek D, Colbert DT, Smalley RE. *J. Phys. Chem*. (**1995**) 99, 10694.

H

Haddon RC. *Acc. Chem. Res.* (**2002**) 35, 997. Carbon nanotubes. Special issue.

Hamers-Casterman C, Atarhouch T, Muyldermans S, Robinson G, Hamers C, Songa EB, Bendahman N, Hamers R. *Nature* (**1993**) 363, 446.

Hamon MA, Chen J, Hu H, Chen Y, Itkis ME, Rao AM, Eklud PC, Haddon RC. *Adv. Mater*. (**1999**) 11, 834.

Harmsen MM, De Haard HJ. *Appl. Microbiol. Biotechnol*. (**2007**) 77, 13.

Hattrup CL, Gendler SJ. *Annu. Rev. Physiol*. (**2008**) 70, 431.

Heister E, Neves V, Tîlmaciu C, Lipert K, Sanz Beltrán V, Coley HM, Silva SRP, McFadden J. *Carbon* (**2009)** 47, 2152.

Heller DA, Jin H, Martinez BM, Patel D, Miller BM, Yeung TK, Jena PV, Höbartner C, Ha T, Silverman SK, Strano MS. *Nat. Nanotechnol*. (**2009**) 4, 114.

Helveg S, López-Cartes C, Sehested J, Hansen PL, Clausen BS, Rostrup-Nielsen JR, Abild-Pedersen F, Nørskov JK. *Nature* (**2004**) 427, 426.

Hirsch A. *Angew. Chem. Int. Ed*. (**2002**) 41, 1853.

Holzinger M, Vostrowsky O, Hirsch A, Hennrich F, Kappes M, Weiss R, Jellen F. *Angew. Chem. Int. Ed.* (**2001**) 40, 4002.

Hong H, Gao T, Cai W. *Nano Today* (**2009**) 4, 252.

Hong SY, Tobias G, Al-Jamal KT, Ballesteros B, Ali-Boucetta H, Lozano-Perez S, Nellist PD, Sim RB, Finucane C, Mather SJ, Green ML, Kostarelos K, Davis BG. *Nat. Mater*. (**2010**) 9, 485.

Hu H, Ni Y, Montana V, Haddon RC, Parpura V. *Nano Lett*. (**2004**) 4, 507.

Hudson JL, Jian H, Leonard AD, Stephenson JJ, Tour JM. *Chem. Mater*. (**2006**) 18, 2766.

Husu H, Canfiled BK, Laukkanen J, Bai B, Kuittinen M, Turunen J, Kauranen M. *Appl. Phys. Lett*. (**2008**) 93, 183115.

I

Iijima S, *Nature* (**1991**) 354, 56.

Iijima S, Ichihashi T. *Nature* (**1993**) 363, 603.

J

Jain K, Kesharwani P, Gupta U, Jain NK. *Int. J. Pharm*. (**2010**) 394, 122.

Jasanada F, Urizzi P, Souchard JP, Le Gaillard F, Favre G, Nepveu F. *Bioconjug. Chem.* (**1996**) 7, 72.

Ji SR, Liu C, Zhang B, Yang F, Xu J, Long J, Jin C, Fu DL, Ni QX, Yu XJ. *Biochim. Biophys. Acta* (**2010**) 1806, 29.

Jiang K, Schadler LS, Siegel RW, Zhang X, Zhang H, Terrones M, *J. Mater. Chem.* (**2004)** 14, 37.

Jorio A, Dresselhaus G, Dresselahus MS. *Carbon nanotubes: advanced topics, in the synthesis, structure, properties and applications.* (**2008**) Berlin: Springer.

Journet C, Maser WK, Bernier P, Loiseau A, Lamy de la Chapelle M, Lefrant S, Deniard P, Lee R, Fischer JE. *Nature* (**1997**) 388, 756.

Journet C, Bernier P. *Appl. Phys. A* (**1998**) 67, 1.

Jue R, Lambert JM, Pierce LR, Traut RR. *Biochemistry* (**1978**) 17, 5399.

K

Kagan VE, Konduru NV, Feng W, Allen BL, Conroy J, Volkov Y, Vlasova II, Belikova NA, Yanamala N, Kapralov A, Tyurina YY, Shi J, Kisin ER, Murray AR, Franks J, Stolz D, Gou P, Klein-Seetharaman J, Fadeel B, Star A, Shvedova AA. *Nat. Nanotechnol*. (**2010**) 5, 354.

Kaiser E, Colescott RL, Bossinger CD, Cook PI. *Anal. Biochem*. (**1970**) 34, 595.

Kam NWS, Jessop, TC, Wender PA, Dai HJ. *J. Am. Chem. Soc.* (**2004**) 126, 6850.

Kam NWS, Dai H. *J. Am. Chem. Soc*. (**2005a**) 127, 6021.

Kam NWS, O'Connell M, Wisdom JA, Dai H. *Proc. Natl. Acad. Sci*. (**2005b**) 102, 11600.

Kam NWS, Liu ZA, Dai HJ. *Angew. Chem. Int. Ed*. (**2006**) 45, 577.

Kang B, Yu D, Dai Y, Chang S, Chen D, Ding Y. *Small* (**2009**) 5, 1292.

Karousis N, Tagmatarchis N, Tasis D. *Chem. Rev*. (**2010**) 110, 5366.

Kauffman DR, Star A. *Angew. Chem. Int. Ed.* (**2008)** 47, 6550.

Kordatos K, Da Ros T, Bosi S, Vázquez E, Bergamin M, Cusan C, Pellarini F, Tomberli V, Baiti B, Pantarotto D, Georgakilas V, Spalluto G, Prato M. *J. Org. Chem*. (**2001**) 66, 4915.

Kostarelos K, Lacerda L, Pastorin G, Wu W, Wieckowski S, Luangsivilay J, Godefroy S, Pantarotto D, Briand JP, Muller S, Prato M, Bianco A. *Nat. Nanotechnol*. (**2007**) 2, 108.

Kostarelos K, Bianco A, Prato M. *Nat. Nanotechnol.* (**2009**) 4, 627.

Koyama S, Kim YA, Hayashi T, Takeuchi K, Fujii C, Kuroiwa N, Koyama H, Tsukahara T, Endo M. *Carbon* (**2009**) 47, 1365.

Kroto HW, Heath JR, O'Brian SC, Curl RF, Smalley RE. *Nature* (**1985**) 381, 162.

Kumar M, Ando Y. *J. Nanosci. Nanotechnol*. (**2010**) 10, 3739.

L

Lacerda L, Pastorin G, Gathercole D, Buddle J, Prato M, Bianco A, Kostarelos K. *Adv. Mater.* (**2007**) 19, 1480.

Lacerda L, Soundararajan A, Singh R, Pastorin G, Al-Jamal KT, Turton J, Frederik P, Herrero MA, Li S, Bao A, Emfietzoglou D, Mather S, Phillips WT, Prato M, Bianco A, Goins B, Kostarelos K. *Adv. Mater*. (**2008a**) 20, 225.

Lacerda L, Bianco A, Prato M, Kostarelos K. *J. Mater. Chem*. (**2008b**) 18, 17.

Lam CW, James JT, McCluskey R, Hunter RL. *Toxicol. Sci*. (**2004**) 77, 126.

Lei J, Ju H. *Wiley Interdiscip. Rev.: Nanomed. Nanobiotechnol.* (**2010**) 2, 496.

Li H, Martin RB, Harruff BA, Carino RA, Allard LF, Sun YP. *Adv. Mater.* (**2004**) 16, 896.

Li R, Wu R, Zhao L, Wu M, Yang L, Zou H. *ACS Nano* (**2010**) 4, 1399.

Liu J, Rinzler AG, Dai H, Hafner JH, Bradley RK, Boul PJ, Lu A, Iverson T, Shelimov K, Huffman CB, Rodriguez-Macias F, Shon YS, Lee TR, Colbert DT, Smalley RE. *Science* (**1998)** 280, 1253.

Liu X, Hurt RH, Kane AB. *Carbon* (**2010**) 48, 1961.

Liu Z, Cai W, He L, Nakayama N, Chen K, Sun X, Chen X, Dai H. *Nat. Nanotechnol*. (**2007a**) 2, 47.

Liu Z, Sun X, Nakayama N, Dai H. *ACS Nano* (**2007b**) 1, 50.

Liu Z, Davis C, Cai W, He L, Chen X, Dai H. *Proc. Natl. Acad. Sci.* (**2008a**) 105, 1410.

Liu Z, Li X, Tabakman SM, Jiang K, Fan S, Dai H. *J. Am. Chem. Soc*. (**2008b**) 130, 13540.

Liu Z, Chen K, Davis C, Sherlock S, Cao Q, Chen X, Dai H. *Cancer Res*. (**2008c**) 68, 6652.

Liu Z, Tabakman S, Welsher K, Dai H. *Nano Res*. (**2009a**) 2, 85.

Liu Z, Fan AC, Rakhra K, Sherlock S, Goodwin A, Chen X, Yang Q, Felsher DW, Dai H. *Angew. Chem. Int. Ed.* (**2009b**) 48, 7668.

Lopez CF, Nielsen SO, Moore PB, Klein ML. *Proc. Natl. Acad. Sci*. (**2004**) 101, 4431.

Lovat V, Pantarotto D, Lagostena L, Cacciari B, Grandolfo M, Righi M, Spalluto G, Prato M, Ballerini L. *Nano Lett*. (**2005**) 5, 1107.

Lu F, Gu L, Meziani MJ, Wang X, Luo PG, Veca LM, Cao L, Sun YP. *Adv. Mater.* (**2009**) 21, 139.

Lu X, Xin T, Wang N, Zhang Q. *J. Am. Chem. Soc*. (**2003**) 125, 10459.

Lucero OM, Dawson DW, Moon RT, Chien AJ. *Curr. Oncol. Rep.* (**2010**) 12, 314.

M

MacDonald RA, Laurenzi BF, Viswanathan G, Ajayan PM, Stegemann JP. *J. Biomed. Mater. Res. A* (**2005**) 74, 489.

Maggini M, Scorrano G, Prato M. *J. Am. Chem. Soc*. (**1993**) 115, 9798.

Marches R, Chakravarty P, Musselman IH, Bajaj P, Azad RN, Pantano P, Draper RK, Vitetta ES. *Int. J. Cancer* (**2009**) 125, 2970.

Mattson MP, Haddon RC, Rao AM. *J. Mol. Neurosci*. (**2000**) 14, 175.

McCullen SD, Stevens DR, Roberts WA, Clarke LI, Bernacki SH, Gorga RE, Loboa EG. *Int. J. Nanomedicine* (**2007**) 2, 253.

McDevitt MR, Chattopadhyay D, Jaggi JS, Finn RD, Zanzonico PB, Villa C, Rey D, Mendenhall J, Batt CA, Njardarson JT, Scheinberg DA. *PLoS One* (**2007**) 2, e907.

Meyyappan M. *Carbon Nanotubes: Science and Applications.* (**2005**) Boca Raton, Fla.: CRC.

Ménard-Moyon C, Venturelli E, Fabbro C, Samorì C, Da Ros T, Kostarelos K, Prato M, Bianco A. *Expert Opin. Drug Discov.* (**2010a**) 5, 691.

Ménard-Moyon C, Kostarelos K, Prato M, Bianco A. *Chem. Biol*. (**2010b**) 17, 107.

Ménard-Moyon C, Fabbro C, Prato M, Bianco A. *Chem. Eur. J.* (**2011**) 17, 3222.

Moghaddam MJ, Taylor S, Gao M, Huang S, Dai L, McCall MJ. *Nano Lett.* (**2004**) 4, 89.

Monthioux M, Kuznetsov VL. *Carbon* (**2006**) 44, 1621.

Muyldermans S. *J. Biotechnol*. (**2001)** 74, 277.

N

Nayak TR, Jian L, Phua LC, Ho HK, Ren Y, Pastorin G. *ACS Nano* (**2010**) 4, 7717.

Niv Y. *World J. Gastroenterol*. (**2008**) 14, 2139.

Novoselov KS, Geim AK, Morozov SV, Jiang D, Zhang Y, Dubonos SV, Grigorieva IV, Firsov AA. *Science* (**2004**) 306, 666.

O

Oberlin A, Endo M, Koyama T. *J. Cryst. Growth* (**1976**) 32, 335.

O'Connell MJ, Bachilo SM, Huffman CB, Moore VC, Strano MS, Haroz EH, Rialon KL, Boul PJ, Noon WH, Kittrell C, Ma J, Hauge RH, Weisman RB, Smalley RE. *Science* (**2002**) 297, 593.

Ou Z, Wu B, Xing D, Zhou F, Wang H, Tang Y. *Nanotechnology* (**2009**) 20, 105102.

P

Pan B, Cui D, Xu P, Ozkan C, Feng G, Ozkan M, Huang T, Chu B, Li Q, He R, Hu G. *Nanotechnology* (**2009**) 20, 125101.

Pantarotto D, Briand JP, Prato M, Bianco A. *Chem. Commun*. (**2004a**) 16.

Pantarotto D, Singh R, McCarthy D, Erhardt M, Briand JP, Prato M, Kostarelos K, Bianco A. *Angew. Chem. Int. Ed.* (**2004b**) 43, 5242.

Pastorin G, Wu W, Wieckowski S, Briand JP, Kostarelos K, Prato M, Bianco A. *Chem. Commun.* (**2006**) 1182.

Pastorin G. *Pharm. Res*. (**2009**) 26, 746.

Pavet V, Beyrath J, Pardin C, Morizot A, Lechner MC, Briand JP, Wendland M, Maison W, Fournel S, Micheau O, Guichard G, Gronemeyer H. *Cancer Res.* (**2010**) 70, 1101.

Plata DL, Gschwend PM, Reddy CM. *Nanotechnology* (**2008**) 19, 185706.

Podesta JE, Al-Jamal KT, Herrero MA, Tian B, Ali-Boucetta H, Hegde V, Bianco A, Prato M, Kostarelos K. *Small* (**2009**) 5, 1176.

Prato M. *J. Mater. Chem*. (**1997**) 7, 1097.

Prato M, Kostarelos K, Bianco A. *Acc. Chem. Res.* (**2008**) 41, 60.

Price BK, Hudson JL, Tour JM. *J. Am. Chem. Soc*. (**2005**) 127, 14867.

R

Ravichandran P, Periyakaruppan A, Sadanandan B, Ramesh V, Hall JC, Jejelowo O, Ramesh GT. *J. Biochem. Mol. Toxicol*. (**2009**) 23, 333.

Rubio N, Herrero MA, de la Hoz A, Meneghetti M, Prato M, Vázquez E. *Org. Biomol. Chem*. (**2010**) 8, 1936.

Ruggiero A, Villa CH, Holland JP, Sprinkle SR, May C, Lewis JS, Scheinberg DA, McDevitt MR. *Int. J. Nanomedicine* (**2010a**) 5, 783.

Ruggiero A, Villa CH, Bander E, Rey DA, Bergkvist M, Batt CA, Manova-Todorova K, Deen WM, Scheinberg DA, McDevitt MR. *Proc. Natl. Acad. Sci.* (**2010b**) 107, 12369.

Russier J, Ménard-Moyon C, Venturelli E, Gravel E, Marcolongo G, Meneghetti M, Doris E, Bianco A. *Nanoscale* (**2011**) 3, 893.

S

Sahay G, Alakhova DY, Kabanov AV. *J. Control. Release* (**2010)** 145, 182.

Saito N, Usui Y, Aoki K, Narita N, Shimizu M, Hara K, Ogiwara N, Nakamura K, Ishigaki N, Kato H, Taruta S, Endo M. *Chem. Soc. Rev*. (**2009**) 38, 1897.

Salvador-Morales C, Basiuk EV, Basiuk VA, Green ML, Sim RB. *J. Nanosci. Nanotechnol*. (**2008**) 8, 2347.

Samorì C, Sainz R, Ménard-Moyon C, Toma FM, Venturelli E, Singh P, Ballestri M, Prato M, Bianco A. *Carbon* (**2010a)** 48, 2447.

Samorì C, Ali-Boucetta H, Sainz R, Guo C, Toma FM, Fabbro C, da Ros T, Prato M, Kostarelos K, Bianco A. *Chem. Commun.* (**2010b**) 46, 1494.

Sarin VK, Kent SB, Tam JP, Merrifield RB. *Anal. Biochem*. (**1981**) 117, 147.

Schnorr JM, Swager TM. *Chem. Mater*. (**2011**) 23, 646.

Shao N, Wickstrom E, Panchapakesan B. *Nanotechnology* (**2008**) 19, 465101.

Shvedova AA, Kisin ER, Mercer R, Murray AR, Johnson VJ, Potapovich AI, Tyurina YY, Gorelik O, Arepalli S, Schwegler-Berry D, Hubbs AF, Antonini J, Evans DE, Ku BK, Ramsey D, Maynard A, Kagan VE, Castranova V, Baron P. *Am. J. Physiol. Lung Cell. Mol. Physiol.* (**2005**) 289, L698-708.

Singh P, Campidelli S, Giordani S, Bonifazi D, Bianco A, Prato M. *Chem. Soc. Rev.* (**2009**) 38, 2214.

Singh PK, Hollingsworth MA. *Trends Cell. Biol*. (**2006**) 16, 467.

Singh R, Pantarotto D, Lacerda L, Pastorin G, Klumpp C, Prato M, Bianco A, Kostarelos K. *Proc. Natl. Acad. Sci.* (**2006**) 103, 3357.

Star A, Tu E, Niemann J, Gabriel JC, Joiner CS, Valcke C. *Proc. Natl. Acad. Sci.* (**2006**) 103, 921.

Steinmetz NF. *Nanomedicine* (**2010**) 6, 634.

T

Tasis D, Tagmatarchis N, Bianco A, Prato M. *Chem. Rev*. (**2006**) 106, 1105.

Tessonnier JP, Villa A, Majoulet O, Su DS, Schlögl R. *Angew. Chem. Int. Ed.* (**2009**) 48, 6543.

Terrones M. *Annu. Rev. Mater. Res*. (**2003**) 33, 419.

Thomas CE, Ehrhardt A, Kay MA. *Nat. Rev. Genet*. (**2003**) 4, 346.

Traut RR, Bollen A, Sun TT, Hershey JW, Sundberg J, Pierce LR. *Biochemistry* (**1973**) 12, 3266.

Tripisciano C, Kraemer K, Taylor A, Borowiak-Palen E. *Chem. Phys. Lett*. (**2009**) 478, 200.

U

Usui Y, Aoki K, Narita N, Murakami N, Nakamura I, Nakamura K, Ishigaki N, Yamazaki H, Horiuchi H, Kato H, Taruta S, Kim YA, Endo M, Saito N. *Small* (**2008**) 4, 240.

V

van der Aa MA, Huth US, Häfele SY, Schubert R, Oosting RS, Mastrobattista E, Hennink WE, Peschka-Süss R, Koning GA, Crommelin DJ. *Pharm. Res*. (**2007**) 24, 1590.

van der Linden RH, Frenken LG, de Geus B, Harmsen MM, Ruuls RC, Stok W, de Ron L, Wilson S, Davis P, Verrips CT. *Biochim. Biophys. Acta* (**1999**) 1431, 37.

Vermes I, Haanen C, Steffens-Nakken H, Reutelingsperger C. *J. Immunol. Methods*. (**1995**) 184, 39.

Venturelli E, Fabbro C, Chaloin O, Ménard-Moyon C, Smulski CR, Da Ros T, Kostarelos K, Prato M, Bianco A. *Small* (**2011**) 7, 2179.

W

Wang CH, Chiou SH, Chou CP, Chen YC, Huang YJ, Peng CA. *Nanomedicine: NBM* (**2011)**, 7, 69.

Wang H, Zhou W, Ho Dl, Winey KI, Fischer JE, Glinka CJ, Hobbie EK. *Nano Lett*. (**2004**) 4, 1789.

Wang HF, Wang J, Deng XY, Sun HF, Shi ZJ, Gu Zn, Liu YF, Zhao YL. *J. Nanosci. Nanotechnol.* (**2004**) 4, 1019.

Weiner LM, Surana R, Wang S. Nat. Rev. Immunol. (**2010**) 10, 317.

Welsher K, Liu Z, Daranciang D, Dai H. *Nano Lett*. (**2008**) 8, 586.

Weng X Wang M, Ge J, Yu S, Liu B, Zhong J, Kong J. *Mol. Biosyst*. (**2009**) 5, 1224.

Wörle-Knirsch JM, Pulskamp K, Krug HF. *Nano Lett.* (**2006**) 6, 1261.

Wu W, Li R, Bian X, Zhu Z, Ding D, Li X, Jia Z, Jiang X, Hu Y. *ACS Nano* (**2009**) 3, 2740.

X

Xiao Y, Gao X, Taratula O, Treado S, Urbas A, Holbrook RD, Cavicchi RE, Avedisian CT, Mitra S, Savla R, Wagner PD, Srivastava S, He H. *BMC Cancer* (**2009**) 9, 351.

Y

Yanagi K, Iakoubovskii K, Matsui H, Matsuzaki H, Okamoto H, Miyata Y, Maniwa Y, Kazaoui S, Minami N, Kataura H. *J. Am. Chem. Soc.* (**2007**) 129, 4992.

Yang H, Wang SC, Mercier P, Akins DL. *Chem. Commun.* (**2006**) 1425.

Yang ST, Guo W, Lin Y, deng Xy, Wang HF, Sun HF, Liu YF, Wang X, Wang W, Chen M, Huang YP, Sun YP. *J. Phys. Chem. C* (**2007**) 111, 17761.

Yang ST, Fernando KA, Liu JH, Wang J, Sun HF, Liu Y, Chen M, Huang Y, Wang X, Wang H, Sun YP. *Small* (**2008**) 4, 940.

Ying Y, Saini RK, Liang F, Sadana AK, Billups WE. *Org. Lett*. (**2003**) 5, 1471.

Yinghuai Z, Peng AT, Carpenter K, Maguire JA, Hosmane NS, Takagaki M. *J. Am. Chem. Soc*. (**2005**) 127, 9875.

Z

Zanello LP, Zhao B, Hu H, Haddon RC. *Nano Lett*. (**2006**) 6, 562.

Zhang XZ, Jiao K, Liu SF, Hu YW. *Anal. Chem*. (**2009**) 81, 6006.

Zhang ZH, Yang XY, Zhang Y, Zeng B, Wang ZJ, Zhu TH, Roden RBS, Chen YS, Yang RC. *Clin. Cancer Res*. (**2006**) 12, 4933.

Zhao Y, Allen BL, Star A. *J. Phys. Chem. A* (**2011**) DOI: 10.1021/jp112324d

Zheng M, Jagota A, Semke ED, Diner BA, McLean RS, Lustig SR, Richardson RE, Tassi NG. *Nat. Mater*. (**2003**) 2, 338.

Publications

_ C. Samorì, R. Sainz, C. Ménard-Moyon, F. M. Toma, E. Venturelli, P. Singh, M. Ballestri, M. Prato, A. Bianco. Potentiometric titration as a straightforward method to assess the number of functional groups on shortened carbon nanotubes. *Carbon* (**2010**) 48, 2447.

_ C. Ménard-Moyon, E. Venturelli, C. Fabbro, C. Samorì, T. da Ros, K. Kostarelos, M. Prato, A. Bianco. The alluring potential of functionalized carbon nanotubes in drug discovery. *Expert Opin. Drug Deliv.* (**2010**) 5*,* 691.

_ J. Russier, C. Ménard-Moyon, E. Venturelli, E. Gravel, G. Marcolongo, M. Meneghetti, E. Doris, A. Bianco. Oxidative biodegradation of single- and multi-walled carbon nanotubes. *Nanoscale* (**2011**) 3, 893.

_ E. Venturelli, C. Fabbro, O. Chaloin, C. Ménard-Moyon, C.R. Smulski, T. Da Ros, K. Kostarelos, M. Prato, A. Bianco**.** Antibody covalent immobilization to carbon nanotubes and assessment of antigen binding. *Small* (**2011**) 7, 2179.

_ L.G. Delogu, E. Venturelli, R. Manetti, G.A. Pinna, C. Carru, R. Madeddu, L. Murgia, F. Sgarrella, H. Dumortier, A. Bianco**.** *Ex vivo* impact of functionalized carbon nanotubes on human immune cells. *Nanomedicine* (**2011**) accepted.

_ M.F. Serag, N. Kaji, E. Venturelli, Y. Okamoto, K. Terasaka, M. Jabasini, M. Tokeshi, H. Mizukami, A. Bianco, Y. Baba. A cellular address tag for controlled biodistribution of single walled carbon nanotubes in plant cells. **2011**, submitted.

Communications

1. GDR-GNT ANNUAL MEETING 2011
   E. Venturelli, C. Fabbro, O. Chaloin, C. Ménard-Moyon, C.R. Smulski, T. Da Ros, K. Kostarelos, M. Prato, A. Bianco.
   "Antibody-functionalized carbon nanotubes towards a targeted anticancer therapy"
   Oral communication and poster presentation
   Dourdan, France (2011)

2. EURONANOFORUM 2011
   L.G. Delogu, E. Venturelli, R. Manetti, G.A. Pinna, C. Carru, R. Madeddu, L. Murgia, F. Sgarrella, H. Dumortier, A. Bianco.
   "Functionalized carbon nanotubes on human immune cells"
   Poster presentation
   Budapest, Hungary (2011)

3. ESF CONFERENCE "NANOCARBONS: FROM PHYSICOCHEMICAL AND BIOLOGICAL PROPERTIES TO BIOMEDICAL AND ENVIRONMENTAL EFFECTS"
   E. Venturelli, C. Ménard-Moyon, A. Bianco.
   "Multiple functionalization of carbon nanotubes"
   Poster presentation
   Acquafredda di Maratea, Italy (2009)

4. SYMPOSIUM ON "CARBON-BASED NANOMATERIALS: FROM CHEMISTRY TO APPLICATIONS"
   E. Venturelli, C. Ménard-Moyon, A. Bianco.
   "Multiple functionalization of carbon nanotubes"
   Poster presentation
   Strasbourg, France (2009)